

TE
662
.A3
no.
FHWA-
RD-
80-198

FUNDAMENTAL STUDIES IN AUTOMATIC VEHICLE CONTROL

August 1981
Final Report



Document is available to the public through
the National Technical Information Service,
Springfield, Virginia 22161




Prepared for
FEDERAL HIGHWAY ADMINISTRATION
Offices of Research & Development
Traffic Systems Division
Washington, D.C. 20590

FOREWORD

This report is the last of a series of three reports resulting from the study "Fundamental Studies in Automatic Vehicle Control". One of the objectives of the study was to extend the development of wire-following longitudinal and lateral control systems to permit such difficult maneuvers as switching, lane changing, and merging under both normal and emergency operating conditions. The controls were to be designed to allow operations in high-speed (~ 100 km/hr), small time-headway (~ 1 sec) situations through complex guideway networks. Another objective was to study the feasibility of using radar for automatic lateral control of vehicles.

The earlier reports in this series covered the work performed during each of the first two years of this study. It was decided that annual reports be issued rather than a single report at the end in order to make the results available on a more timely basis. Very limited copies of the two previous reports are available upon request from Mr. Lyle Saxton, Federal Highway Administration, Office of Research (HRS-32), Washington, D.C. 20590.


Charles F. Schreffey
Director, Office of Research

NOTICE

This document is disseminated under the sponsorship of the Department of Transportation in the interest of information exchange. The United States Government assumes no liability for its contents or use thereof.

The contents of this report reflect the views of the authors who are responsible for the facts and accuracy of the data presented herein. The contents do not necessarily reflect the official views or the policy of the Department of Transportation.

This report does not constitute a standard, specification, or regulation.

The United States Government does not endorse products or manufacturers. Trademarks or manufacturers' names appear herein only because they are considered essential to the object of this document.

<p>1. Report No. FHWA/RD-80/198</p>	<p>2. Government Accession No.</p>	<p>3. Recipient's Catalog No.</p>	
<p>4. Title and Subtitle Fundamental Studies in Automatic Vehicle Control</p>		<p>5. Report Date August 1981</p>	<p>6. Performing Organization Code 784712</p>
<p>7. Author(s) R. Fenton, R. Mayhan, R. Bishel, R. Kneifel, R. Magee, S. Murthy, L. Rakocy, R. Smith, L. Thayer</p>		<p>8. Performing Organization Report No. 784712-3</p>	
<p>9. Performing Organization Name and Address Transportation Control Laboratory Department of Electrical Engineering The Ohio State University Columbus, Ohio 43210</p>		<p>10. Work Unit No. (TRAIS) FCP 32J1-032</p>	<p>11. Contract or Grant No. DOT-FH-11-9257</p>
<p>12. Sponsoring Agency Name and Address Department of Transportation Federal Highway Administration Office of Research - HRS-32 Washington, D.C. 20590</p>		<p>13. Type of Report and Period Covered Final Report May 1979 - Sept. 1980</p>	
<p>15. Supplementary Notes FHWA Contract Manager: Fred Okano (HRS-32)</p>		<p>14. Sponsoring Agency Code T-0411</p>	
<p>16. Abstract</p> <p>During the past year, which was the final one on a 3-year program, the research efforts were focused principally on the continuing development of a physical test facility which was employed to study control and communication problems at, and below, the sector level. This was done in the context of high-speed (to 26.8 m/s) operations at time headways as small as 1 s.</p> <p>The principal accomplishments during this final year were: (1) The selection of a sector-level control concept, the design and implementation of hardware required for sector-level operations, and the choice of geometrics over which online control would be realized; (2) The development and successful field evaluation of a sector computer-to-controlled vehicle communication link; (3) The design, development, and field evaluation (with very promising results) of a "radar" approach to lateral control; and (4) The design and field evaluation of a vehicle longitudinal controller which provided excellent performance --a small-position error, a comfortable ride, and a relative insensitivity to disturbance forces-- on a consistent basis over a wide range of environmental conditions. The secondary accomplishments included the construction of a sidewall structure for radar steering, and the implementation (and successful field evaluation) of previously designed lateral and longitudinal controllers with microprocessor-based units.</p>		<p>DEPARTMENT OF TRANSPORTATION</p> <p>FEB 8 1982</p>	
<p>17. Key Words Automatic highway, AHS, dual-mode, automatic longitudinal control, automatic lateral control, radar steering microprocessor controllers, sector communications, sector computer.</p>	<p>18. Distribution Statement</p> <p>This document is available to the public through the National Technical Information Service, Springfield, Virginia 22161.</p>		
<p>19. Security Classif. (of this report) Unclassified</p>	<p>20. Security Classif. (of this page) Unclassified</p>	<p>21. No. of Pages</p>	<p>22. Price</p>

METRIC CONVERSION FACTORS

APPROXIMATE CONVERSIONS FROM METRIC MEASURES

SYMBOL WHEN YOU KNOW MULTIPLY BY TO FIND SYMBOL

LENGTH

in	inches	* 2.5	centimeters	cm
ft	feet	30	centimeters	cm
yd	yards	0.9	meters	m
mi	miles	1.6	kilometers	km

AREA

in ²	square inches	6.5	square centimeters	cm ²
ft ²	square feet	0.09	square meters	m ²
yd ²	square yards	0.6	square meters	m ²
mi ²	square miles	2.6	square kilometers	km ²
	acres	0.4	hectares	ha

MASS (weight)

oz	ounces	28	grams	g
lb	pounds	0.45	kilograms	kg
	short tons(2000lb)	0.9	tonnes	t

VOLUME

tsp	teaspoons	5	milliliters	ml
tbsp	tablespoons	15	milliliters	ml
fl oz	fluid ounces	30	milliliters	ml
c	cups	0.24	liters	l
pt	pints	0.47	liters	l
qt	quarts	0.95	liters	l
gal	gallons	3.8	liters	l
ft ³	cubic feet	0.03	cubic meters	m ³
yd ³	cubic yards	0.76	cubic meters	m ³

TEMPERATURE (exact)

°F	Fahrenheit temperature	5/9 (after subtracting 32)	Celsius temperature	°C
----	------------------------	----------------------------	---------------------	----

*1 in = 2.54 (exactly). For other exact conversions and more detailed tables, see NBS Misc. Publ. 286, Units of Weights and Measures. Price \$2.25, SD Catalog No. C13.10:286.

APPROXIMATE CONVERSIONS FROM METRIC MEASURES

SYMBOL WHEN YOU KNOW MULTIPLY BY TO FIND SYMBOL

LENGTH

mm	millimeters	0.04	inches	in
cm	centimeters	0.4	inches	in
m	meters	3.3	feet	ft
m	meters	1.1	yards	yd
km	kilometers	0.6	miles	mi

AREA

cm ²	square centimeters	0.16	square inches	in ²
m ²	square meters	1.2	square yards	yd ²
km ²	square kilometers	0.4	square miles	mi ²
ha	hectares(10,000m ²)	2.5	acres	

MASS (weight)

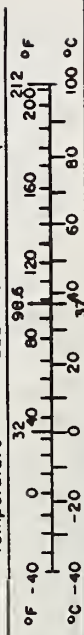
g	grams	0.035	ounces	oz
kg	kilograms	2.2	pounds	lb
t	tonnes (1000kg)	1.1	short tons	

VOLUME

ml	milliliters	8.03	fluid ounces	fl oz
l	liters	2.1	pints	pt
l	liters	1.06	quarts	qt
l	liters	0.26	gallons	gal
m ³	cubic meters	36	cubic feet	ft ³
m ³	cubic meters	1.3	cubic yards	yd ³

TEMPERATURE (exact)

°C	Celsius temperature	9/5 (then add 32)	Fahrenheit temperature	°F
----	---------------------	-------------------	------------------------	----



FUNDAMENTAL STUDIES
IN
AUTOMATIC VEHICLE CONTROL

EXECUTIVE SUMMARY

The control required for an automated highway system can be achieved via a hierarchy wherein a centralized computer would oversee network operations with this including the coordination of activities in the individual geographic regions comprising the network. A second level of control would be at the regional level. Each regional controller would supervise the activity of a number of sectors and control the vehicles in those sectors via appropriate commands to the sector computers which comprise the third level of control. The fourth, and lowest, level of control is that of the individual vehicle. The concern here is with control of the sector level which is comprised of four essential facets:

- a) The specification of the desired state of each vehicle;
- b) The determination of the actual state of each vehicle;
- c) Communications between each vehicle and sector-control; and
- d) The control of each individual vehicle.

Each of the facets can be viewed in the context of either longitudinal or lateral control.

During the past year, which was the final year of a three-year program, the research efforts were focused principally on the continuing development of a physical test facility which will be employed to study control and communication problems at, and below, the sector level. This will be done in the context of high-speed (to 26.8 m/s) operations at time headways as small as 1 s.

The principal accomplishments during this year were:

1. The selection of a sector-level control concept, the design and implementation of hardware required for sector-level operations, and the choice of geometrics over which online control would be realized;
2. The development and successful field evaluation of a sector computer-to-controlled vehicle communication link;
3. The design, development and field evaluation (with very promising results) of a "radar" approach to lateral control; and
4. The design and field evaluation of a vehicle longitudinal controller which provided excellent performance -- a small-position error, a comfortable ride, and a relative insensitivity to disturbance forces -- on a consistent basis over a wide range of environmental conditions.

These accomplishments were integrated and a demonstration of online control, which involved 2 test vehicles operating at a time headway of 1 s, was given. The highlight of this demonstration involved the merging of an initially stationary vehicle into a position 1 s ahead of a mainline vehicle traveling at a speed of 26.8 m/s.

The secondary activities included the design, construction, and field evaluation of a guidewall structure for use in radar steering, and a start toward converting the analog electronics, employed in the vehicle lateral and longitudinal controllers, to a discrete digital realization. The latter was accomplished using microprocessors and involved the digital realization of both a lateral and a longitudinal controller. The former, which involved a previously designed, velocity-adaptive controller, was extensively tested and yielded excellent performance -- tracking error < 0.063 m, a good insensitivity to disturbance forces, and a comfortable ride. The latter, which involved the realization of a simple velocity controller, was also field tested with good results; however, it remains to similarly implement a more complex, better-performing longitudinal controller which was selected for final implementation. The microprocessors employed here can also be employed in a vehicle-based, decision-making role.

In view of the results obtained from this study, it is proposed that future AHS technology development efforts should be focused on the following:

- a) The continued development of the automated vehicle test facility at TRCO;
- b) The implementation of an online computing system which could accomplish all sector-level control tasks;
- c) An intensive study of a multi-processor system for in-vehicle use;
- d) Studies of radar-sensing techniques for use in both lateral and longitudinal control; and
- e) Studies in vehicle longitudinal control with an emphasis on both emergency operations and the tradeoffs between fuel usage, vehicle tracking accuracy and ride comfort.

TABLE OF CONTENTS

		Page
	EXECUTIVE SUMMARY	iii
	FIGURES	x
	TABLES	xviii
	<u>CHAPTER</u>	
I	INTRODUCTION	1
	A. Automated highway system concept	1
	B. AHS control hierarchy	3
	C. Overview	7
II	SECTOR-LEVEL CONTROL STUDIES	9
	A. Network control policy	9
	B. Control functions	11
	C. Merging high-speed traffic streams	13
	D. Sector computer hardware	20
	E. Sector geometrics	23
III	SECTOR-LEVEL COMMUNICATIONS	27
	A. Introduction	27
	B. Synchronization and data rates	32
	C. System configuration	36
	D. System testing and modifications	40
	E. Field test evaluation	51
IV	A TWO-FREQUENCY RADAR FOR USE IN PASSIVE LATERAL CONTROL	52
	A. Theory of the two-frequency radar	60
	B. The laboratory investigation of the two-frequency radar	75
	C. Full scale studies	100
	D. Conclusions	127

Table of Contents (Cont.)

V.	A MICROPROCESSOR-BASED, VEHICLE LATERAL CONTROLLER	129
	A. Introduction	129
	B. Lateral controller design	129
	C. Compensator realization	138
	D. Selection of T and word length	143
	E. Simulation studies	153
	F. Full-scale studies	159
	G. Discussion	164
VI	STUDIES IN VEHICLE LONGITUDINAL CONTROL	168
	A. Overview of previous studies	168
	B. Controller implementation	174
	C. Full-scale testing of selected controller	183
	D. Commentary	192
VII	A MICROCOMPUTER-BASED LONGITUDINAL CONTROLLER	195
	A. Introduction	195
	B. Microcomputer functions	195
	C. Velocity controller tests	209
	D. Longitudinal position controller implementation	224
VIII	SUMMARY AND FUTURE EFFORTS	225
	A. Summary	225
	B. Future directions	228
	REFERENCES	229
	<u>APPENDIX</u>	
A	ON THE LATERAL RIDE QUALITY OF A WIRE-FOLLOWING SYSTEM	238
B	A COORDINATE SYSTEM FOR AUTO- MATIC LATERAL CONTROLLER DESIGN	244
	A. Introduction	244
	B. Inertial reference frame	245
	C. Path-dependent coordinates	252
	D. Conclusions	257

Table of Contents (Cont.)

BB	AN APPROXIMATION FOR ΔS_{cg}	258
C	A MICROPROCESSOR-BASED LATERAL CONTROLLER -- HARDWARE IMPLEMEN - TATION	262
D	MICROCOMPUTER HARDWARE FOR A LONGITUDINAL CONTROLLER	265
	A. Introduction	265
	B. Address Allocations	265
	C. Program PROM	266
	D. I/O ports	269
	E. Multiplier interface	269
	F. Interrupt considerations	277
	G. Summary	277

FIGURES

<u>FIGURE</u>		<u>Page</u>
1-1	A general control hierarchy	5
1-2	A sector-level, control configuration	6
2-1	A 3-into-1 junction with synchronous slots	15
2-2	A network of sectors	15
2-3	(a) Vehicles entering a 3-into-1 junction (b) Cycles formed with $M_m = 6$ (c) Cycles after resolution of conflicts	15
2-4	A block diagram of the sector computer	21
2-5	Selected sector geometrics	25
2-6	Relationship of selected geometrics to TRCO skid pad	25
3-1	Communications time base	31
3-2	Derivation of timing signals at the vehicle level	35
3-3	System configuration	37
3-4	Vehicle timing circuit	39
3-5	TDM timing	41
3-6	Sector computer timing circuit	42
3-7	The biquad configuration	45
3-8	Filter characteristics	47
3-9	Matched filter response for a rectangle pulse	48

Figures (Cont.)

3-10	Integrate and dump filter	48
3-11	Input-output waveforms	50
3-12	Geometries of TRCO skid pad	50
4-1	Geometrics for a passive lateral position sensor	54
4-2	Illustration defining the operating region, ΔR , and the operating range, R_o , of a passive lateral position sensor	56
4-3	Signal spectrum of the two-frequency radar	61
4-4	Block diagram of system I	64
4-5	Block diagram of system II	67
4-6	Modulation frequency vs. maximum unambiguous range	69
4-7	Spatial phase distribution for low-frequency modulation	71
4-8	Spatial phase distribution for high-frequency modulation	72
4-9	Schematic diagram of the indoor test configuration	77
4-10	Front view of the indoor test facility and a portion of the 8.4 GHz radar	79
4-11	Rear view of the indoor test facility and the 8.4 GHz radar	80
4-12	The 10.5 GHz radar	81
4-13	Block diagram of the 8.4 GHz radar	82
4-14	Block diagram of the 10.5 GHz radar	83
4-15	Measured phase shift vs. lateral distance using the 8.4 GHz radar ($\Delta f = \text{MHz}$)	84

Figures (Cont.)

4-16	Measured phase shift vs. lateral distance using the 10.5 GHz radar ($\Delta f = 300$ MHz)	85
4-17	Possible leakage paths for the 10.5 GHz radar	87
4-18	Phase vs. distance with no leakage signals present -- theoretical calculation	90
4-19	Theoretical results for Case I where $S/N = 10$ dB	93
4-20	Phasor diagram of \hat{V}_1 and \hat{V}_2 with \hat{V}_1 as the reference phasor	94
4-21	Measured phase shift vs. lateral distance (20° B.W. antennas and 1m x 1m screen wire reflector)	95
4-22	Theoretical results for Case II where $S/N = 20$ dB	97
4-23	Measured phase shift vs. lateral distance (20° B.W. antennas, and 1m x 1m screen wire reflector)	98
4-25	Front view of reflector structure	101
4-26	Front view of radar unit mounted on the vehicle	102
4-27	Top view of radar unit mounted on the vehicle	102
4-28	Vehicle-sidewall geometry with outboarded antennas	103
4-29	Profile of the wall structure referenced to the embedded wire	104
4-30	Geometrical optics analysis of reflection from a distorted reflector	106
4-31	Two different traces of lateral position error vs. travelled distance as measured by the radar sensor	108

Figures (Cont.)

4-32	The output of the three position sensing devices at one point on the test tract	110
4-33	Lateral position error vs. distance as measured by the amplitude sensor and the radar sensor	111
4-34	Lateral position error vs. distance as measured by the amplitude sensor and the radar sensor.	113
4-35	Lateral position error vs. distance as measured by the amplitude sensor and radar sensor	115
4-36	Lateral position error vs. distance as measured by the amplitude sensor and the radar sensor	116
4-37	Cross-sectional view of the modified reflecting wall	117
4-38	Lateral position error vs. distance with the reflecting wave only partially covered with foil (wire-following control)	119
4-39	Radar and phase-sensor output vs. lateral distance at one point of the test track	121
4-40	Lateral position error vs. distance as obtained from the phase-sensor and the radar (wire-following control at $v = 3.4$ m/s).	122
4-41	Lateral position error vs. distance as obtained from the phase-sensor and the radar (radar control at $v = 3.4$ m/s)	123
4-42	Lateral position error vs. distance as obtained from the phase-sensor and the radar (wire-following control at $v = 12$ m/s)	125
4-43	Lateral position error vs. distance as obtained from the phase-sensor and the radar (radar control at $v = 14$ m/s)	126

Figures (Cont.)

5-1	A single-loop, lateral controller	130
5-2	Lateral dynamics model as a function of forward velocity	132
5-3	Block diagram of inverse compensator	139
5-4	ΔS_f vs. t for $T = 100$ ms and $I \rightarrow \infty$	145
5-5	ΔS_f vs. t for $T = 70$ ms, $I \rightarrow \infty$, and 4 values of V_f	146
5-6	ΔS_f vs. t for $T = 50$ ms, $I \rightarrow \infty$, and 4 values of V_f	147
5-7	ΔS_f vs. t for $T = 25$ ms, $I \rightarrow \infty$, and 4 values of V_f	148
5-8	ΔS_f vs. t for $T = 75$ ms, $I = 8$ ($J = 4$), and 4 values of V_f	150
5-9	ΔS_f vs. t for $T = 50$ ms, $I = 16$ ($J = 9$), and 4 values of V_f	151
5-10	Simulation structure	154
5-11	Step responses (ΔS_f vs. t) for 4 speeds (simulation)	155
5-12	Tracking performance on a curve with a 100-m radius and $V_f = 13.4$ m/s (simulation)	157
5-13	Tracking performance on a curve with preview information ($R = 100$ m and $V_f = 13.4$ m/s)	158
5-14	Step responses (ΔS_f vs. t) for 6 speeds	161
5-15	Tracking performance on a straight roadway for 5 speeds	162
5-16	Tracking performance on a 100-m radius curve for $V_f = 9$ m/s	165
5-17	Tracking performance on a 100-m radius for $V_f = 13.4$ and 17 m/s	166

Figures (Cont.)

6-1	One basic propulsion system model	170
6-2	Small-signal linear velocity controller with internal velocity feedback	172
6-3	State dependent controller/vehicle combination	173
6-4	Two linear velocity controllers	175
6-5	1st gear limit cycle data example	177
6-6	Limit cycle with state-dependent controller and vehicle at constant velocity	178
6-7	Limit cycle with state-dependent controller and accelerating vehicle in first gear	179
6-8	Block diagram of modified controller	182
6-9	System entry commands employed by Fenton and Chu [52]	184
6-10	Selected acceleration/velocity reference profile	185
6-11	Acceleration-versus-velocity plots	186
6-12	System entry response	188
6-13	Larger A_c yields less stable system response	189
6-14	Move-up and move-back command acceleration trajectories	191
6-15	Move-up / move-back acceleration responses	193
7-1	A block diagram of the vehicle longitudinal control system	197
7-2	Estimation of position between absolute markers	198
7-3	Estimation of position using a wheel tachometer output	200

Figures (Cont.)

7-4	A technique for interpolating between tachometer pulse intervals	201
7-5	Graphical illustration of example of the proposed state estimator	206
7-6	A longitudinal, position controller	208
7-7	Flow chart for linear controller	210
7-8	An analog velocity controller	212
7-9	A microcomputer realization of a velocity controller	214
7-10	Flow chart for velocity controller	216
7-11	Step response of velocity controllers, $V_{CO} = 9.15 \text{ m/s}$	218
7-12	Step responses of velocity controllers, $V_{CO} = 12.2 \text{ m/s}$	219
7-13	Step responses of velocity controllers $V_{CO} = 15.2 \text{ m/s}$	220
7-14	Step responses of velocity controllers $V_{CO} = 18.3 \text{ m/s}$	221
7-15	Step responses of velocity controllers, $V_{CO} = 21.3 \text{ m/s}$	222
7-16	Steady-state tracking of digital velocity controller around a curved portion of track	223
A-1	Acceleration (rms) at a vehicle's cg	241
A-2	Accelerations (rms) at front center of vehicle	242
A-3	Tracking error (rms) at the vehicle's front center	243
B-1	A simplified model of a vehicle's lateral dynamics	248

Figures (Cont.)

B-2	Vehicle motion as described in an inertial reference frame	248
B-3	A lateral controller described in inertial coordinates	251
B-4	Steering controller for operation along a straight-line path (inertial coordinate system).	
B-5	A path-dependent coordinate system	253
B-6	Steering controller described in path-dependent coordinates	253
B-7	Simplified block diagram for a path-dependent coordinate system	256
C-1	Block diagram of SDK-86 microcomputer with hardware modifications	263
D-1	Basic microcomputer structure	266
D-2	Memory Allocations	267
D-3	PROM interface	268
D-4	Output port interface	270
D-5	Input port interface	271
D-6	Multiplier X-register interface	274
D-7	Multiplier Y-register interface	275
D-8	Least-significant, product output interface	276
D-9	Most-significant, product output interface	278

TABLES

<u>TABLE</u>		<u>Page</u>
4-1	Radar system parameters for two modulation frequencies, Δf	74
4-2	Measured lateral accelerations for wire-following (W-F) control and radar (R) control at two different longitudinal velocities	127
5-1	Parameter values for instrumented Plymouth sedan	134
5-2	Definition of parameters	144
6-1	Parameter set for modified controller	181
B-1	Definition of symbols	246

CHAPTER I

INTRODUCTION

A. Automated Highway System Concept

One approach toward the amelioration of both present and anticipated future transportation problems is individual-vehicle, automated ground transport. One form of such transport, "dual-mode," is an attractive candidate for further study.

The general dual-mode concept involves a roadway complex which consists of both automated and nonautomated roads. Various main arteries would probably be equipped for automation while various secondary streets/roads would not be equipped. Ultimately, it would be expected that public vehicles and both individual private vehicles and commercial traffic would use the system; however, it seems likely that initially only mass transit vehicles would be employed.

An individual vehicle would enter the system at a special entrance point where it would first undergo a rapid automatic checkout, and the driver would indicate his destination. If it "passed" the checkout, the vehicle would move to an entrance ramp from which it would be automatically merged into the traffic stream. However, if it "failed" the vehicle would not be allowed

to merge into the traffic stream; instead, it would be rejected and guided to a nearby service facility for repair. The traffic stream velocity would be fixed by a central traffic controller and would be dependent on weather, roadway conditions, the state of the traffic stream, etc. Once in the traffic stream, the vehicle would remain under automatic control until the driver's preselected exit was reached. Then the vehicle would be guided off the roadway onto an exit ramp, and control would be returned to the driver.

In the event of vehicle disability, the vehicle would be ejected from the main traffic stream. If it were controllable, it would be routed to the nearest emergency exit. If it were not, the use of one lane would be lost until the vehicle could be moved off the highway. Hence, it would be temporarily necessary to direct the mainstream vehicles around the disabled one. Clearly, some provision must be made for clearing the roadway as quickly as possible.

The potential advantages of this type of system include substantial increases in both traffic flow capacity and traffic safety as well as some modest reduction in fuel usage [1] - [2].

Dual-mode systems have been suggested for both ubiquitous coverage of urban areas [3] and for intercity highway applications. Here, the emphasis is on the latter, and the term "Automated Highway System" (AHS) will hereforth be used to refer to this application.

The initial studies on the automated highway were conducted in the late 1950's and, subsequently, limited efforts were undertaken, both here and abroad, by various industrial organizations, government laboratories and academic institutions [4]-[19]. This type of system would probably be first considered for an already congested network (e.g., the Northeast corridor).

B. AHS Control Hierarchy

The control required for the automated part of an AHS is dependent upon the selected system structure. The structure selected here involves a post-deterministic synchronous approach to traffic management (as is described in detail in Chapter II), and it is comprised of two intimately related facets. The first, macro-control, embodies the entire hierarchy of control which is necessary for system coordination. This is, of course, the "systems" level of control, and it includes such operations as vehicle scheduling and routing, the determination and specification of traffic speeds, and system response to abnormal and emergency situations. The second facet, micro-control, is explicitly concerned with individual vehicle position regulation and maneuvering and encompasses both vehicle lateral control and longitudinal control.

A general control hierarchy, which could be employed with an automated vehicle system, includes a central controller to over-

see network operations with this including the coordination of activities in the individual geographic regions comprising the network (see Fig. 1-1). A second level of control would be at the regional level. Each regional controller would supervise the activity in a number of sectors and control the vehicles in those sectors via appropriate commands to the sector computers which comprise the third level of control. The fourth, and lowest, level of control is that of the individual vehicle.

Note from Fig. 1-2 that a sector-level, control configuration would be comprised of four basic elements:

- 1) A sector computer;
- 2) A communication link for achieving both computer-to-vehicle and vehicle-to-computer transmissions;
- 3) An information source for directly providing the computer with state information on each vehicle; and
- 4) An information source embedded in, or located nearby, the guideway and intended to supply state information to each controlled vehicle.

With this general configuration, the sector computer would have two independent indications of the state of each vehicle -- one from the guideway-to-sector computer information source and one transmitted from the vehicle. This would provide desired redundancy. Further, if the information received were of sufficient accuracy and timeliness, the system could be designed for a quick

CONTROL LEVEL

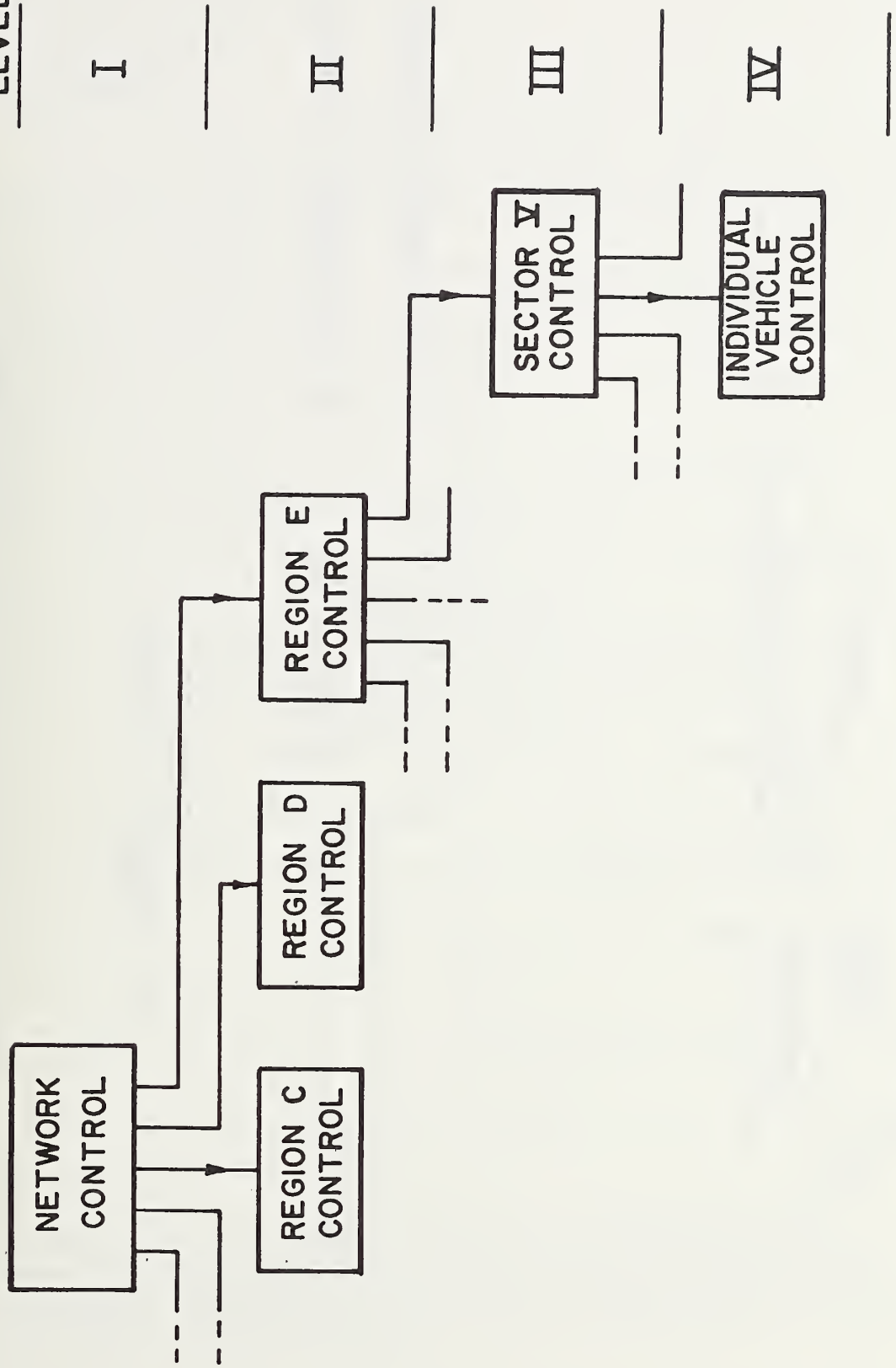


Fig. 1-1. A general control hierarchy.

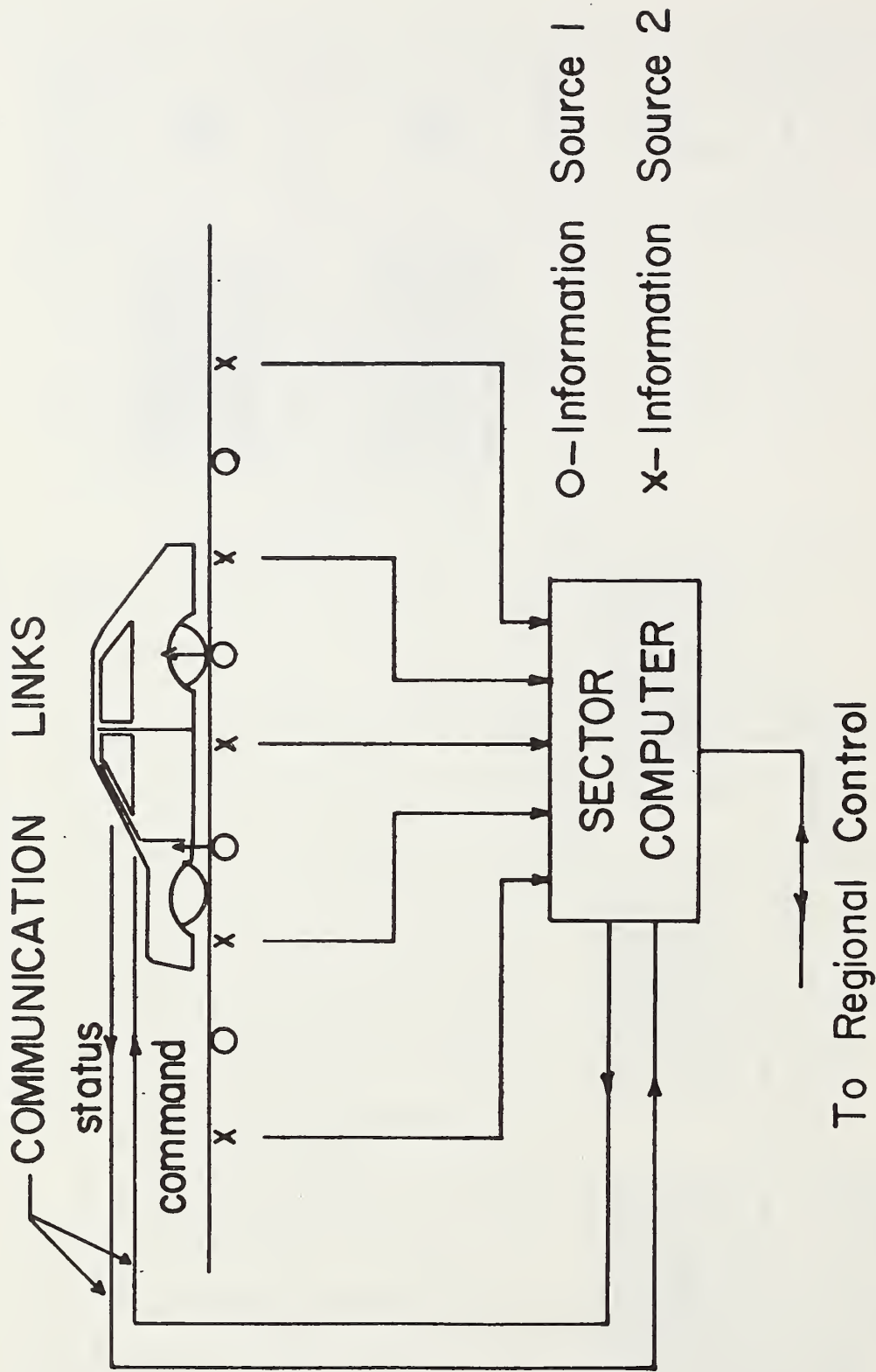


Fig. 1-2. A sector-level, control configuration.

response to an anomalous situation .

C. Overview

During the past year, which was the final year of a three-year program, the research efforts were focused principally on the continuing development of a physical test facility which will be employed to study control and communication problems at, and below, the sector level.¹ This will be done in the context of high-speed (to 26.8 m/s) operations at time headways as small as 1 sec. The primary activities undertaken were:

- 1) The selection of a sector-level control concept, the design and implementation of hardware required for sector-level operations, and the choice of geometrics over which online control is to be realized;
- 2) The development and field evaluation of a sector computer-to-controlled vehicle communications link;
- 3) The design, development and field evaluation of a "radar" approach to lateral control; and

1

The results obtained during the first two years, as well as a description of the test facility geometrics and the various wire configurations embedded in the roadbed are described in the previous interim reports [20]-[21].

- 4) The design and field evaluation of a vehicle longitudinal controller which provided excellent performance -- a small-position error, a comfortable ride, and a relative insensitivity to disturbance forces -- on a consistent basis over a wide range of environmental conditions.

The secondary activities included the design, construction, and field evaluation of a guidewall structure for use in radar steering, and a start toward converting the analog electronics, employed in the vehicle longitudinal and lateral controllers, to a discrete digital realization. The latter was accomplished using microprocessors which can also be employed in a vehicle-based, decision-making role.

CHAPTER II

SECTOR-LEVEL CONTROL STUDIES

A. Network Control Policy

Three network control policies have been suggested for achieving safe and efficient operation under high-speed, small time-headway conditions -- asynchronous, synchronous, and quasi-synchronous. The asynchronous, or car-following approach, involves stochastic vehicular control (i.e., control with respect to the state of the surrounding traffic). The earliest paper dealing with such control was presented by Zworykin and Flory [22] in 1958; subsequently, numerous others have been presented in the literature; e.g., [23]-[25]. One problem with this approach is the resolution of vehicle conflicts at merging junctions where the coordinated control of many vehicles is essential. The required vehicle-based technology for achieving such control is currently unavailable.

The synchronous, or point-follower, approach is characterized by deterministic vehicular control. This involves the concept of slots (of H_t in time units) moving through a network so that slot synchronization is achieved at all merging junctions. This approach was first suggested by Gluck [26] and has subsequently

been studied in detail by many others including Godfrey [27], Boyd and Lucas [28], and Howson [29].

A deterministic implementation involves the computing of a vehicle's entire trajectory (i.e., its schedule over a selected route) prior to its entry into the system. A sequence of slot assignments, that would allow an uninterrupted trip from origin to destination, would be specified for that vehicle. This predetermined approach involves possibly excessive waiting time (i.e., delay) for an entering vehicle, a restrictive scheduling algorithm, and an inability to effectively respond to failures.

Another approach, which is less rigid and more adaptive, is to remove the requirement for a priori slot assignments. Instead, a vehicle is merged into mainline traffic, possibly into the first available empty slot, and then moved in synchronization with other traffic until a conflict point (e.g., a merging junction) is reached; then maneuvering may be required to effect safe and efficient operation. This postdeterministic approach was introduced by Munson [30] and subsequently extended by numerous investigators including Rule [31], Roseler et al [32], and Kornhauser and McEvaddy [33]. This policy involves minimal waiting time at an entry point, a distribution of the computational load, and a potentially simpler resolution of failures.

The quasi-synchronous approach is a combination of the synchronous and asynchronous approaches. Vehicles on connecting

links would be under vehicle-follower control while those in the vicinity of a merging junction would be under point-follower control. This approach is similar to the postdeterministic synchronous one.

The evidence for the superiority of one policy over another is not conclusive, and the results presented to date appear to be dependent upon the choice of network configuration, its geographical extent, and the nature of the imposed travel demands. It does appear, however, that greater operating flexibility, less travel delays, and a simpler implementation results with the choice of a postdeterministic synchronous policy and therefore this choice is made here.

B. Control Functions

The network computer (see Fig. 1-1) would maintain frequently updated statistics on the network state (as based on data received from the regional levels) and use this information to control vehicle entry, routing, scheduling, and system response to failures. This would be a macroscopic level of control with the required commands being transmitted to the appropriate regional level. A second essential function would be the collection, processing, and storing of operational data for later use.

The primary function of each regional computer would be the supervision and coordination of all activity within its assigned

boundaries. Command decisions would be based on gross commands from the network controller, data received from adjacent regional computers, and data from the sector computers within its jurisdiction. The selected vehicle commands would be sent to the sector computers for subsequent transmission (possibly in a modified form) to the controlled vehicles.

A sector computer would transmit a command trajectory to each vehicle prior to its entering the sector.¹ This information would be either the command selected at the regional level or that command as modified by the sector computer to meet local conditions. Once in the sector, each vehicle would periodically transmit its status (i.e., operating normally (as commanded) or operating abnormally). If each vehicle were operating normally, the sector computer would continue to monitor operations; however, if one or more vehicles were operating abnormally, the sector computer would cause an emergency braking command to be transmitted to all affected vehicles.

Each individual vehicle, upon receiving command information, would act so as to maintain the desired lateral and longitudinal states. The vehicle could take independent action only in the event of certain emergency conditions in which case the sector

1

This communication approach, as opposed to transmitting command information online (e.g. every 100 mss), greatly reduces the complexity of the required communications.

computer would be promptly notified.

The most difficult, normal (nonemergency) control problem, which must be frequently solved within this hierarchy, is the safe and efficient merging of two or more lanes of high-speed traffic into a single lane. This problem, which involves regional-level, sector-level, and vehicle-level control is considered in detail here.

C. Merging High-Speed Traffic Streams

a) Overview

The merging problem has two principal aspects -- junction saturation and vehicle conflicts. The former occurs when the vehicle flow-rate into a junction exceeds the slot flow-rate out, and the latter when two or more vehicles occupy upstream slots that will merge into one downstream slot.

Long-term junction saturation would be prevented by the network controller which would distribute vehicle entry times based on the current network statistics. Thus, the average input flow-rates would not exceed a junction's capacity. Short-term saturation, however, could occur and would need to be handled locally. This could be accomplished by routing overflow traffic into a special waiting area, or by reducing stream speed and creating more slots. Both approaches result in additional trip-time delay and trip-time variance as well as complicate the control process.

In contrast, by exiting excess vehicles onto adjacent non-automated highways, waiting in queues can be avoided, stream speed maintained and a simplified control process implemented. With a well-designed network controller, such forced exiting would be a very low-probability event. This approach is employed here resulting in the ability to resolve merging conflicts without internal delays.

Conflicts are resolved by maneuvering one or more vehicles forward or backward into other slots. Thus, the sector level of control would do the following:

- 1) Examine the arrangement of vehicles allowed into the junction;
- 2) Detect any conflicts; and
- 3) Resolve these by specifying which vehicles are to maneuver and issuing the proper commands.

b) An Algorithm for Merging Conflict Resolution

The merging conflicts can be solved by employing an algorithm which uses the cycle concept [28]. Here, a cycle, which is a group of adjacent slots, varies in length from 1 to M_m .

The two aspects of the selected algorithm are readily described using the 3-into-1 merging junction shown in Fig. 2-1. This corresponds, for example, to that portion of an intersection wherein some northbound and some southbound traffic are routed

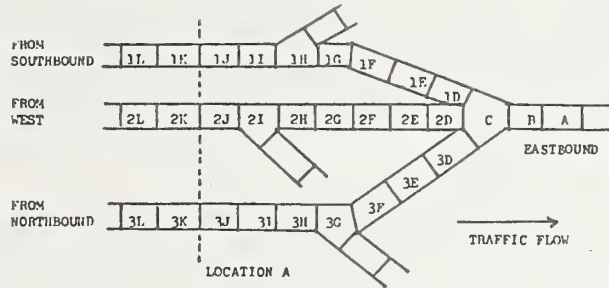


Fig. 2-1. A 3-into-1 junction with synchronous slots.

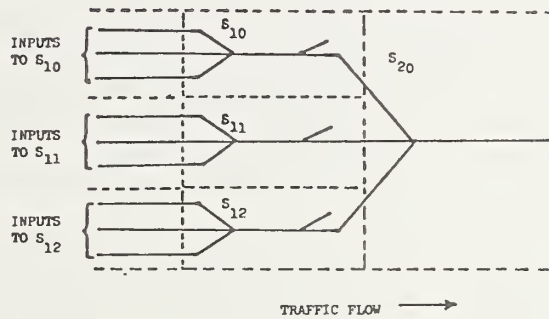


Fig. 2-2. A network of sectors.

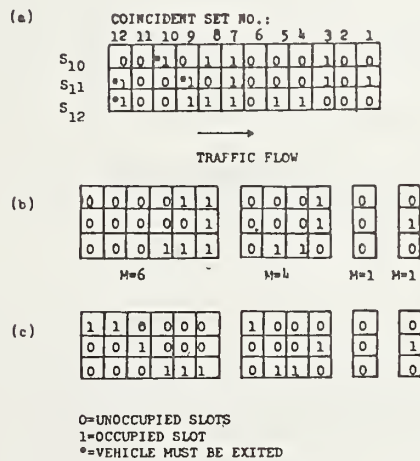


Fig. 2-3. (a) Vehicles entering a 3-into-1 junction.
 (b) Cycles formed with $M_m = 6$.
 (c) Cycles after resolution of conflicts.

onto an eastbound lane. Slots on the three "feeder" lanes which have the same letter will be referred to as a coincident set because they will merge into one slot.

At location A, i.e., a point on each feeder lane prior to the last exit before the merge, the coincident set of slots would be checked. If the total number of vehicles in the set were zero or one, no conflict would exist and the cycle would be ended (with a cycle length of one). H_t seconds later the next coincident set would be similarly checked. If it contained two or three vehicles, a conflict would exist and the cycle would be continued into the following coincident set. As each set reached Location A, it would be processed and the cycle length incremented by one until one of the following conditions were met:

- 1) $V \leq m$
or
2) $V \geq M_m$,

where

- V = running total of the number of
vehicles in the cycle, and
 m = current value of cycle length .

If condition one were met, a cycle would be complete with one slot in the cycle for each vehicle, M (the final value of the cycle length) would be set equal to m , and since $m < M_m$ no vehicle(s) would be exited. However, if condition two were met, $V-M$ vehicles

(if any) from the last coincident set and all vehicles (if any) in the next $M_m - m$ coincident sets must be exited, and a cycle length of M_m would result.

Using variable rather than fixed-length cycles results in a more efficient use of empty coincident sets. The number of slots in a cycle is equal to the number of vehicles in the cycle unless the cycle length is one (in which case it may be unoccupied) or if empty slots are reserved for upcoming traffic. A more subtle advantage is that vehicles are effectively "preloaded" towards the front of a cycle so that conflicts can be resolved without using move-up maneuvers. Such maneuvers are undesirable because of the increased fuel consumption and the safety problems associated with operation at a speed greater than the stream speed.

Various move-back maneuvering strategies could be employed. One of these is to minimize the number of vehicles maneuvered since a maneuvered vehicle would consume more fuel than one not maneuvered [24]. This is the choice made here.

c) Example

The algorithm will be demonstrated using the geometrics of Fig. 2-2, which are comprised of four sectors, each having the geometrics of Fig. 2-1. Here, the three sectors S_{10} , S_{11} , and S_{12} receive vehicle-string inputs which have been processed to provide conflict-free merges in these sectors; i.e., the future

configuration of vehicles after the merges in S_{10} , S_{11} , and S_{12} has been determined. An example of such a configuration (arbitrarily chosen) is shown in Fig. 2 - 3(a) by a matrix with 1's representing occupied slots and 0's unoccupied ones. It is this matrix which must be processed to eliminate both short-term saturation and merging conflicts in S_{20} .

Short-term saturation would be prevented by the regional computer which is in communications with each of the sectors. It would process the matrix of Fig. 2-3(a), prior to the vehicle's entry into S_{10} , S_{11} , and S_{12} , to form cycles and decide which vehicles (if any) need to be exited before entering S_{20} . The exiting decisions would be communicated to S_{10} , S_{11} , and S_{12} which would then generate the proper routing commands. Choosing $M_m = 6$ in the example, the cycles of Fig. 2-3 (b) result. Starting from the right the first coincident set of Fig. 2-3(a) contains one vehicle, so the cycle is complete with a length of one (i.e., $M = m = 1$). The second set has no vehicles so another cycle of $M = 1$ results. The third set, however, contains two vehicles, and it is necessary to continue the cycle through the sixth set, when a cycle with $M = m = 4$ results. The next cycle begins with the seventh set which contains three vehicles. This cycle is completed in the ninth set when $V > M_m$ ($V = 7$). Since $V \geq M_m = 6$, M is set equal to six, and the vehicles in the tenth, eleventh, and twelfth sets must be exited. One of the two vehicles in the ninth set

also must be exited (an arbitrary choice is made here). In this manner, short-term saturation is eliminated and only merging conflicts remain to be resolved.

The cycle data, as generated by the regional computer in the matrix form of Fig. 2-3(b), is passed to S_{20} which specifies the vehicle maneuvering necessary for the resolution of any conflicts. Conceptually, this task involves manipulating a matrix so that there is only one "1" per column. The results, for the specified maneuvering strategy, are shown in Fig. 2-3(c). No conflict exists in the first two cycles, for the third a three-slot moveback by the vehicle in lane one suffices, while three vehicles must be maneuvered in the fourth case. These results may be verified readily.

d) Discussion

The suggested merging algorithm is characterized by the following:

- 1) Control flexibility;
- 2) An efficient distribution of the computational load;
- 3) Minimal communications to and from the vehicles;
- 4) Minimal trip-time delay and trip-time variance; and
- 5) Vehicle fuel economy.

It is flexible as it can be applied to the merging geometries commonly encountered in a highway environment. In particular, it is easily modified for a two-into-one merge.

The computational load is distributed with the network controlling long-term saturation, the region short-term saturation, and the sector resolving conflicts.

Communications between a sector computer and a vehicle may be reduced by providing command trajectories, which contain all necessary routing and maneuvering information, prior to sector entry. This was the approach employed here.

By avoiding internal queues and using forced exiting, minimal trip-time delays and trip-time variance may be obtained for the vehicles remaining under AHS operation.

Some vehicle fuel economy could be achieved by avoiding slowdowns, an efficient choice of stream speed, and a conflict-resolution strategy that minimizes the number of vehicles to be maneuvered.

D. Sector Computer Hardware

The hardware efforts, which have dealt with systems-level control, have been principally focused on the realization of a sector computer which can be employed for the online control of vehicles at the Transportation Research Center of Ohio (TRCO). The selected computer, which is shown in Fig. 2-4, is comprised of two primary units -- a DEC PDP 11/03 minicomputer and special-purpose hardware -- and peripheral equipment which includes a high-speed teletype, a paper tape reader/punch, a video terminal,

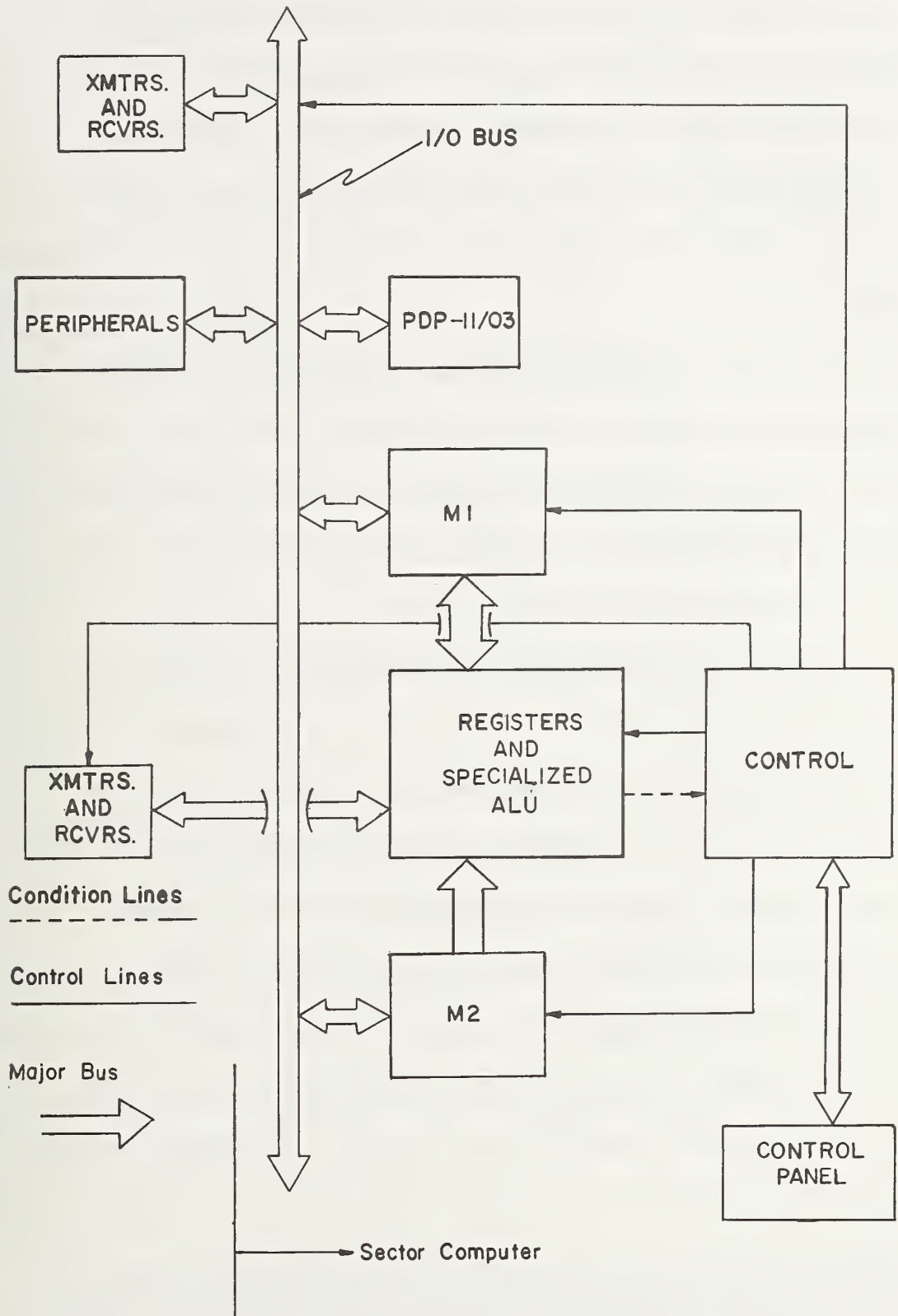


Fig. 2-4. A block diagram of the sector computer.

and a disc system.² In addition, transmitters and receivers are included so that communication can be achieved between this computer and both a regional computer and individual vehicles. During the past year, some interfacing between the various elements within this computer and between this computer and its peripherals was designed.

Note that the Special-Purpose Hardware is interfaced to the bus through the memory blocks M1 and M2, which are each comprised of 4096, 16-bit words. The two required interfaces, which were implemented on a single, printed circuit board, are similar and much of the circuitry is shared.

Presently, two peripherals are available -- a DECwriter and a paper tape punch/reader. The former is a keyboard/printer, and it has been procured and the necessary interfacing provided. The latter, which will facilitate the storage and loading of frequently run programs, was assembled, and a simple parallel interface was designed and built to connect this unit to the sector computer. In the future, it may be desirable to include two more peripherals -- a CRT (video display) and a disc-operating system -- to greatly enhance the computers capability and flexibility. Both would involve the design and construction of a DMA (direct-memory access) interface.

2

A detailed description of this computer is contained in the interim report "Fundamental Studies in Automatic Vehicle Control," dated May 15, 1979 [21].

The communication link interface (which at this time is not complete) is the subchannel 1 transmitter and receiver. This link, which is described in detail in Reference 21, provides trajectory and routing information to each vehicle as it enters the sector.³

E. Sector Geometrics

In order to complete the development of the sector controller (i.e., the implementation of both the software and some additional hardware), it was necessary to specify the sector geometrics, to be controlled. Two primary restrictions were involved:

- 1) the maximum number of vehicles that can be controlled (which fixes the controlled mileage);
and
- 2) the maneuvering requirements which relate to the merging and diverging of traffic.

Previously, the maximum sector capacity was chosen as 256 vehicles, and the special-purpose computer was designed (and partially constructed) to control up to this number [21]. If the sector were operating at maximum capacity, the controlled mileage (L) would be

3

Additional interfaces will eventually be required for a regional computer receiver and adjacent sector-computer transmitters and receivers.

$$256 H_t V_s \quad (m)$$

where V_s is the stream speed in m/s. This mileage is fixed by the minimum speed for which maximum-capacity operation is desired.

If, as is the case here, L were selected as 3.43 km and $H_t = 1s$, then the maximum capacity of 256 vehicles would be achieved for 13.4 m/s (30 mph) and would decrease to 128 vehicles for $V_s = 26.8$ m/s (60 mph).

In regard to maneuvering, the geometrics must be selected so that a variety of vehicle control operations could be performed over a wide speed range. These operations would include

- i) vehicle entry and exiting
- ii) the merging of two main lines of traffic at line speed,
- iii) on-line maneuvering,
- iv) constant-speed operation, and
- v) responses to emergencies.

After a careful consideration of such factors and the evaluation of many possible geometrics, those shown in Fig. 2-5, which comprise 3.43 km of roadway, were selected for implementation. One part of these geometrics is comprised of an already-instrumented section of the TRCO skid pad as shown in Fig. 2-6. Also shown are the two required additions -- a "real" addition (consisting of a diverge, a parallel lane, and a merge) and a

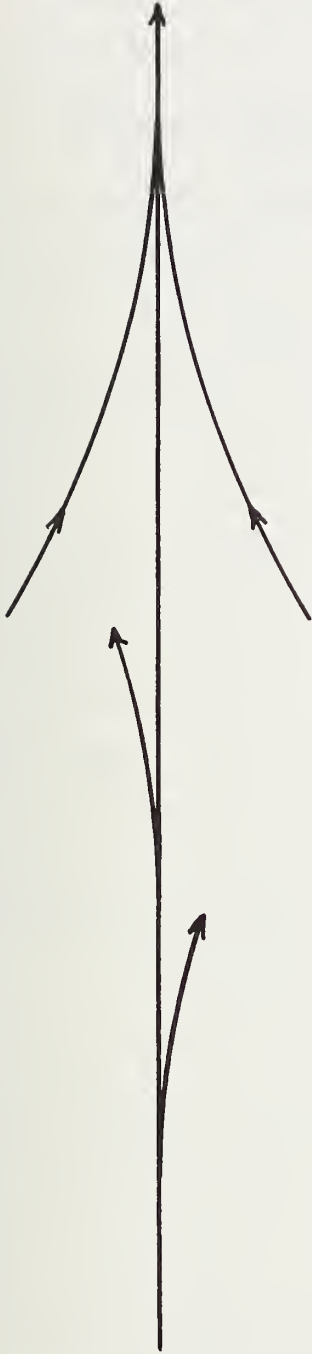


Fig. 2-5 Selected sector geometrics

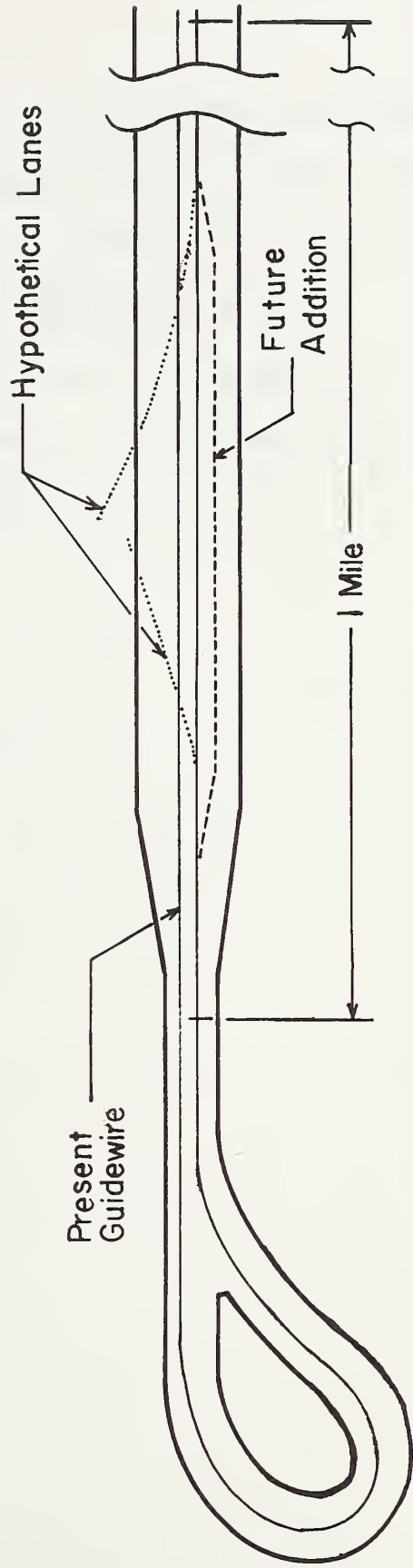


Fig. 2-6 Relationship of selected geometrics to TRCO skid pad.

hypothetical addition (consisting of a diverge and a merge). The latter would be computer generated and only exist in the computer's memory (and be displayed on a video terminal if one were available).

Using this combination of real and hypothetical roadways, it will be possible to demonstrate various high-capacity, vehicle-control operations over a wide speed range.

CHAPTER III

SECTOR-LEVEL COMMUNICATIONS

A. Introduction

One essential part of a sector-level control facility is communications between the controller and each vehicle in the sector. At present, it appears as if this function could be most efficiently realized via an inductive link (e.g., inductive loops embedded in the roadbed and transmitting/receiving coils on each vehicle); however, during this study it was not possible to design and install the necessary equipment at TRCO, especially that required in the 4-mile long roadbed. Instead, it was expedient to employ an available RF system.

This system is comprised of "off the shelf" equipment, manufactured by Electro-Mechanical Research Inc. (EMR), which was originally designed for the simultaneous transmission of up to 21 frequency-division multiplexed (FDM) channels with relatively low data rates (from 6 Hz to 2500 Hz). A typical application for this equipment would be transmitting several channels of low-bandwidth measurement data from a remote test site; i.e., an aircraft, industrial machinery, etc. Since the equipment is not capable of transmitting digital data at appreciable bit rates (the highest band-

width channel can operate at a maximum of 2500 bits/sec) the restricted bandwidths were a major design consideration in the development of a small-scale link.

At present, three vehicles have been instrumented for automatic control, and it was desired to effect two-way communications between those vehicles and the sector computer. In addition, it was desired that the selected approach be expandable so that operations with more vehicles (e.g., 256 as suggested by Takasaki [35]) could be simulated.

The data transfers which were chosen are composed of the following messages:

- 1) Status Signals

Each vehicle transmits a status word every .1 seconds. This word is composed of three binary bits; 2 bits reflect the present state of the vehicle (normal, failing but not severely, and failing severely) and 1 bit indicates that a sector failure has been detected. The vehicle status is determined by the individual vehicle controller which monitors both state-error signals and various vital functions (e.g., differences between planned and actual acceleration, velocity, and position values and engine oil pressure).

2) Emergency Commands

After receiving the status words (a total of 9 bits received), an emergency command is selected for each vehicle. This command is a 2-bit braking command transmitted to the vehicles affected by a failure. When a vehicle receives this data, it decodes the command and determines if it should continue on its present longitudinal trajectory or halt at one of two emergency braking levels.

For example, a typical control test might involve three vehicles at small time headways executing a series of move-up and move-back maneuvers. If any vehicle indicates that it is off course, the sector computer would select a braking command for the failing vehicle and the vehicles behind it. "Continue normal" commands would be chosen for the vehicles in front of the failing one.

3) Normal Commands

The final configuration of this particular communication system does not allow for the normal command transmissions.¹ These are the subject of current

¹Normal commands are those which define the vehicle's planned course through the sector. These are transmitted prior to a vehicle's entry into the sector.

investigations which may lead to a set of normal commands differing from those previously suggested by Takasaki [35]. However, with the communication system described here, the inclusion of any normal commands will be a simple process -- the highest bandwidth FDM channel is reserved for normal command transmission.

4) Time Base

The transfers of status signals and emergency commands occur periodically and at a rate of once every .1 seconds. These transmissions follow the timing cycle shown in Fig. 3-1. The transmissions are time-division multiplexed (TDM). The time at which each vehicle transmits and receives data is defined by its current ID number and the elapsed time since the beginning of the last .1 second cycle. In this configuration, as opposed to an asynchronous one, it is unnecessary to label each data word with the ID number of the vehicle which transmits or receives it -- the order in which data is received determines its source (or intended destination).

In reference to Fig. 3-1 the sequence of events is as follows:

Time t_a is the beginning of the system cycle and, at this time, the vehicle controllers sample both the state-error signals and

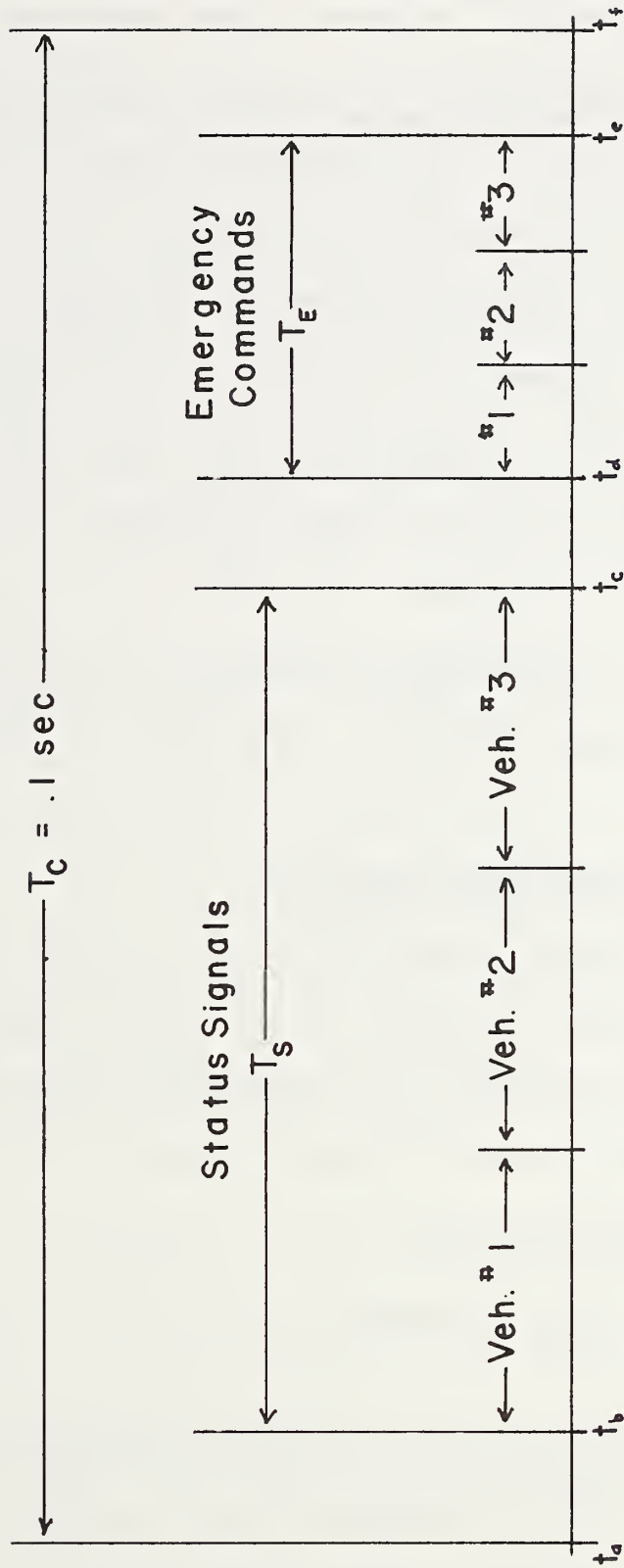


Fig. 3-1. Communications time base

various vital functions. By time t_b , the vehicle controllers must determine the status word that correctly describes these sampled values. From time t_b to t_c the sector computer receives one status word (3 bits) from each of the three vehicles. From t_c to t_d the sector computer decodes this information to determine the operating condition of the sector, and then selects the appropriate braking command for each vehicle. During the t_d to t_e time interval three emergency commands (2 bits each) are transmitted to the vehicles. If a vehicle controller determines that the vehicle must brake in response to an emergency command, the braking occurs at time t_f . This cycle is repeated every .1 seconds.

B. Synchronization and Data Rates

The durations chosen for the $t_c - t_b$ and $t_e - t_d$ time intervals (hereafter referred to as T_S and T_E respectively) define the bit rates and therefore the bandwidths required for the communications that occur in these intervals. The bit rate for the status transmissions is

$$\frac{9}{T_S} \quad (\text{bits/sec}) \quad (3-1)$$

while that for the emergency command transmissions is

$$\frac{6}{T_S} \quad (\text{bits/sec}) \quad (3-2)$$

Several other factors should be considered before values of T_S and T_E are chosen.

A requirement for any synchronous (or coherent) communications system is the availability of a stable reference frequency for the demodulation of received signals. (A similar reference frequency is also needed in a digital communications system.) This frequency² is used to clock data into or out of a shift register or similar storage elements. This is of particular importance since the concern here is with a digital link in which serialized binary data is transferred.

Several methods have been developed to provide a reference frequency. One involves filtering the desired frequency component from the raw serialized data.³ In another method, the necessary timing frequency is derived from a crystal oscillator located at the receiver. Still another method involves transmitting a reference frequency with the data. Since an adequate number of FDM channels were available in the EMR equipment, this latter method was employed.

In a general application of this procedure, the sector computer would transmit two timing frequencies f_S and f_E to each

² This signal is usually a square wave at a frequency equal to the serial data bit rate. It is used to synchronously deserialize received data or serialize transmitted data.

³ This filtering can only be done if enough signal energy is available at that frequency, i.e. there is a high density of low-to-high and high-to-low transitions.

vehicle. The frequency f_S (equal to the bit rate of the status transmissions) would be applied to the input of a shift register to synchronize the output of serialized status, or in the case of the sector computer, synchronize the input of serialized status. The frequency f_E (equal to the bit rate of the emergency command transmissions) would be used similarly in both the vehicles and sector computer to clock emergency commands into or out of a shift register.

Consider a situation where:

$$Mf_S = Nf_E \quad (3-3)$$

(M and N are any positive integers). This relationship implies that the timing frequencies f_S and f_E are harmonically related to some fundamental frequency equal to:

$$\frac{N}{M} f_E \quad \text{or} \quad \frac{M}{N} f_S \quad (3-4)$$

If condition (3-3) is satisfied, the sector computer need only transmit one timing frequency

$$f_T = Mf_S = Nf_E \quad (3-5)$$

Vehicle circuitry can derive f_S and f_E (shown pictorially in Fig. 3-2) from f_T . Since satisfying (3-5) simplifies the system, values for T_S and T_E were selected according to this criterion.

With $T_S = .06$ seconds and $T_E = .02$ seconds, the status transmission bit rate is

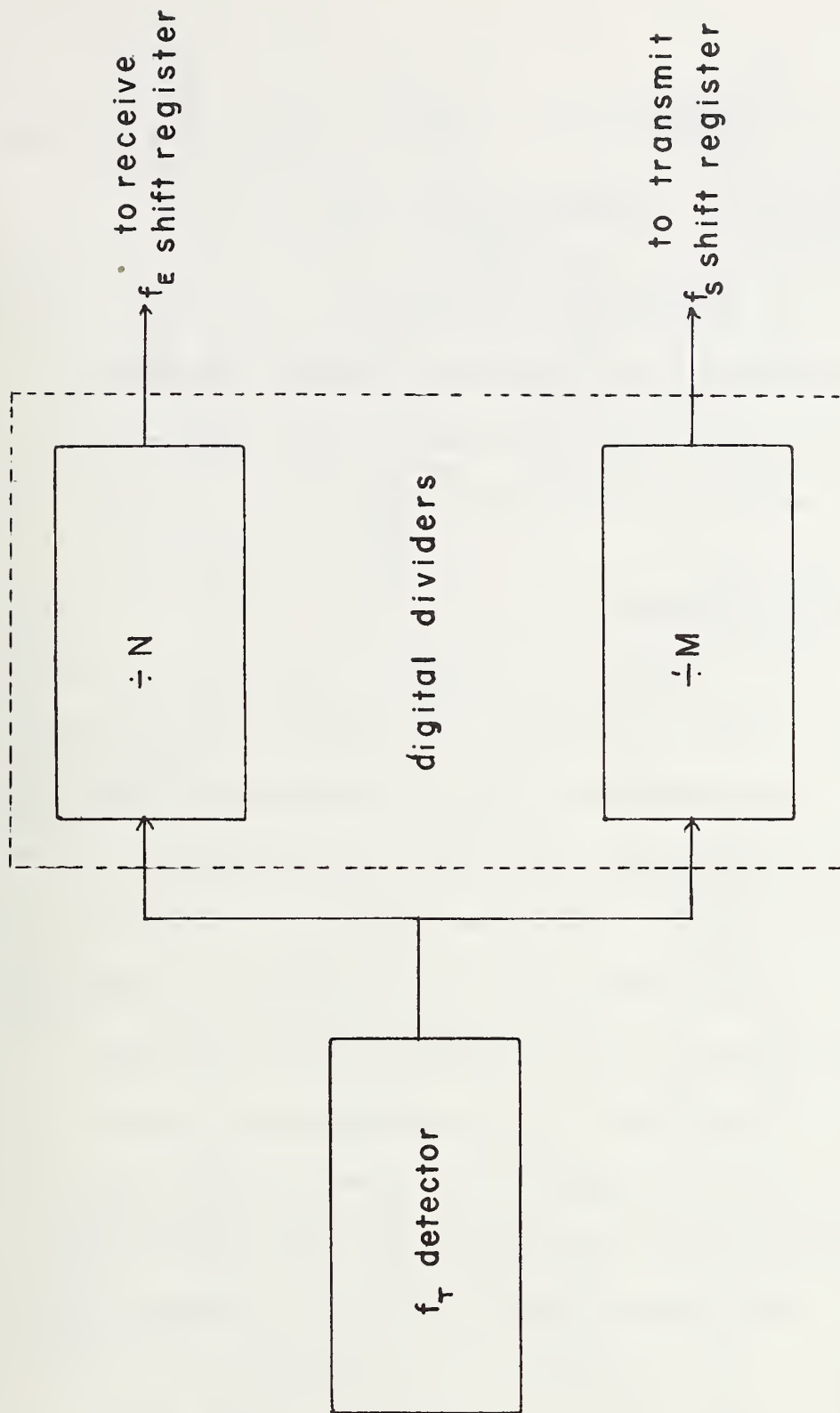


Fig. 3-2 Derivation of timing signals at the vehicle level

$$\frac{9 \text{ bits}}{.06 \text{ sec}} = 150 \text{ bits/sec.}, \quad (3-6)$$

and the emergency command bit rate is

$$\frac{6 \text{ bits}}{.02 \text{ sec}} = 300 \text{ bits/sec.} \quad (3-7)$$

With these bit rates, only one timing frequency, $f_T = 300 \text{ Hz}$ need be transmitted to the controlled vehicles. This rate is within the capabilities of the EMR equipment.

C. System Configuration

The block diagram of the system incorporating the EMR equipment is shown in Fig. 3-3. For sector-to-vehicle transmissions, three channels are used -- each dedicated to the transfer of a particular signal. One FDM channel provides a 10-Hz signal to the vehicles. This signal consists of a pulse occurring at the beginning of each T_c cycle and is necessary to coordinate vehicle maneuvering. It is also used to preset the timing circuitry at the beginning of each communications sequence. Another FDM channel is utilized for the 300-Hz timing frequency.⁴ This frequency is used to coordinate the TDM transmitting and receiving. Still another channel carries the serialized emergency commands.

⁴It is possible to derive this 300-Hz timing frequency from the transmitted 10-Hz signal thereby eliminating the 300-Hz channel. This may be done via a phase-locked loop multiplier.

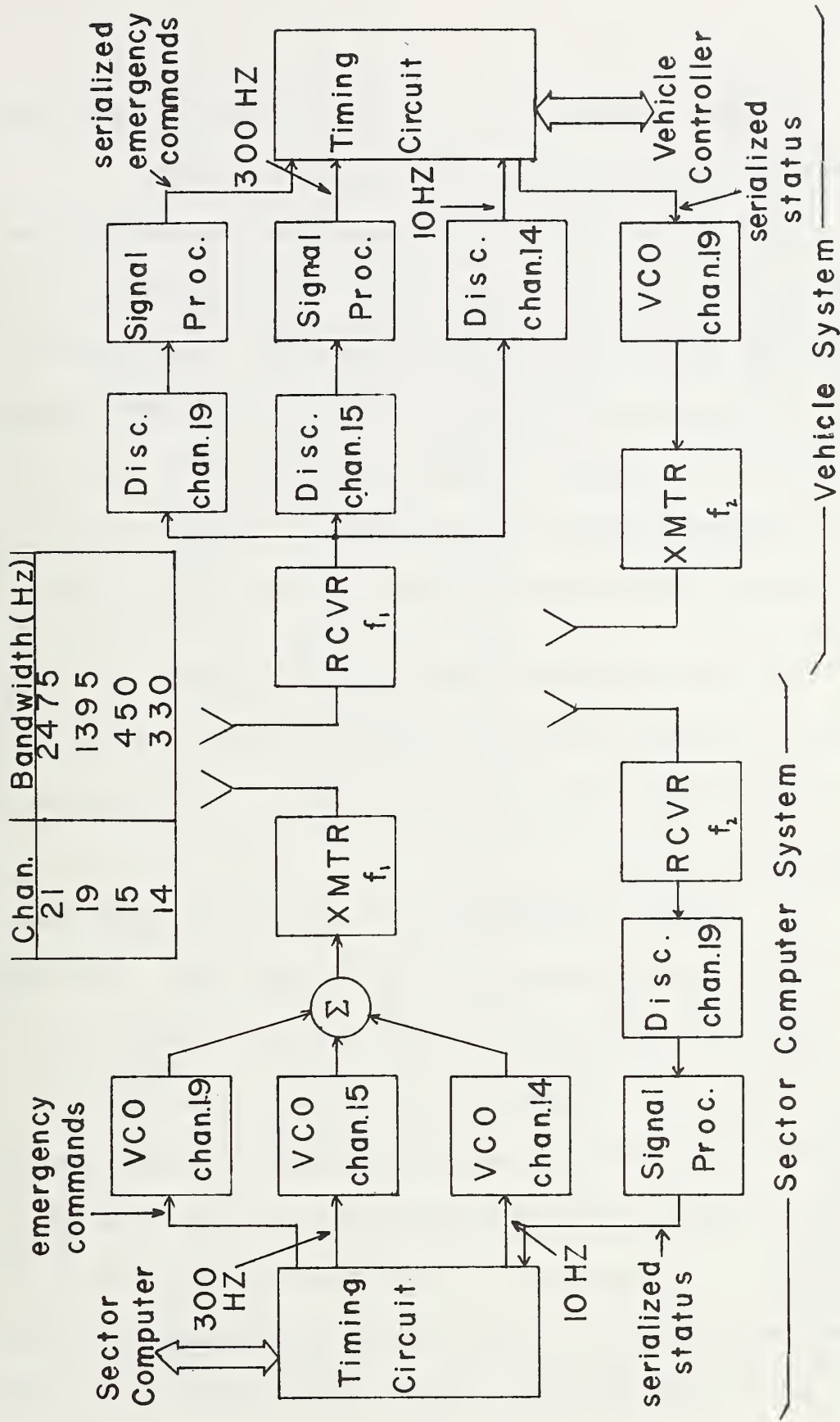


Fig. 3-3. System configuration

Only one FDM channel is needed for vehicle-to-sector status transmissions and again these transmissions are TDM.

After the vehicle receives, demodulates and separates the incoming signals, they are processed (as is discussed in the next section) and applied to the timing circuit inputs. The processed 300-Hz timing frequency is applied to the input of a shift register and clocks in the received emergency commands. A 150-Hz timing frequency (derived from the processed 300-Hz signal) is used to perform the parallel-to-serial conversion of the status word.

The sector-computer timing circuitry uses these two frequencies in a similar fashion -- 300-Hz is utilized to serialize the emergency commands and 150-Hz is used to deserialize the received status signals.

The reception of a 10-Hz pulse from the sector computer initializes the vehicle timing circuitry (see Fig. 3-4). The rising edge of this pulse resets two counters which are driven by the 300-Hz signal. The outputs of these counters are decoded and compared to the current ID number of the vehicle. More simply, the timing circuitry counts 300-Hz pulses starting at the beginning of every .1 second period. The combination of a particular counter output and an ID number uniquely describes a time slot where data is transmitted or received serially (see Fig. 3-1 for the time slot designations).

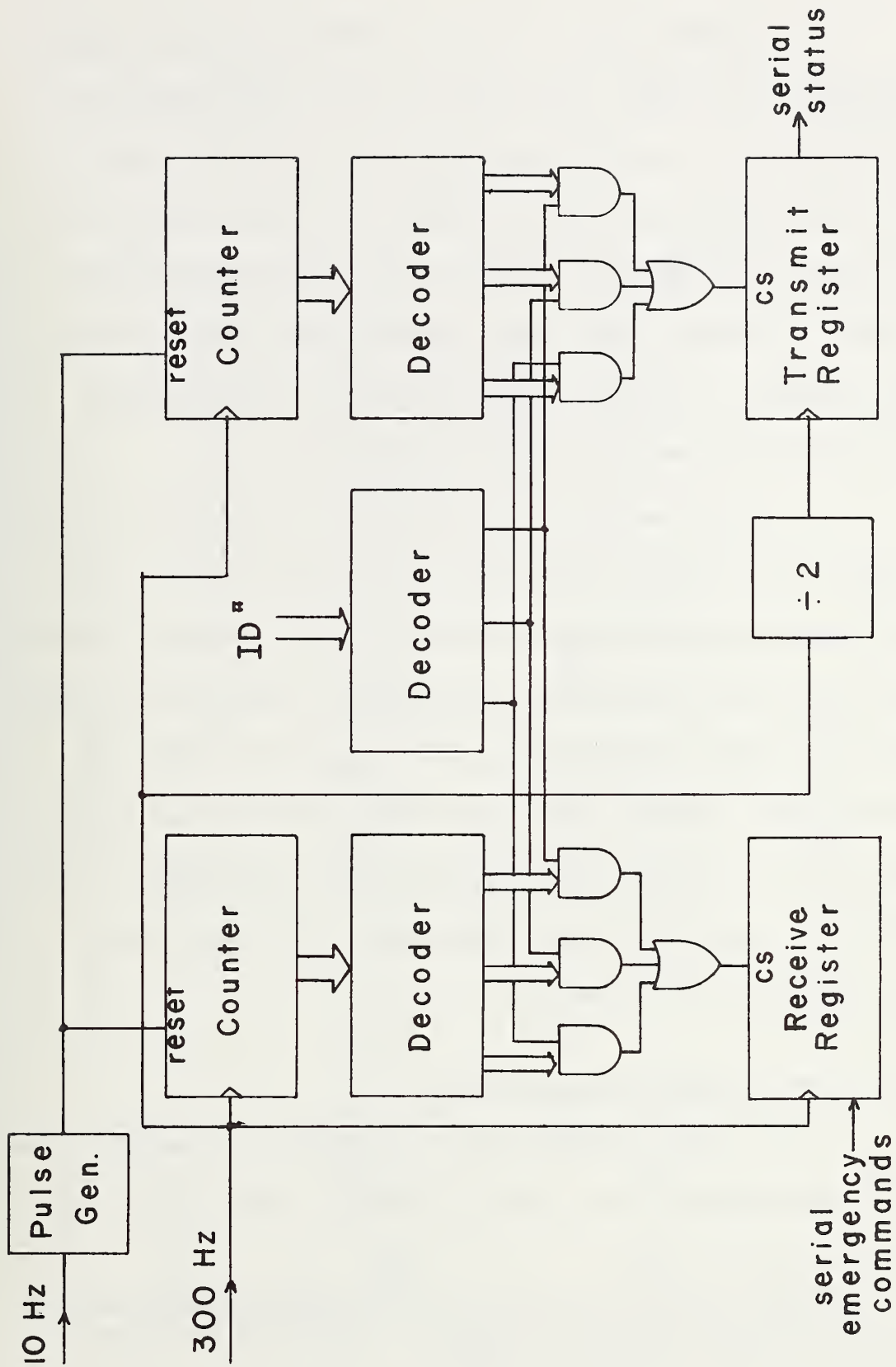


Fig. 3-4. Vehicle timing circuit

For example (see Fig. 3-5), a vehicle currently assigned ID#2 transmits a status word from the 9th to 14th 300-Hz count. During this time, the 150-Hz timing frequency is bypassed to the input of a shift register which contains the current status word (provided by the vehicle controller). The word is clocked out serially on the next three 150-Hz positive edges that occur in that time slot. A vehicle with ID#1 receives its emergency⁵ command on the 23rd and 24th 300-Hz pulses.

The sector-computer timing circuitry operates in a similar manner, but one level of decoding is eliminated (see Fig. 3-6). This circuit need only input or output data on a particular 300-Hz count making the ID decoding unnecessary. The sector computer receives 9 status bits (see Fig. 3-5) from the 3rd to the 20th 300-Hz count, and the order in which they are received specifies the vehicle ID number from which they were transmitted. From the 23rd to 28th 300-Hz count, emergency commands (6 bits) are transmitted to the vehicles.

D. System Testing and Modifications

In any communications system, the effects of additive noise on the detection process must be considered. With this in mind,

⁵In actuality, the 23rd and 24th 300-Hz positive edges used for this purpose are delayed somewhat to ensure that the serial input to the shift register is stable.

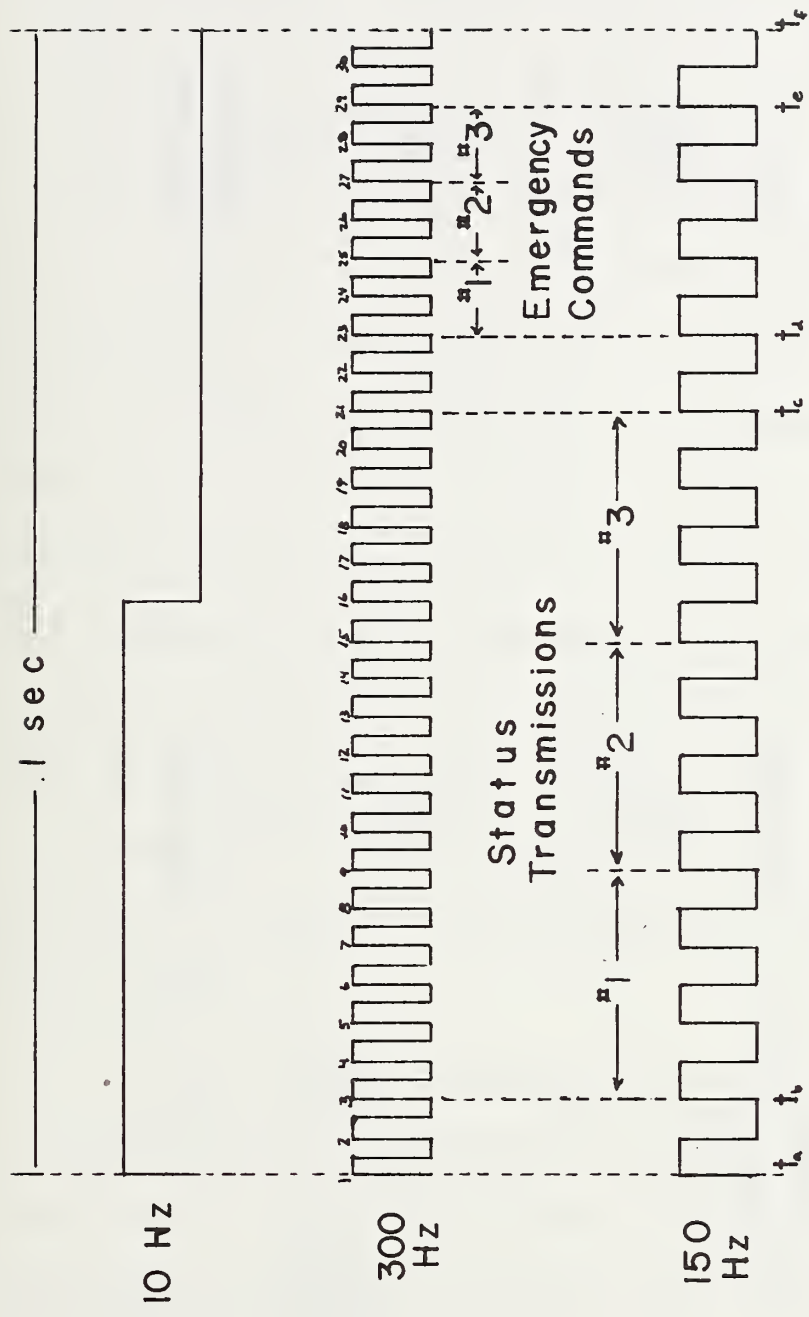


Fig. 3-5. TDM timing

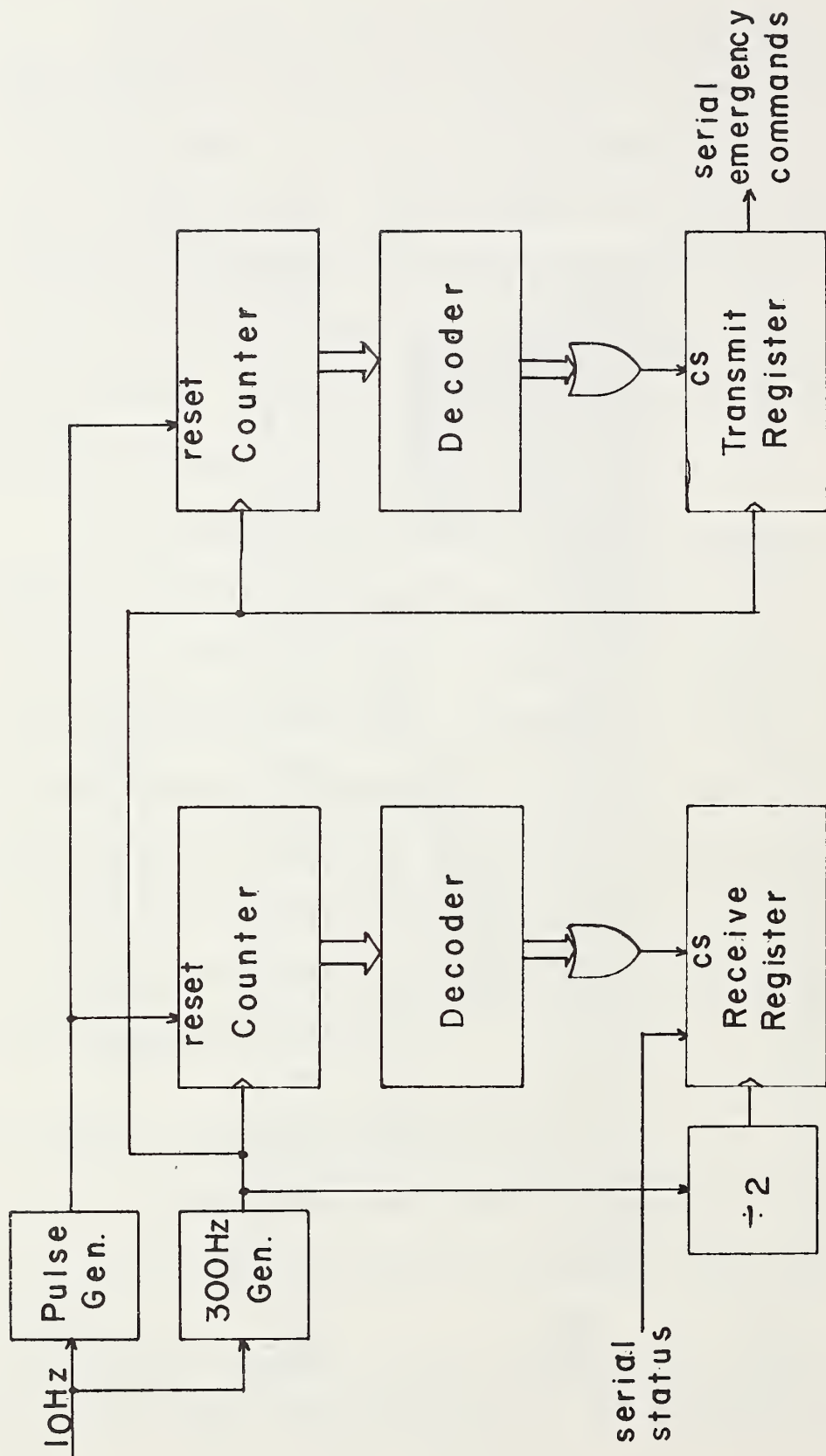


Fig. 3-6. Sector computer timing circuit

signal processors can be incorporated into the communication system to reduce or eliminate undesirable effects. With digital circuitry additive noise can cause false triggering and undefined states in the logic gates. Regardless of the noise source, given a large enough signal-to-noise ratio (S/N), noise effects can be effectively eliminated without processing.

At the operating range of the EMR equipment (220–260 MHz), line of sight must be achieved between the transmit and receive antennas or a large signal attenuation will be experienced. The result, of course, is a drastic reduction of the (S/N) ratio. Unfortunately, line of sight could not be maintained on all parts of the TRCO Skid Pad without erecting an unusually high antenna mast. A smaller mast was permanently installed, but even with its use there were still areas of the Skid Pad where the S/N ratio was too low to ensure proper operation of the timing circuitry. For this reason, it was decided that processing the incoming signals would be necessary to eliminate detection errors and loss of synchronization.

a) Timing Frequency Processing

To determine what processing was needed, the timing circuits were tested at TRCO with no signal processing and with simulated inputs. The narrow bandwidth of the 10-Hz channel⁶

⁶ The bandwidth specifications of each channel are shown in Fig. 3-3.

prevented any appreciable noise power from passing that discriminator (the input stage of the discriminators is a band-pass amplifier), and no false triggering of the 10-Hz pulse generator was observed. Unfortunately, this was not the case for the 300-Hz channel.

The higher bandwidth of this channel resulted in a lower signal-to-noise ratio (more noise power was passed through this discriminator), and the higher noise levels caused false triggering in the 300-Hz counters. This was eliminated by inserting a 4-pole, active, band-pass filter on the output of the discriminator.

The choice of filter configuration was based on several factors. It was desired to maintain a constant phase relationship between the 10-Hz and 300-Hz signals to ensure proper system operation . A narrow bandpass filter has a very steep phase change near its center frequency, and this can be a source of unwanted phase shift. Phase shifts could result from either frequency drifts of the input signal (these are assumed to be negligible), or filter component variations resulting in a change of the filter characteristics. In this application, the latter effects must be eliminated and, therefore, a filter whose characteristics were relatively insensitive to the component variations was needed. A biquad circuit satisfies this requirement, and a filter of this type was designed. A schematic diagram of the circuit is shown in Fig. 3-7 with the filter frequency characteristics shown in

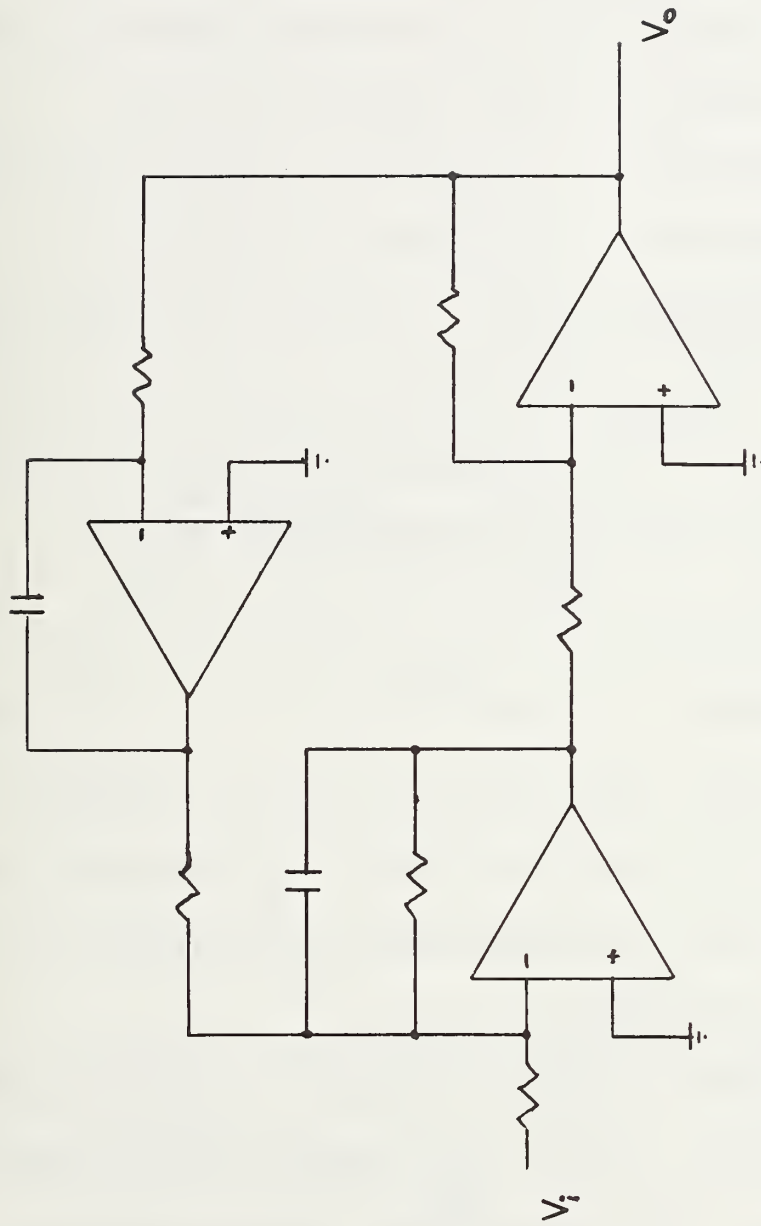


Fig. 3-7. The biquad configuration

Fig. 3-8. With the use of this filter, the 300-Hz counting errors previously observed in the vehicle timing circuitry were eliminated.

b) Data Processing

The larger bandwidths of the emergency command and status channels caused a large reduction in the S/N ratio where line of sight was not achieved. A method was required to eliminate the possible detection errors caused by the noise.

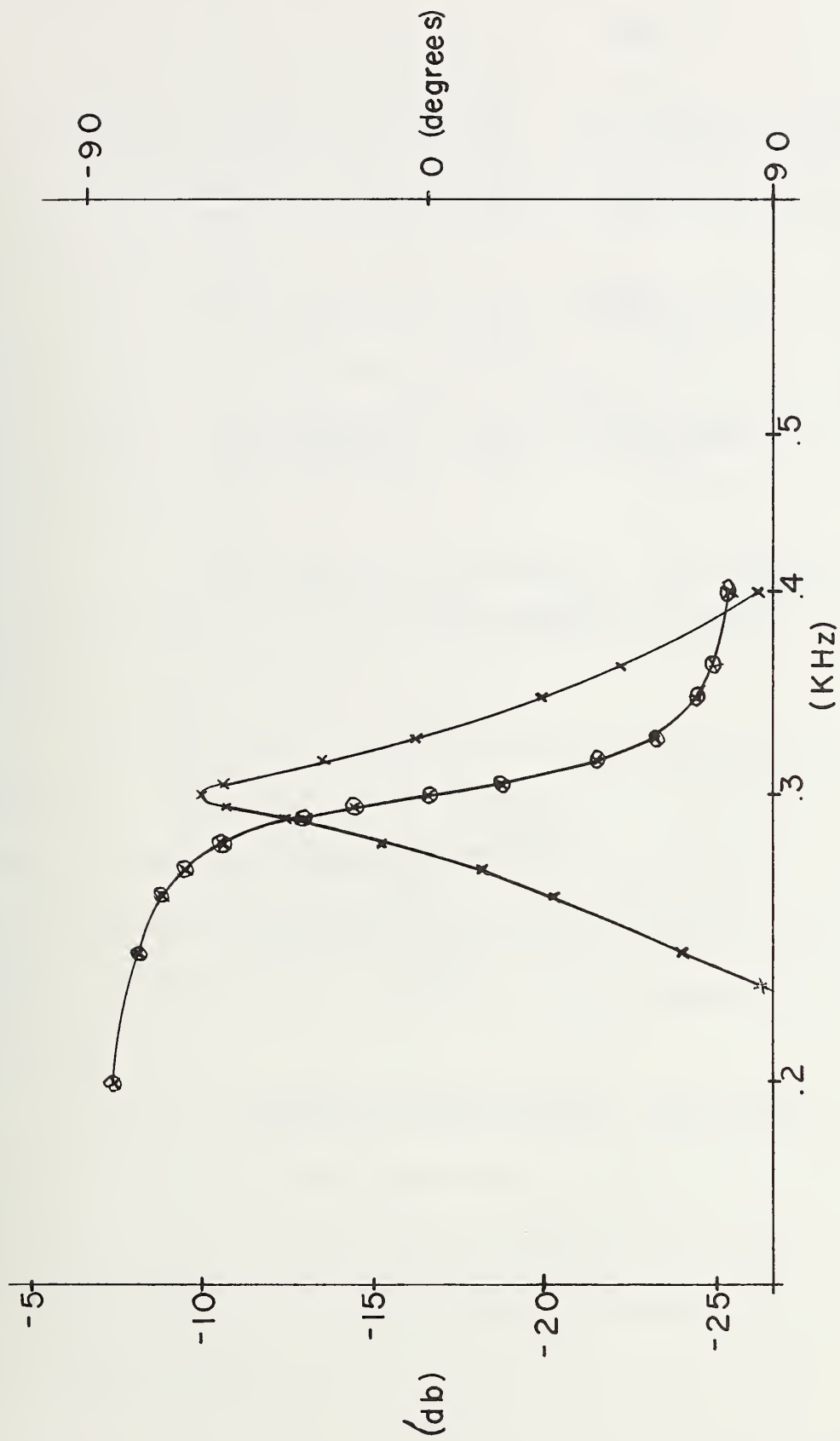
In any digital system it is desired to maximize the peak pulse power (information) in the presence of additive noise in order to aid the detection process. To do this, the signal plus noise (assumed white) is passed through a linear, time-invariant filter. The optimum filter for this purpose is a matched filter [36], and has the impulse response and transfer function:

$$h(t) = kf^*(t_m - t) \quad (3-8)$$

$$H(\omega) = kF^*(\omega)e^{-j\omega t_m} \quad (3-9)$$

where $f(t)$ is the input signal, $F(\omega)$ is its Fourier transform, t_m is the best time to observe the output, k is an arbitrary constant (assumed to be 1 for convenience), and the asterisk indicates the complex conjugate.

The realization of a matched filter for an incoming pulse train is quite simple. Consider the rectangular pulse waveform shown in Fig. 3-9a. The matched filter impulse response is given by:



x - amplitude response
 o - phase response

Fig. 3-8. Filter characteristics

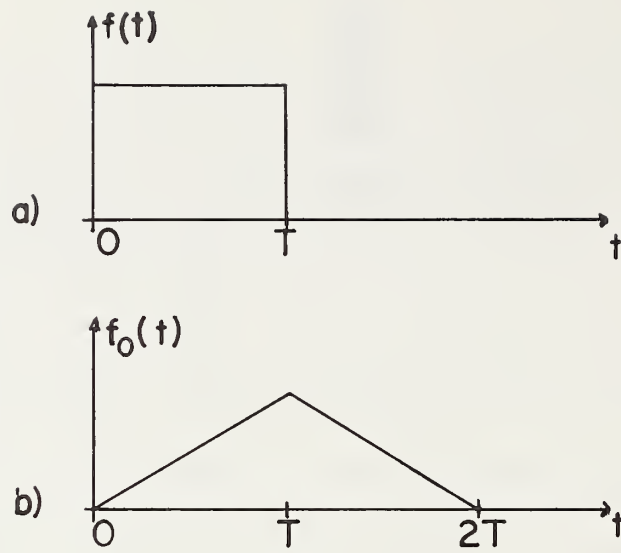


Fig. 3-9. Matched filter response for a rectangle pulse

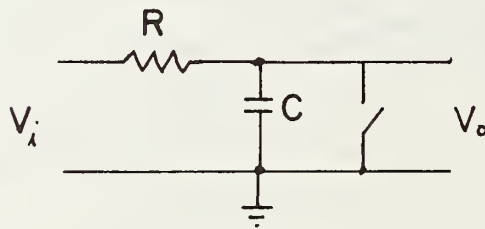


Fig. 3-10. Integrate and dump filter

$$h(t) = f(T-t) = f(t) \quad (3-10)$$

so that Fig. 3-9a also describes $h(t)$. The convolution of $h(t)$ and $f(t)$, the matched filter output, yields the triangular waveform shown in Fig. 3-9b.

The linearly increasing portions of this waveform ($t < T$) can be realized by integrating the pulse input. The result (the filter output) is sampled at $t = T$, when this output is a maximum, and then the integrator is reset (dumped). In effect, the trailing portion of the filter output, which occurs for $t > T$, is ignored. A simple circuit to accomplish this integrate-and-dump filtering is shown in Fig. 3-10.

For $RC \gg T$, the circuit acts like an integrator on the pulse waveform. The output $V_o(t)$ is sampled at $t = T$ and then the capacitor is shorted momentarily to reset the integrator ($V_o(t) = 0$). Examples of input-output waveforms are shown in Fig. 3-11. Note that synchronization is required for the sampling and reset operations.

Filters of this type were designed for both the emergency command channel and the status channel. The synchronization necessary for the sampling and reset operations was achieved by deriving the appropriate sampling and reset signals from the 300-Hz timing frequency.

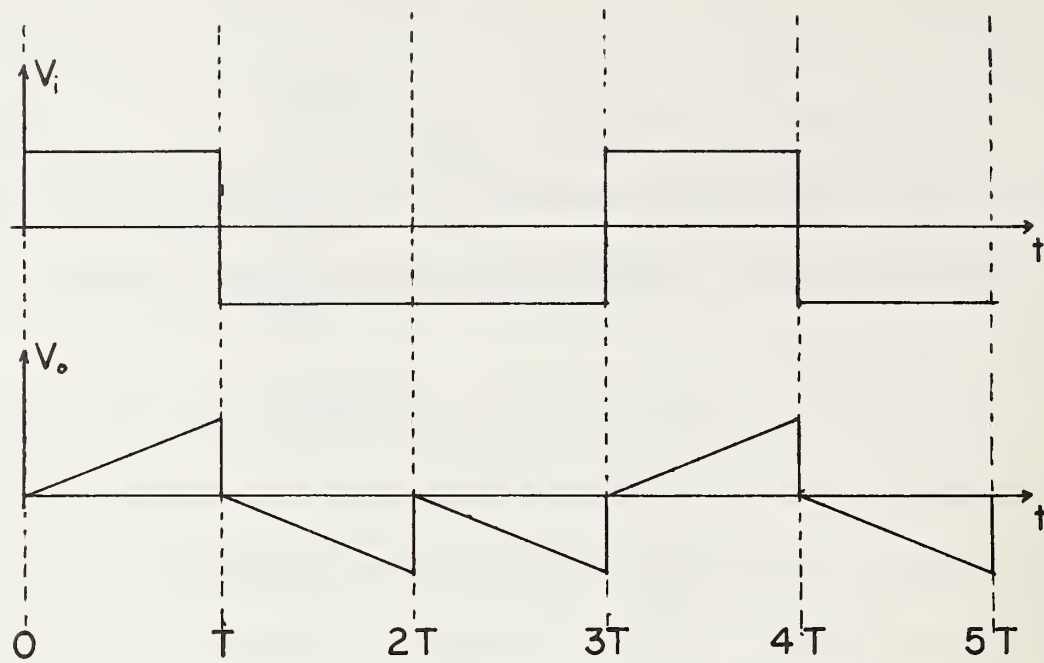


Fig. 3-11. Input-output waveforms

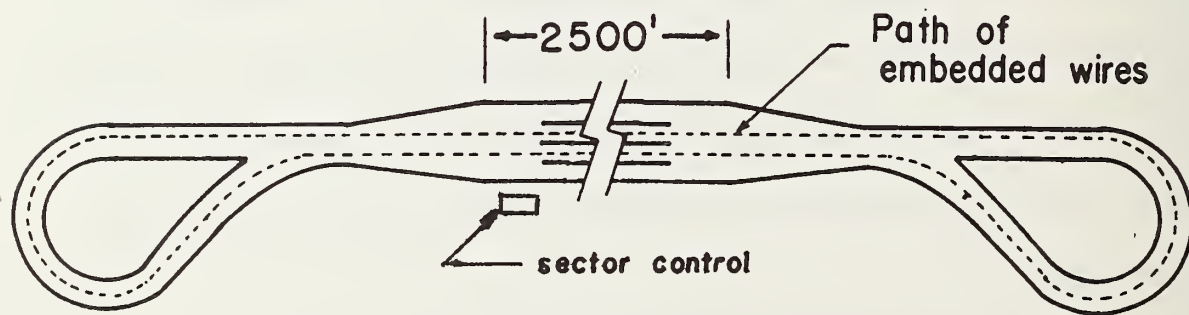


Fig. 3-12. Geometries of TRCO skid pad

E. Field Test Evaluation

The communications system was tested at TRCO by evaluating the transmissions between a base station, which was located at the sector control facility (see Fig. 3-12) and a vehicle being driven over the skid pad. Only one vehicle was employed because of equipment limitations.⁷ An evaluation of the observed performance showed that:

- a) Continuous synchronization between the vehicle and the sector computer was maintained even in those areas where the S/N ratio was low; and
- b) Reliable, error-free transmission of data was achieved from all locations on the skid pad.

It should be noted that, regardless of the S/N ratio, some probability of a detection error exists. With suitable processing, it is possible to reduce the probability of an error to a very small number. However, there is always a chance that a received signal will be detected improperly. This must be remembered when designing overall system operation procedures.

⁷A detailed account of this effort is contained in Reference 37.

CHAPTER IV
A TWO-FREQUENCY RADAR FOR USE IN
PASSIVE LATERAL CONTROL

The success of the wire-following approach to vehicle lateral control has been well documented [15], [21]. The approach, however, requires actively-excited, roadway-based elements to provide the necessary lateral position information to the controller. As recently indicated by Saxton [38], the use of "passive" (all active elements are onboard the vehicle) sensors to provide this information greatly improves the feasibility of implementing the AHS. The results of the design, construction, and testing of one such passive sensor are reported in this chapter.

There are many ways of implementing a passive sensor for lateral distance measurement. Most would rely on the generation of a signal on board the vehicle and its transmission and subsequent reflection off a sidewall reflector. The signal returned to the sensor would be processed to determine the distance between the vehicle and the reflector. The distance information would be contained -- in some manner -- in the time delay between transmission and reception due to the finite speed of the signal.

Acoustic or optical signals could be used. However, the dependence of the speed of sound on the temperature of air would greatly decrease the accuracy of the sensor unless some means were provided to compensate for the environmental conditions present in the highway application. Any opaque obstruction -- such as dirt, mud, or snow -- that might form on the output port of the device would completely terminate its operation.

Conventional electromagnetic methods appear to be the most feasible. Essentially, an ultra-short-range radar operating at frequencies that are unaffected by changes in the environment is needed. The general configuration is shown in Fig. 4-1. The parameter R_0 will be used to represent the desired lateral position of the vehicle as measured with respect to the side-wall reflector. The actual position will be denoted by d .

When implemented and deployed on a controlled vehicle, an ideal radar would measure the distance d . With a knowledge of R_0 , an error signal would be generated and supplied to the controller which would act to maintain the vehicle at R_0 . Perturbations in position about R_0 are to be expected due to random external forces acting on the vehicle.

Ideally, a radar used for lateral position measurement should be able to accurately and unambiguously determine lateral distances of

$$d = R_0 \pm (\Delta R/2) . \quad (4-1)$$

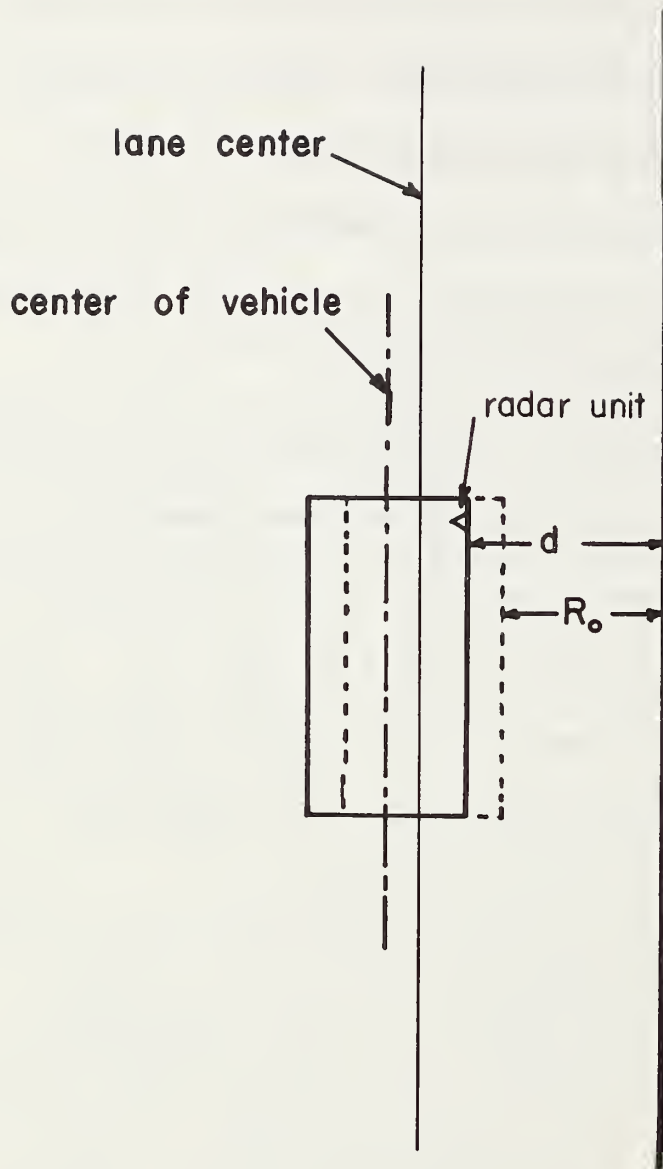


Fig. 4-1. Geometrics for a passive lateral position sensor.

The parameter ΔR will be referred to as the operating region of the radar (Fig. 4-2). Since R_0 is the desired position of the vehicle, the error signal input to the controller will be proportional to $d - R_0$. Obviously, ΔR must be large enough to include all expected lateral deviations of the vehicle -- with some margin for error.

Since ΔR will usually be small compared to the desired position, R_0 can be used to indicate the operating range of the radar. In normal applications R_0 will be less than 2 or 3 meters -- depending upon the configuration of the highway. However, in lane changing operations a range of 8 meters or more might be required.

It is instructive to compare the operating philosophy of this passive radar approach to the active wire-following method. The reference for the wire-follower is a conductor buried along lane-center. Thus, the desired position is effectively $R_0 = 0$. Any deviations from lane center result in an error signal.

For the wire-follower of Olson's [15], the maximum deviation that can be accommodated is $\Delta R/2 = 12.5$ cm. For a well designed controller [21], this has proven to be more than adequate. The accuracy of the wire-follower is essentially ± 0.64 cm. This too has proven to be quite adequate for the controllers tested.

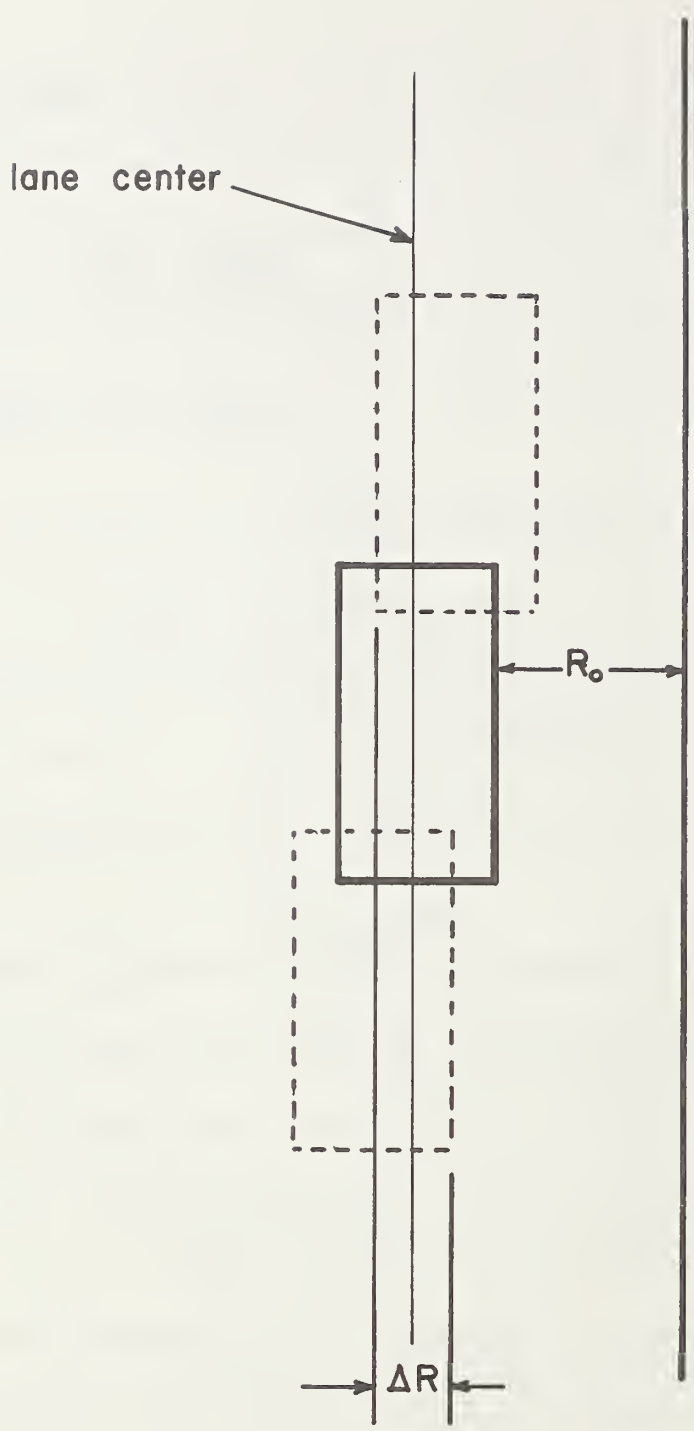


Fig. 4-2. Illustration defining the operating region, ΔR , and the operating range, R_o , of a passive lateral position sensor.

Since the operating specification of the sensor is a function of the controller used, it is convenient to insist that any passive radar device be able to determine lateral deviations to the same accuracy and over the same operating region as the wire-follower. A device having a performance degraded from this would have to be tested in conjunction with a given controller to see if its performance is still adequate. Thus, for the present, we shall specify that the passive radar system have an accuracy and operating region equal to that of Olson's wire-following system. Its range should be between 0 and 3 meters.

Many conventional radar systems were examined and the following are a few of the more promising systems that might be utilized as a passive sensor:

- 1) A continuous-wave (CW) radar
- 2) An AM-CW radar
- 3) A two-frequency radar
- 4) A two-frequency, Doppler radar
- 5) A FM-CW radar
- 6) A short-pulse, baseband radar.

CW radars are the easiest to implement. A single sinusoid of radian frequency ω is generated and transmitted. Distance is determined from the phase difference between the transmitted and received signals that occurs due to the finite propagation time of

the transmitted signal. However, the measured phase can only be determined within $\pm 180^\circ$. Since a total round trip path of a wavelength, λ , will introduce a total phase shift of 360° , the maximum unambiguous range, d_{\max} , that can be determined by the radar is

$$d_{\max} \leq \lambda/2 \quad (4-2)$$

where $\lambda = 2\pi c/\omega$ and c is the velocity of light.

Thus, a wavelength of approximately 4 meters would be needed for $R_0 = 2$ meters. Unfortunately, at this frequency, the size of the antenna (for a reasonably directive beamwidth) is quite large. At shorter wavelengths the antenna could be smaller, but the range would be ambiguous.

The AM-CW radar overcomes this ambiguity problem. It determines range by measuring the phase difference between the amplitude modulation of the transmitted and echo signals. Here, the range is a function of the modulation frequency and the antenna size is a function of the carrier frequency. Nilssen and Boyer [39] describe such a short-range radar which operates over a range of 0 to 15.24 m with a maximum error of 15.24 cm. The modulation frequency was 20 MHz.

The two-frequency radar is similar to the AM-CW radar.¹ It utilizes the phase-difference of the difference-frequency signals

¹

An AM-CW radar with suppressed-carrier is a two-frequency radar.

to obtain a distance measurement. This difference-frequency determines the maximum unambiguous range.

The two-frequency, Doppler radar offers another approach; however, the vehicle must be moving laterally to obtain a distance measurement. Its main advantage is that the phase measurement can be made at audio frequencies.

A conventional FM-CW radar cannot measure very close range with the needed resolution. A modified form of the FM-CW radar was developed by Marukawa and Namekawa [40]. Their system measures short distances with the accuracy equal to approximately one-half the carrier wavelength.

Another clever scheme for measuring short distances is described by Nicolson and Ross [41]. In their paper on short-pulse, baseband radar, they achieved resolutions less than 30.48 cm for distances of 15.24 m. Their method uses very few microwave components, and is quite cost-effective.

After a detailed examination of the characteristics of these radar systems, both the two-frequency and the AM-CW radars seemed to show the most promise for the automated highway application. Because of the initial availability of equipment, the two-frequency radar was chosen for a more detailed study and eventual full-scale implementation. Specifically, the necessary design equations were derived assuming ideal conditions. Some

analysis was devoted to anomalous situations such as the effect of leakage signals on the radar performance. A prototype was constructed using available laboratory equipment to validate some of the initial conclusions on the radar operation. On the basis of these results, a special purpose two-frequency radar was designed and constructed for a particular vehicle-guardrail configuration. The final implementation was then tested in full-scale operation on a controlled vehicle.

A. Theory of the Two-Frequency Radar

Two approaches for implementing the two-frequency radar were examined. The major difference is in the detection process -- i.e., the method of obtaining the signals to be input to the phase measuring device.

a) System I

Here three sinusoids

$$V_1(t) = A \cos \omega_1 t \quad (4-3)$$

$$V_2(t) = A \cos \omega_2 t \quad (4-4)$$

$$V_3(t) = A \cos \omega_3 t \quad (4-5)$$

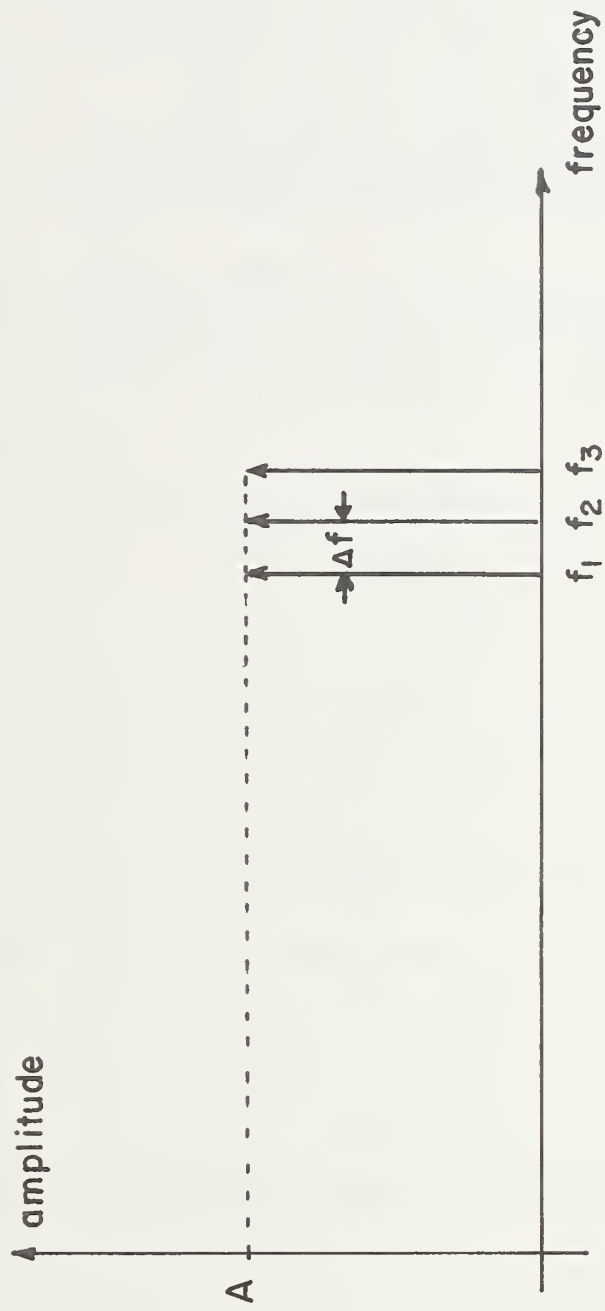
are generated. The frequencies are related by

$$f_1 = f_2 - \Delta f \quad (4-6)$$

and

$$f_3 = f_2 + \Delta f . \quad (4-7)$$

The spectrum is shown in Fig. 4-3.



$$f_1 = f_2 - \Delta f$$

$$f_3 = f_2 + \Delta f$$

Fig. 4-3. Signal spectrum of the two-frequency radar.

The transmitted signal V_t consist of the upper two frequencies; specifically

$$V_t(t) = A \cos \omega_2 t + A \cos \omega_3 t . \quad (4-8)$$

The returned signal V_r is attenuated and delayed in time; i.e.,--

$$V_r = \alpha A \cos \omega_2 (t-\tau) + \alpha A \cos \omega_3 (t-\tau) \quad (4-9)$$

where α is the attenuation factor and τ is the round trip time delay,

$$\tau = 2d/c \quad (4-10)$$

The received signal can be mixed with $V_1(t)$ to yield

$$\begin{aligned} V_{c1} = & \alpha A^2 [\cos \omega_1 t \cos \omega_2 (t-\tau)] + \\ & \alpha A^2 [\cos \omega_1 t \cos \omega_3 (t-\tau)] \end{aligned} \quad (4-11)$$

and also mixed with $V_2(t)$ to give

$$\begin{aligned} V_{c2} = & \alpha A^2 [\cos \omega_2 t \cos \omega_2 (t-\tau)] + \\ & \alpha A^2 [\cos \omega_2 t \cos \omega_3 (t-\tau)] \end{aligned} \quad (4-12)$$

Using the trigonometric relationship

$$\cos \alpha \cos \beta = \frac{1}{2} \cos (\alpha-\beta) + \frac{1}{2} \cos (\alpha+ \beta) \quad (4-13)$$

and expanding the expressions, one obtains the following signals at the output of each mixer:

$$\begin{aligned} V_{c1} = & \frac{\alpha A^2}{2} \left[\cos \left((\omega_2 - \omega_1)t - \omega_2 \tau \right) + \cos \left((\omega_2 + \omega_1)t - \omega_2 \tau \right) \right. \\ & \left. + \cos \left((\omega_3 - \omega_1)t - \omega_3 \tau \right) + \cos \left((\omega_3 + \omega_1)t - \omega_3 \tau \right) \right] \end{aligned} \quad (4-14)$$

and

$$V_{c1} = \frac{\alpha A^2}{2} \left[\cos \omega_2 \tau + \cos (2\omega_2 t - \omega_2 \tau) + \cos \left((\omega_3 - \omega_2)t - \omega_3 \tau \right) + \cos \left((\omega_3 + \omega_2)t - \omega_3 \tau \right) \right]. \quad (4-15)$$

With proper filtering to eliminate frequency components such as $\omega_3 + \omega_1$, $\omega_2 + \omega_1$, $2\omega_2$, $\omega_3 - \omega_1$, $\omega_3 + \omega_2$, and DC, the signals reduce to

$$V'_{c1} = \frac{\alpha A^2}{2} \cos (\Delta \omega t - \omega_2 \tau). \quad (4-16)$$

and

$$V'_{c2} = \frac{\alpha A^2}{2} \cos (\Delta \omega t - \omega_3 \tau). \quad (4-17)$$

The phase difference $\Delta \phi$ between the two signals is

$$\Delta \phi = (\omega_3 - \omega_2) \tau = \Delta \omega \tau. \quad (4-18)$$

Since $\Delta \omega = 2\pi \Delta f$ and $\tau = 2d/c$, then

$$\Delta \phi = \frac{4\pi \Delta f d}{c} \quad (4-19)$$

and it follows that a phase measurement will be proportional to the distance the signal travels:

$$d = \frac{c \Delta \phi}{4\pi \Delta f}. \quad (4-20)$$

A block diagram of the radar is shown in Fig. 4-4 where the frequencies of the signals at various points are shown.

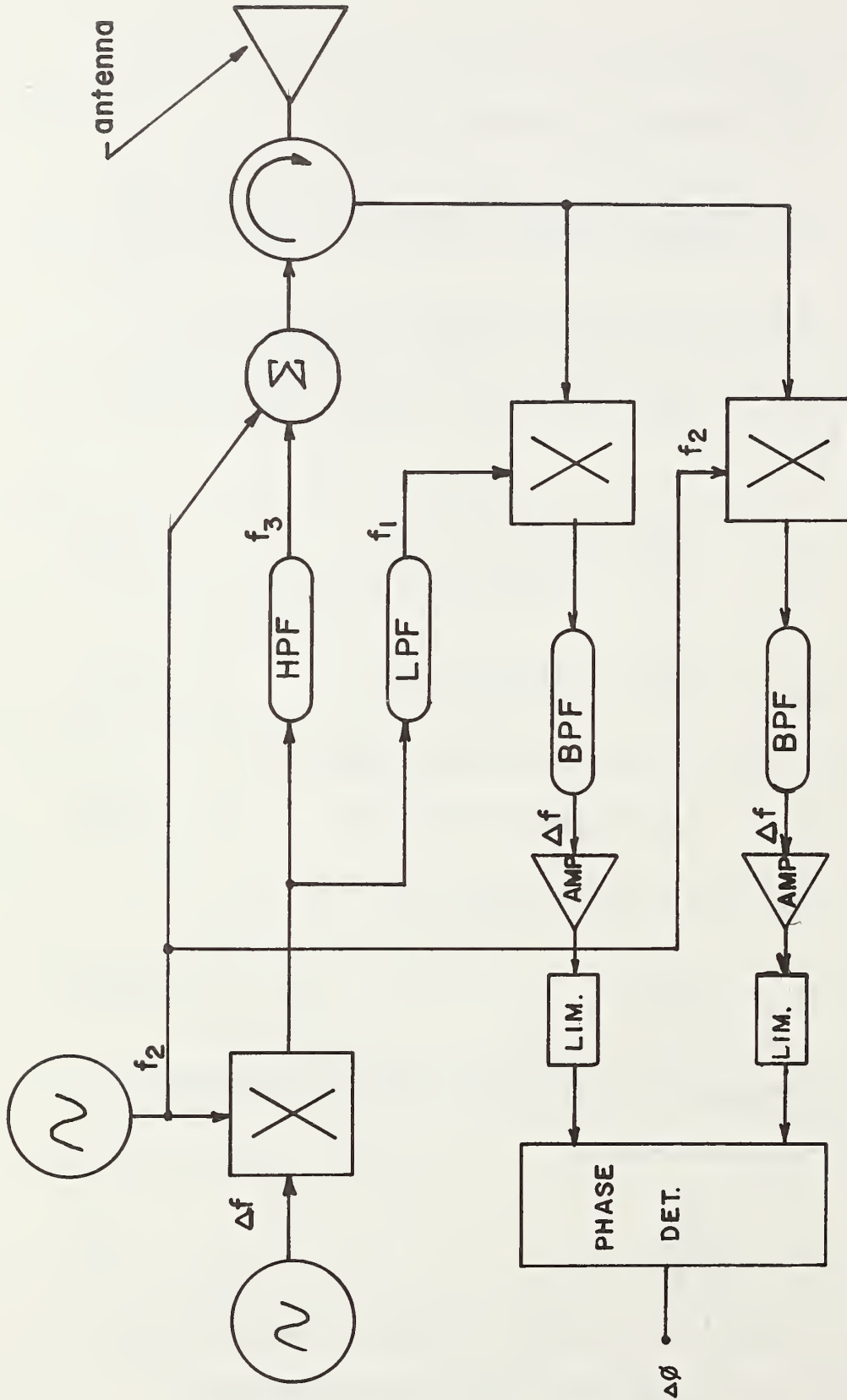


Fig. 4-4. Block diagram of system I.

b) System II

In the second approach, the transmitted signals consist of the highest and lowest frequencies rather than the upper two. As will be seen later, this affects the detection process.

The transmitted signal is

$$V_t(t) = A \cos \omega_1 t + A \cos \omega_3 t . \quad (4-21)$$

The received signal at the antenna now becomes

$$V_r(t) = V_{r_1} + V_{r_2} \quad (4-22)$$

where

$$V_{r_1} = \alpha A \cos \omega_1(t - \tau) \quad (4-23)$$

and

$$V_{r_2} = \alpha A \cos \omega_3(t - \tau). \quad (4-24)$$

It is assumed that V_{r_1} and V_{r_2} can be separated by narrow bandpass filters. Each can then be mixed together to yield

$$V_c = \frac{(\alpha A)^2}{2} \left[\cos \left((\omega_3 - \omega_1)t - (\omega_3 - \omega_1)\tau \right) + \cos \left((\omega_3 + \omega_1)t - (\omega_3 + \omega_1)\tau \right) \right] \quad (4-25)$$

With another narrow bandpass filtering process passing only the $\omega_3 - \omega_1$ frequency, the signal

$$V_c = \frac{(\alpha A)^2}{2} \cos (2 \Delta \omega t - 2 \Delta \omega \tau) \quad (4-26)$$

can be obtained where $2\Delta\omega = \omega_3 - \omega_1$ and $\Delta\omega = \omega_3 - \omega_2$.

A reference signal can be generated by frequency doubling the modulation signal, Δf . This gives

$$V_{\text{ref}} = A_{\text{ref}} \cos(2\Delta\omega t) \quad (4.27)$$

Obviously, the distance information is contained in the phase shift of V_c with respect to the reference signal. This phase difference is

$$\Delta\phi = 2\Delta\omega\tau. \quad (4-28)$$

Again, since $\Delta\omega = 2\pi\Delta f$ and $\tau = 2d/c$, then

$$\Delta\phi = 8\pi \frac{\Delta f d}{c} \quad (4-29)$$

and it follows that

$$d = \frac{\Delta\phi c}{8\pi\Delta f}. \quad (4-30)$$

A block diagram of this radar system is shown in Fig. 4-5, and the frequencies involved are shown at various points in the diagram.

There is not a great difference between the two methods of implementation. System II has the advantage that one of the signals to the phase detector will be of constant amplitude which could aid in the detection process. However, it has the disadvantage of requiring a microwave amplifier to bring the returned signals up to the proper level for mixing, and microwave amplifiers are expensive.

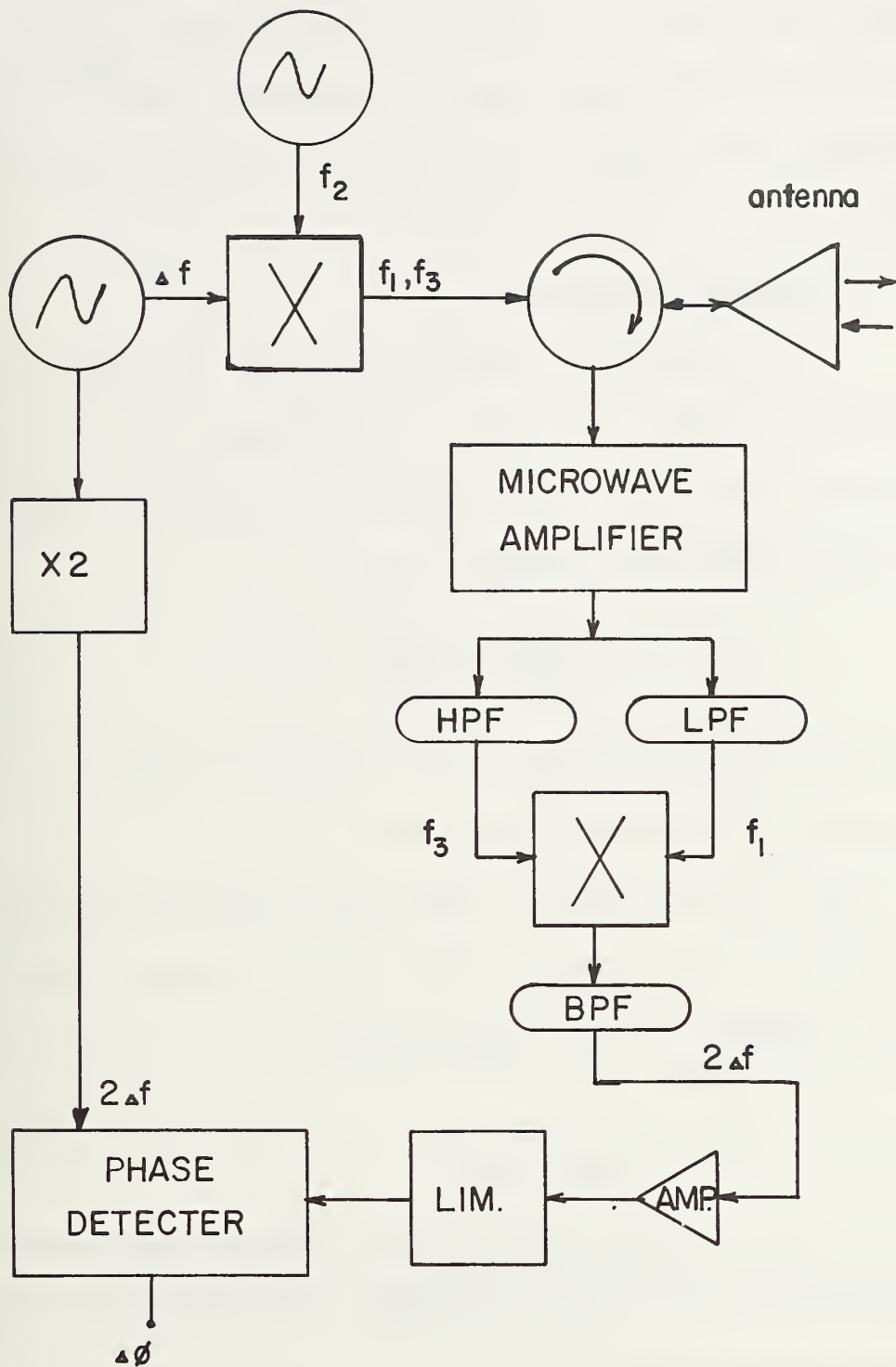


Fig. 4-5. Block diagram of System II.

Because most of the components for System I could be obtained either from the available FHWA equipment or from the OSU ElectroScience Lab, this was the system chosen for implementation. Consequently, only System I will be discussed hereafter.

c) System Parameters

The modulation frequency determines the maximum unambiguous range. Since the phase difference can only be measured within $\pm 180^\circ$ or 2π radians, the maximum distance that can be determined unambiguously is

$$d_{\max} = \frac{c\Delta\varphi}{4\pi\Delta f} = \frac{c(2\pi)}{4\pi\Delta f} = \frac{\Delta\lambda}{2} \quad (4-31)$$

where $\Delta\lambda$ is the wavelength of the modulation frequency. This relationship is illustrated in Fig. 4-6.

The modulation frequency also determines the theoretical r.m.s. range error δd with which the two-frequency radar can measure distance. It can be expressed as

$$\delta d = \frac{c}{4\pi\Delta f(2S/N)^{1/2}} \quad (4-32)$$

where S is the energy contained in the received signal and N is the noise power per cycle of bandwidth. The derivation of (4.32) is given by Skolnik [42].

The result, (4-32), indicates that the greater the modulation frequency, the less will be the r.m.s. error. However, the

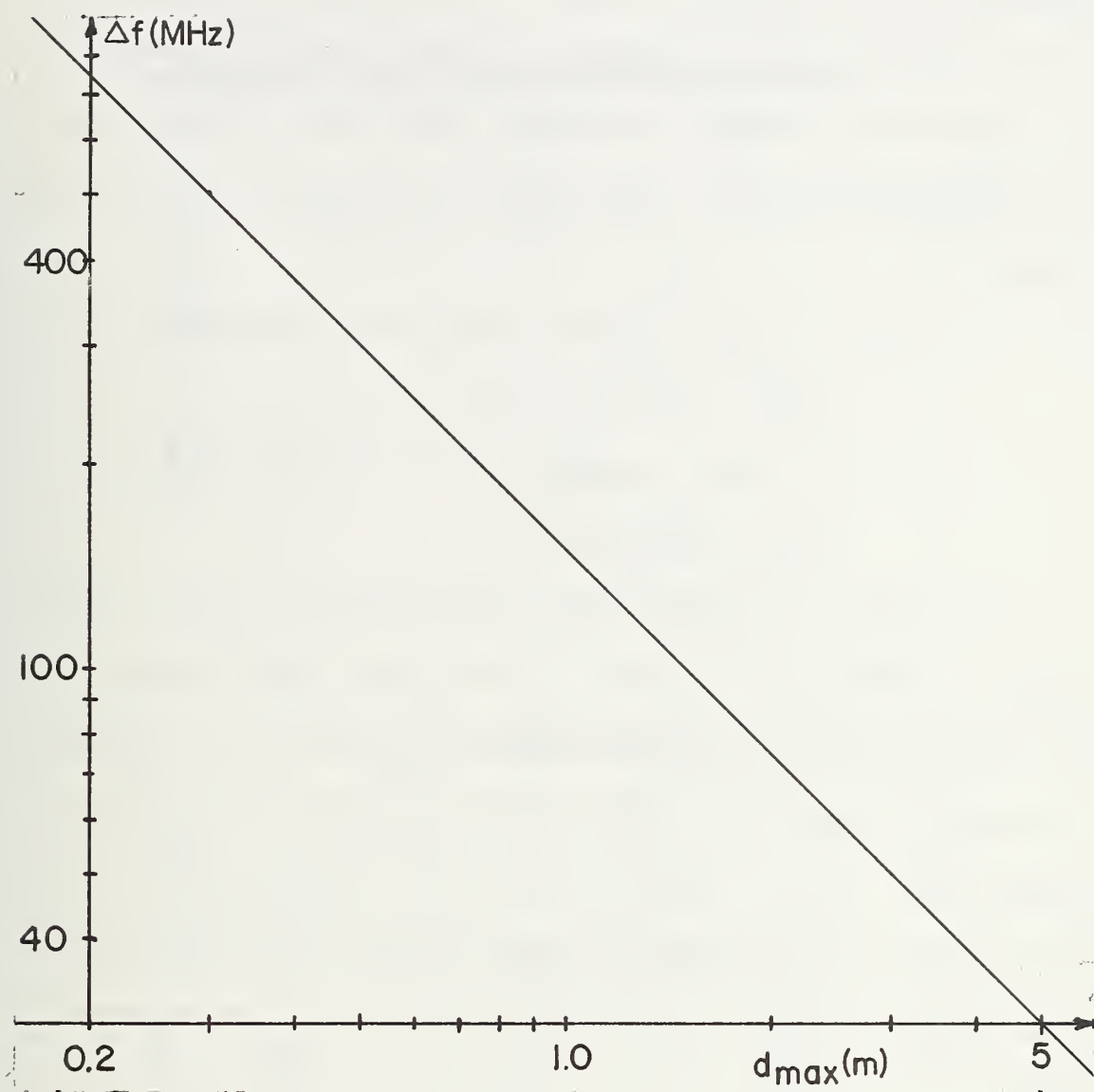


Fig. 4-6. Modulation frequency vs. maximum unambiguous range.

frequency cannot be made too large if unambiguous measurements are to be made. Thus, the selection of the modulation frequency, Δf , represents a tradeoff between the requirements of accuracy and unambiguous distance measurement. Two cases can be considered:

- a) the vehicle operates within the unambiguous range -- low Δf , and
- b) the vehicle operates outside the unambiguous range -- high Δf .

If the radar is operated within its unambiguous range -- the situation is depicted in Fig. 4-7 -- the phase measurements will produce the absolute distance between the radar and reflector. For example, suppose $R_0 = 2\text{m}$ is desired. If we select $\Delta f = 60\text{ MHz}$, then $d_{\text{max}} = 2.5\text{ m}$ from (4-31). Using $R_0 = 2\text{m}$ in (4-1), we find that the operating region ΔR is 1 m. For an rms range error of 0.5 cm, a S/N ratio of 35 db would be required, (4-32).

In contrast, consider operation outside the unambiguous range. The phase measurement will only produce the position of the vehicle relative to some fixed distance R_{0i} , $i = 1, 2, \dots$. Each value of R_{0i} is an integer multiple of $\Delta\lambda/2$ -- see Fig. 4-8. For example, if $\Delta f = 300\text{ MHz}$, then $\Delta R = 0.5\text{ m}$ and $R_{01} = 0.25\text{ m}$, $R_{02} = 0.75\text{m}$, $R_{03} = 1.25\text{ m}$, etc.

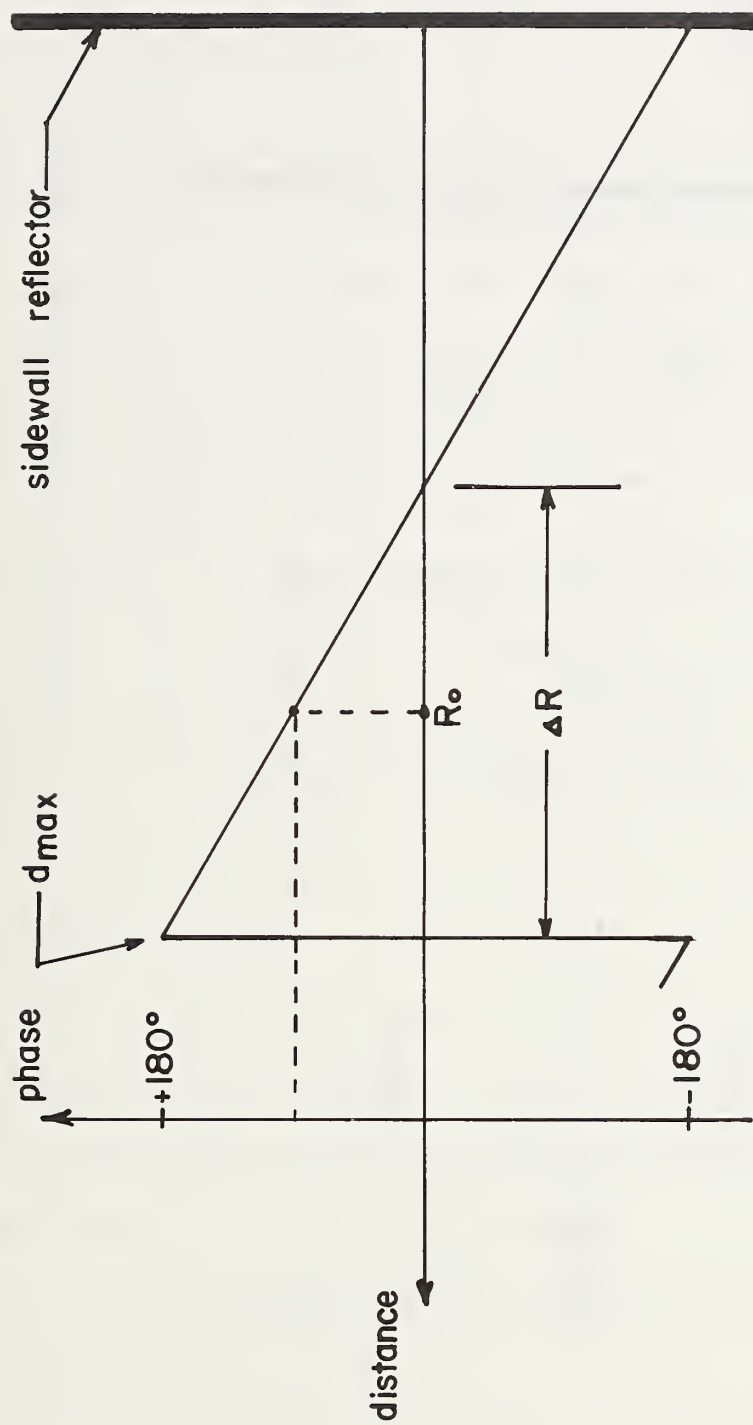


Fig. 4-7. Spatial phase distribution for low-frequency modulation.

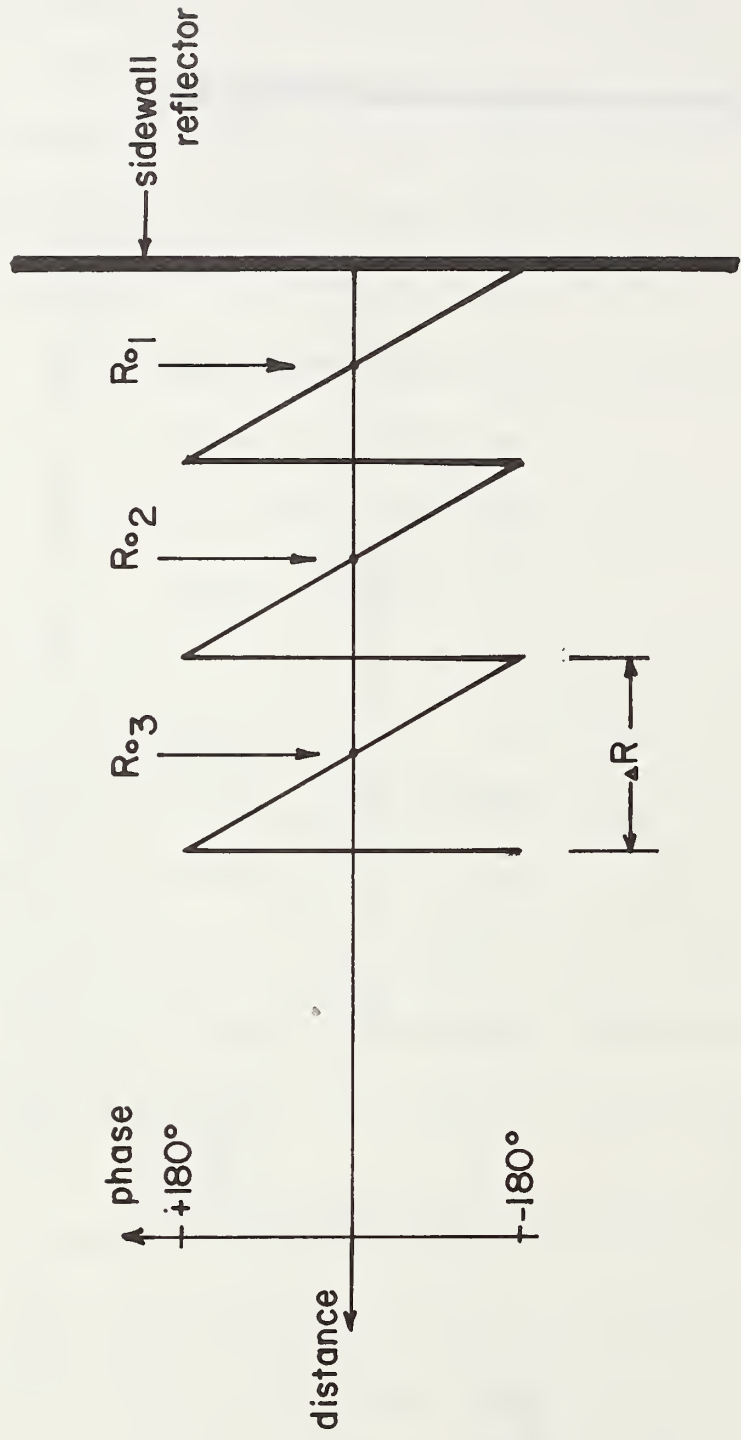


Fig. 4-8. Spatial phase distribution for high-frequency modulation.

The advantage of operating outside the unambiguous range is that the required S/N ratio for a given δd is less because Δf is larger. For $\delta d = 0.5$ cm a S/N ratio of only 21 db would be required in contrast to the 35 db ratio needed when operating inside the unambiguous range. The disadvantage is that absolute lateral distance cannot be measured. The vehicle must be placed, on entrance to the guideway, at some fixed value of R_{0i} . The important system parameters are listed in Table 4-1 for the choice of $\Delta f = 60$ MHz and 300 MHz.

The sizes of the antenna and reflector required are determined by the carrier frequency. X-band frequencies appear to be a logical first choice for two reasons. Antennas having reasonable directivity are of moderate size suitable for mounting on a vehicle. Also, the band is well used and the necessary components are all available "off-the-shelf".

While the previous discussion of the radar's operation involved a single antenna with circulator, it was discovered that for adequate suppression of leakage signals a circulator with more than 50 db of isolation would be needed. Such circulators are not readily available. In the remaining part of the study, the dual-antenna approach was used.

TABLE 4-1

Radar System Parameters for Two Modulation Frequencies, Δf .

Δf	Maximum unambiguous range, d_{\max}	ΔR	R_0	S/N for $\delta d_{r.m.s.} = 0.5\text{cm}$
60 MHz	2.5m	1.0m	2.0m	35 dB
300 MHz	0.5m	0.5m	$R_{01} = 0.25\text{m}$ $R_{02} = 0.75\text{m}$ $R_{03} = 1.25\text{m}$	21 dB

B. The Laboratory Investigation of the Two-Frequency Radar

The two-frequency radar was implemented with two different modulation frequencies ($\Delta f = 60$ MHz and 300 MHz) and was tested under static conditions in a laboratory environment. The full-scale field tests conducted at TRCO will be reported in Section C of this chapter.

The first model, a 8.4 GHz prototype, was constructed from the available waveguide components on loan from the OSU Electro-Science Laboratory and the Federal Highway Administration. The model was quite large, required various laboratory-sized power supplies, utilized a Klystron source and operated with a modulation frequency of 60 MHz.

The second model, a 10.5 GHz radar, was designed for a modulation frequency of 300 MHz and constructed in microstrip form. It required a 15V power source and used a Gunn oscillator to obtain the microwave signal. The unit was very compact and could be mounted on a vehicle to demonstrate its operation in a full-scale situation.

The two radars were tested in an indoor laboratory environment under similar conditions to illustrate the differences associated with different modulation frequencies. In both cases, it was found that leakage was the major problem for this particular radar configuration. Unwanted signals from the transmitter

section combined with the desired signals in the receiver. The leakage was noted in both prototypes and was the dominate factor contributing to the error in the measurement of lateral distance. A theoretical model was found to explain how the unwanted signals affected the sensor performance. The theoretical analysis and experimental tests showed that the amount of desired signal compared to the leakage signals (which can be called a signal-to-"noise" ratio -- S/N) is directly related to the measurement error as indicated by (4-32).

a) Effects of Using High and Low Modulation Frequencies

To determine whether a low or high modulation frequency should be used, an experimental investigation of the two-frequency radar at $\Delta f = 60$ MHz and 300 MHz was conducted using the two prototypes. Fig. 4-9 is a diagram of the indoor test configuration. Instead of moving the radar (such motion would occur if the sensor were mounted on a vehicle), the reflector was moved. This arrangement was necessary due to the large size of the 8.4 GHz prototype. The position of the reflector plate was controlled by a servo-motor. The measured phase, $\Delta\phi$, which corresponds to the lateral distance (4-19) is plotted against the actual lateral distance, d , obtained via the "follow-up" potentiometer.

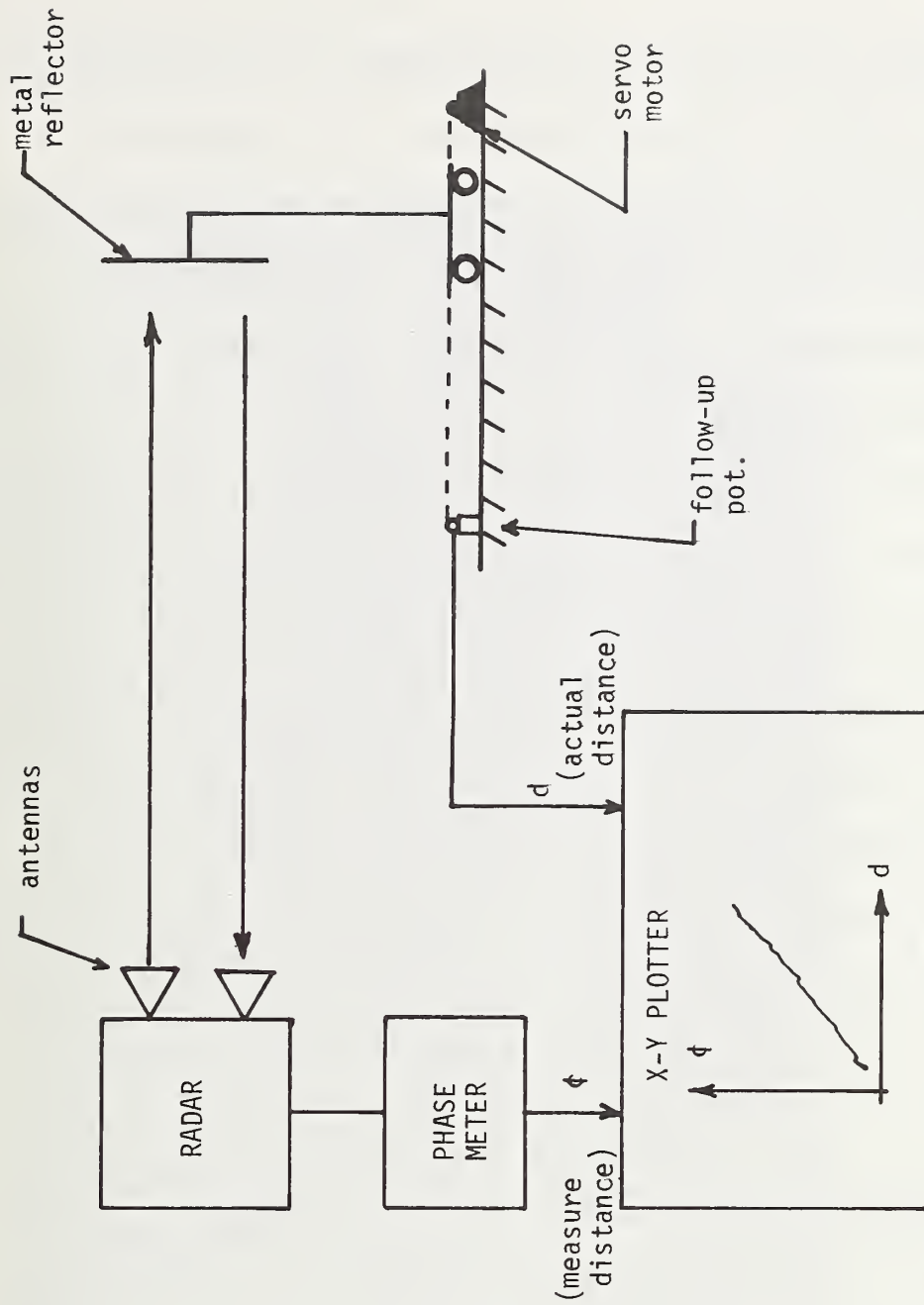


Fig. 4-9. Schematic diagram of the indoor test configuration.

Figs. 4-10 and 4-11 are photographs of the laboratory configuration using the 8.4 GHz prototype. For comparison of physical size, Fig. 4-12 is a photograph of the 10.5 GHz radar. The detailed block diagrams of the two radars are shown in Figs. 4-13 and 4-14. A HP-8405A vector voltmeter was used as the phase detector.

Experiments were performed to evaluate the performance characteristics of each radar. Figs. 4-15 and 4-16 show typical results using each prototype under similar conditions.

With $\Delta f = 60$ MHz (Fig. 4-15), each centimeter of distance should correspond to 1.44° while with $\Delta f = 300$ MHz (Fig. 4.16) this changes to one centimeter per 7.2° . Comparing the two results, one notes that the maximum uncertainty in the measured phase for each was:

$\pm 4^\circ$ for the 8.4 GHz radar, and

$\pm 2.4^\circ$ for the 10.5 GHz radar.

The increased phase-measurement accuracy for the 10.5 GHz is attributed to the use of components ordered to desired specifications as opposed to the 8.4 GHz prototype wherein components with marginal specifications were used simply because of their availability.

However, even if the phase-measurement accuracy were the same, the distance measurement uncertainty would be better by a



Fig. 4-10. Front view of the indoor test facility and a portion of the 8.4 GHz radar.



Fig. 4-11. Rear view of the indoor test facility and the 8.4 GHz radar.

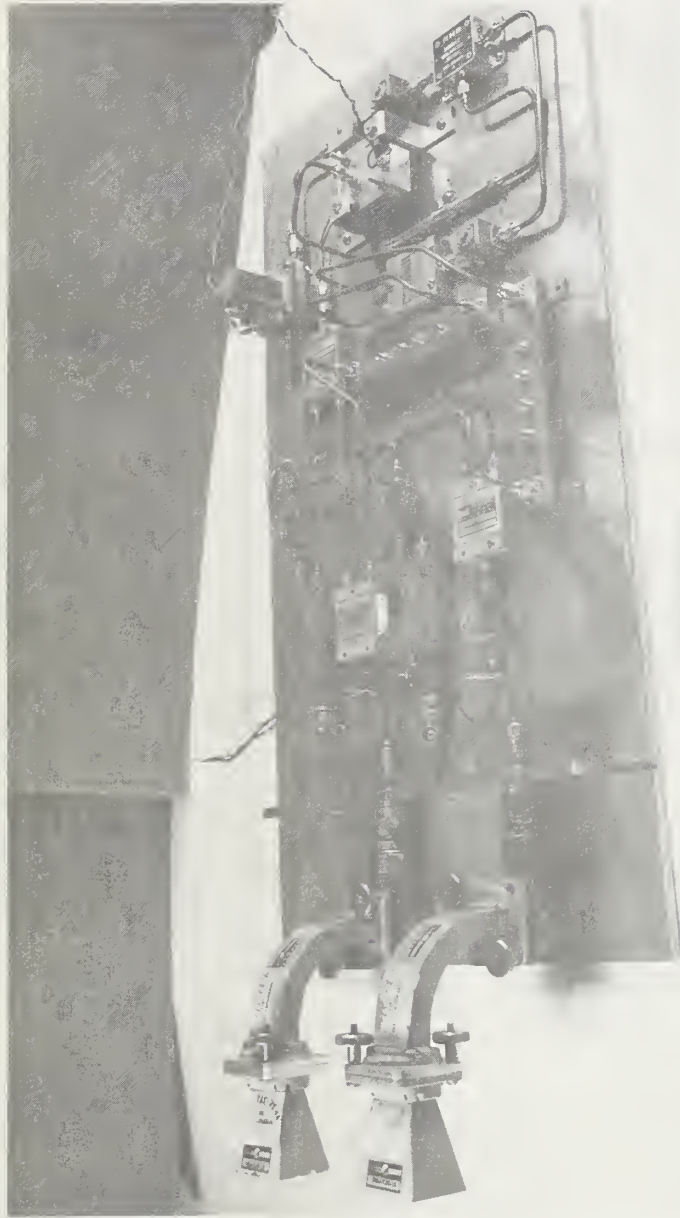


Fig. 4-12. The 10.5 GHz Radar.

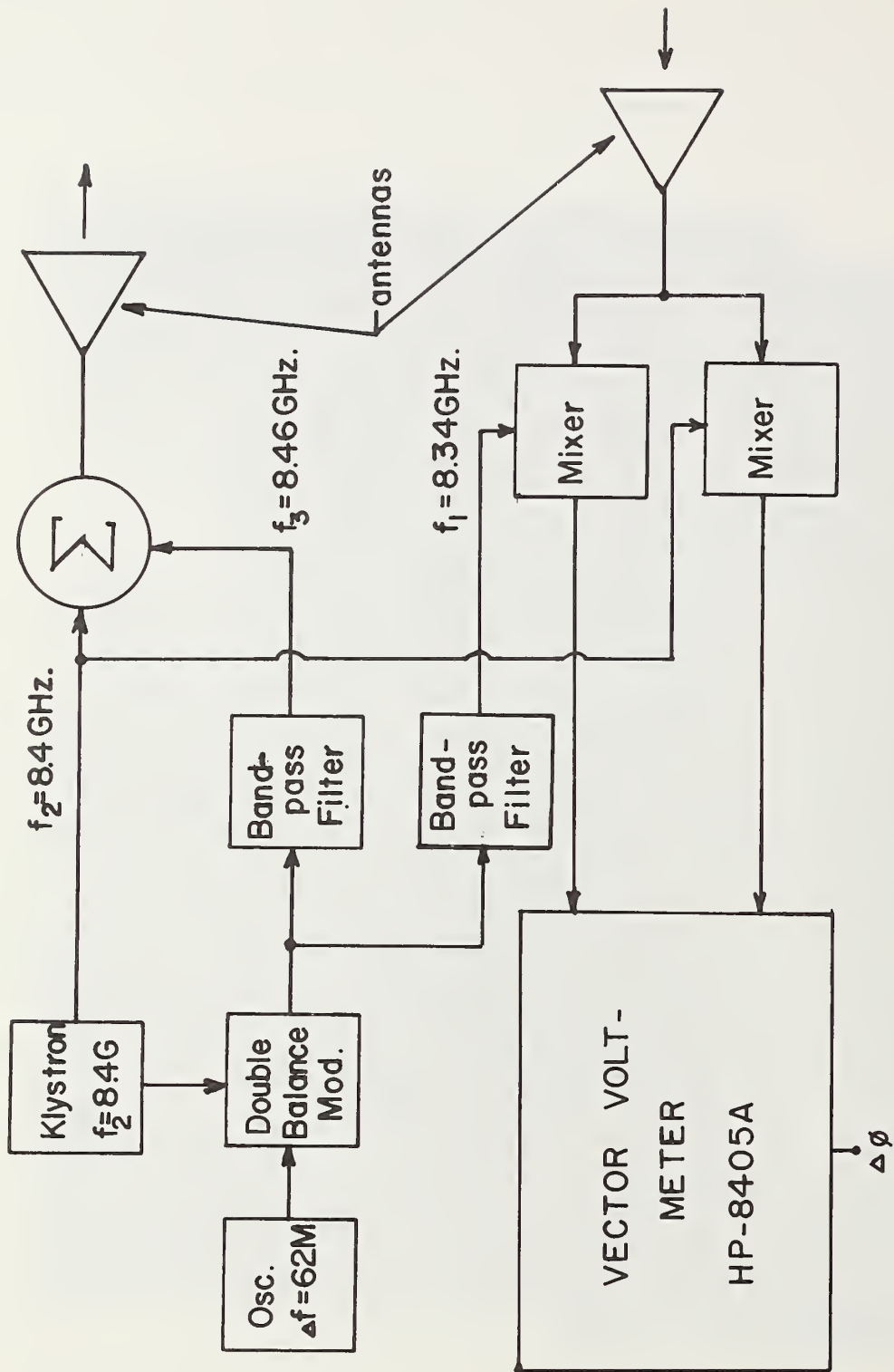


Fig. 4-13. Block diagram of the 8.4 GHz radar.

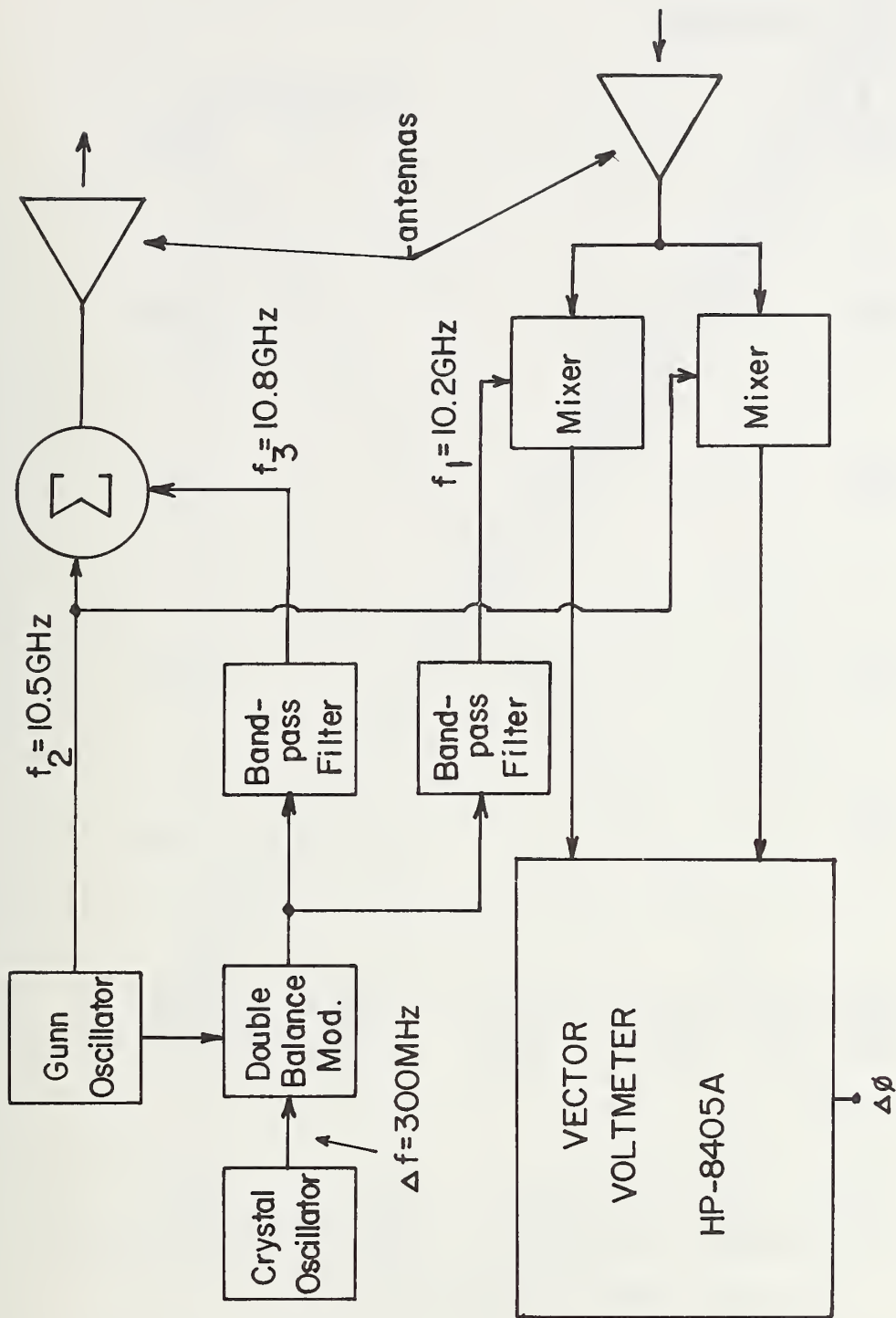


Fig. 4-14. Block diagram of the 10.5 GHz radar.

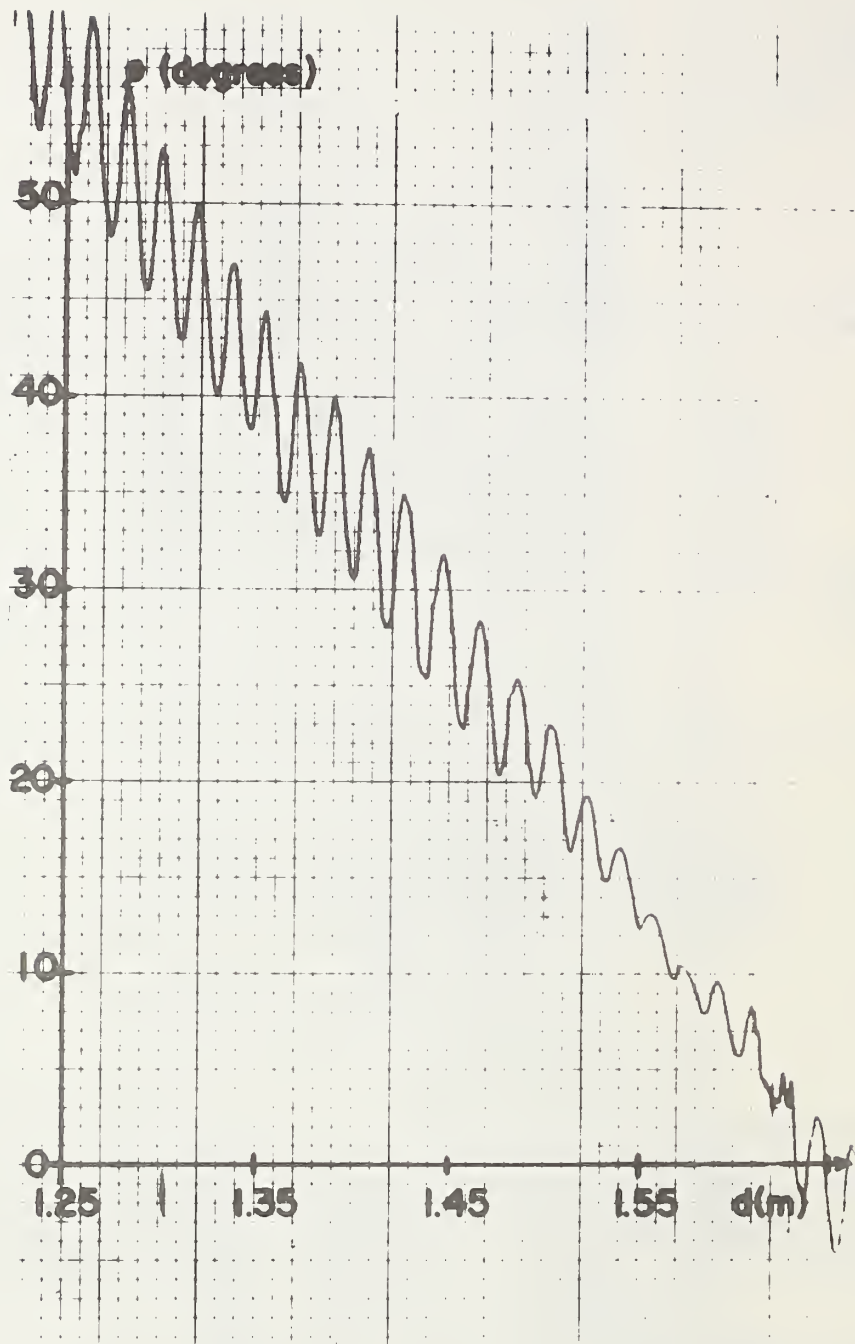


Fig. 4-15. Measured phase shift vs. lateral distance using the 8.4 GHz radar ($\Delta f = 60$ MHz).

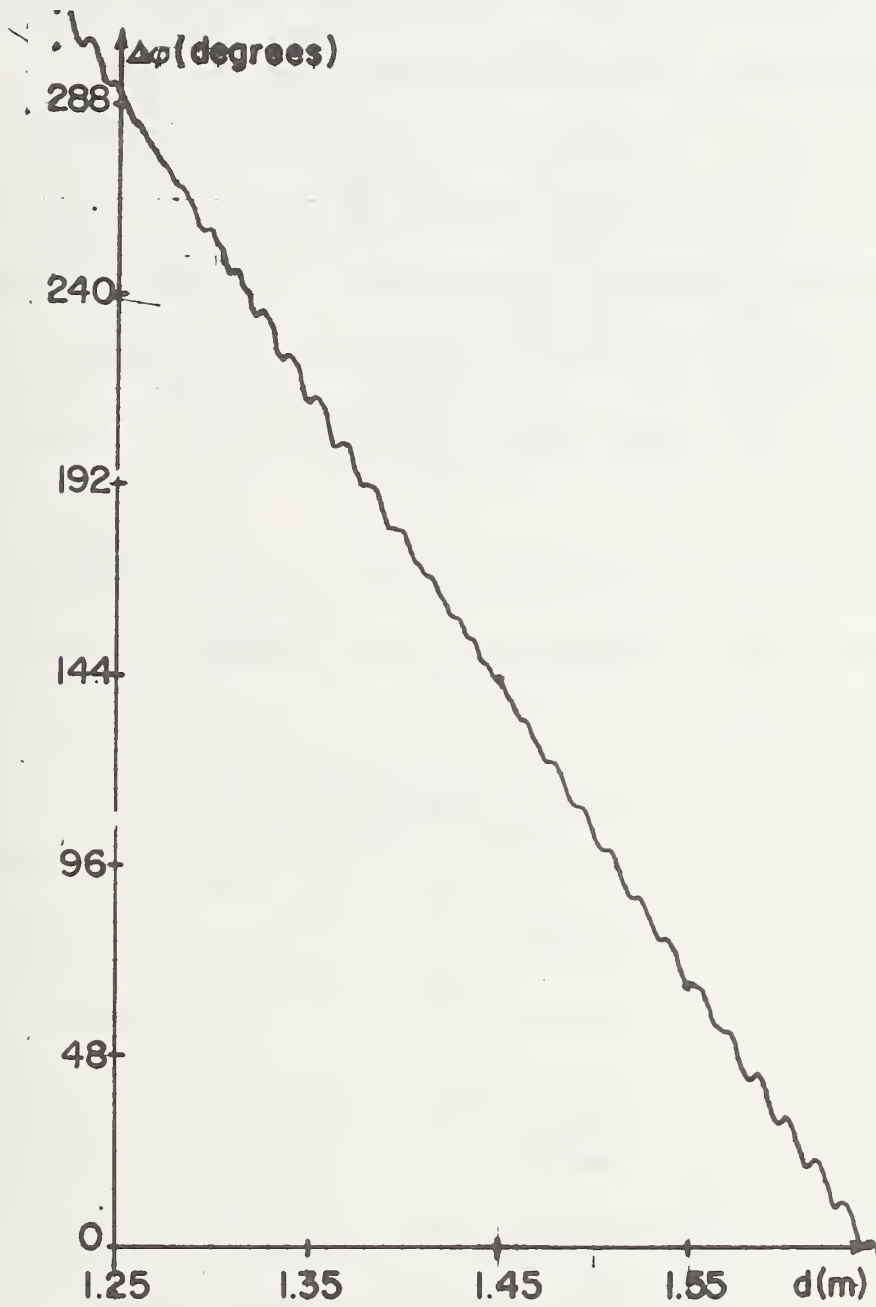


Fig. 4-16. Measured phase shift vs. lateral distance using the 10.5 GHz radar ($\Delta f = 300$ MHz) .

factor of 5 due to the difference in modulation frequency. For the results shown, the measured uncertainty in phase translates into the following uncertainty in distance :

$$\begin{aligned} & \pm 2.78 \text{ cm for the 8.4 GHz radar, and} \\ & \pm 0.33 \text{ cm for the 10.5 GHz radar.} \end{aligned}$$

This decreased uncertainty is dramatically illustrated by the two figures (4-15 and 4-16) because the vertical axis scales (in degrees) were chosen to be approximately the same in terms of lateral position.

Since the higher position accuracy is very desirable in a steering application, Δf was selected at 300 MHz for use in the microstrip prototype.

b) Theoretical Model for the Effects of Leakage

The main cause for the inaccuracy in the measurement of position is the introduction of unwanted signals at the mixers of the radar. There are various paths which these undesired signals can follow to combine with the desired signal. Figure 4-17 shows the major leakage paths in the 10.5 GHz prototype. They are:

- 1) The transmitted signals crossing directly over to the receiver via the antennas,
- 2) the transmitted signal reflecting off other objects rather than the reflector,
- 3) the LO signal, 10.5 GHz, crossing over to mixer #1 via the RF port,

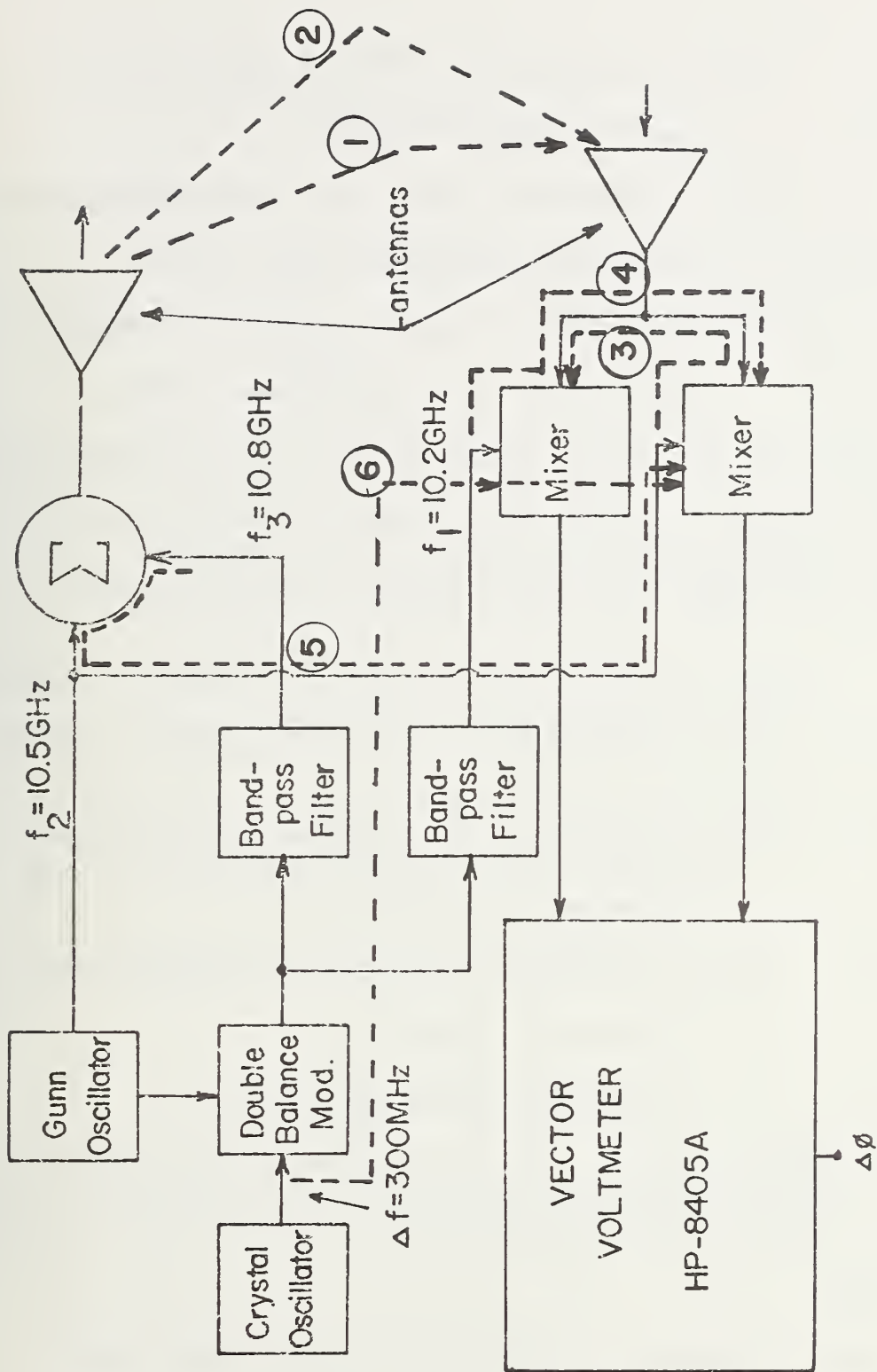


Fig. 4-17. Possible Leakage Paths for the 10.5 GHz radar.

- 4) the LO signal, 10.2 GHz, crossing over to mixer #2 via the RF port,
- 5) the transmitted signal, 10.8 GHz, leaking back into the LO port of mixer #2, and
- 6) the modulation frequency, 300 MHz, leaking over to the mixers via the power leads.

Theoretically, each of these undesired signals influence the composite signal; however, as a simple but realistic model, the signals at the input of the phase detector can be expressed as

$$v_1 = \alpha \cos \Delta \omega t + A \cos (\Delta \omega t - \omega_2 \tau) \quad (4-33)$$

$$v_2 = \beta \cos \Delta \omega t + A \cos (\Delta \omega t - \omega_2 \tau) \quad (4-34)$$

where

α = amplitude of the resultant undesired signal obtained in mixer #1,

β = amplitude of the resultant undesired signal obtained in mixer #2,

and

A = amplitude of the desired signal.

A mathematical analysis of the six undesired signals combining with the desired signals would reduce to forms similar to (4-33) and (4-34).

Without leakage, the input signals at the phase detector would be

and
$$v_1 = A \cos (\Delta \omega t - \omega_2 \tau) \quad (4-35)$$

$$v_2 = A \cos (\Delta \omega t - \omega_3 \tau) . \quad (4-36)$$

The phase difference would be

$$\Delta \varphi = -\omega_2 \tau - (-\omega_3 \tau) = \Delta \omega \tau \quad (4-37)$$

which equals

$$\Delta \varphi = \frac{4\pi d \Delta f}{c} . \quad (4-38)$$

Note that (4-38) is the same as (4-19). Now if $\Delta f = 300$ MHz, the phase measurement would represent the actual distance between antennas and the reflector. Figure 4-18 shows this ideal case. As expected, a straight line with a slope of $7.2^\circ/\text{cm}$ results.

With leakage included, the calculations of the phase difference is most easily performed if the signals are converted to phasors.

The phasor representations of (4-33) and (4-34) are

$$\hat{V}_1 = \alpha + Ae^{-j\omega_2 \tau} = Be^{j\varphi_1} \quad (4-39)$$

and

$$\hat{V}_2 = \beta + Ae^{-j\omega_3 \tau} = Ce^{j\varphi_2} . \quad (4-40)$$

After some trigonometric manipulation, the phase difference becomes

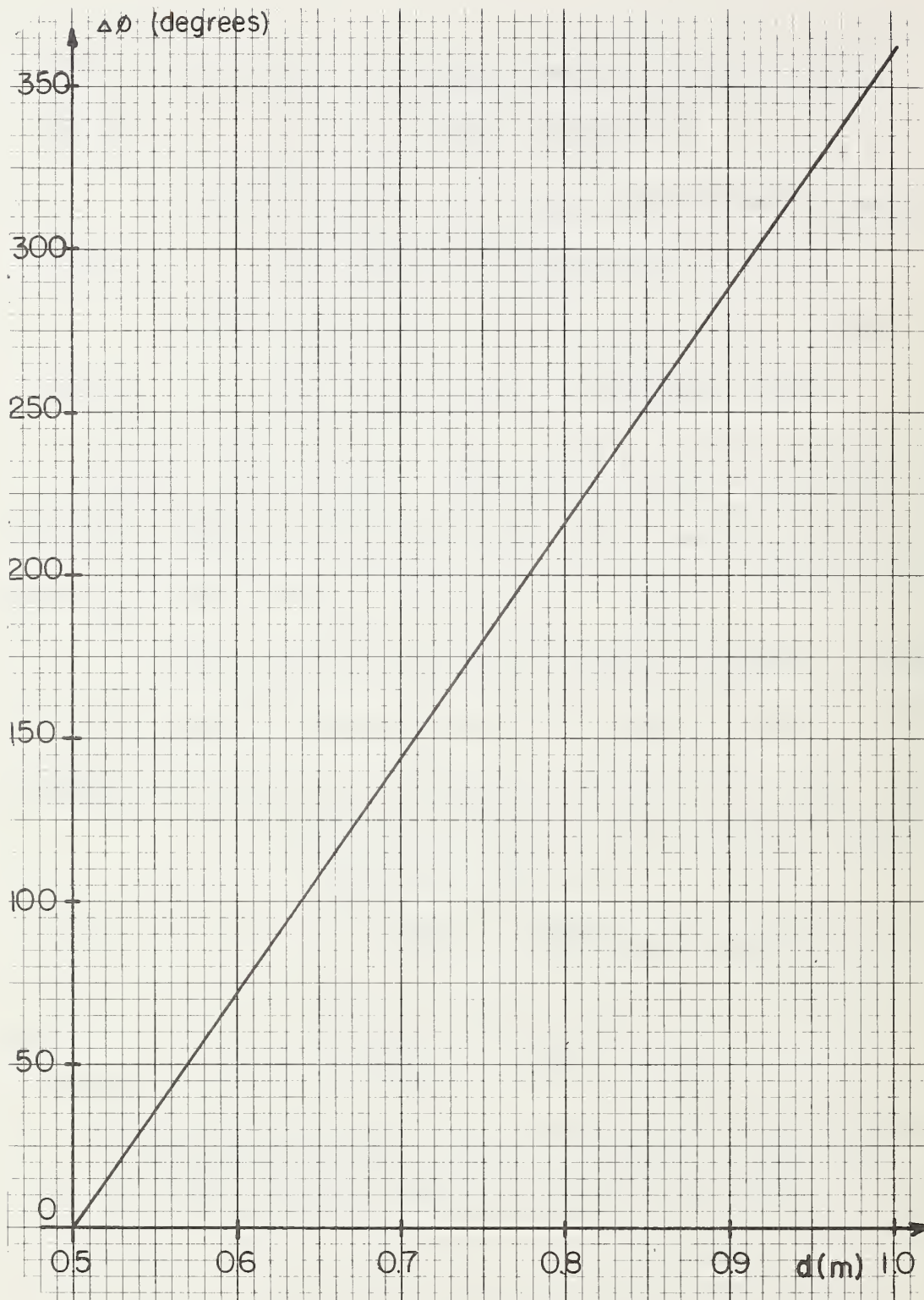


Fig. 4-18. Phase vs. distance with no leakage signals present -- theoretical calculation.

$$\begin{aligned} \Delta\varphi &= \varphi_1 - \varphi_2 \\ &= \tan^{-1} \left[\frac{A \sin \Delta\omega\tau + \alpha \sin \omega_3\tau - \beta \sin \omega_2\tau}{A \cos \Delta\omega\tau + \alpha \cos \omega_3\tau + \beta \cos \omega_2\tau + \frac{\beta\alpha}{A}} \right]. \end{aligned} \quad (4.41)$$

To illustrate the effects of leakage, two cases will be considered:

- 1) Leakage from one component only; i.e. --

$$A = 1.0$$

$$\beta = 0.1$$

$$\alpha = 0$$

$$S/N = 20 \text{ dB}$$

and

- 2) Leakage from both components

$$A = 1.0$$

$$\beta = 0.05$$

$$\alpha = 0.05$$

$$S/N = 20 \text{ dB}$$

1. Case I -- One Leakage Component Only

With one leakage component, the phase difference,

(4-41) becomes

$$\Delta\varphi = \tan^{-1} \frac{\sin \Delta\omega\tau - 0.1 \sin \omega_2\tau}{\cos \Delta\omega\tau + 0.1 \cos \omega_2\tau} \quad (4-42)$$

where

$$\tau = 2 \text{ d/c} .$$

The calculated phase versus distance is shown in Fig. 4-19 for $\Delta f = 300$ MHz and $f_2 = 10.5$ GHz. Note the effects of the unwanted signal. The undesired component causes an uncertainty in measurement of $\pm 5.8^\circ$ or ± 0.8 cm. Here, the r.m.s. error, $\delta d = 0.57$ cm and the peak error, $\delta d_p = 0.8$ cm. These values are in full agreement with (4-32).

For a better understanding of this leakage problem, a phasor diagram can be used. Figure 4-20 shows \hat{V}_1 and \hat{V}_2 on such a diagram. Here,

$$\hat{V}_1 e^{j\omega_2 \tau} = 1 \quad (4-43)$$

that is, all phasors are referenced to the $e^{j\omega_2 \tau}$ term. Thus,

$$\hat{V}_2 e^{j\omega_2 \tau} = 0.1 e^{j\omega_2 \tau} + e^{-j\Delta\omega\tau} \quad (4-44)$$

The undesired component adds or subtracts from the desired component and makes 35 revolutions for a change of 0.5 m of distance whereas the desired phasor only makes one revolution ($\omega_2 \tau = [252.0^\circ / \text{cm}]d$ and $\Delta\omega\tau = [7.2^\circ / \text{cm}]d$ for $\Delta f = 300$ MHz and $f_2 = 10.5$ GHz).

Figure 4-21 is the measured phase shift vs. lateral distance of the reflector as obtained under experimental static tests. Comparing the two results (Figs. 4-19 and 4-21), one notes the following similarities:

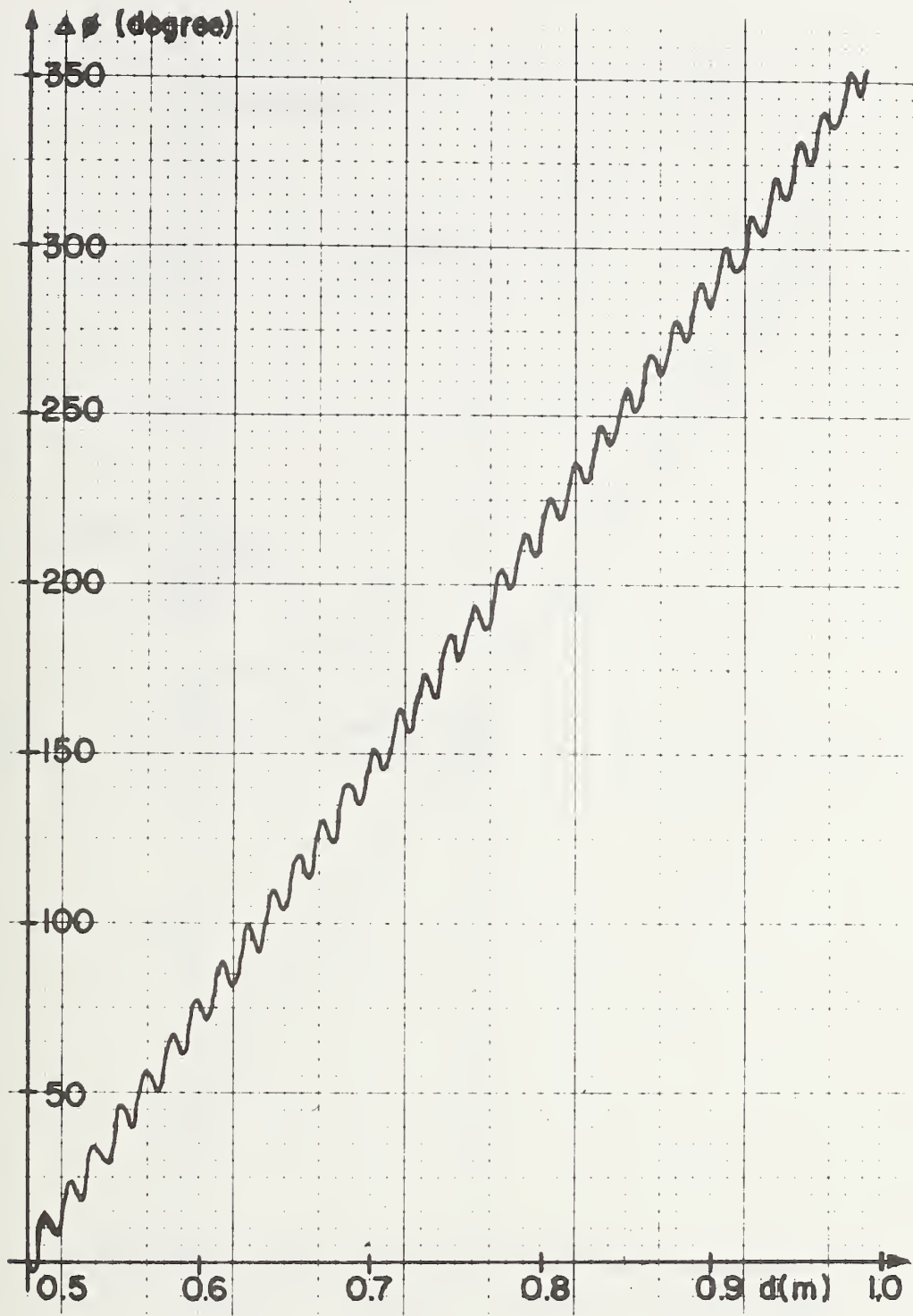


Fig. 4-19. Theoretical results for Case I where $S/N = 20$ dB.

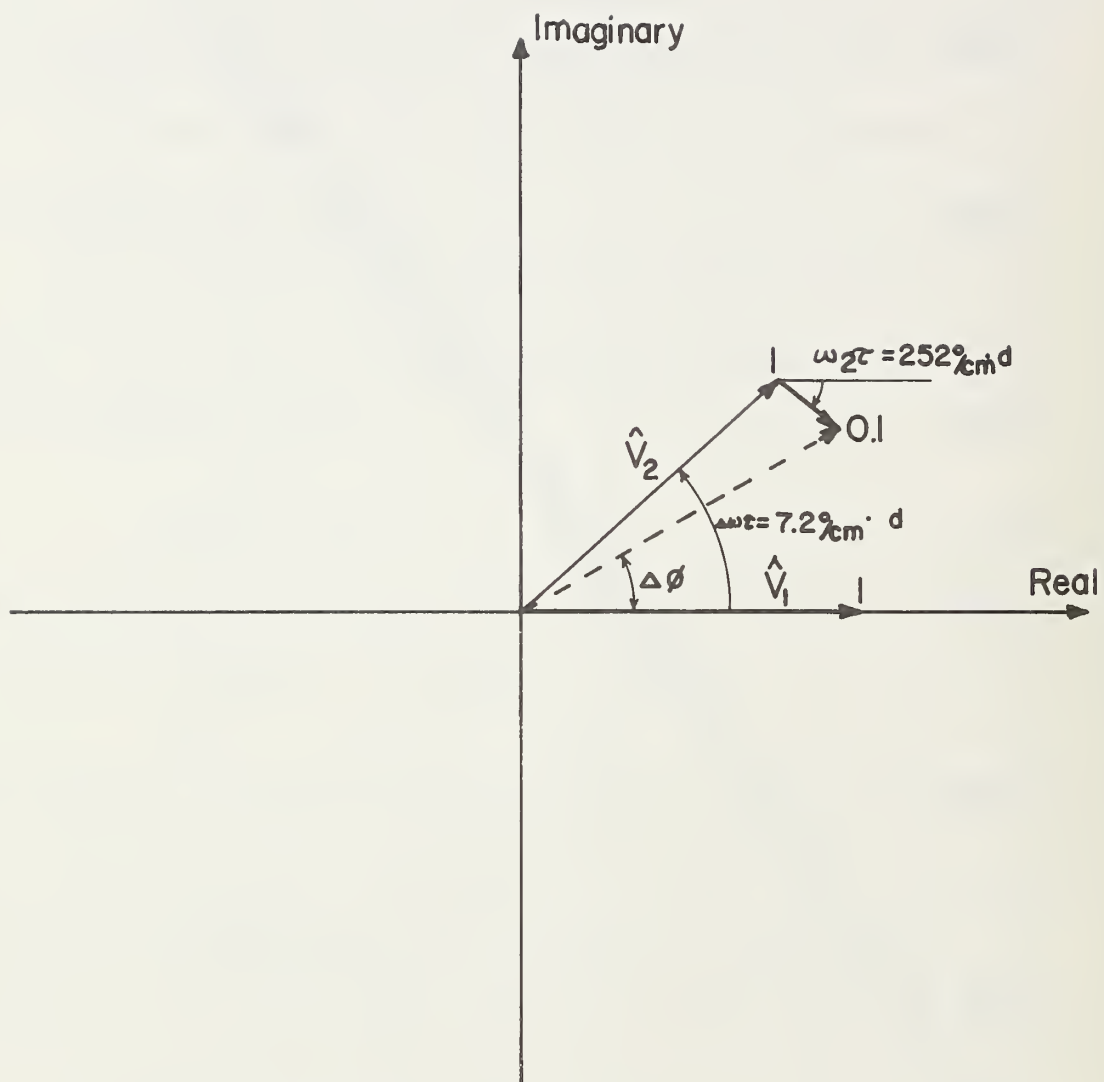


Fig. 4-20 . Phasor diagram of \hat{V}_1 and \hat{V}_2 with \hat{V}_1 as the reference phasor.

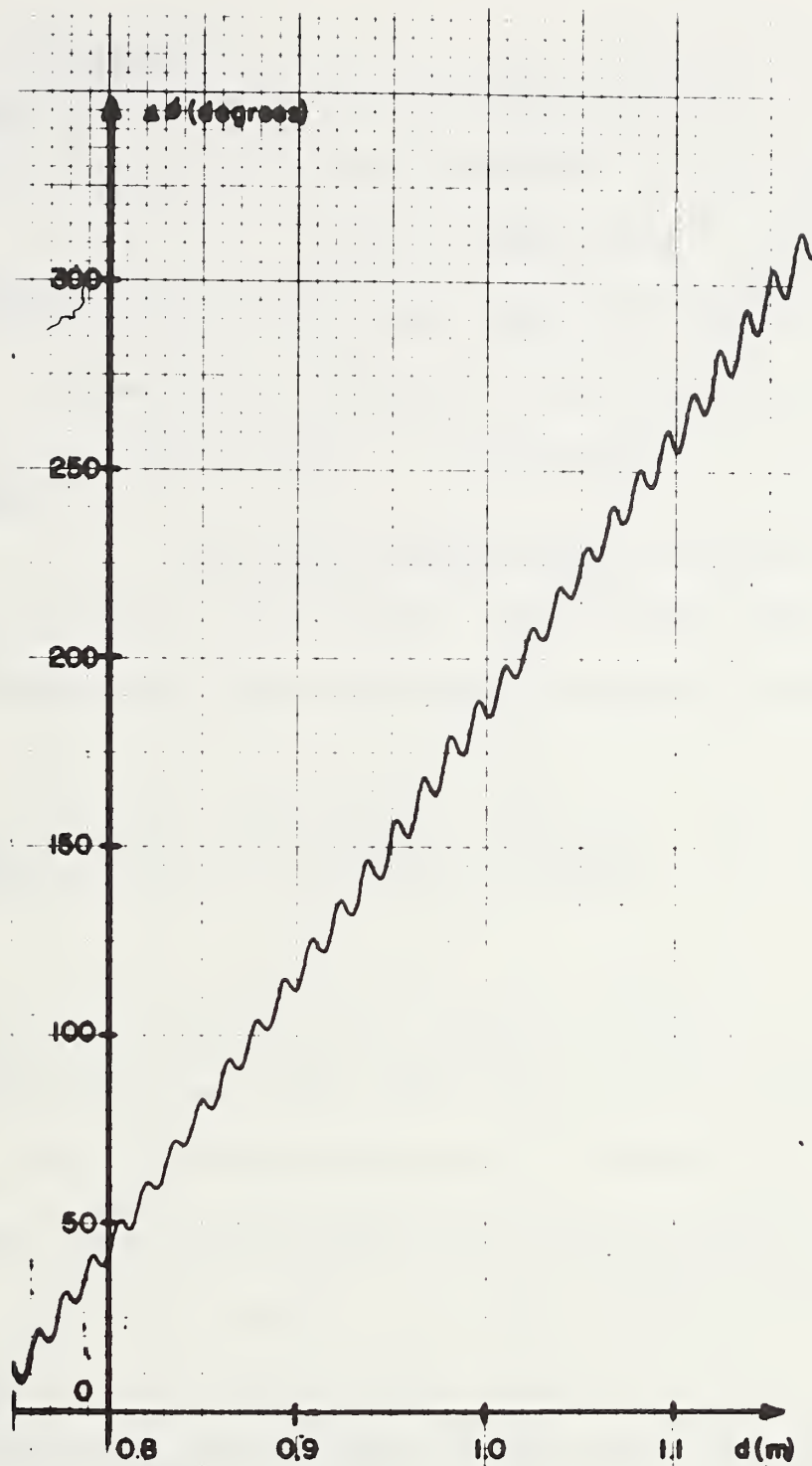


Fig. 4-21. Measured phase shift vs. lateral distance (20° B.W. antennas and $1\text{m} \times 1\text{m}$ screen wire reflector).

- i) δd_p are approximately equal (0.8 cm for the theoretical result and 0.9 cm for the experimental result).
- ii) The average slopes are identical, 7.2°/cm.
- iii) Unwanted oscillations have the same "wavelengths" -- approximately 1.5 cm.

2. Case II -- Two Leakage Components

When both leakage components are included, the phase difference for the specific parameters chosen becomes

$$\Delta\phi = \tan^{-1} \frac{\sin \Delta\omega\tau + 0.05 \sin \omega_3\tau - 0.05 \sin \omega_2\tau}{\cos \Delta\omega\tau + 0.05 \cos \omega_2\tau + 0.05 \cos \omega_3\tau + 0.0025} \quad (4.45)$$

A plot of $\Delta\phi$ versus d is shown in Fig. 4-22 for $\Delta f = 300$ GHz, $f_2 = 10.5$ GHz, and $f_3 = 10.8$ GHz. With two leakage components present, the possibility of destructive interference between the two exists. At various points of the phase-distance curve, the two components cancel each other and a straight line results.

Figure 4.23 is one such experimental result. A comparison of Fig. 4-22 and 4-23 illustrates that both components must, in general, be accounted for to explain the observed results.

Having an analytical model to predict the effects of leakage does not, in itself, result in the reduction of its effects. However,

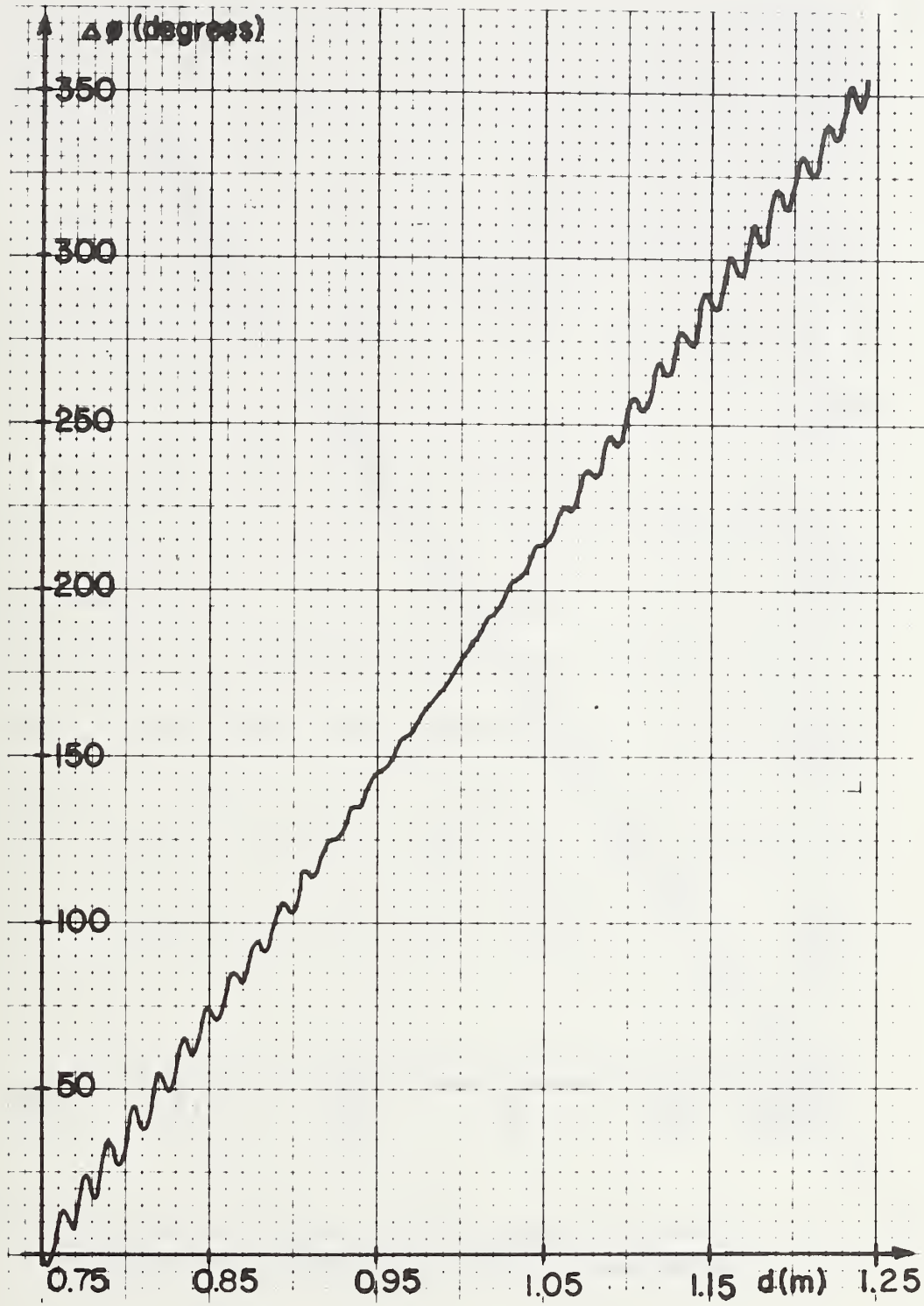


Fig. 4-22. Theoretical results for Case II where $S/N = 20$ dB.

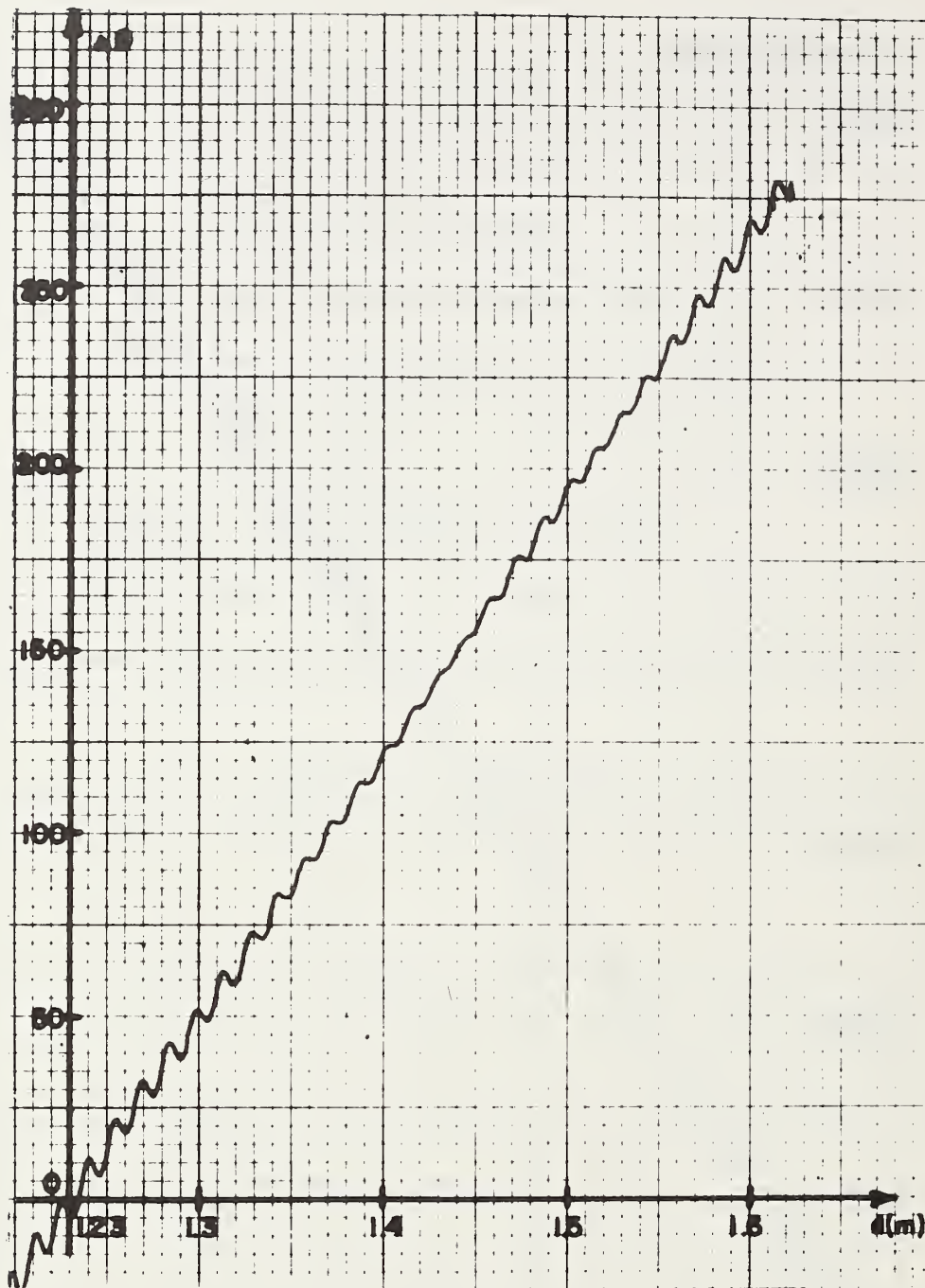


Fig. 4-23. Measured phase shift vs. lateral distance (20° B.W. antennas, and 1m x 1m screen wire reflector).

it was found that the interrelated factors influencing the amount of externally generated leakage entering through paths 1 and 2 shown in Fig. 4.17 were:

- 1) position, h , of the antennas above ground,
- 2) spacing, s , between antennas,
- 3) beamwidth, BW ,
- 4) the range of operation, R_o , and
- 5) the size and type of reflector.

An extensive discussion of the resulting peak-position-error δd_p as these parameters were varied over reasonable ranges can be found in [43] and is not repeated here. In summary, it was determined that under ideal static conditions and with the use of 20 db isolators in paths 3, 4, 5, and 6 (see Fig. 4.17) to reduce the internally generated leakage, δd_p could be kept below 0.5 cm. The appropriate values of the geometric parameters were

$$0.5 \text{ m} < h < 1.0 \text{ m}$$

$$s = 11.5 \text{ cm.}$$

$$BW = 20^\circ$$

$$.8 \text{ m} < R_o < 2 \text{ m.}$$

and a .7 m wide, flat, metallic reflector (aluminum) was used.

The corresponding factors in the full-scale, vehicle-mounted radar tests were chosen as close as possible to the above values or range of values.

C. Full Scale Studies

A specially constructed reflector wall, 152 meters in length, was built at TRCO for the purposes of dynamically testing the 10.5 GHz prototype in an automatic steering application. The wall was constructed parallel to an existing embedded conductor so that a comparison between the performance of the wire-following system and the radar system could be made.

The reflector wall consisted of a 0.71 m wide wire screen. The screen was used rather than a solid plate because of the possibly excessive wind loads that could occur due to high winds in this region of the test track. A cross-sectional and front view of the wall is illustrated in Figs. 4-24 and 4-25.

The radar was mounted 85 cm high on the front of a 1965 Plymouth sedan near the side closest to the wall. Figures 4.26 and 4.27 show the sensor's mounting arrangement. Amplitude and phase sensors were used to detect the embedded, current-carrying conductor. The antennas were outboarded by about 60 cm from the vehicle to achieve sufficiently large signal return. Here, $R_0 = 1.4$ m. This configuration is shown in Fig. 4.28.

The wall was placed as parallel as possible to the embedded wire; however, an uncertainty of ± 0.9 cm still exists between the two. Figure 4-29 shows the profile of the 152 m structure

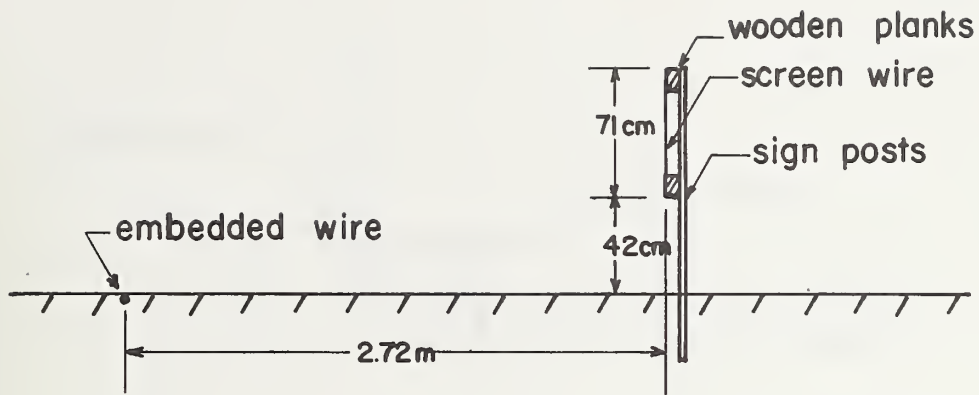


Fig. 4-24. Cross-sectional view of reflector structure.

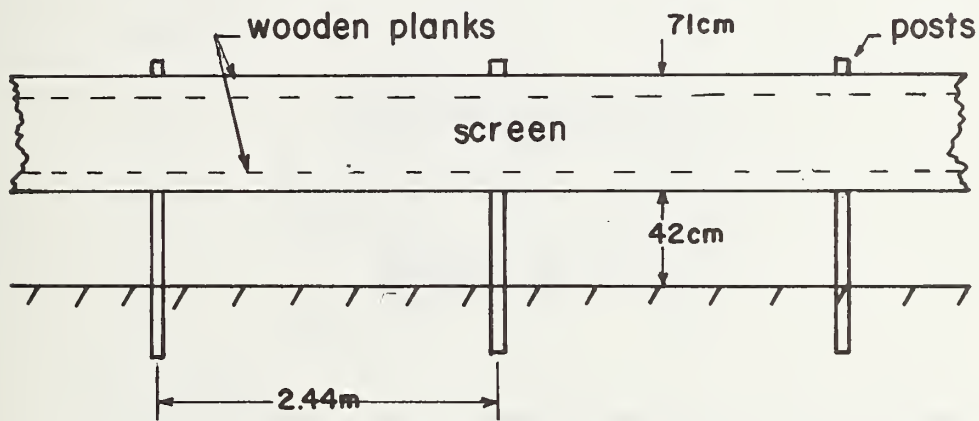


Fig. 4-25. Front view of reflector structure.

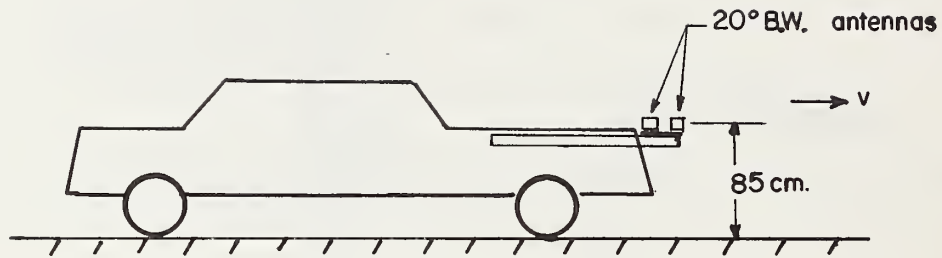


Fig. 4-26. Front view of radar unit mounted on the vehicle.

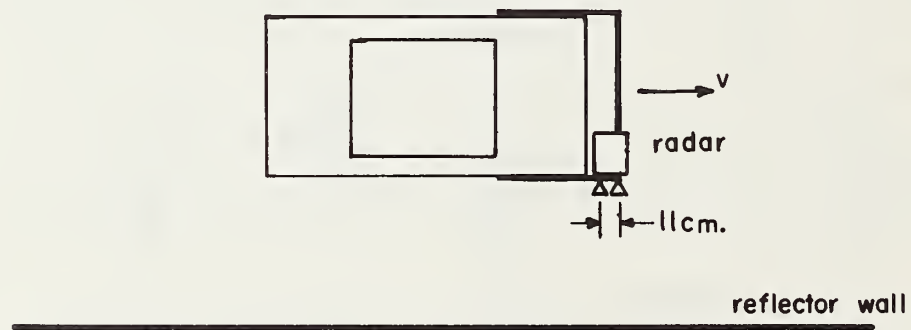


Fig. 4-27. Top view of radar unit mounted on the vehicle.

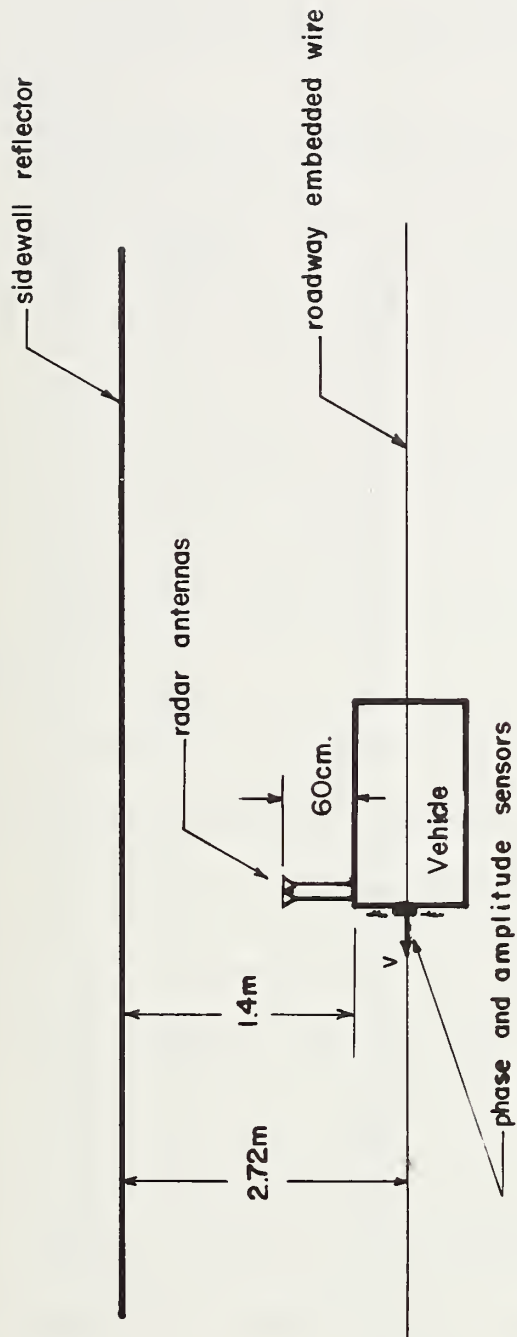


Fig. 4-28. Vehicle-sidewall geometry with outboarded antennas.

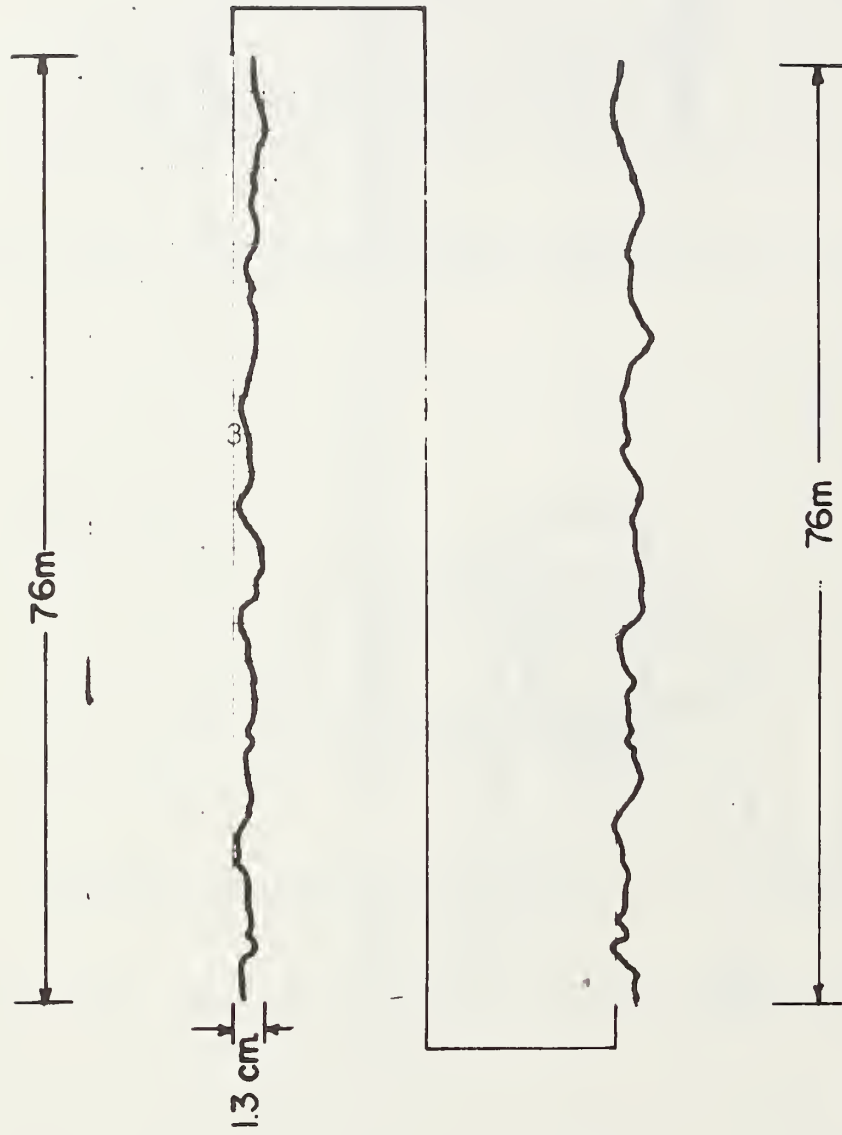
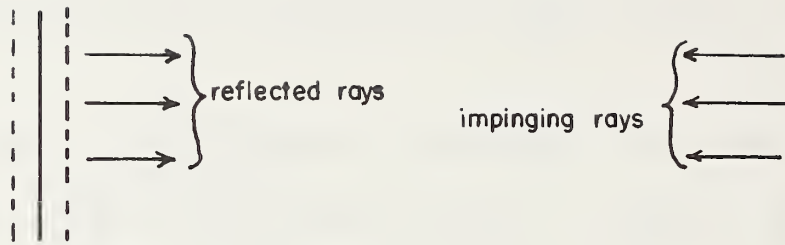


Fig. 4-29. Profile of the wall structure referenced to the embedded wire.

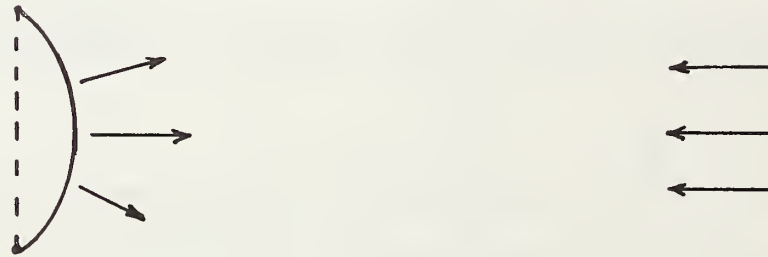
and the slight irregularities. This profile was determined by taking measurements every 15 cm along the track using the wire as reference.

In construction, the screen was kept taut in order to form a flat, rigid reflector. It was expected that air would easily flow through the screen and no heavy wind loading would occur. However, over time the wind did deform the reflector. Eventually, the wire screen was able to move back and forth under wind action. Its precise position at any given time depends upon the environmental conditions; however, its motion is constrained to a few centimeters.

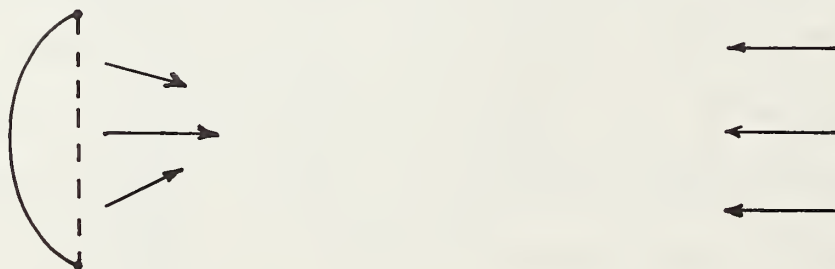
This relaxation and distortion of the screen reflecting wall introduced some unexpected problems in the operation of the radar sensor. In theory, if the reflector moves back and forth only a few centimeters (as shown in Fig. 4.30a) only a slight perturbation in the phase indication should result. However, the screen is rigidly attached to the two parallel wooden planks on the upper and lower portions of the fence (see Fig. 4.25). When the screen is slack, only the middle portion is able to move under wind loading as depicted in Fig. 4.30 b and c. Both configurations occur randomly as the wind changes. Because of the focusing and defocusing effects, large, random changes in the received signal amplitude occurs and the phase meter is often unable to measure



a) parallel motion of the reflector



b) concave outward distortion



c) concave inward distortion

Fig. 4-30. Geometrical optics analysis of reflection from a distorted reflector.

the phase -- a condition referred to as "dropout".

Examples are shown in Fig. 4.31. Here the vehicle was accurately controlled using the wire-following sensor and a recording of the radar's measurement of lateral position was taken. Note the large swings in the "apparent vehicle position" even though no actual lateral motion of the vehicle occurred.

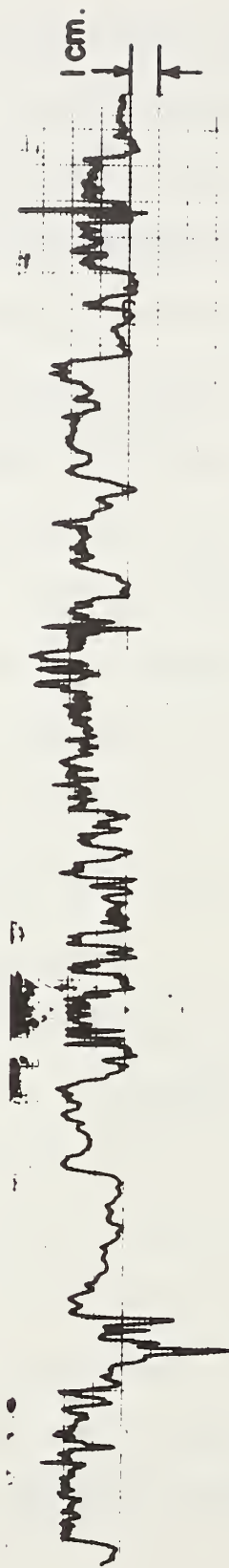
In spite of this undesirable property of the reflecting wall, a series of dynamic tests were conducted to assess the radar performance. Eventually, however, the screen deteriorated to such an extent that it was unusable. In the last month of the contractual period, the entire wall was modified and the tests were partially repeated. Both sets of results are included in the following sections as well as a description of the modified reflector used in the later tests.

a) Comparison of the Lateral Sensors Using the Screen Reflector.

A comparison between the performance of the phase sensor, the amplitude sensor, and the radar sensor was made at two velocities -- 3 m/s and 15 m/s -- using the original screen reflector. The specific controller used was designed by Cormer [44]. The outputs of each sensor were uniformly scaled so that any sensor output could be used as an input to the controller.



→ | ← 1 sec.



→ | ← 1 sec.

Fig. 4-31. Two different traces of lateral position error vs. travelled distance as measured by the radar sensor. The vehicle was controlled by the signal of the amplitude sensor ($v = 3 \text{ m/s}$).

1. Sensor Accuracy.

For comparison of the accuracies of these three sensors, consider the quasi-static results shown in Fig. 4-32. The three devices were activated simultaneously with the vehicle stationary at one point on the test track. The vehicle was then steered slightly off center while remaining almost exactly at the same longitudinal position.

The analog output of the amplitude sensor is highly accurate when no steel reinforcing is present -- as at TRCO. Thus, this signal is assumed to be a true measure of lateral error. Due to its discrete nature, the phase sensor indicates position error to within ± 0.64 cm. The output of the radar sensor clearly follows the same general trend as the outputs of the active sensors but the signal is contaminated with an oscillatory component due to the internal leakage of various RF signals within the radar (Section B). The corresponding peak uncertainty (as determined from Fig. 4-32) is $\delta d_p = 0.63$ cm.

2. Low-Speed Tests

The vehicle was first controlled by the amplitude sensor, at 3 m/s, and the outputs of both the radar and amplitude sensors were recorded. A typical result is shown in Fig. 4-33. The amplitude sensor/controller combination was able to maintain a

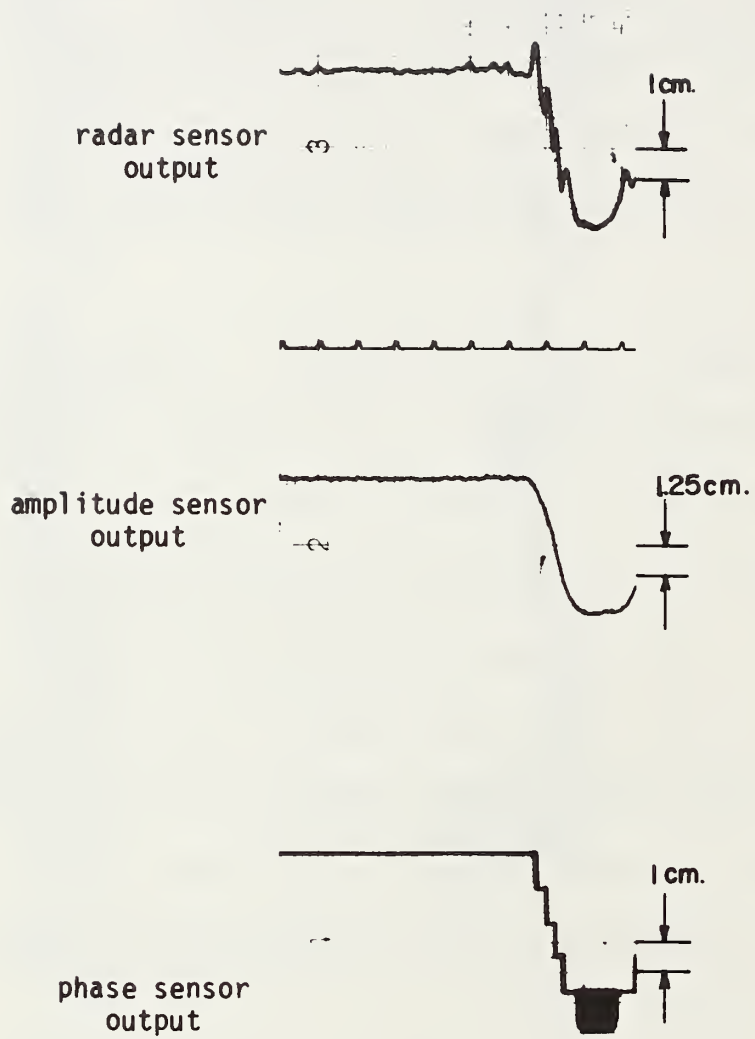


Fig. 4-32. The output of the three position sensing devices at one point on the test track.



a) radar sensor position error signal



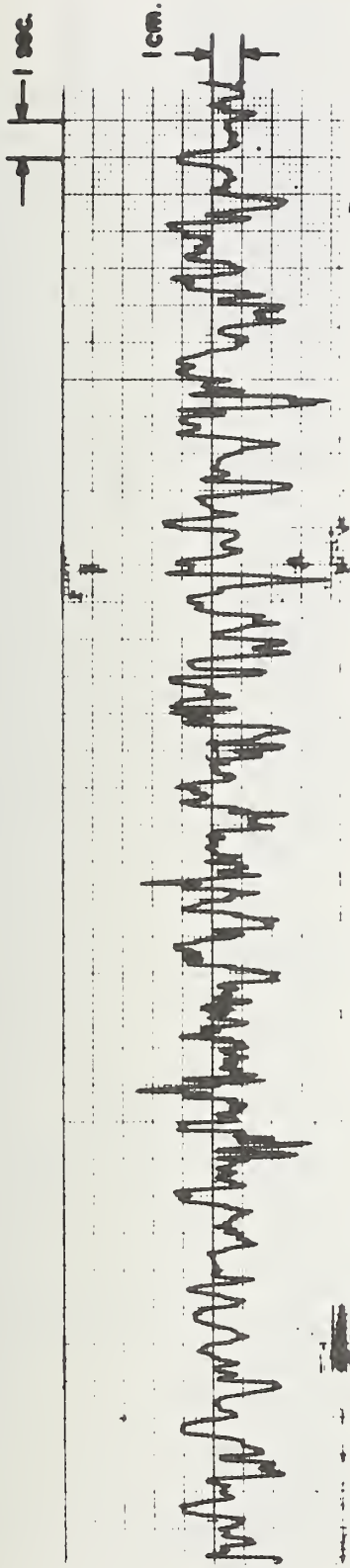
b) amplitude sensor position error signal

Fig. 4-33. Lateral position error vs. distance as measured by the amplitude sensor and the radar sensor. The vehicle was controlled by the signal of the amplitude sensor ($v = 3 \text{ m/s}$).

peak-to-peak position error deviation of less than 1.0 cm. Here, the peak-to-peak position error deviation will be denoted by ΔS_f and referred as the tracking accuracy.

Assuming the output of the amplitude sensor is a true indication of the vehicle's position error and, since the radar antennas are firmly mounted on the vehicle, the actual deviation of the antennas can be no more than 1 cm. Yet, the deviation as indicated by the radar sensor is as much as 4 to 5 cm. (The large spikes in the signal due to dropout were ignored.) This discrepancy is due to the deteriorated screen-wall and the ± 0.63 cm uncertainty in radar's output.

Other tests were made using the output of the radar sensor as the controller input. A typical low-speed result is shown in Fig. 4-34a. Clearly, the signal from the radar unit can be used to control the vehicle in spite of the rather rapid undulations of the signal. Because of these undulations, it is difficult to measure the deviation in the position error directly from the radar signal. However, the output of the amplitude sensor indicates that the radar/controller combination is able to maintain the vehicle to a deviation of less than 5 cm (see Fig. 4-34b). Here, the tracking accuracy ΔS_f of the radar/controller combination is 4.25 cm -- as measured by the amplitude sensor. This is consistent with the wall-position deviation measurements obtained earlier. Thus, the vehicle may be trying to follow the local deformations of the wall.



a) radar sensor position error signal



b) amplitude sensor position error signal

Fig. 4-34. Lateral position error vs. distance as measured by the amplitude sensor and the radar sensor. The vehicle was controlled by the signal of the radar sensor ($v = 3 \text{ m/s}$).

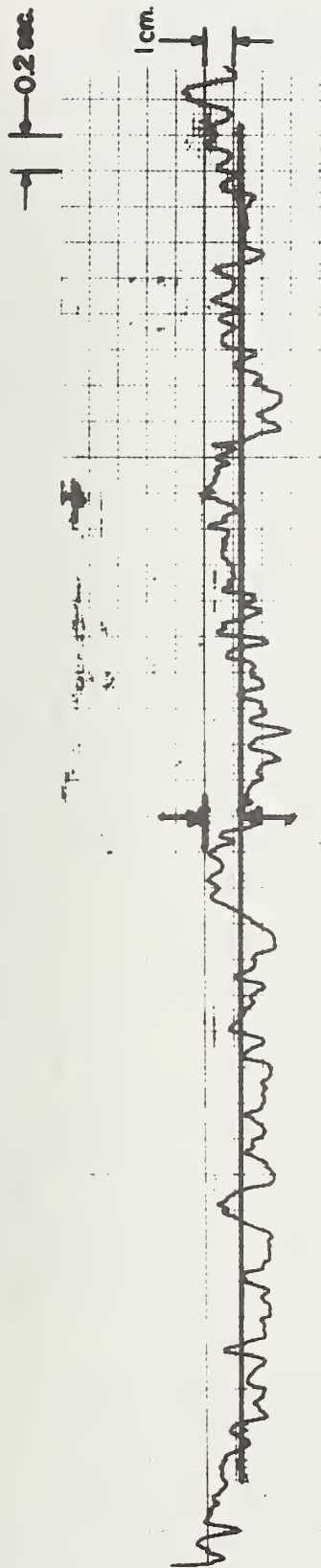
3. High-Speed Tests

The low-speed tests were repeated at a vehicle velocity of 15 m/s (higher speeds were impractical due to the short length of the reflecting wall). Typical results are shown in Fig. 4-35 for an amplitude-sensor controlled vehicle and in Fig. 4-36 for the case of the radar-sensor control.

The tracking accuracy of the amplitude sensor/controller combination is approximately 3.5 cm (here, $\Delta S_f = 3.5$ cm). At the same time, the radar sensor was indicating a position error deviation of less than 4 cm. With the radar controller combination, the tracking accuracy was 4.75 cm. Again it appears that the vehicle might be trying to follow the undulations of the screen-wall reflector.

b) Comparison of the Sensors Using the Modified Reflecting Wall

Several months before the expiration of the contract, the screen reflector had deteriorated to such an extent that it was unuseable. Dropouts occurred so often that adequate control of the vehicle could not be maintained. It was decided to modify the wall using 3/4 inch (1.9 cm) sheets of plywood. These were placed on the roadway side of the wall as depicted in Fig. 4.37. Several methods of changing the reflecting portion of the wall were tried.

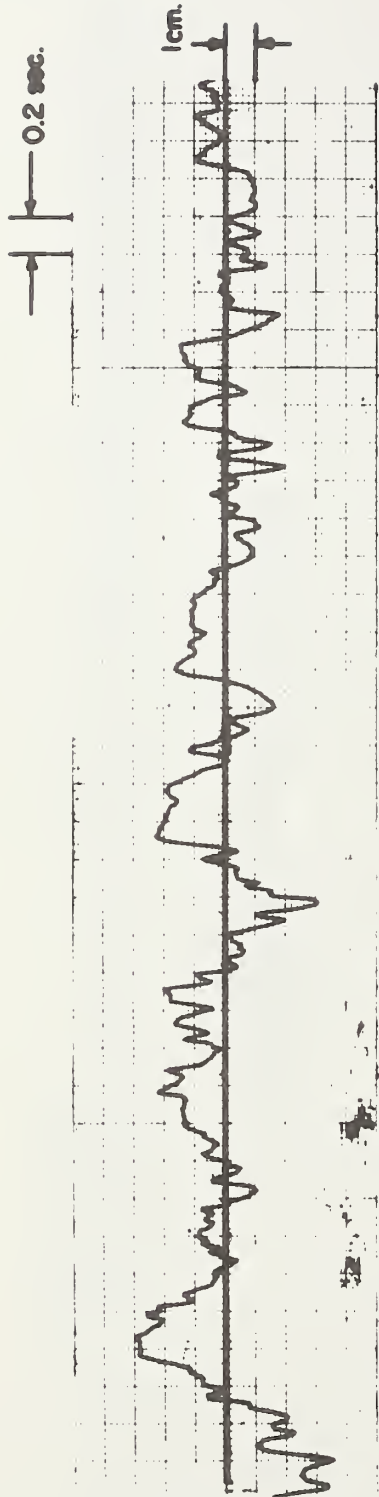


a) radar sensor position error signal



b) amplitude sensor position error signal

Fig. 4-35. Lateral position error vs. distance as measured by the amplitude sensor and radar sensor. The vehicle was controlled by the signal of the amplitude sensor ($v = 15 \text{ m/s}$).



a) radar sensor position error signal



b) amplitude sensor position error signal

Fig. 4-36. Lateral position error vs. distance as measured by the amplitude sensor and the radar sensor. The vehicle was controlled by the signal of the radar sensor ($v = 15 \text{ m/s}$).

First, the screen was affixed firmly to the inner face of the plywood (see Fig. 4.37). Since wind forces could not now move the screen, it was hoped that no undulation in the signal level would occur. Unfortunately the signal attenuation through the plywood was great enough (8-10db) to make the performance marginal.

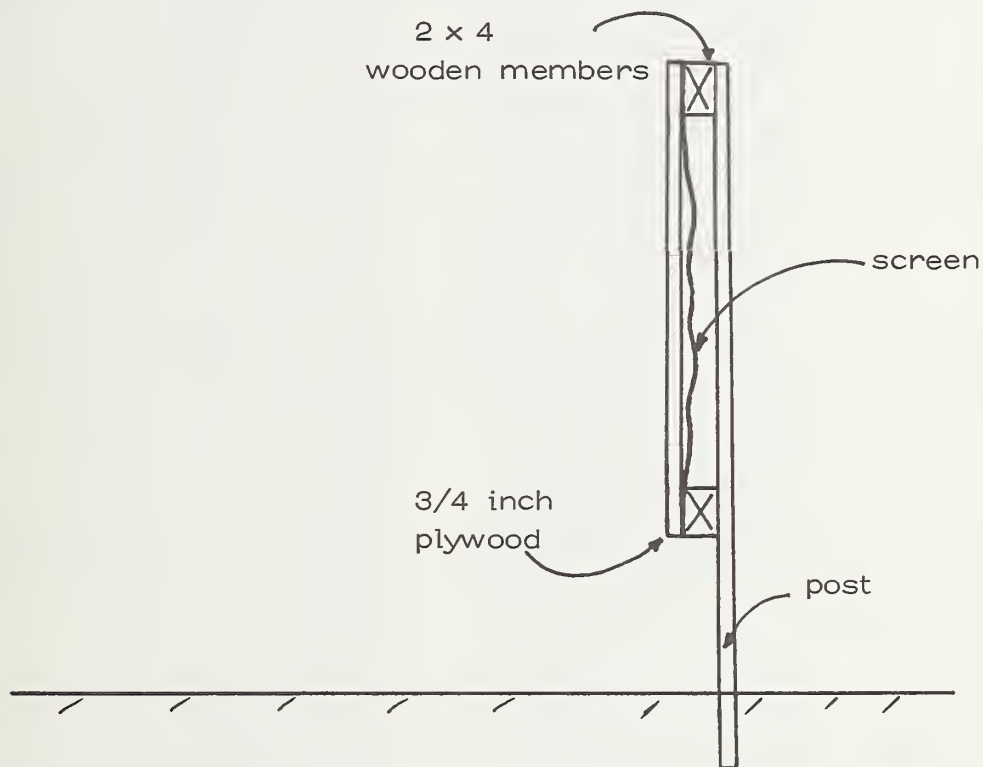


Fig. 4-37. Cross-sectional view of the modified reflecting wall.

Next, aluminum paint (purchased locally) was tried on the outer surface of the wall but the reflecting properties were not adequate. It appears that a paint with much higher metallic con-

tent than that available "off the shelf" would be needed.

Finally, ordinary household aluminum foil was glued to the outer surface of the plywood. The improvement was dramatic. Laboratory tests indicated that the reflecting properties were equal to that obtained with thick metallic reflectors. In the full scale tests, the plywood wall could not move and the only position uncertainty was that caused by the leakage component of the radar.

To illustrate the difference in the radar performance using the screen versus using the foil, a test was made before the entire fence was covered with foil. The result is shown in Fig. 4.38. The vehicle was controlled by the phase - sensor method of wire-following. The transition between the screen portion and the foil portion of the fence is obvious. Dropouts no longer occur and the signal is much less noisy.

Further tests were conducted at low and high speeds using both wire-following control and radar control. It must be noted that in all tests, the need for outboarding the radar antennas as shown in Fig. 4.28 was eliminated. Use of the foil reflector increased the signal strength to such an extent that the antennas could be placed flush with the vehicle side as depicted in Fig. 4.27. In fact, the dynamic range was so improved that the vehicle could be adequately operated several meters from the fence. Quantitative data on this could not be obtained, however, because

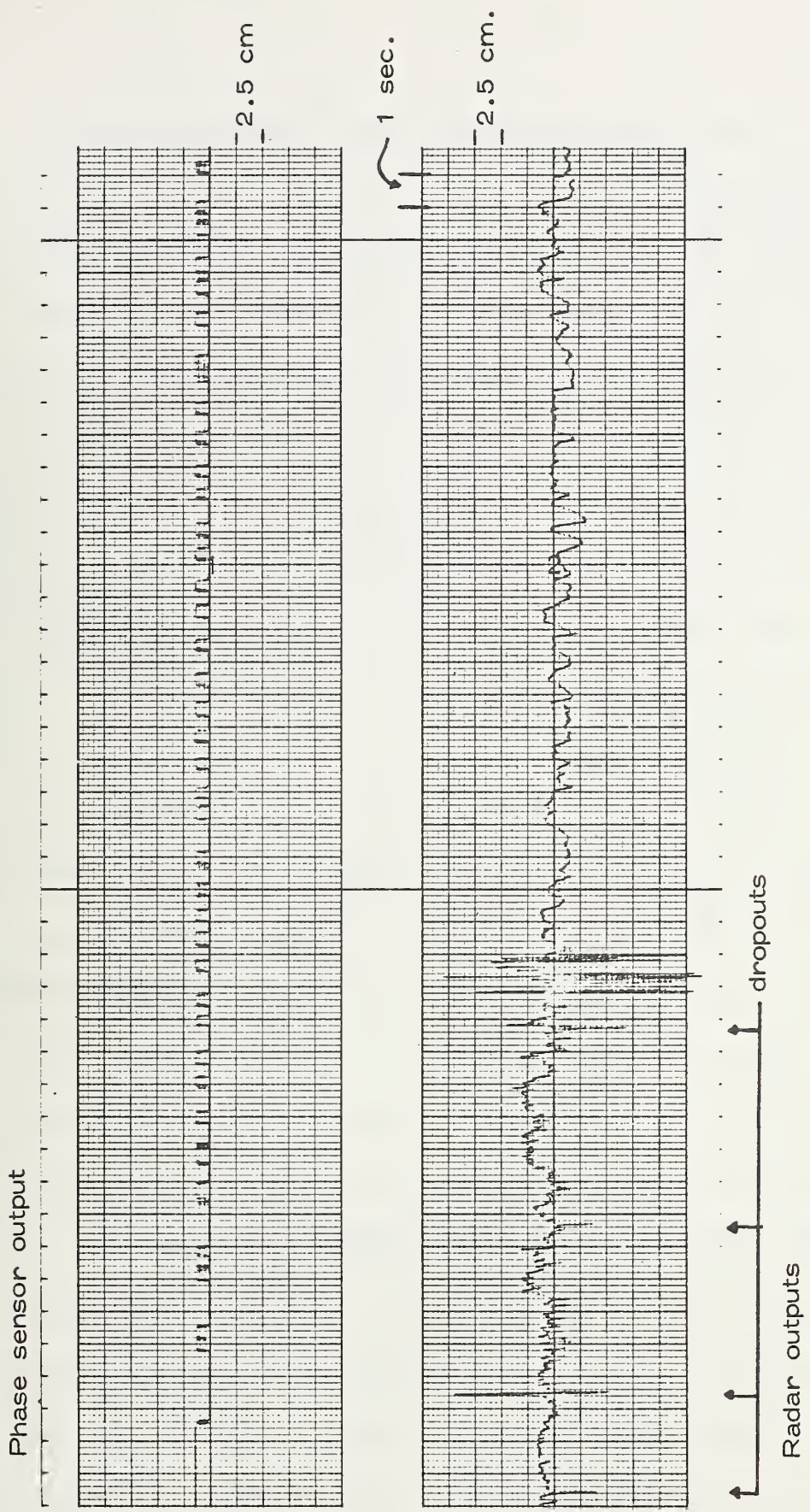


Fig. 4-38. Lateral position error vs. distance with the reflecting wall only partially covered with foil (wire-following control).

no wire reference was available at larger distances from the reflecting surface.

The results of a quasistatic calibration are shown in Fig. 4.39. Note that while this calibration is different (by a factor of 2) from that used for the tests with the original screen reflector, the signals from the phase-sensor and the radar were uniformly scaled and either could be used as an input to the lateral controller. The effects of the leakage components in the radar can be noted in Fig. 4.39. These are now the major cause of error in the lateral position measurement.

1. Low-Speed Tests

Here the vehicle was maintained at a constant longitudinal velocity of approximately 3.4 m/sec. The lateral tracking performances using the wire-following sensor and the radar sensor are shown in Figs. 4.40 and 4.41, respectively. The wire follower clearly maintains the vehicle to within ± 0.6 cm ($\Delta S_f = 1.2$ cm) of the desired position. (A more precise figure cannot be determined due to the discrete nature of the signal.) At the same time, the radar is indicating a relative fence-to-wire deviation (from Fig. 4.40) of about ± 2.5 cm ($\Delta S_f = 5.0$ cm). The major cause of this larger deviation is the inherent limitation of this radar sensor due to the leakage signals. However, because the foil is now being used as the reflector, no dropouts

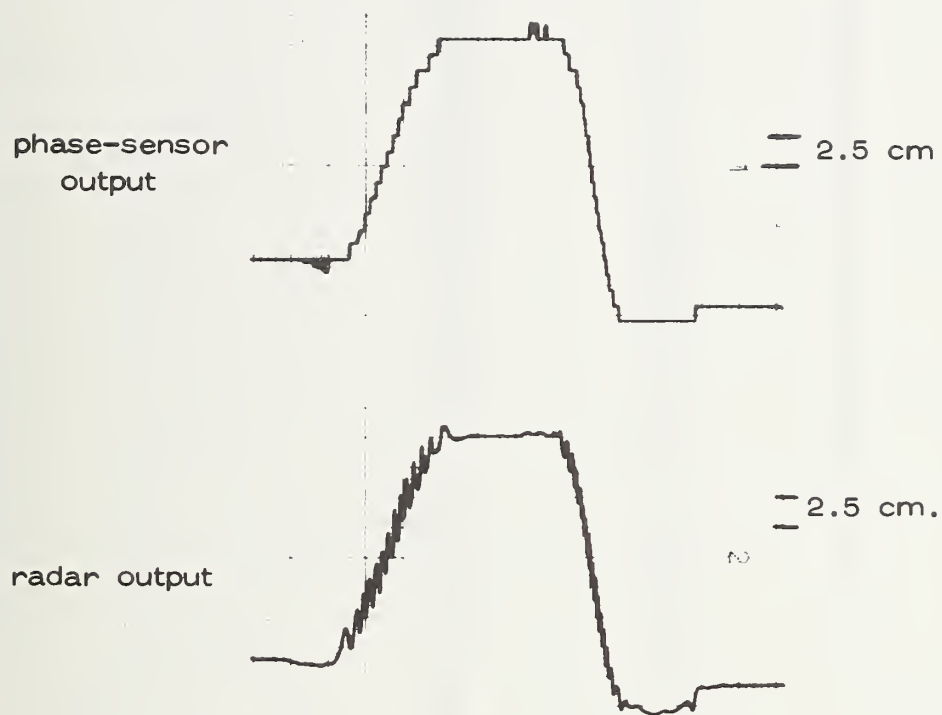


Fig. 4-39. Radar and phase-sensor output vs. lateral distance at one point of the test track.

Phase-sensor output



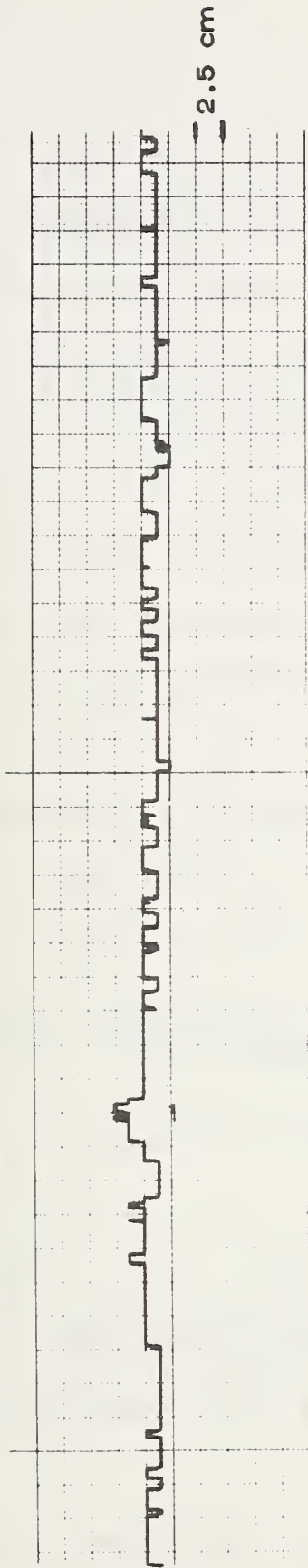
1 sec



Radar output

Fig. 4-40. Lateral position error vs. distance as obtained from the phase-sensor and the radar (wire-following control at $v = 3.4$ m/s).

Phase sensor output



Radar output

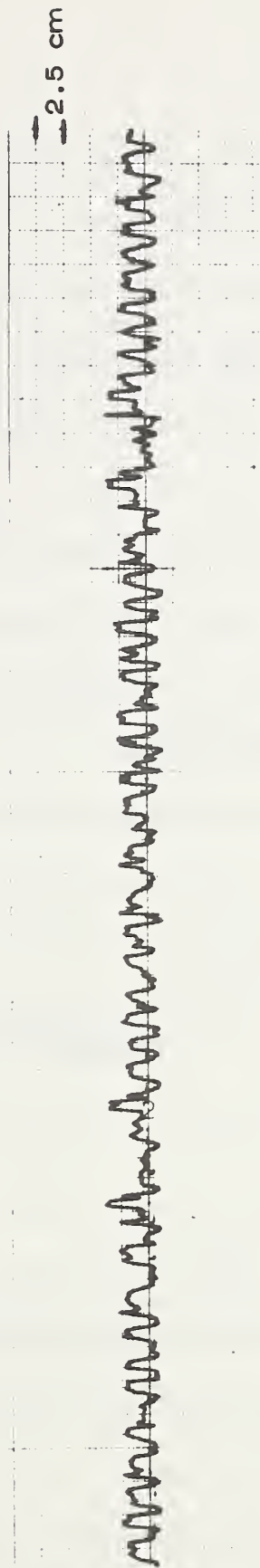


Fig. 4-41. Lateral position error vs. distance as obtained from the phase-sensor and the radar (radar control at $v = 3.4$ m/s).

(which would appear as large changes in the error signal input to the controller) are present. This results in a smoother ride as compared with the ride when the screen was used as the reflector even though the position deviation is about ± 2.5 cm (see Fig. 4.41). Of course, the smoothest ride occurs when the wire-following control is used. It was found that the rms lateral acceleration at both the center-of-gravity and the front of the vehicle using the radar input was about twice that which resulted when wire-following control was used (see Table 4.2)

2. High-Speed Tests

The high-speed tests were conducted at approximately 12 to 14 m/sec -- an upper limit due to the short length of fence available. The results are displayed in Figs. 4.42 and 4.43 and are analogous to Figs. 4.40 and 4.41 except that the longitudinal velocity is greater.

Observe from Fig. 4.42 that the lateral deviation of the vehicle using wire-following control is now about ± 1.2 cm ($\Delta S_f = 2.5$ cm) at this higher longitudinal velocity. Again, a more precise figure cannot be given due to the discrete nature of the signal. The corresponding indication of lateral position deviation by the radar is ± 2.5 cm.

The tracking performance when the radar signal is used for control is shown in Fig. 4.43. Using the wire-following sensor

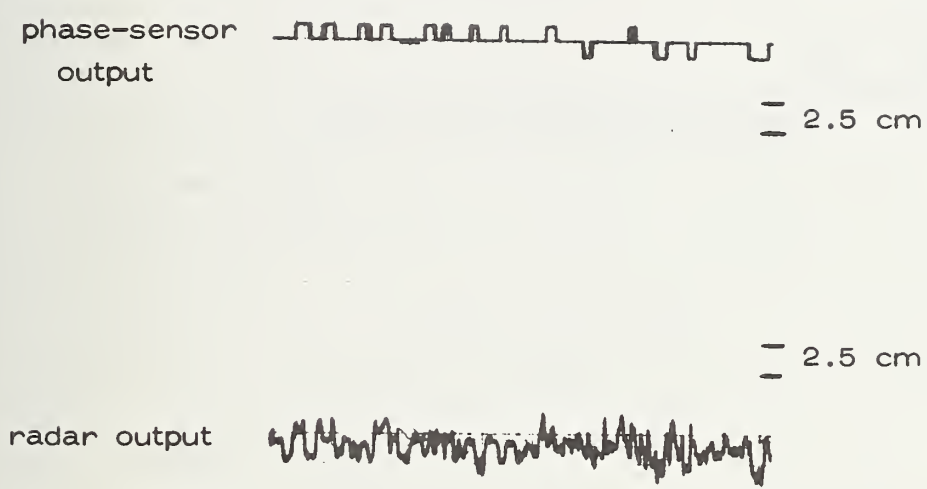


Fig. 4-42. Lateral position error vs. distance as obtained from the phase-sensor and the radar (wire-following control at $v = 12$ m/s).

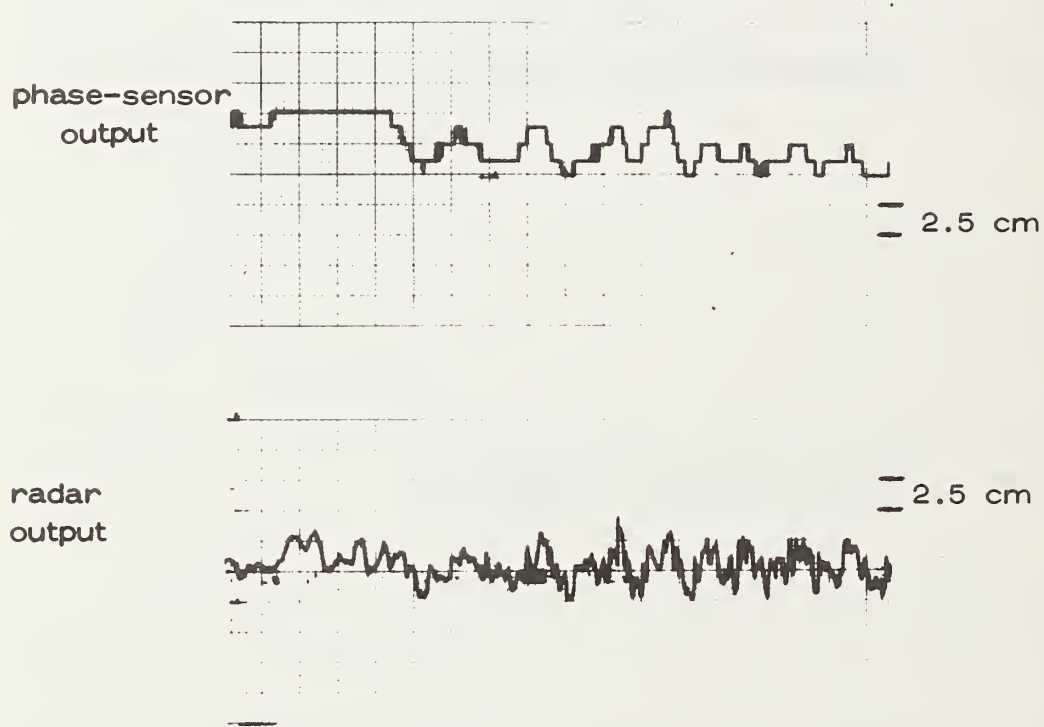


Fig. 4-43. Lateral position error vs. distance as obtained from the phase-sensor and the radar (radar control at $v = 14$ m/s).

as an absolute measure, one finds that the tracking accuracy is ± 2.5 cm (or $\Delta S_f = 5.0$ cm). The actual tracking ability may be somewhat inferior to this because the radar signal (lower trace of Fig. 4.43) indicates a figure of about ± 3.5 cm ($\Delta S_f = 7.0$ cm).

The ride comfort with radar-signal control was again somewhat deteriorated from that with wire-following control. The rms lateral acceleration measurements at the center-of-gravity and at the front of the vehicle are shown in Table 4.2. The values obtained with radar control were about twice those obtained with wire-following control.

TABLE 4.2

Measured lateral accelerations for wire-following (W-F) control and Radar (R) control at two different longitudinal velocities.

Longitudinal velocity, m/sec	Acceleration at the center of gravity , m/sec ²	Acceleration at the front of the vehicle, m/sec ²
3.4	0.09 (W-F)	0.24 (W-F)
	0.17 (R)	0.57 (R)
12 to 14	0.11 (W-F)	0.29 (W-F)
	0.22 (R)	0.65 (R)

D. Conclusions

A two-frequency radar was designed and constructed to assess the feasibility of "passively" obtaining position information for automatic lateral control. The final prototype was evaluated

both in the laboratory and in a full-scale situation.

The performance of the radar-based controller was determined with respect to the wire-following one by comparing observed lateral position error for each simultaneously. It must be noted that the reliability of this procedure is highly dependent upon the actual variation of the "wire-to-reflector" spacing. In any full-scale application, extreme accuracy in installation would not be required. It would only be necessary that the wall follow the general path of the roadway with no abrupt discontinuities.

The full-scale results clearly indicated that a passive approach of obtaining a lateral reference signal for automatic steering is viable. Tracking accuracies roughly one-half those for the wire-following approach were obtained. Since the sensing accuracy was limited due to the presence of internal leakage signals, further improvement should result by reducing this leakage in subsequent redesigns. There is no apparent reason why the eventual performance of a radar-based system should not be equal to, or better than, that of a wire-following system.

In the course of the full-scale testing, it was determined that rigidity of the reflecting surface must be maintained in order to provide sufficient signal level at the receiving antenna. The final version of the 150 meter reflector installed at TRCO satisfies this requirement and should be extremely useful in the evaluation of future radar designs.

CHAPTER V
A MICROPROCESSOR-BASED,
VEHICLE LATERAL CONTROLLER

A. Introduction

In a previous study [21], a velocity-adaptive lateral controller was designed to meet requirements pertaining to lateral-position tracking accuracy, ride comfort, and an insensitivity to both changes in critical vehicle parameters and disturbance forces. This controller, which was realized with analog components, was tested under full-scale conditions and excellent performance was achieved.

During the past year, as part of an effort to increase a vehicle's onboard decision-making capability, an Intel 8086 micro-computer was installed in the 1965 Plymouth sedan to implement the previously designed velocity-adaptive controller and to monitor various vital functions (e.g., engine oil pressure, generator current and lateral position deviation).

B. Lateral Controller Design

Consider the closed-loop controller shown in Fig. 5-1. The command inputs are a null, which corresponds to lane center

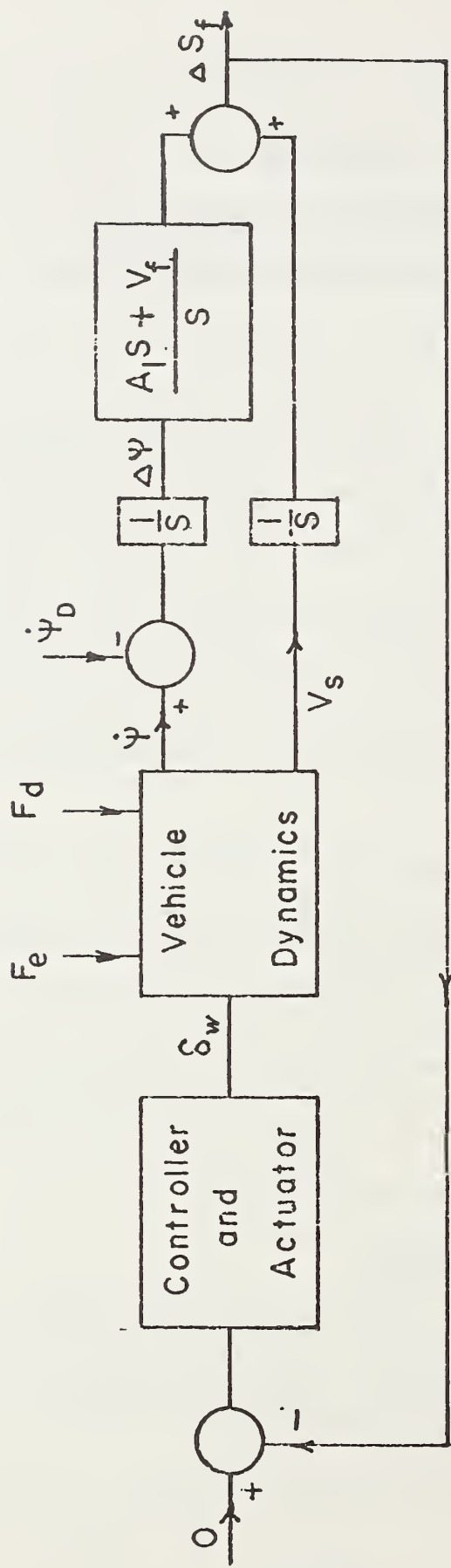


Fig. 5-1 A single-loop, lateral controller .

when a wire-following reference is employed, and the desired yaw rate $\dot{\psi}_D$.¹ The block labeled "controller" is to be specified in the design process, and that labeled actuator corresponds to an electrohydraulic servo coupled to the power-steering unit. This actuator is a closed-loop subsystem whose output, the front-wheel angle (δ_w), is obtained via a "follow-up" potentiometer. The subsystem transfer function, as obtained from empirical tests, is

$$\frac{\delta_w}{E_i} = \frac{1.14}{s + 14.2}, \quad (\text{rad/V}) \quad (5-1)$$

where E_i is the actuator input voltage.

The block labeled "Vehicle Dynamics" represents the lateral dynamics of the test vehicle. These dynamics are characterized by the inputs δ_w , a superelevation force (F_e), and a disturbance force (F_d), and the outputs yaw rate ($\dot{\psi}$) and side velocity (V_s). A detailed model, which was validated for nonemergency control situations in a previously reported study [15], is shown in Fig. 5-2 together with a model of a wire-following reference/measurement configuration.

1

A justification for this choice of inputs is contained in Appendix B.

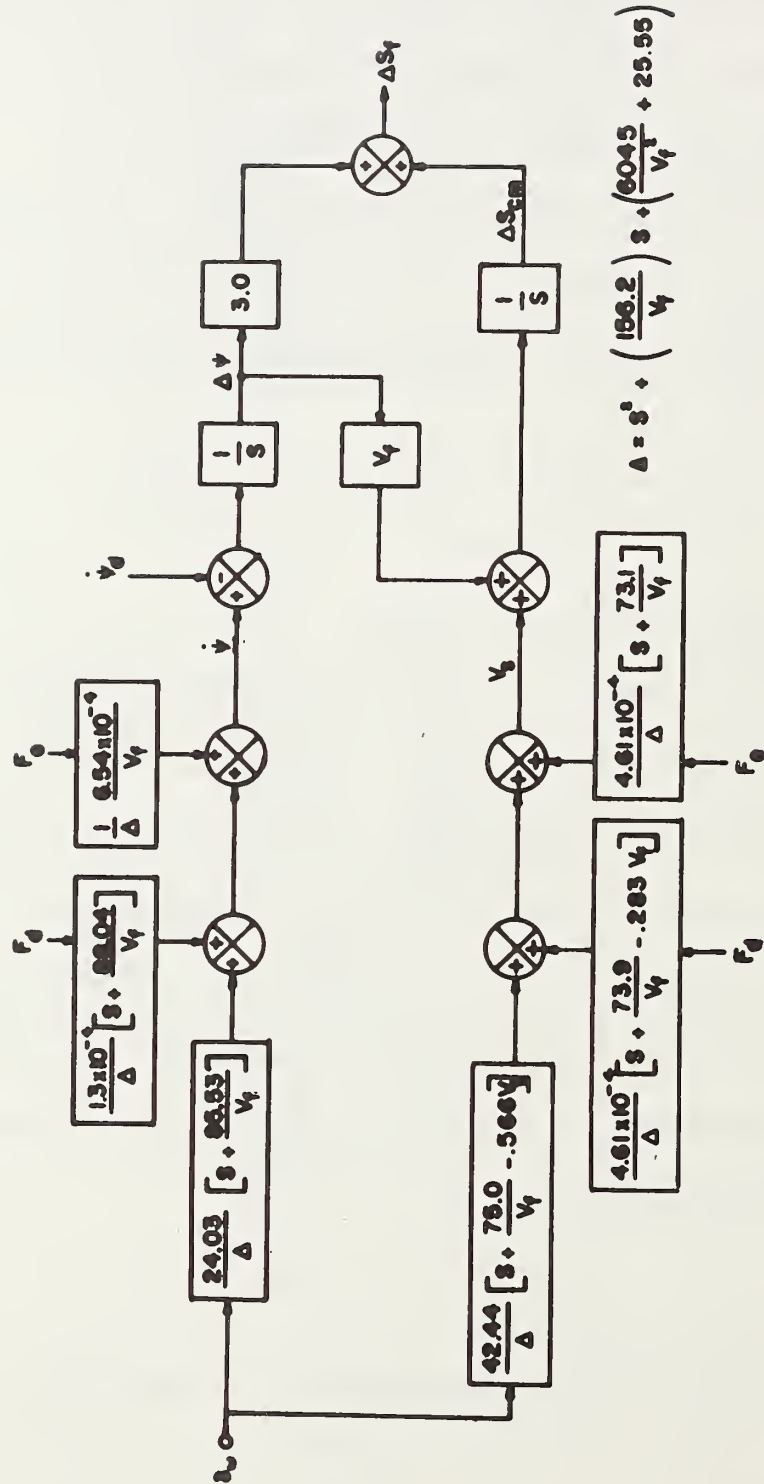


Fig.5.2 Lateral dynamics model as a function of forward velocity.

The parameters associated with these models are listed in Table 5-1. Of these parameters, the vehicle's forward velocity V_f and the front- and rear-cornering stiffness coefficients (C_f and C_r , respectively) vary to such an extent as to substantially affect the performance of the closed-loop system. Since it is impractical to measure C_r and C_f on line, the system should be designed to be relatively insensitive to variations in these quantities. In contrast, V_f can be accurately measured; therefore, the system can be made nominally independent of this quantity by employing inverse compensation. This was the approach previously adopted in designing the analog, velocity-adaptive controller.

The transfer function relating ΔS_f , the position of the vehicle relative to lane center, and δ_w can be derived from Fig. 5-2 and is

$$\Delta S_f = \frac{114.5 (s^2 + \frac{81.65}{V_f} s + 17.95)}{s^2 (s^2 + \frac{156.2}{V_f} s + \frac{6045}{V_f^2} + 25.5)} \delta_w \quad (5-2)$$

Here, C_f and C_r are equal to the nominal values specified in Table 5-1.

The discrete-time equivalent of the cascade combination of Eqns. (5-1) and (5-2) is

TABLE 5-1

Parameter Values Selected for Instrumented Plymouth Sedan

<u>Symbol</u>	<u>Definition</u>	<u>Value</u>
M	Total mass of vehicle	2168.00 kg
a	Distance from cg to front axle	1.40 m
b	Distance from cg to rear axle	1.55 m
A_1	Distance from cg to sensor location	3.00 m
I	Moment of inertia about vertical axis	5360 m N-s ²
c	Distance from cg to wind force center	0.70 m
C_f	Linearized cornering rate of front tires	46,000 N/rad
C_r	Linearized cornering rate of rear tires	44,000 N/rad
M_s	Sprung mass of vehicle	1950 kg
h	Vertical distance between sprung and unsprung mass centers	0.6 m
L_ϕ	Roll stiffness	25,000 Nm/rad
ϵ_r	Rear roll steer rate	0.2 rad/rad
Y_ϕ	Lateral force increment due to camber changes of the wheels which occur at the front suspension and the roll steering angle of the rear suspension.	3000 N/rad

$$\Delta S_f(z) = \frac{z-1}{z} \left[\frac{AT^2 z(z+1)}{2(z-1)^3} + \frac{BTz}{(z-1)^2} + \frac{Cz}{(z-1)} + \frac{Dz}{z-e^{-14.2T}} + \frac{F(z^2 - ze^{-aT} \cos \omega t) + G Ze^{-at} \sin \omega t}{z^2 - 2ze^{-aT} \cos \omega t + e^{-2aT}} \right]$$

where

$$A = \frac{165}{K_1},$$

$$B = \frac{.64734 \left[\frac{1159.43 K_1}{V_f} - 254.89 K_1 - \frac{3.98 \times 10^4}{V_f} \right]}{K_1^2},$$

$$C = .6473 \left\{ 28.4 K_1 + \frac{1159.43 K_1}{V_f} + \frac{1.811 \times 10^5}{V_f} \right\} K_1^2$$

$$- \left\{ \frac{81.65 K_1}{V_f} - 17.95 K_1 + \frac{2.8038 \times 10^3}{V_f} \right\}$$

$$\times \frac{(28.4 K_1 + 2 K_1^2)}{201 K_1^4},$$

$$D = \frac{10.013 - \frac{52.87}{V_f}}{(227.19 + \frac{6045}{V_f^2} - \frac{2218}{V_f})},$$

$$F = -(C + D),$$

$$G = -\left(\frac{156.2}{V_f} (D + C) + 14.2 (C + E) + B\right),$$

$$a = \frac{78.1}{V_f},$$

$$\omega = 25.55 - \frac{54.61}{V_f^2},$$

and

$$K_1 = \frac{6045}{V_f^2} + 25.55.$$

This can be reduced to the form

$$\frac{\Delta S_f(z)}{E_i(z)} = \frac{A_3 z^3 + A_2 z^2 + A_1 z + A_0}{(z-1)^2 (z-e^{-14.2T}) (z^2 - 2ze^{-aT} \cos \omega t + e^{-2aT})}. \quad (5-3)$$

Two discrete-time approaches may be used to compensate for changes in velocity. The first involves designing an inverse compensation to cancel velocity-dependent poles and zeros in Eqn. (5-3) and to replace these with corresponding velocity-independent quantities. The cancellation of such poles and zeros involves many

multiplications and divisions, and the evaluation of complex, velocity-dependent functions like e^x , $\sin x$, and $\cos x$. In a real-time environment, these complex computations would result in an increase in both the transport delay and the greatest lower bound on the sampling time. The result is detrimental to stability and, to compensate for this, a fast and therefore expensive system is required.

A second approach involves simulating a continuous-time compensator with discrete elements. Thus, an inverse compensator of the form

$$G_V(s) = \frac{s^2 + 2as + a^2 + b^2}{s^2 + \frac{81.65}{V_f}s + 17.95} \times \frac{s^2 + \frac{156.2}{V_f}s + \frac{6045}{V_f^2} + 25.55}{s^2 + 2hs + h^2 + K^2} \quad (5-4)$$

can be used to cancel the velocity-dependent poles and zeros of Eqn (5-2). Here a , b , h and K are design parameters which affect both the stability of the system and the damping. The values chosen here were the same as those employed by Cormier

[44] and were as follows:

$$a = 3, \quad b = 2, \quad h = 12, \quad K = 0$$

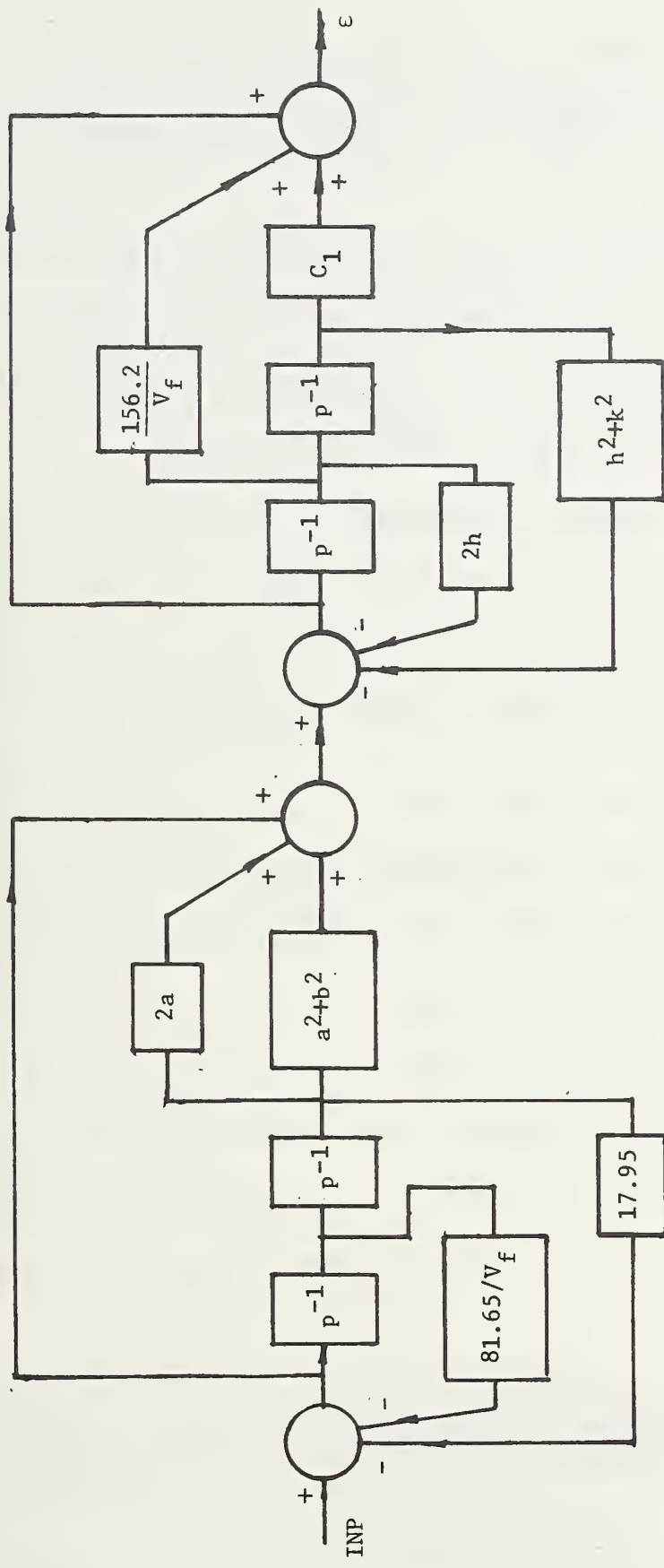
A block diagram of this continuous-time compensator is shown in Fig. 5-3. If each integrator were replaced by a discrete-time equivalent unit, the resulting structure could be easily realized on a microprocessor. If a good simulation of the continuous-time compensator were achieved, system response would be nominally independent of velocity.

Fewer computations are involved than in the previous approach, and thus transport delay and the greatest-lower bound on sampling time can be reduced. Also, the computations can be easily performed on slow machines like microprocessors and this decreases system cost. For these reasons, the second approach was used to compensate for velocity dependence in this study.

C. Compensator Realization

The discrete approximation selected to replace each integration term in Eqn. (5-4) (or Fig. 5-3) must be selected so that the following requirements are satisfied:

- i) The continuous-time transfer function should be accurately approximated so that a good system response is obtained.



Note: $C_1 = 25.55 + 6045/V_f^2$

Fig. 5-3. Block diagram of inverse compensator.

- ii) The sampling frequency is sufficiently small so that adequate time is available for processor computations;
- iii) These computations must be few and uncomplicated (e.g., no computation of transcendental functions) so that an inexpensive processor can be employed.
- iv) Transport delay² should be minimized.
- v) The smallest feasible word length should be used for representing internal variables and coefficients. (Increased word length requires either greater computation time or the use of a more complex processor.)

Four integration approximators were selected and evaluated against these criteria. Subsequently, it was noted that the use of a second-order approximator (e.g., one derived from Simpson's approximation) resulted in an eighth-order, discrete transfer function which involved an excessive number of somewhat complex online computations; therefore, such approximators were not considered further. In contrast, the use of a first-order approximator resulted in a fourth-order transfer function and a lesser

²

In a discrete-time system, transport delay is the time from the input being sampled to the output being changed. This delay arises due to computation time and adversely affects stability.

number of simpler computations.

The trapezoidal approximator, which has the input/output characteristic

$$\frac{T}{2} \frac{E+1}{E-1} ,$$

was selected for this study.³ Here, T is the sampling period and E is the advance operator.

On replacing s by $\frac{2}{T} \frac{E-1}{E+1}$ in Eqn. (5-4), there results

$$G_V(E) = \frac{E^2(4+2TK_2 + T^2K_1) + E[-8 + 2T^2K_1] + [4-2TK_2 + T^2K_1]}{E^2(2+12T)^2 + 2E(12T+2)(12T-2) + (12T-2)^2} \times$$

$$\frac{E^2[4 + 12T + 13T^2] + E[-8 + 26T^2] + 4[-12T + 13T^2]}{E^2[4 + 2TK_3 + 17.95T^2] + E[-8 + 35.9T^2] + [4 - 2TK_3 + 17.95T^2]} ,$$

(5-5)

where

$$K_1 = \frac{6045}{V_f^2} + 25.5, \quad K_2 = \frac{156.2}{V_f}, \quad \text{and}$$

$$K_3 = \frac{81.65}{V_f} .$$

³

A detailed description of the evaluation process is contained in Reference [45].

This equation can be readily converted to a state-variable form which is especially convenient for a digital-computer implementation. This was accomplished by using the direct-programming approach, as it resulted in a minimal number of calculations.

In essence, $G_V(E)$ was considered as being comprised of two stages; i.e.,

$$G_V(E) = G_{V1}(E) G_{V2}(E) = \frac{E_i(k)}{INP(k)} .$$

Two state variables, $X_6(k)$ and $X_7(k)$, are used to represent the first stage which has the input $INP(k)$ and the output $OUT_8(k)$. Correspondingly, $X_8(k)$ and $X_9(k)$ are employed in the second stage which has the input $OUT_8(k)$ and the output $E_i(k)$. The latter signal should be recognized as the actuator input. The resulting formulation is as follows:

$$\begin{aligned} X_6(k+1) &= E[X_6(k)] = X_7(k) , \\ X_7(k+1) &= E[X_7(k)] = [INP(k)a_1x_7(k) - a_2X_6(k)]/a_3 , \\ OUT_8(k) &= b_1X_7(k+1) + b_2X_7(k) + b_3X_6(k) , \end{aligned} \tag{5-6}$$

$$\begin{aligned} X_8(k+1) &= E[X_8(k)] = X_9(k) , \\ X_9(k+1) &= E[X_9(k)] = [OUT_8(k) - C_1X_9(k) - C_2X_8(k)]/C_3 , \end{aligned}$$

and

$$E_i(k) = d_1X_9(k+1) + d_2X_9(k) + d_3X_8(k) .$$

The quantities a_1 , a_2 , a_3 , b_1 , b_2 , b_3 , c_1 , c_2 , c_3 and d_1 , d_2 , and d_3 are shown in Table 5-2.

D. Selection of T and Word Length

The effects of different selections for both T and word length (I) was evaluated by employing a C.S.M.P.⁴ simulation of the system shown in Fig. 5-1. The compensation selected was comprised of a discrete part (Eqn. 5-6) in cascade with the analog lead-lag term,

$$1.05 \frac{s + 0.5}{s} \frac{s + 5.2}{s + 15.3} \quad (5-7)$$

The detector gain was selected as 35 and the loop gain as 2900. These choices were the same as those previously employed in the development of the analog, velocity-adaptive controller [44].

The simulated system was excited with a step input and the response $\Delta S_f(t)$ was recorded. Responses were obtained for T ranging from 5 to 100 ms and V_f from 10 to 40 m/s. Initially, no restriction was placed on the word length representing the state variables and coefficients (i.e., $I \rightarrow \infty$).

4

The Continuous System Modeling Program (C.S.M.P.) was developed by IBM to model both continuous- and discrete-time systems.

TABLE 5-2

Definition of Parameters

Parameter	Definition
a_1	$2(2 + 12T)(2 - 12T)$
a_2	$-(12T - 2)^2$
a_3	1
b_1	$4 + 2TK_2 + K_1T^2$
b_2	$2T^2K_1 - 8$
b_3	$4 - 2TK_2 + T^2K_1$
c_1	$8 - 35.9T^2$
c_2	$2TK_3 - 4 - 17.95T^2$
c_3	$4 + 2TK_3 + 17.95T^2$
d_1	$4 + 12T + 13T^2$
d_2	$-8 + 26T$
d_3	$4(-12T + 13T^2)$

The results are shown in Figs. 5-4 to 5-7. The response for $T = 100$ ms is highly velocity dependent with an overshoot of approximately 75% at all speeds. At $T = 70$ ms, the response is essentially velocity independent, and the overshoot is some 30%. The responses for 50 ms, and 25 ms are virtually identical; i.e., there is little velocity dependence and the overshoot is 20%. The

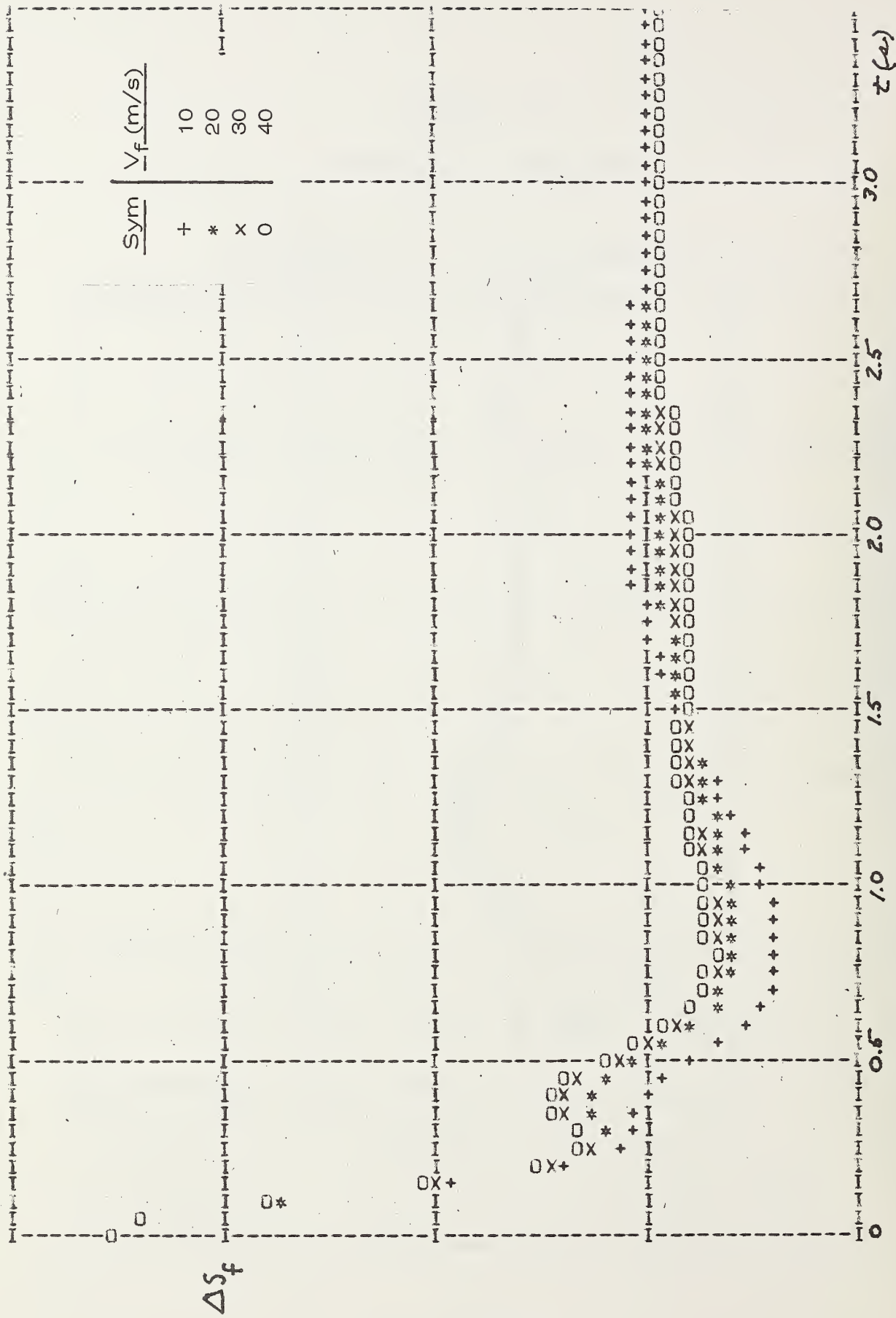


Fig. 5-5. ΔS_f vs. t for $T = 70$ ms, $I \rightarrow \infty$ and 4 values of V_f .

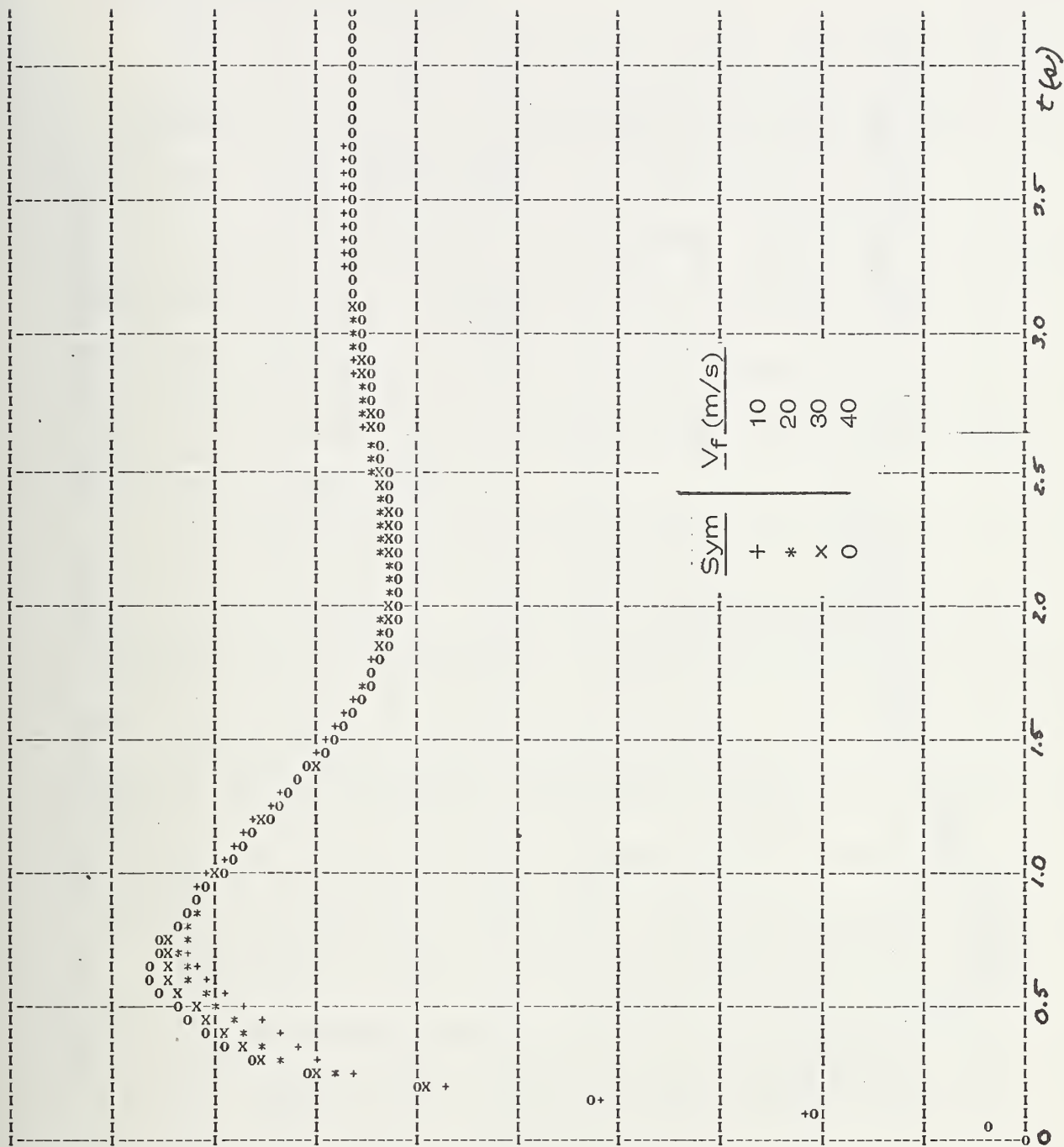


Fig. 5-6. ΔS_f vs. t for $T = 50 \text{ ms}$, $I \rightarrow \infty$, and 4 values of V_f .

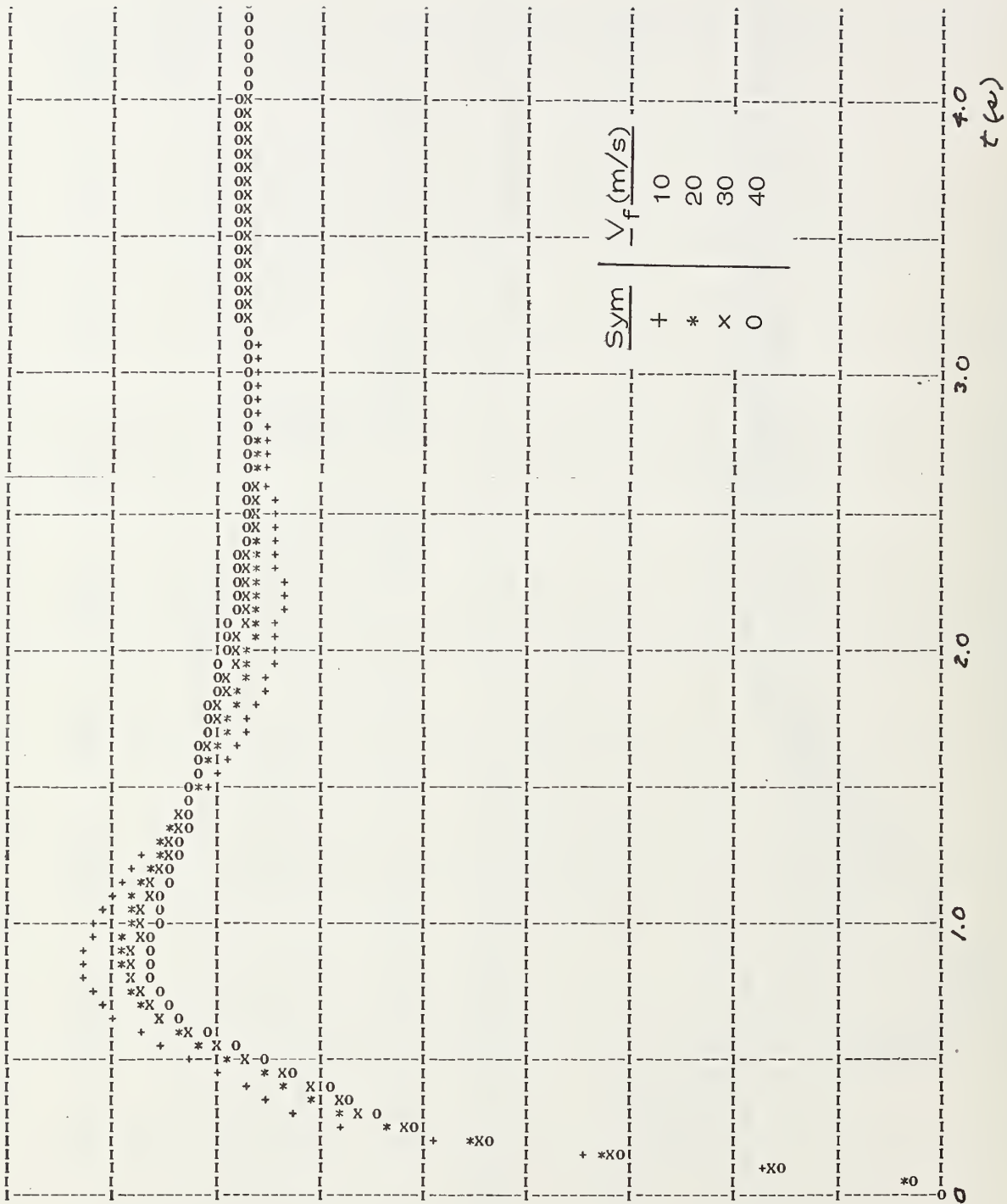


Fig. 5-7. ΔS_f vs. t for $T = 25$ ms, $I \rightarrow \infty$, and 4 values of V_f .

latter results are similar to those previously obtained using a continuous-time compensator.

The word lengths evaluated were 8, 16, and 32 bits as most microprocessors handle 8- or 16-bit data. All variables and coefficients were represented in a fixed-point form, as this results in a smaller number of computational steps relative to a floating-point choice. In essence, after a computation was made, the derived quantity was rounded off. Here again, the evaluation was made by considering the response ($\Delta S_f(t)$ vs. t) of the closed-loop system to step inputs.

The results are shown in Figs. 5-8 to 5-9. When $I = 8$ and $J = 4$ (J is employed to denote the fractional part of a word), a choice of $T = 75$ ms results in a considerably degraded response with respect to the unlimited word-length case; i.e., it is velocity dependent with an overshoot of some 50%.⁵ When T was further decreased, the responses were increasingly velocity dependent. In essence, no satisfactory choice of T resulted by choosing $I = 8$.

A choice of $I = 16$ ($J = 8, 9, 10$) results in step responses that were quite similar to those for $I = \infty$ provided $20 < T < 50$ ms (e.g., see Fig. 5-9). However, when T was decreased to

5

As T is decreased, the quantities a_1, a_2, \dots, d_4 generally decrease in magnitude. Hence for I and J fixed, the accuracy with which these quantities are represented becomes poorer and a degraded response results.

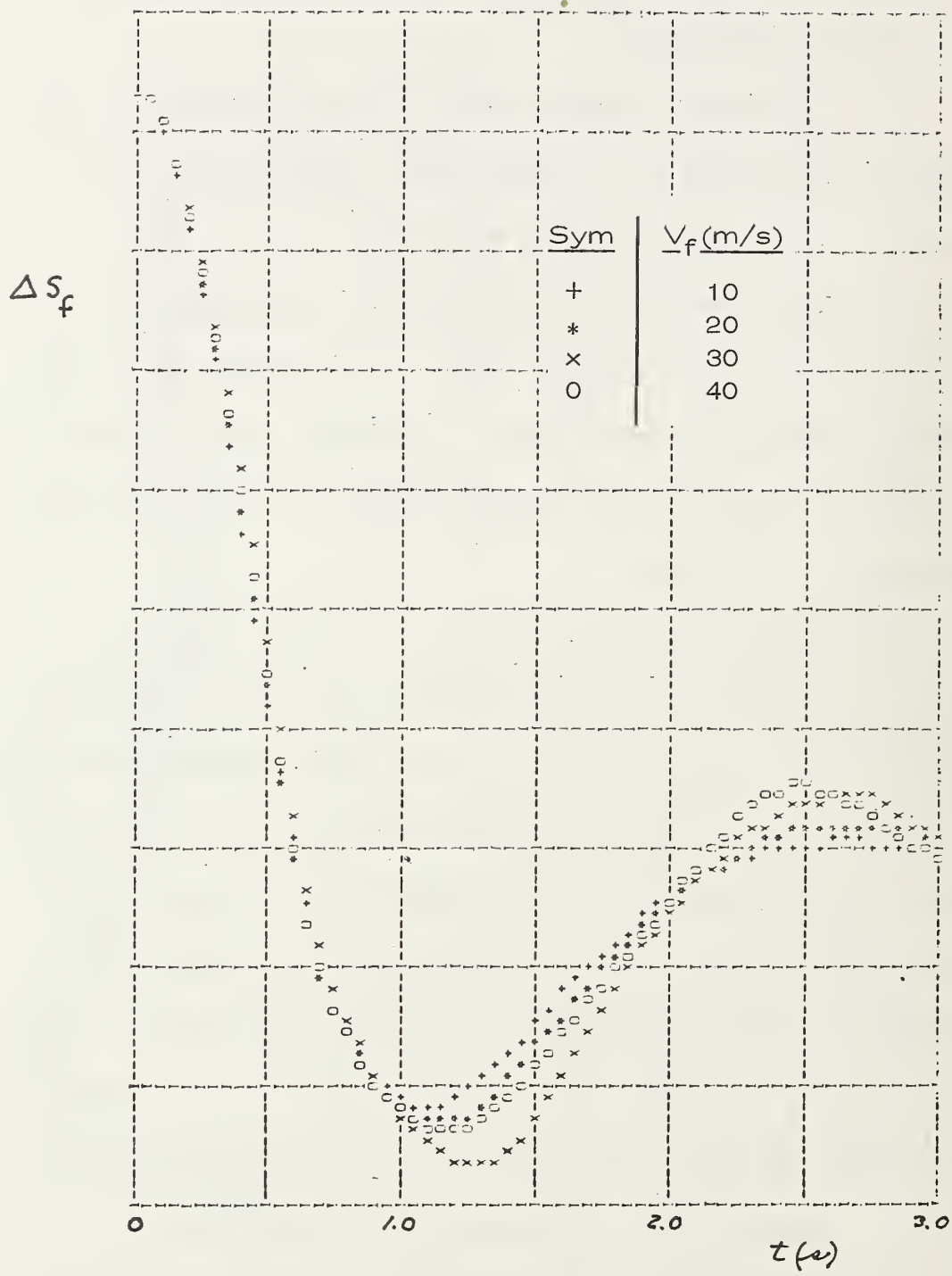


Fig. 5-8. ΔS_f vs. t for $T = 75$ ms, $I = 8$ ($J = 4$), and four values of V_f .

ΔS_f

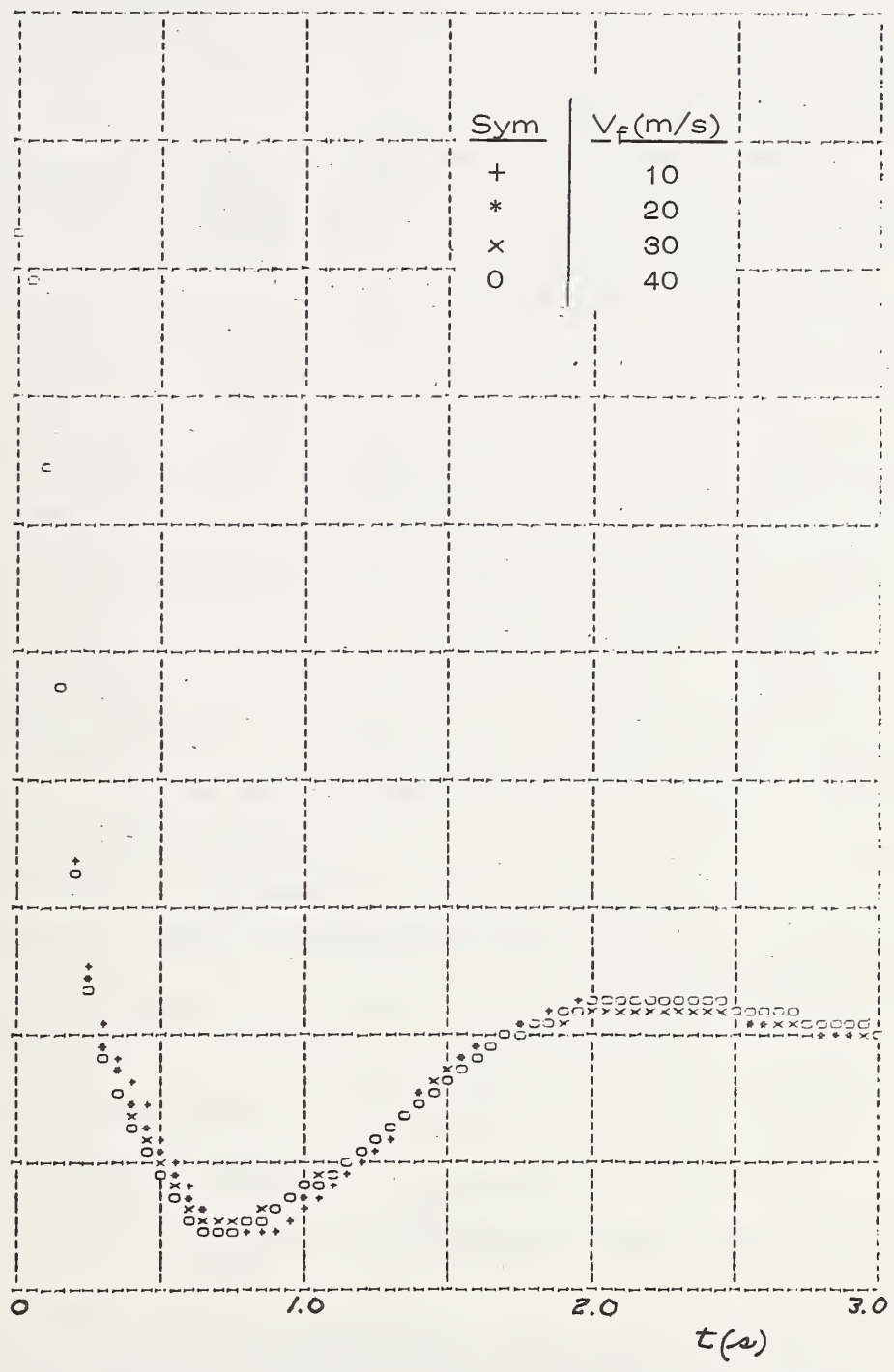


Fig. 5-9. ΔS_f vs. t for $T = 50$ ms, $I = 16$ ($J = 9$), and four values of V_f .

5 ms, the response was quite velocity dependent. The responses for $I = 32$ with $J = 16$ were quite similar to those for $I = \infty$ for all values of T considered.

These results were evaluated in terms of the criteria listed in Section C, and T and I were selected as 50 ms and 16 bits (with $J = 8$), respectively. The computations involved in realizing Eqn. (5-5) involve some 10 divisions and 20 multiplications of 16-bit operands. If an 8-bit machine were employed, these computations could not be completed in 50 ms unless a hardware multiplier were used. It is less expensive to employ a 16-bit machine with built-in, fast multiply-and-divide instructions. This conclusion resulted in the selection of an INTEL 8086-based microcomputer. This was realized by constructing a commercially available SDK-86 Design Kit and interfacing it with appropriate A/D and D/A converters as is described in detail in Appendix C. The developed software, which realized the lead-lag compensation,

$$G(E) = 0.75 \left[1 + \frac{0.0151_H}{E-1} \right] \left[\frac{1 - \frac{0.1_H}{E - 0.7FFF_H}}{E - 0.7FFF_H} \right] G_V(E) , \quad (5-8)$$

is documented in Reference [45].⁶

⁶ The transfer function $G(E)$ corresponds to a discrete equivalent of Eqn (5-7) in cascade with $G_V(E)$ as given by Eqn. (5-5). The former was an "exact" realization, while the latter involved a trapezoidal approximation for integrators.

E. Simulation Studies

The closed-loop system employed for the simulation studies is shown in Fig. 5-10. The compensation (Eqn. 5-8) was realized on the SDK-86, and the remaining components were simulated on an analog computer. The lateral position sensors were represented by a gain of 35, the actuator by Eqn.(5-1), and the lateral dynamics were obtained from the model shown in Fig. 5-2.

The system input V_r represented the desired lateral position of the vehicle relative to lane center (in subsequent, full-scale tests $V_r = 0$ corresponded to a desired vehicle position directly over the lane-centered, lateral reference). A second input $\dot{\psi}_D$ corresponded to the desired yaw rate, while F_e was the corresponding superelevation force.

a) Velocity Independence

Command step changes in lateral position were simulated by switching in a voltage $V_r > 0$ for a fixed V_f . The responses obtained at each of 4 speeds are given in Fig. 5-11. Essentially the same response -- an overshoot of 45% and a response time of some 2s -- was obtained in each case.

b) Curve tracking

A superelevated curve was simulated by employing $\dot{\psi}_D$ and F_e inputs. The former was increased linearly from 0 to 0.134 rad/s, and thereafter was fixed at this value. F_e was

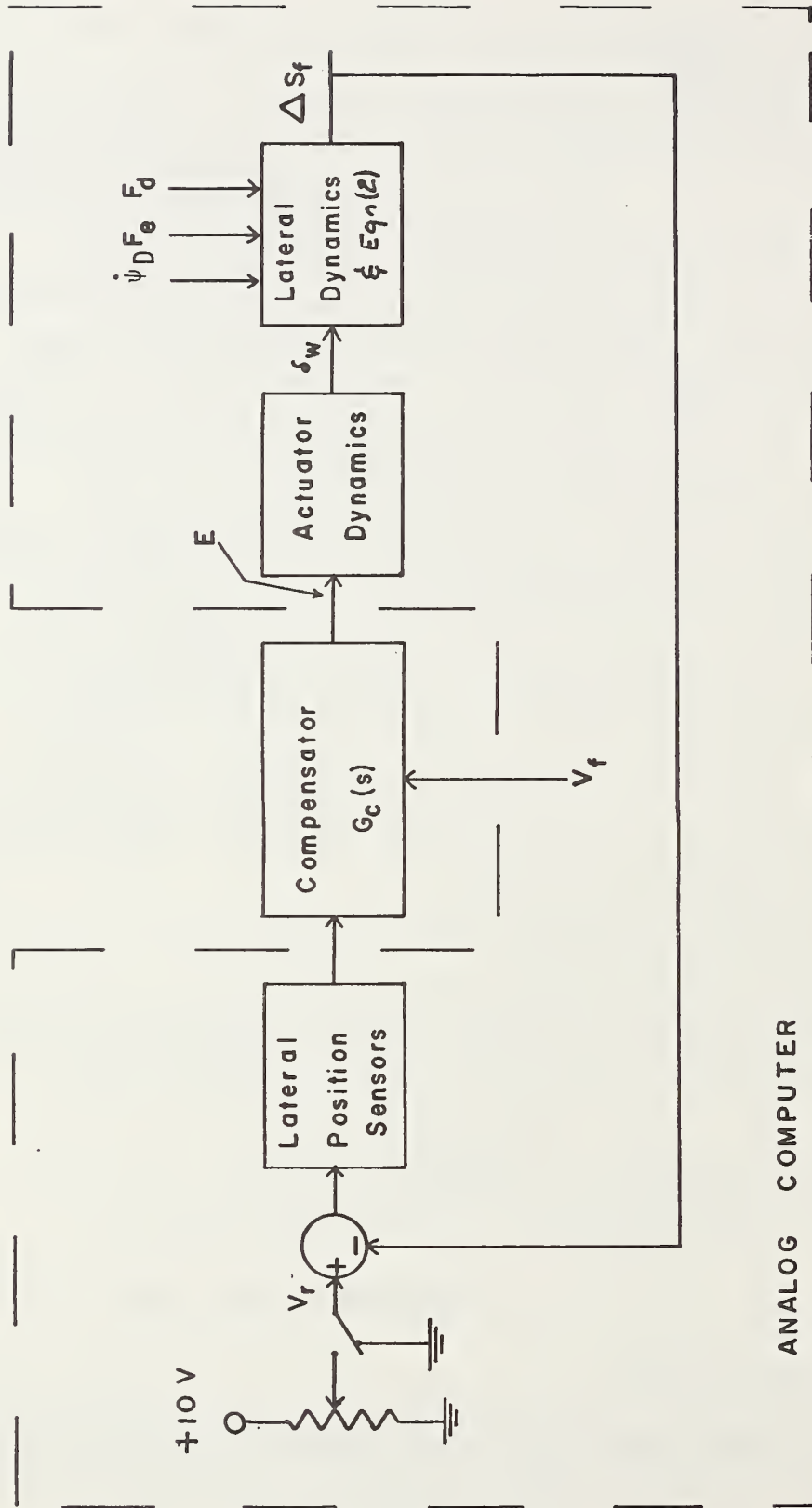


Fig. 5-10. Simulation Structure.

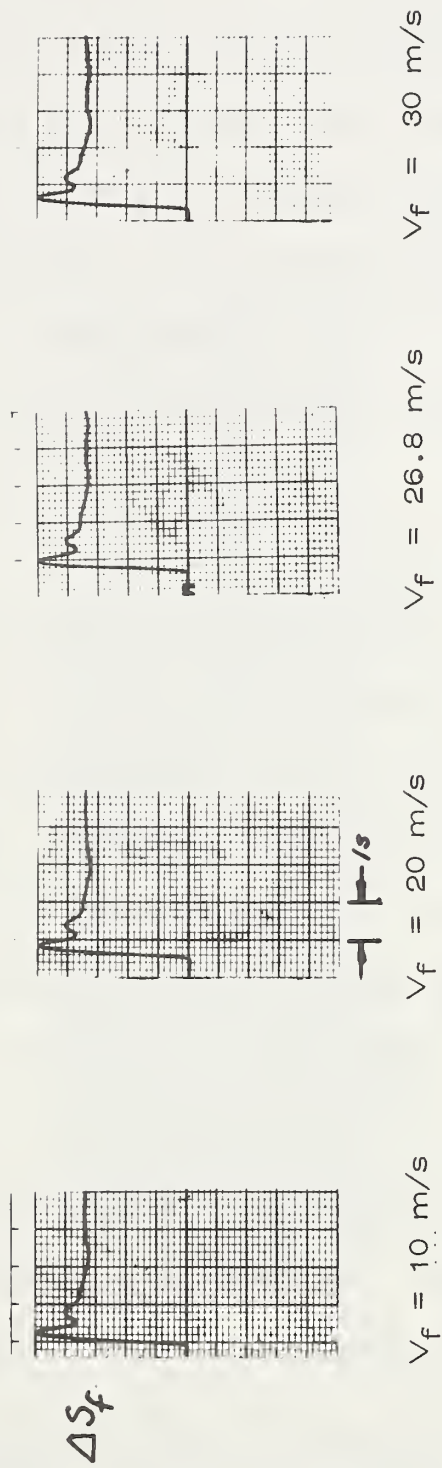


Fig. 5-11. Step responses (ΔS_f vs. t) at four speeds (simulation) .

directly proportional to $\dot{\psi}_D$ and reached a maximum of 1777N. This corresponded to a vehicle, traveling at $V_f = 13.4$ m/s, traversing a spiral transition into a 100-m radius curve.

The response, $\Delta S_f(t)$ versus t , is shown in Fig. 5-12. The quantity ΔS_f , which was initially zero, quickly built up to a peak value of 7 cm and then slowly decayed toward zero. This was essentially the response previously obtained with a corresponding controller.

c) Preview Information

If advance information about the location and radius of an upcoming curve were available, then E_i could be increased when the curve were reached. If this were done properly, it would prevent ΔS_f from significantly increasing. Then, the controller could be employed to traverse curves with smaller radii at higher speeds than might otherwise be practical.

Here, the microcomputer was provided with an advance indication of an upcoming curve and its radius (in this case, 100 m), and the system response ($\Delta S_f(t)$ versus t) was obtained at a speed of 13.4 m/s (see Fig. 5-13). Note that the peak deviation was only 1 cm -- a significant decrease over that shown in Fig. 5-12.⁷

⁷This experiment was not conducted under full-scale conditions as insufficient time was available to install the required roadway markers.

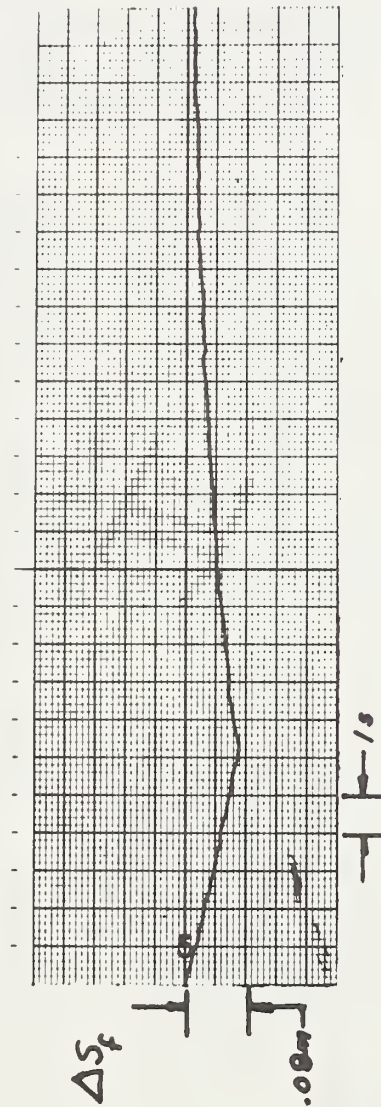


Fig. 5-12. Tracking performance on a curve with a 100-m radius and $V_f = 13.4$ m/s (simulation) .

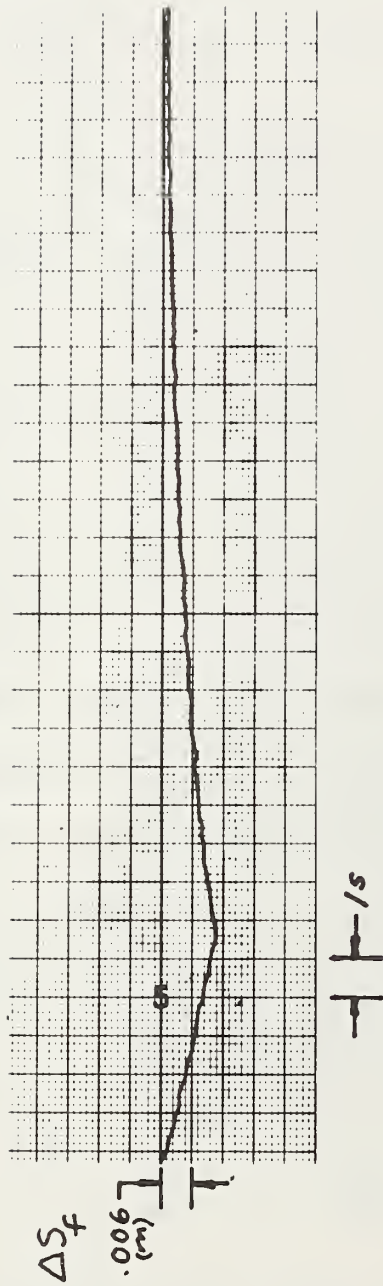


Fig. 5-13. Tracking performance on a curve with preview information ($R = 100$ m and $V_f = 13.4$ m/s).

d) Ride Quality

No attempt was made to evaluate ride quality during these studies. Ride comfort is affected by factors such as vehicle roll, engine vibrations, roadway irregularities and wind disturbances. Hence, it cannot be measured from a simple model in which these factors were largely ignored. Consequently, ride quality was evaluated only under full-scale conditions.

F. Full-Scale Studies

The microcomputer was installed in the 1965 Plymouth test vehicle, which was previously employed by Cormier [44], and the developed controller was tested at the Transportation Research Center of Ohio (TRCO) Skid-Pad Facility (see Fig. 2-6). The steering reference consisted of a single conductor buried 1.9 cm beneath the pavement and running longitudinally around the entire facility -- a distance of some 6400 m. This conductor was excited with a 2.5a (peak-to-peak), 600-Hz signal to produce the desired guidance field. The phase sensors developed by Olson [15] were employed to provide a discretized measurement of ΔS_f , which was the controller input.

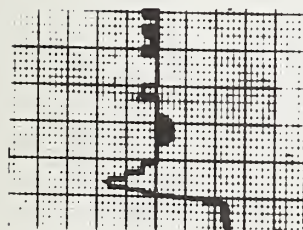
The collected data consisted of $\Delta S_f(t)$, the lateral accelerations at the vehicle's center of gravity and front center (i.e., $a_{cg}(t)$ and a_f , respectively), and rms estimates of these three quantities when appropriate.

a) Velocity Independence

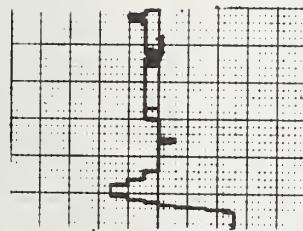
Command step changes in lateral position were obtained by summing a small voltage step with the signal feedback from the lateral-position sensors when the vehicle was traveling at a constant speed along a straight section of roadway. The results, $\Delta S_f(t)$ vs. t , for each of five speeds are shown in Fig. 5-14. First, it should be noted that consistent responses were obtained at each speed (i.e., an overshoot of some 45-50 % and a 1.5 - 2.0 s settling time); and second, that these responses approximate those obtained in the simulation study (see Fig. 5-11). Thus, at least insofar as control was concerned, the velocity dependence was greatly reduced by inverse compensation which lends credence to the validity of both the model employed, and the approximation of the continuous-time compensator.

b) Straight-Road Tracking

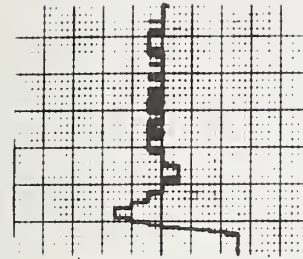
The tracking capabilities of the controller were evaluated on straight portions of the skid pad at various fixed speeds. Typical results (i.e., $\Delta S_f(t)$ vs. t), which are shown in Fig. 5-15, are excellent; e.g., the maximum tracking error for $V_f = 30$ m/s was less than 3.8 cm. The corresponding rms tracking error ranged from 0.5 cm at 5 m/s to 1.5 cm at 30 m/s. The corresponding values of $(a_{cg})_{rms}$ and $(a_f)_{rms}$ were 0.1 and 0.15 m/s^2 , respectively, at 5 m/s and 0.2 and 0.3 m/s^2 ,



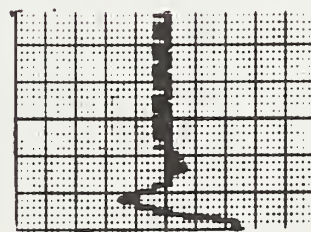
$V_f = 6.1 \text{ m/s}$



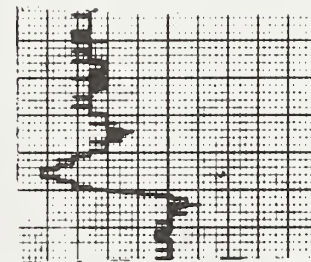
$V_f = 9.1 \text{ m/s}$



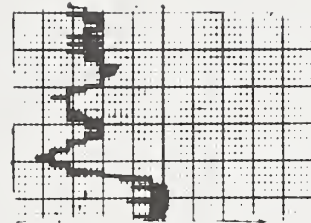
$V_f = 15.2$



$V_f = 21.3 \text{ m/s}$

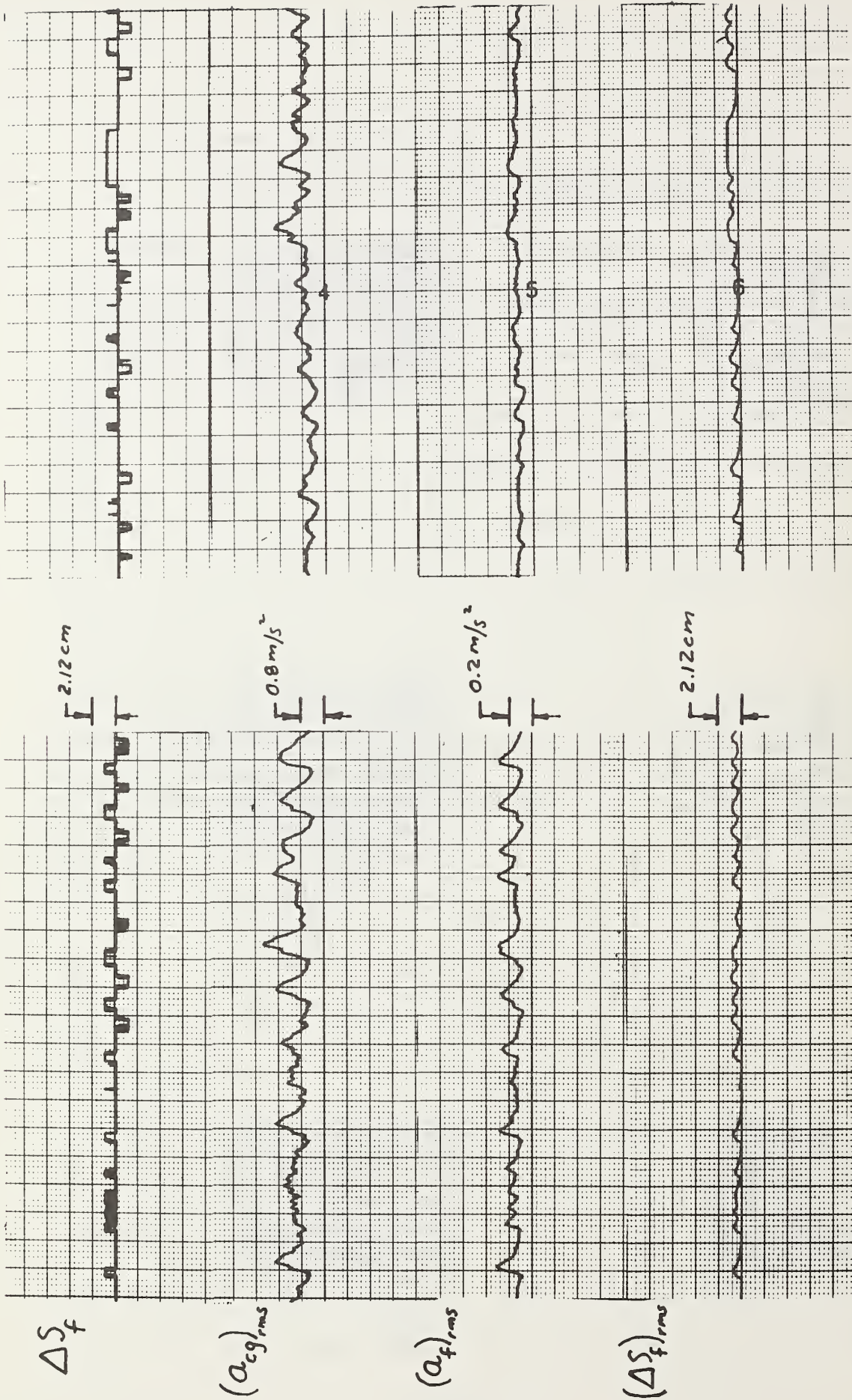


$V_f = 24.4 \text{ m/s}$



$V_f = 31 \text{ m/s}$

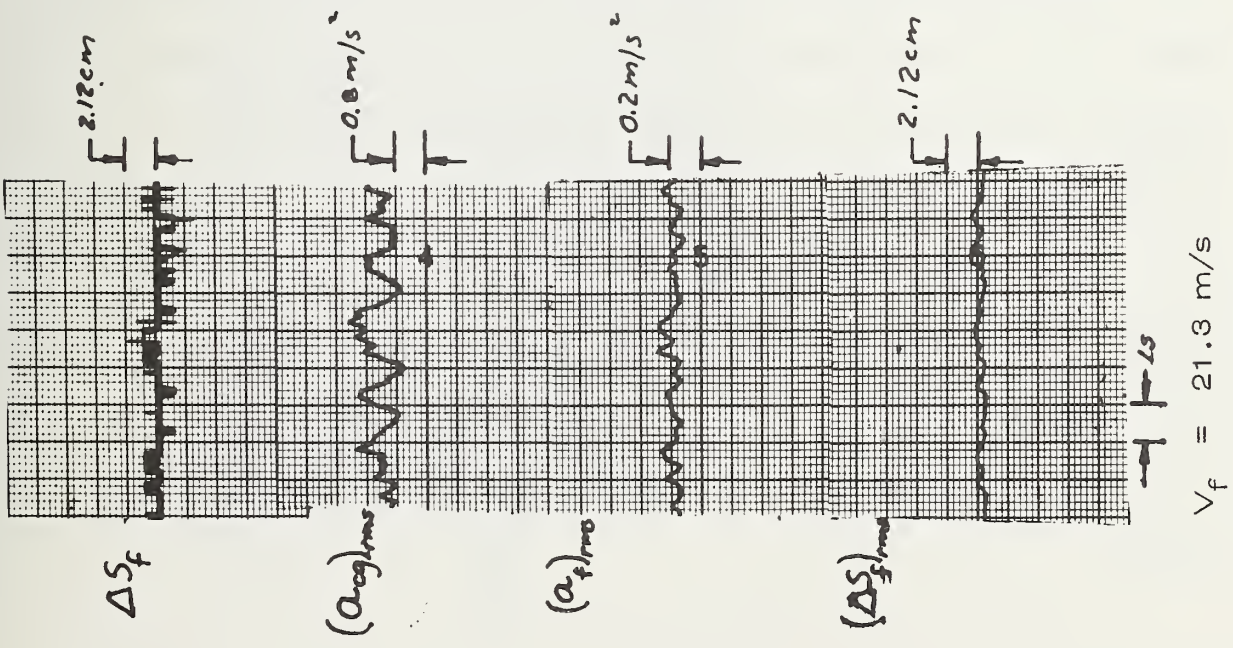
Fig. 5-14. Step responses (ΔS_f vs. t) for 6 speeds.



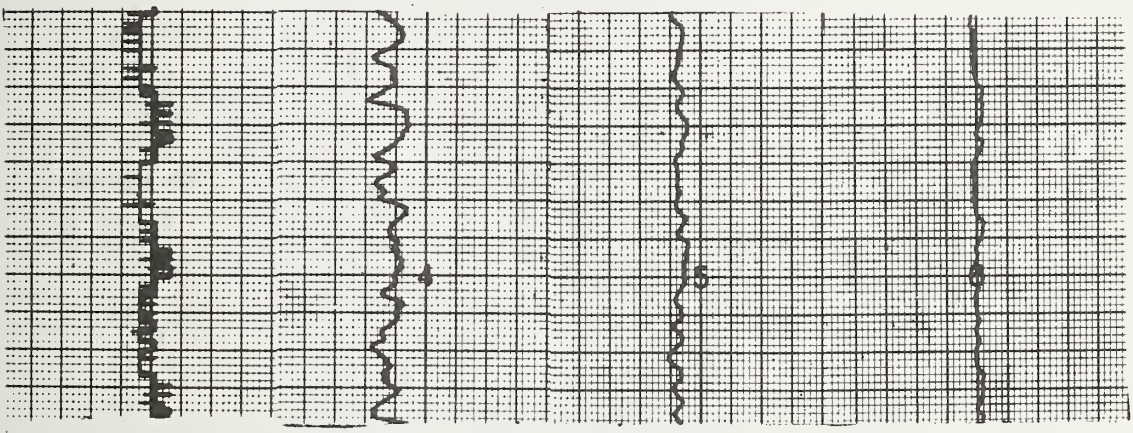
$V_f = 15.2 \text{ m/s}$

$V_f = 9.1 \text{ m/s}$

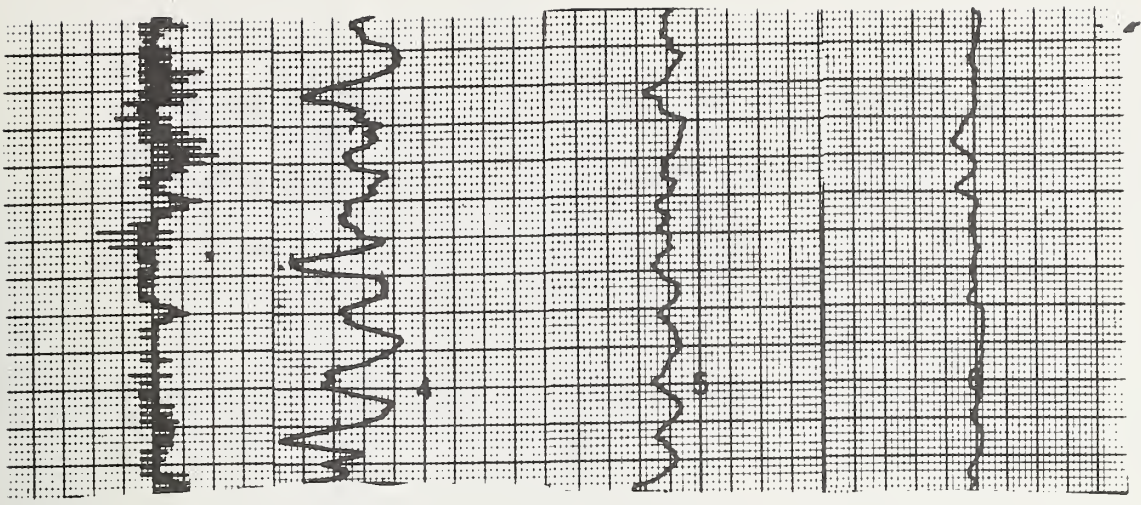
Fig. 5-15. Tracking performance on a straight roadway for 5 speeds (cont.).



$V_f = 21.3 \text{ m/s}$



$V_f = 28.2 \text{ m/s}$



$V_f = 31 \text{ m/s}$

Fig. 5.15 (cont.)

respectively at 30 m/s. These results are slightly higher than those obtained using the analog controller (see Appendix A); however, the ride quality was still characterized as excellent.

c) Curve Tracking

The tracking capabilities of the system, while negotiating one of the 100-m radius curves at TRCO at each of three speeds are illustrated in Figs. 5-16 and 5-17. Excellent tracking ($|\Delta S_f| < 2.5$ cm at 9 m/s, $|\Delta S_f| < 5$ cm at 13.4 m/s, and $|\Delta S_f| < 7.5$ cm at 17 m/s) was obtained together with a smooth, comfortable ride in all cases. Here again, the results are consistent with both those from the simulation study and those obtained using an all-analog controller.

G. Discussion

Clearly, excellent lateral control can be achieved by employing a microprocessor-based controller in a single-loop, position feedback configuration with inverse compensation. Since the microcomputer employed could be used effectively for other tasks (e.g., to monitor vital functions and to provide controller redundancy), it could provide a substantial improvement in onboard vehicle capabilities.

Some aspects which should be investigated in future studies include:

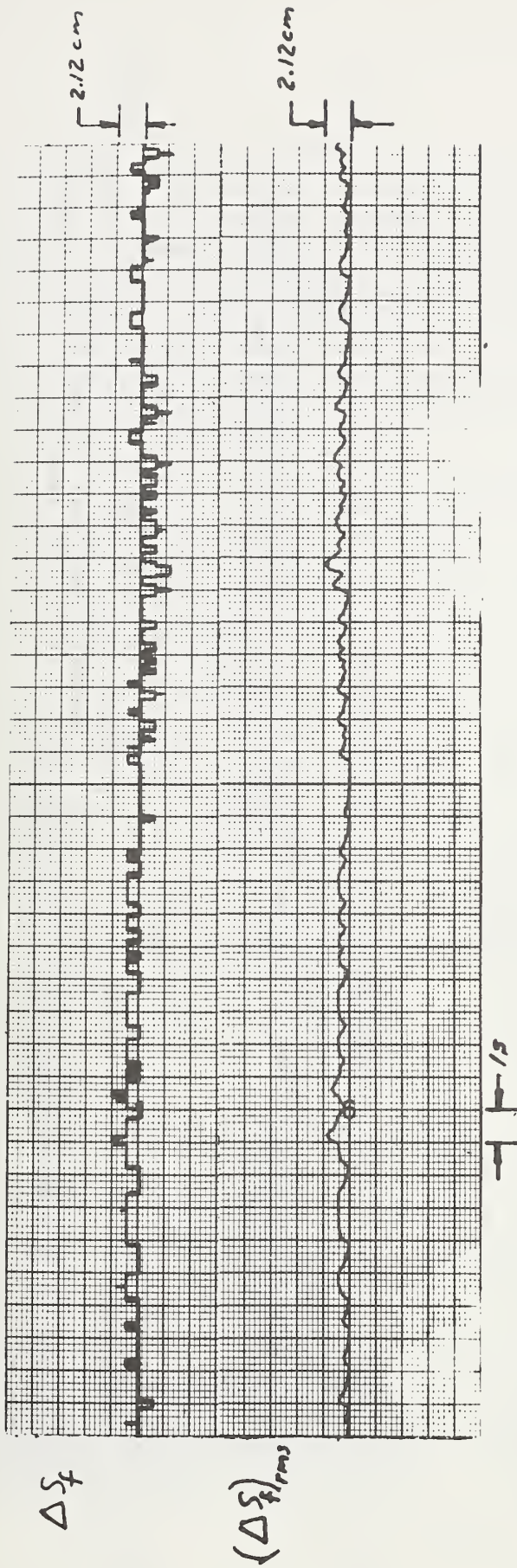
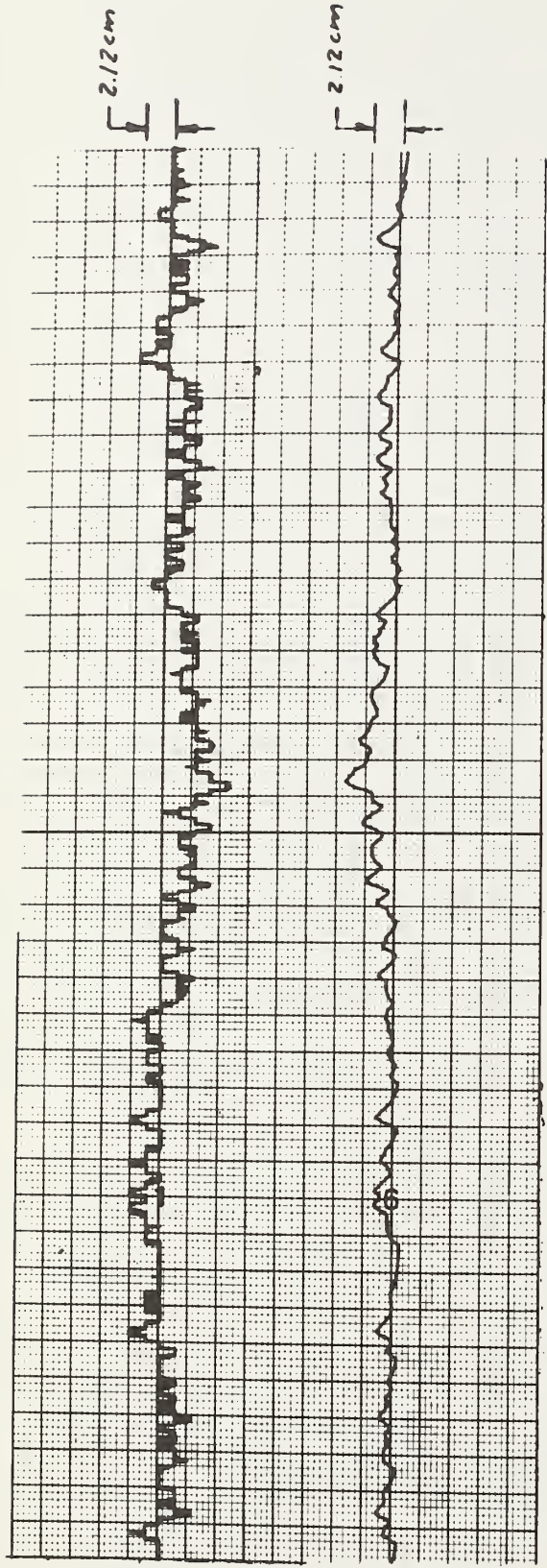
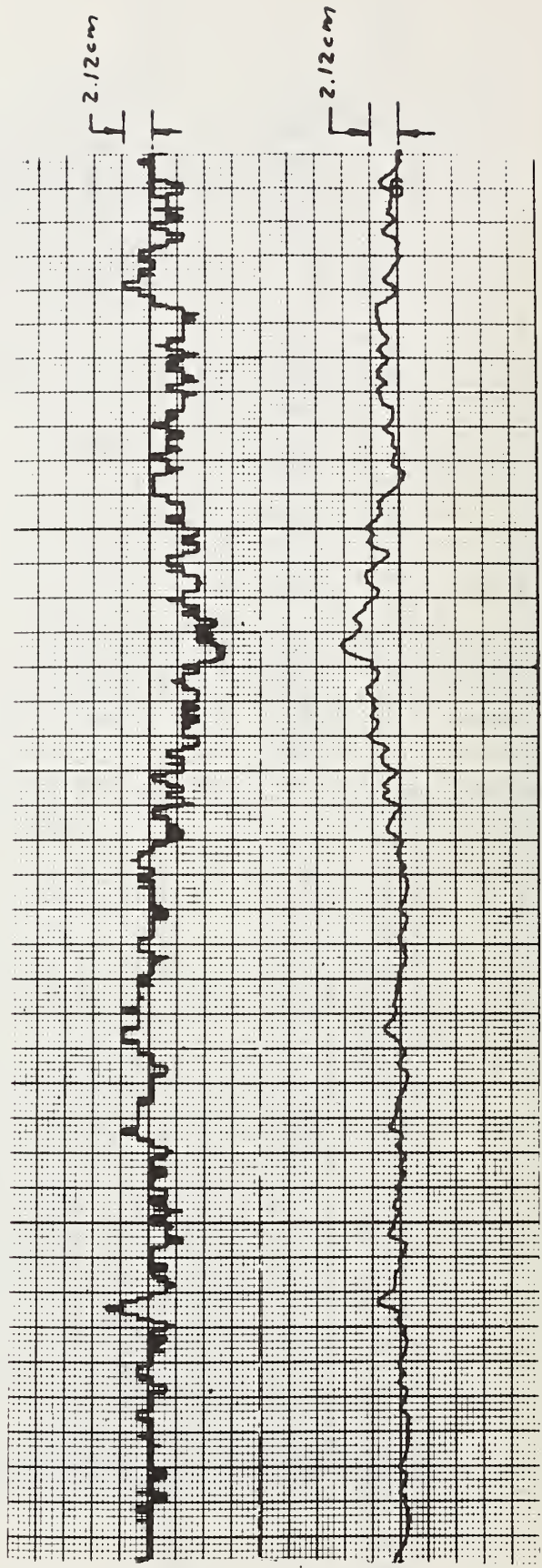


Fig. 5-16. Tracking performance on a 100-m radius curve for $V_f = 9$ m/s .



→ | ← / s

a) $V_f = 13.4 \text{ m/s}$



b) $V_f = 17 \text{ m/s}$

Fig. 5-17. Tracking performance on a 100-m radius curve for $V_f = 13.4$ and 17 m/s .

- i) The monitoring of system functions;
- ii) The development of fault-tolerant controllers to enhance system reliability; and
- iii) The development of a capability for a rapid response to emergencies.

The first of these would be easily accomplished as the available microcomputer has the necessary A/D converters available, and the required software development would be trivial.

Redundant electronics can be used to decrease the probability of controller failure. Such redundancy could involve the use of multiple processors performing the same calculations with software polling being employed to detect any processor failure. Also, since it is generally easier to detect and correct an error in a digital circuit than in an analog one, this may result in enhancing vehicle safety.

A microcomputer can be used as a source of vehicle-based intelligence and, in this role, would be especially useful in reducing the response time to emergencies.

In the application, lateral control, which was evaluated here, the processor was idle 90% of the time. Thus, it could easily accommodate a number of other duties.

CHAPTER VI

STUDIES IN VEHICLE LONGITUDINAL CONTROL

A. Overview of Previous Studies

Several tasks, which are important to the development of a longitudinal controller, are:

- i) The identification of the propulsion system dynamics;¹
- ii) The design of the controller; and
- iii) Its implementation and field evaluation.

Several approaches have been used to specify a propulsion system model that relates vehicle velocity to the throttle input. The U.S. automotive industry uses computer simulation models [46] - [48], which are based on the interpolation of steady-state operating data, to predict vehicle performance for specific driving schedules; however, the dynamic characteristics necessary for the design of a propulsion control system are not included in such models.

¹ Operations in which the brakes must be applied are not considered here. An earlier effort on this subject was discussed in Reference [21].

Many attempts have been made (e.g., [16 - 20, 35, 49 - 50]), to develop dynamical models of an internal-combustion engine, hydrodynamic torque converter, automatic transmission, drivetrain and vehicle combination. These models range in complexity from a first-order linear model, which relates throttle position (V_i) and vehicle velocity (V), to a multiple pole-zero model with state-dependent parameters.

One simple model, which was developed by Blackwell [49] using Newton's Second Law of Motion, is shown in Fig. 6-1. The vehicle time constant M/k_d associated with this model was excessively large relative to values obtained from field testing. This discrepancy was overcome by modifying the model to account for rotating inertias and velocity-dependent, tractive force characteristics. During subsequent field evaluation studies, it was found that uncontrollable factors such as air temperature and pressure, road surface conditions, and slight road grades resulted in erratic response data -- a condition which is not well-suited to the selection of adequate model parameters [51]. Two efforts were made to partially isolate the vehicles from such factors. First, Blackwell employed a chassis dynamometer with only modestly successful results. (The dynamometer provided an insufficient load for the powerful test vehicle -- a 1965 Plymouth sedan.) Second, the closed-loop velocity controller shown in

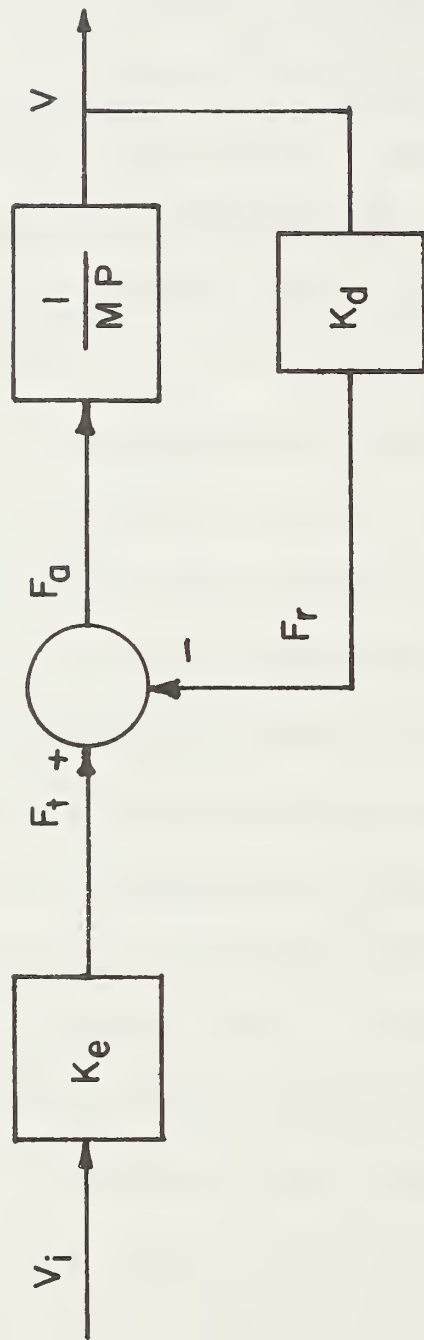


Fig. 6-1. One basic propulsion system model .

Fig. 6-2 was employed to obtain a model which was valid under small-signal, non-demanding conditions [51]. This controller, which employed internal velocity feedback to reduce the controller's susceptance to disturbances, was subsequently modified to a position controller by adding a position feedback loop and appropriate compensation [16]. This controller was employed in low-required acceleration, system entry operations.² Consistent performance was obtained with maximum offline position errors of 4.267 meters (14 feet) and position errors at point of entry of 0.366 meters (1.2 feet). When attempts were made to lessen these errors, degrading, higher-order effects, that weren't predictable with the simple model employed, limited the controller performance.

The requirement for better position control, without any degradation in ride comfort, led to the development of more complex models and corresponding controllers. Takasaki [50] developed a state-dependent model of the vehicle dynamics for small-signal conditions. Subsequently, this model was utilized to design the position controller shown in Fig. 6-3. that resulted in mainline position errors of less than 0.3048 meters (1 foot),

2

System-entry operations pertain to the accelerating of an initially stationary vehicle to mainline speed and its insertion into mainline traffic.

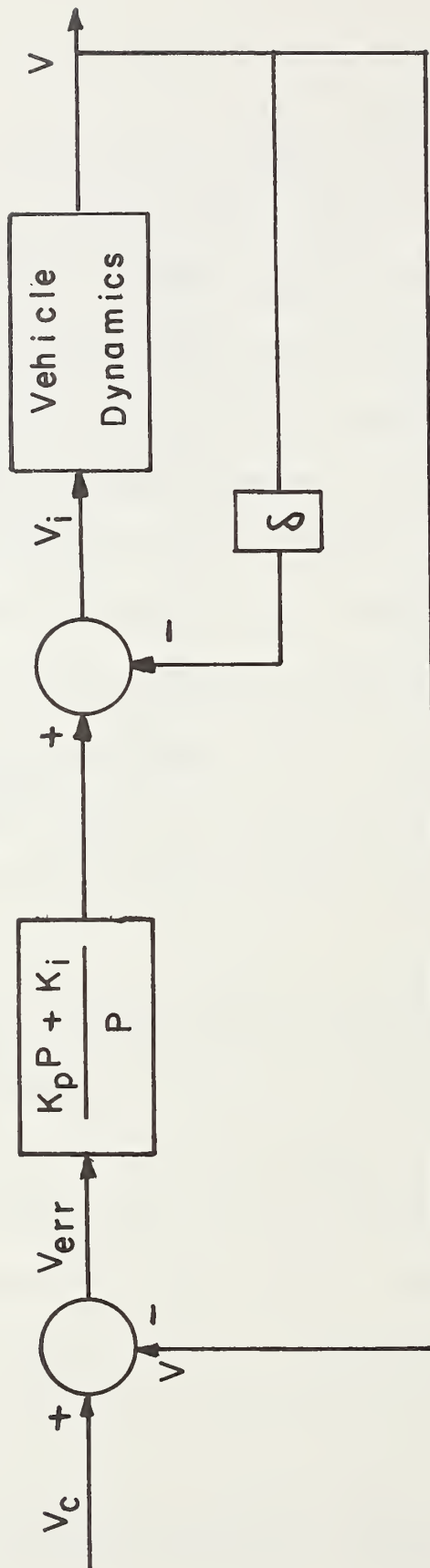


Fig. 6-2 : Small-signal linear velocity controller
with internal velocity feedback.

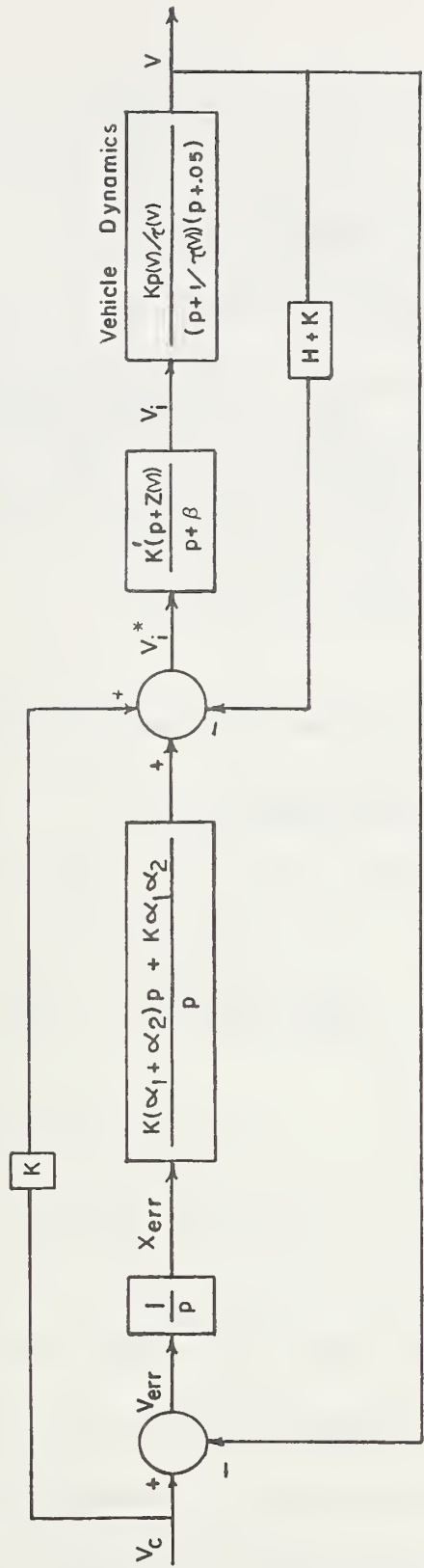


Fig. 6-3 : State-dependent controller / vehicle combination .

system entry, maximum-position errors of 0.366 meters (1.2 feet), and point-of-entry position errors of 0.122 meters (0.4 feet) [52]; however, these results could not be obtained consistently over a wide range of environmental conditions. Subsequently, more complex, state-dependent models were developed [35], [53]. Unfortunately, these models were inadequate to describe controlled vehicle performance -- especially for system entry operations over a wide range of environmental conditions.

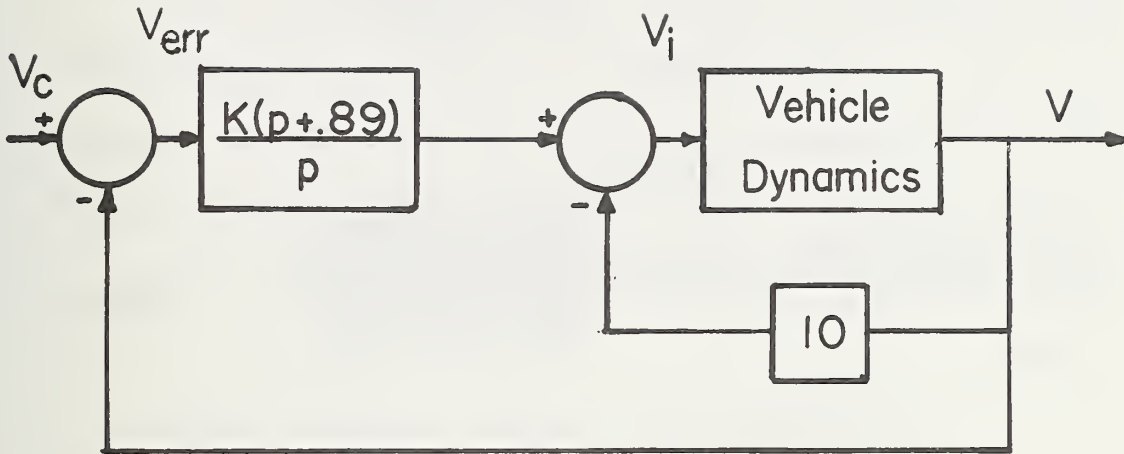
B. Controller Implementation

Extensive field testings were undertaken with the objective of either obtaining useful extensions to one or more of the above models so that higher-order effects, which have been heretofore ignored, could be accounted for in the controller design process, or an adequate new model. An initial step was the specification of some higher-order effects.

a) Limit-Cycle Data

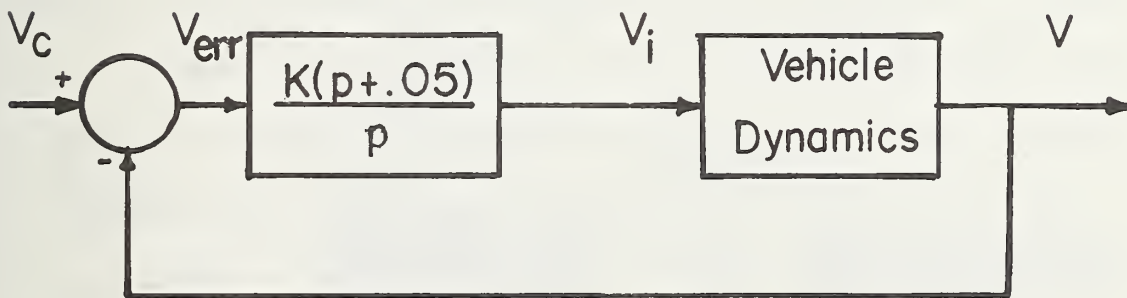
Two linear velocity controllers, hereafter referred to as System I and System II, are shown in Figs. 6-4a and 6-4b, respectively. These controllers were implemented on a 1969 Plymouth test vehicle, which had been used in earlier studies, and controller performance for fixed-gear, fixed-speed operation was observed over the speed range from 0-9.1 m/s. Typically, a limit cycle was present for each gear/speed combination. As

$K=23.8$



a) System I

$K=23.8$



b) System II

Fig. 6-4: Two linear velocity controllers .

an example, consider the data shown in Fig. 6-5 for first-gear operation with $V = 6.1$ m/s. The observed limit cycles are apparently due to nonlinearities in the drivetrain dynamics; i.e., high-frequency components which are present in the signal $V_{err} = V_c - V$ do not appear in the engine rpm (ω_{eng}) signal. (The quantity V_c is a command velocity signal and was constant for these tests.) The other data depicted in this figure are $V_i(t)$, the input to the carburetor, and P_{man} , the manifold pressure.

The state-dependent "position" controller depicted in Fig. 6-3 also exhibited limit cycles for constant-velocity operation.³ These oscillations for $V = 7.6$ m/s were comprised of a slowly varying component at 0.25 Hz and a periodically recurring unstable oscillation at 1.7 Hz (see Fig. 6-6). At 1.7 Hz this controller also has a stability problem while accelerating in first gear above 6.1 m/s (see Fig. 6-7). This is due to state-dependent terms in the vehicle dynamics that were not properly accounted for in either the model employed or in the controller design.

3

This controller was also implemented on the 1969 Plymouth sedan.

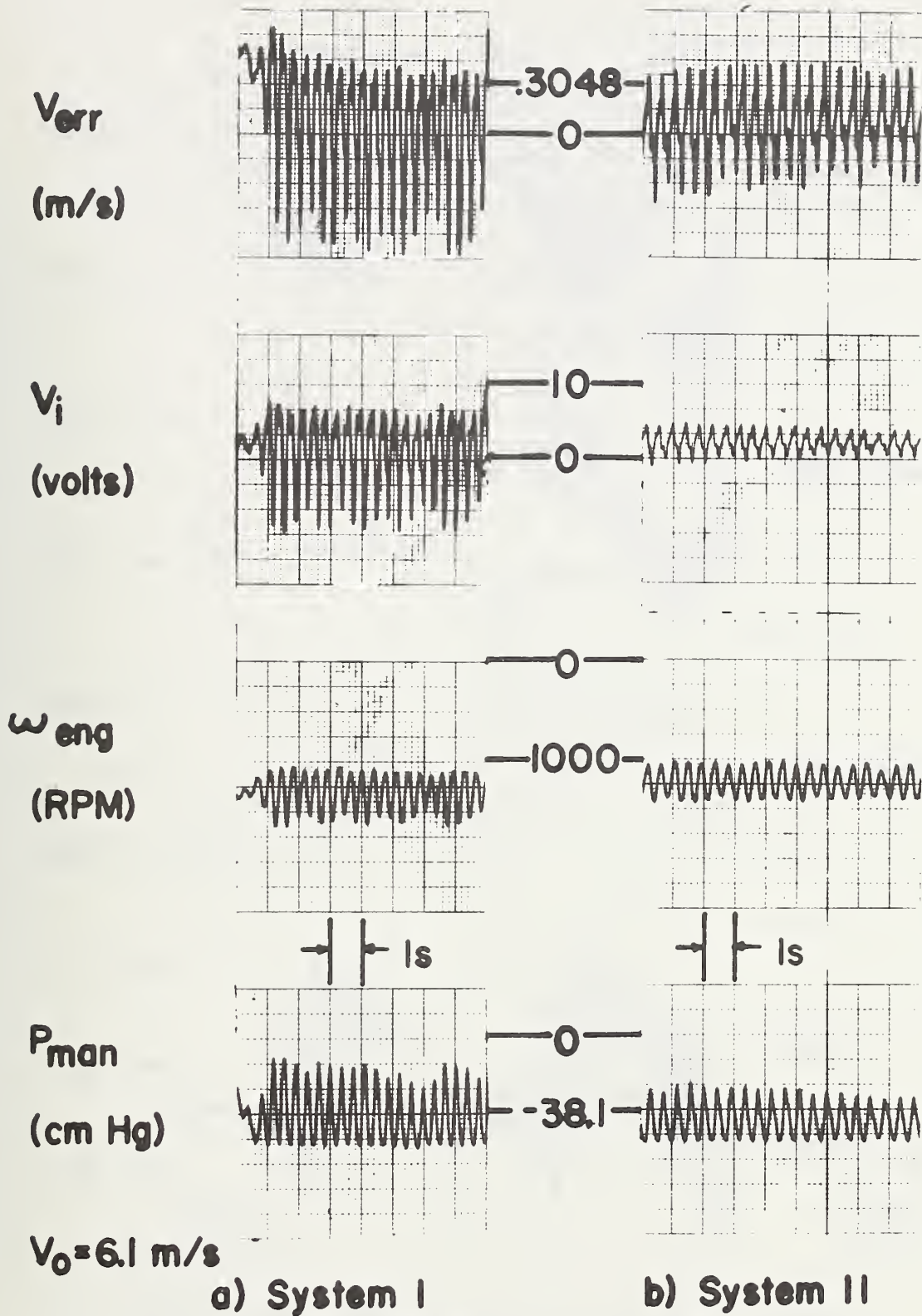


Fig. 6-5: 1st gear limit cycle data example .

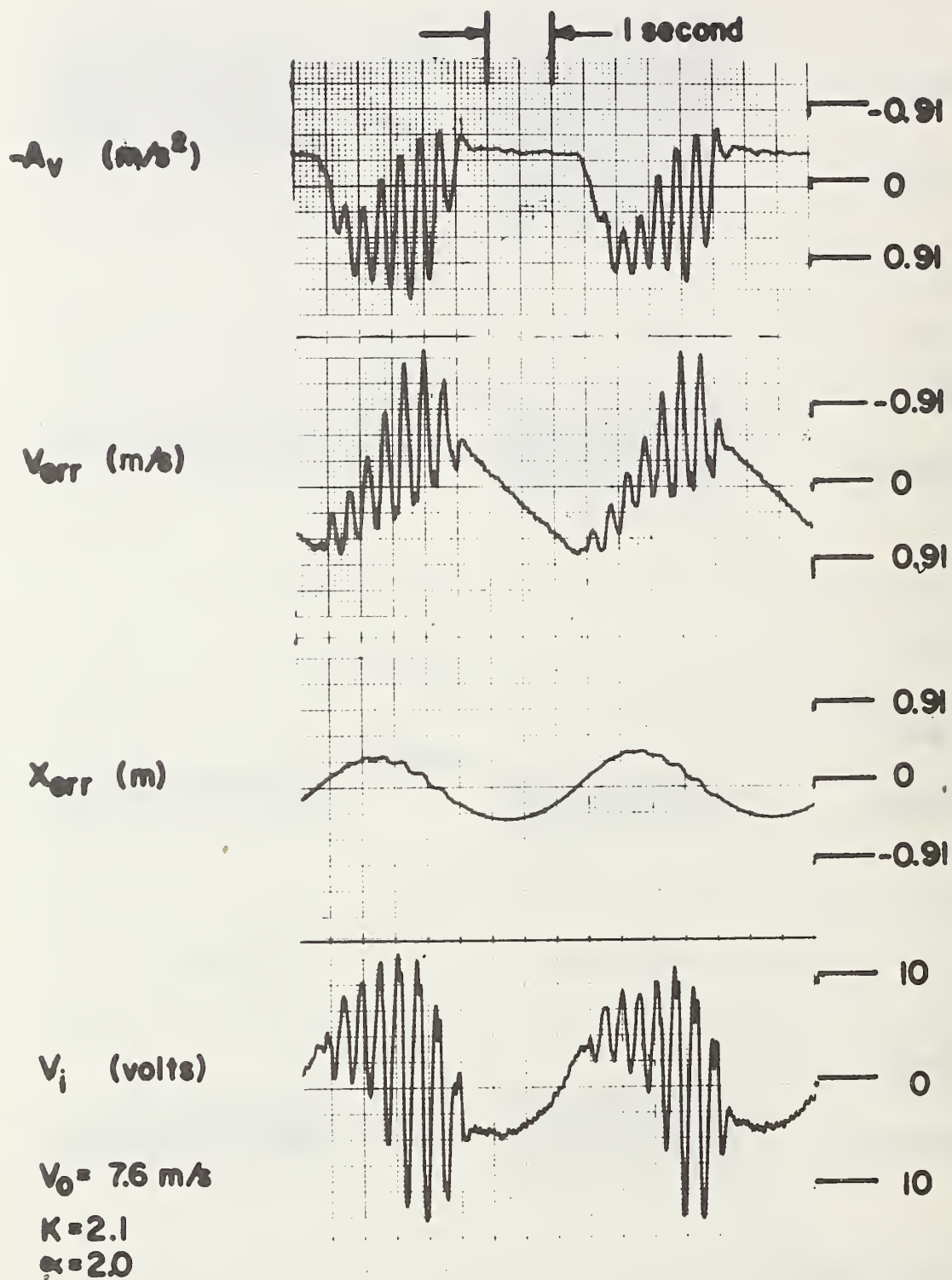


Fig. 6-6: Limit cycle with state-dependent controller and vehicle at constant velocity .

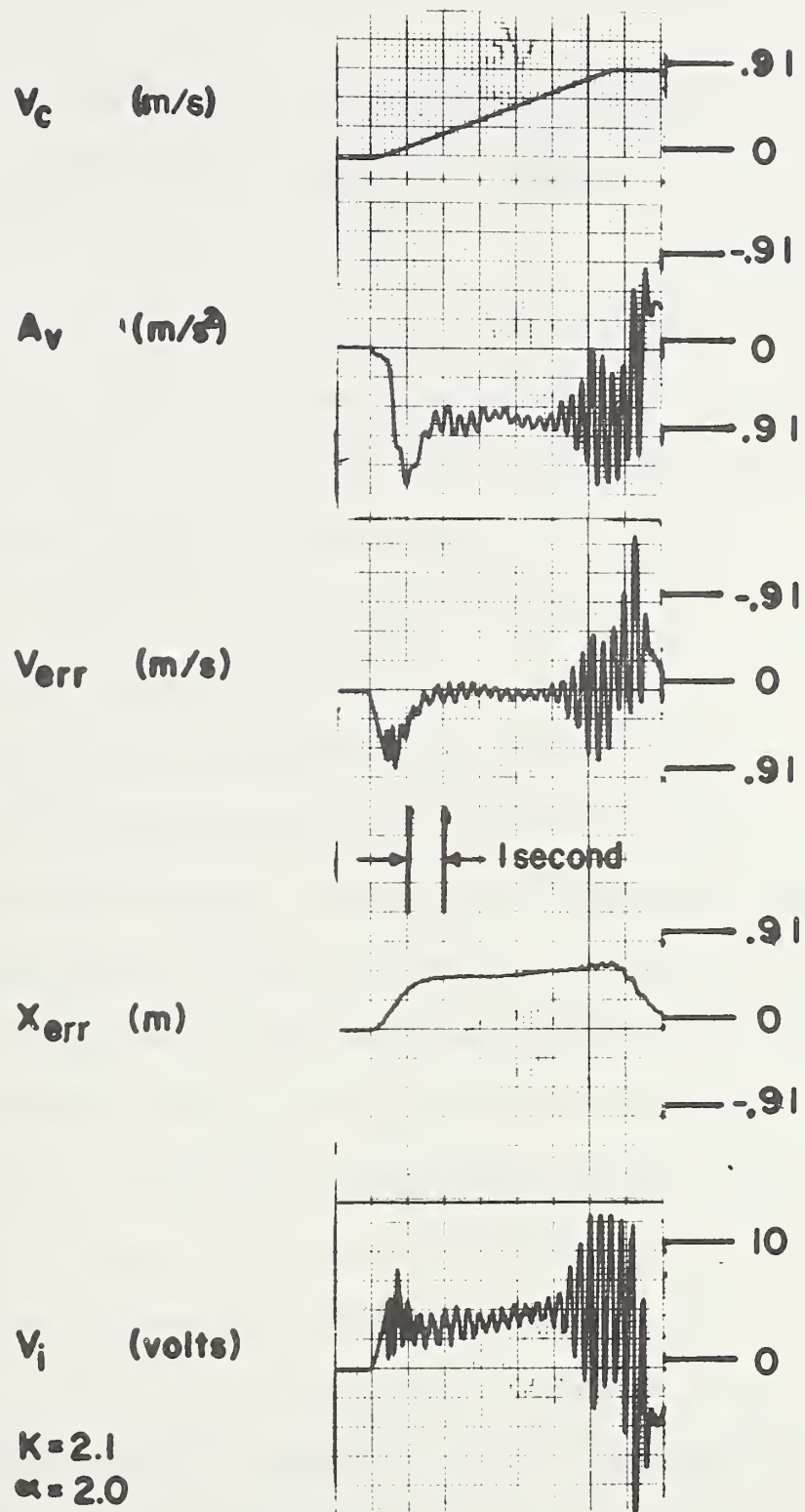


Fig. 6-7: Limit cycle with state-dependent controller and accelerating vehicle in first gear.

b) Limit Cycle Analyses

The condition for a limit cycle in a negative feedback system is

$$G_{OL}(j\omega) = -1 ,$$

where $G_{OL}(j\omega)$ is the open-loop transfer function of that system.

This condition was applied to the previously described controllers for each of the following representations of vehicle dynamics:

- i) Blackwell's model [49],
- ii) Bender and Fenton's first-order model [51],
- iii) Takasaki's state-dependent model [50], and
- iv) A more complex, state-dependent model [35].

In essence, as Kneifel has discussed in detail, the observed limit cycles were not predicted in any of the cases examined [54].

The listed models are best characterized as low-frequency approximations and should be modified if the observed performance-degrading, higher-order effects are to be predicted.

c) Controller Modifications

In concept, the observed limit cycles could be accounted for by cascading a high-frequency term (e.g., a ratio of two quadratic terms) to the low-frequency models previously studied. In practice, this approach was inadequate and resulted in a poor approximation to the field test data [54].

TABLE 6-1

Parameter Set for Modified Controller

Parameter	Value
K_{FF}	1.5
K_X	20.0
K_{IX}	7.0
K'	13.0
K_{ILF}	40.0
$Z(V)$	$0.715 + 3.75 V$
β	10.0

It was thus decided, principally for reasons of convenience and time/economic constraints, to adopt an empirical approach to both the model and controller specifications.⁴ In essence, the selected design, which is shown in Fig. 6-8, is a modification of that shown in Fig. 6-3. The structures are the same; however, the parameters K_{FF} , K_X , K_{IX} , K_{ILF} , and K' were changed to achieve a consistent, stable, and comfortable response during a system entry operation. The selected parameter values, which were determined on the basis of extensive empirical testing, are

⁴ Kneifel [54] examined an automotive propulsion system in some detail and noted that many of its components, especially the carburetor, engine and torque converter, are complex, highly nonlinear and generally undocumented from an input/output, dynamic modeling point of view. On this basis, he concluded it would be a difficult task to obtain a model from first principles.

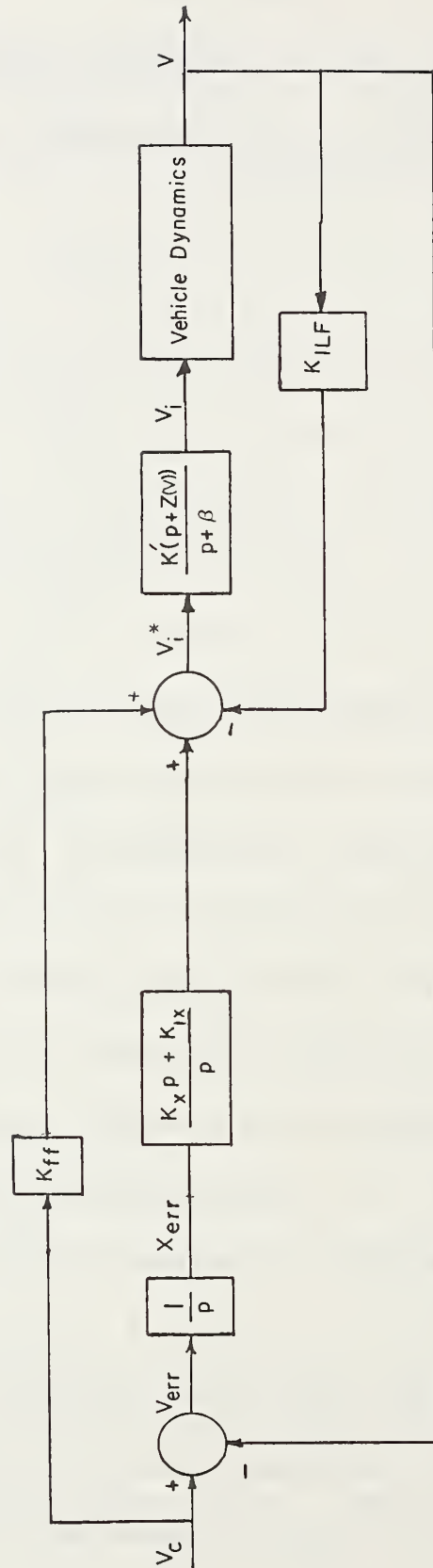


Fig. 6-8: Block diagram of modified controller .

shown in Table 6-1.

d) Reference Trajectory Modifications

The system entry command previously employed is shown in Fig. 6-9. Note that it is applied for an entry time (T) of 30 s -- a time which was selected to satisfy a trade-off between vehicle capabilities, controller bandwidth, ride comfort, and system entry distance (X_m). The inconsistency observed during entry operations was partially due to this choice of command -- especially the required step change in acceleration at $t = 0$.

The modified reference command shown in Fig. 6-10 was specified to coincide more closely with the capabilities of the test vehicle. This is shown in Fig. 6-11 where the command acceleration is presented as a function of command velocity together with the vehicle's maximum acceleration capabilities (as reported by the manufacturer). The quantities T and X_m for this command are 30 s and 480 m, respectively.

C. Full-Scale Testing of Selected Controller

The position controller shown in Fig. 6-8 was implemented with analog components in the 1969 Plymouth test vehicle and extensively tested under both large-signal (i.e., system entry operations) and small-signal (i.e., mainline speed changes and maneuvering commands) conditions.

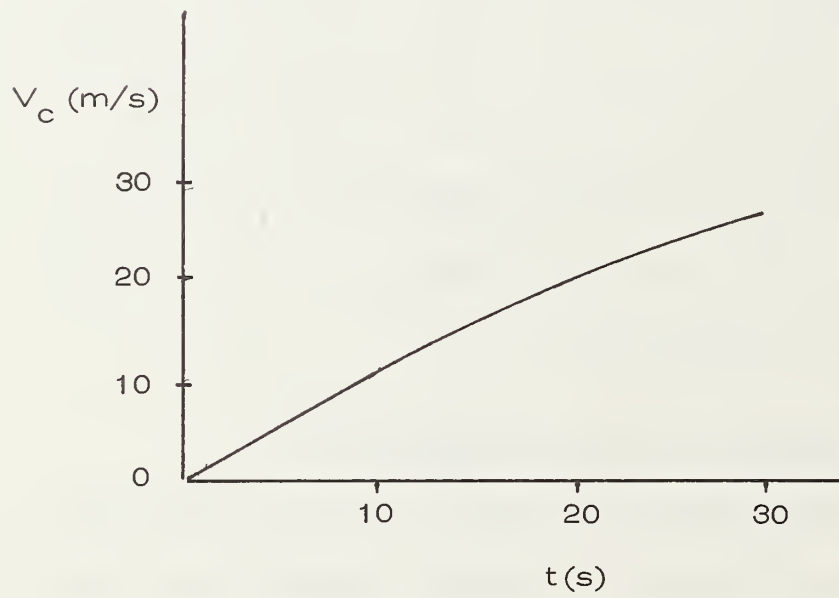
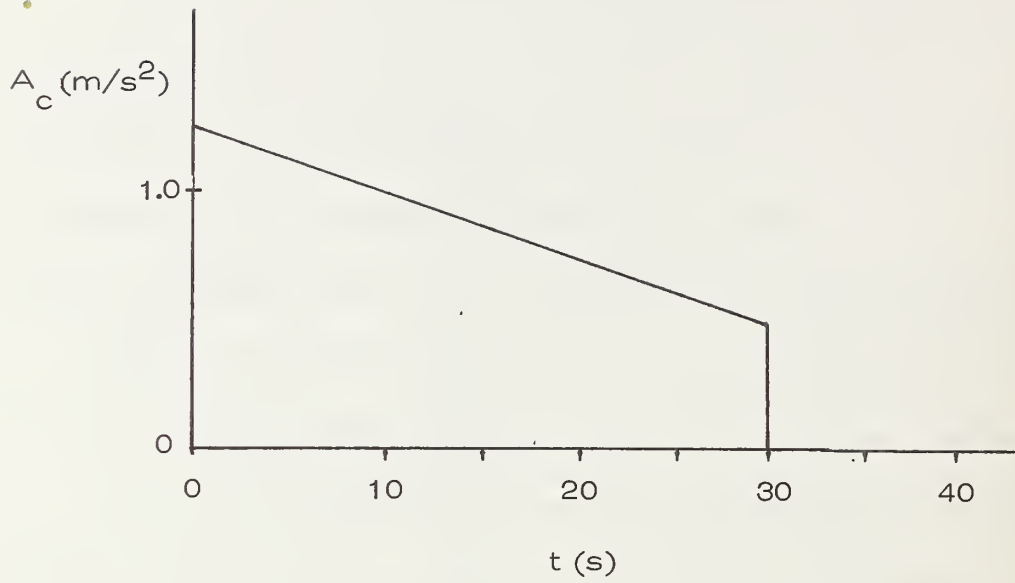


Fig. 6-9: System entry commands employed by Fenton and Chu [52].

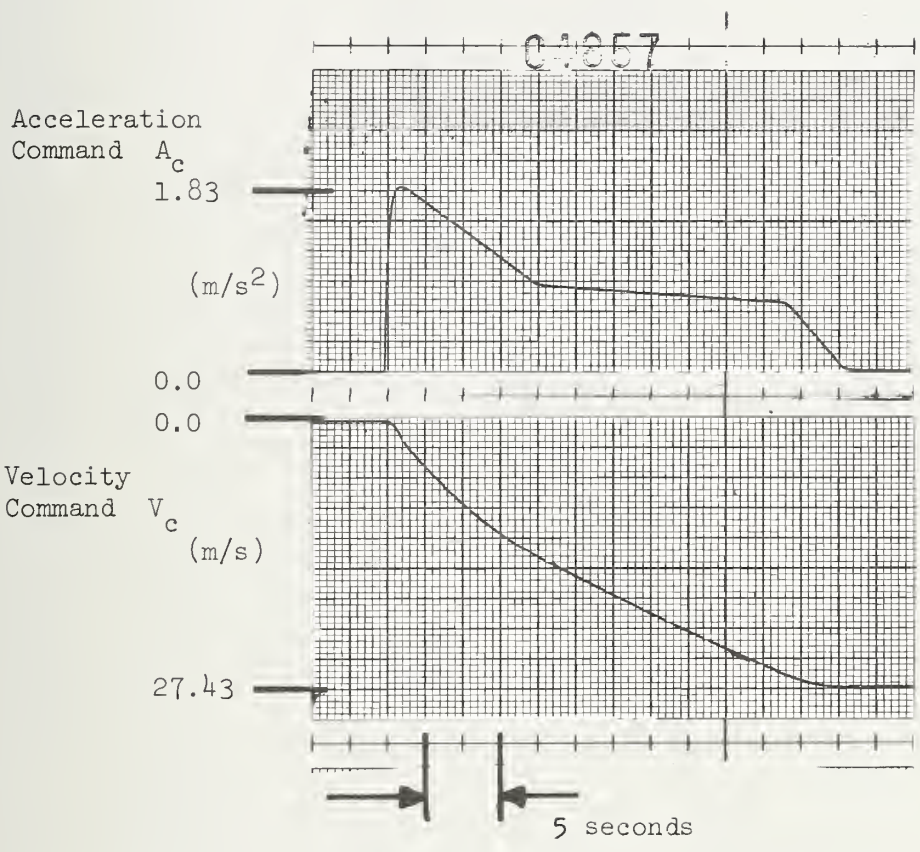


Fig. 6-10: Selected acceleration/velocity reference profile.

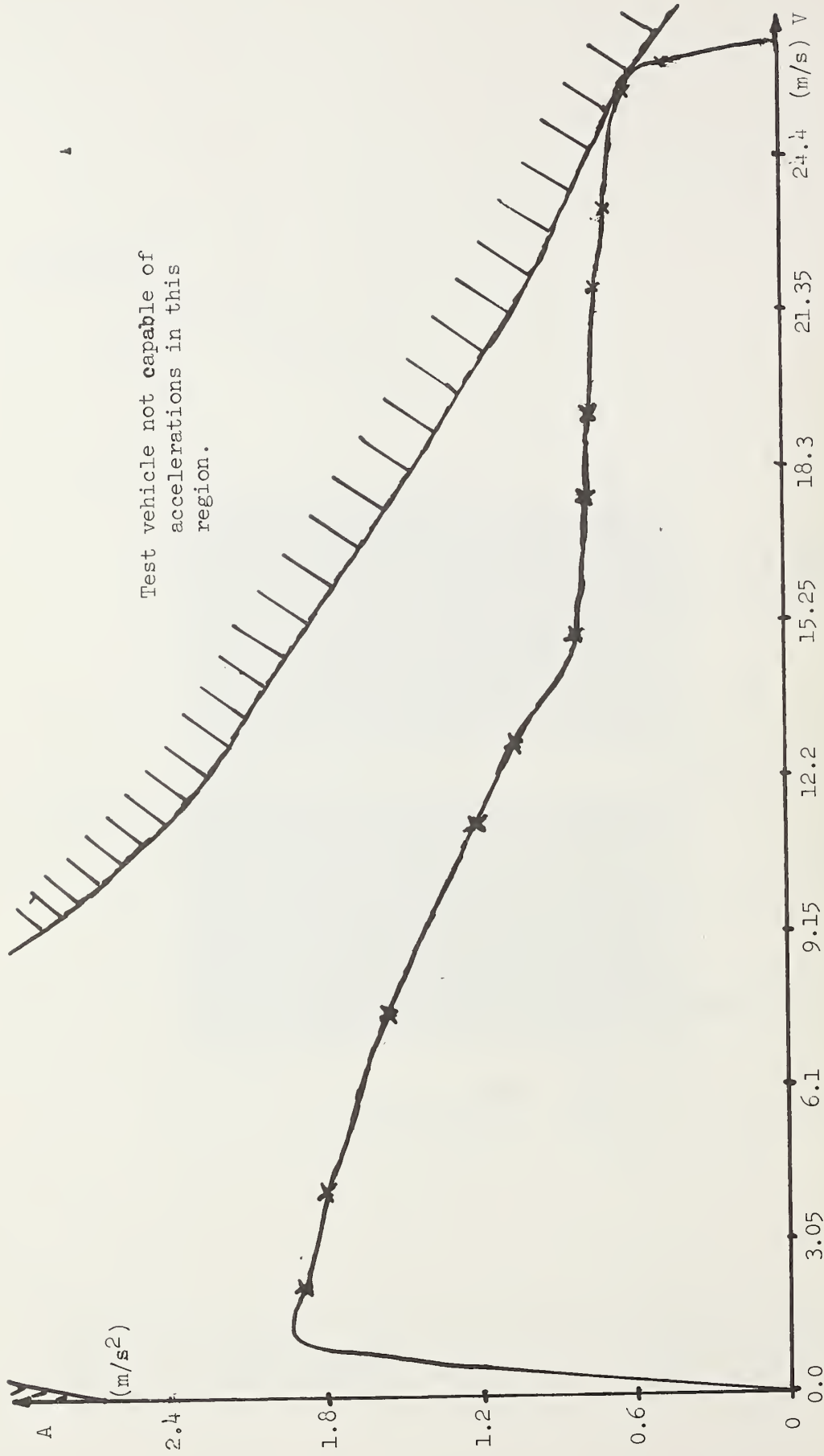


Fig. 6-11: Acceleration versus velocity plots .

a) System Entry Tests

In a typical large-signal test, the initially stationary vehicle was required to follow a specified X_c , V_c , and A_c as it accelerated to a mainline speed of 26.8 m/s. The quantities command position (X_c) and command velocity (V_c) are readily derived from the command acceleration A_c which is given in Fig. 6-10.

Typical results are shown in Fig. 6-12 where the velocity error ($V_c - V$), the position tracking error ($X_c - X$), and several other quantities are presented. Note that these errors are relatively small (e.g., $X_c - X$ has a peak value of 0.80 m and, at the time of vehicle insertion ($T = 30$ s) into a mainstream lane, a value of some 0.27 m). The maneuver was performed smoothly with no ride discomfort being perceived by the test vehicle occupants. Significantly, such results were obtained under both conditions of high humidity and air temperatures up to 35° C and low humidity and temperatures as low as 15° C.⁵

Various tradeoffs exist here. For example, increases in the maximum value of A_c result in severe demands on the vehicle and, as a result, system saturation and decreased stability as can be observed by comparing Figs. 6-12 and 6-13. Also the

⁵ It remains to evaluate this controller at very low temperatures (e.g., -20° C).

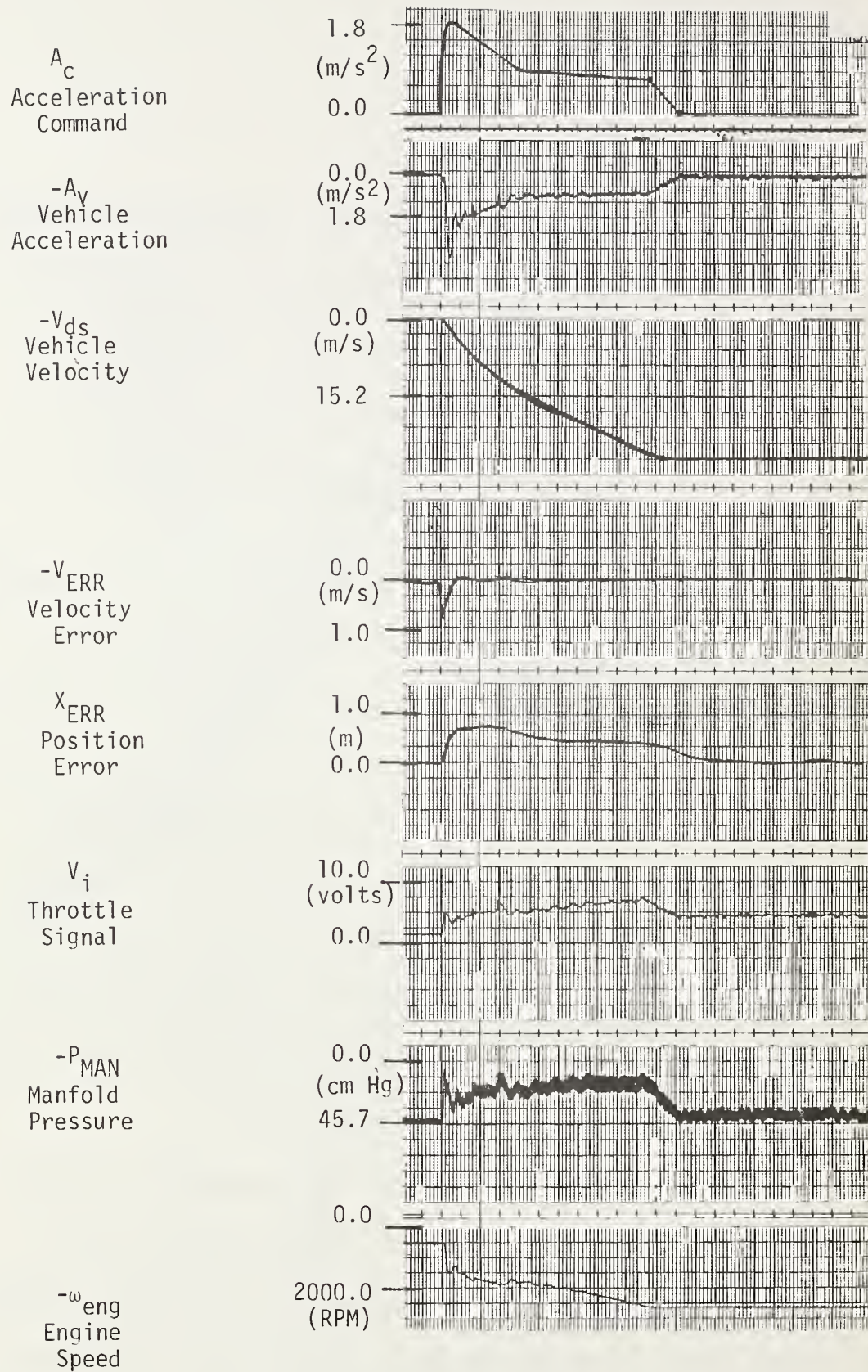


Fig. 6-12: System entry response .

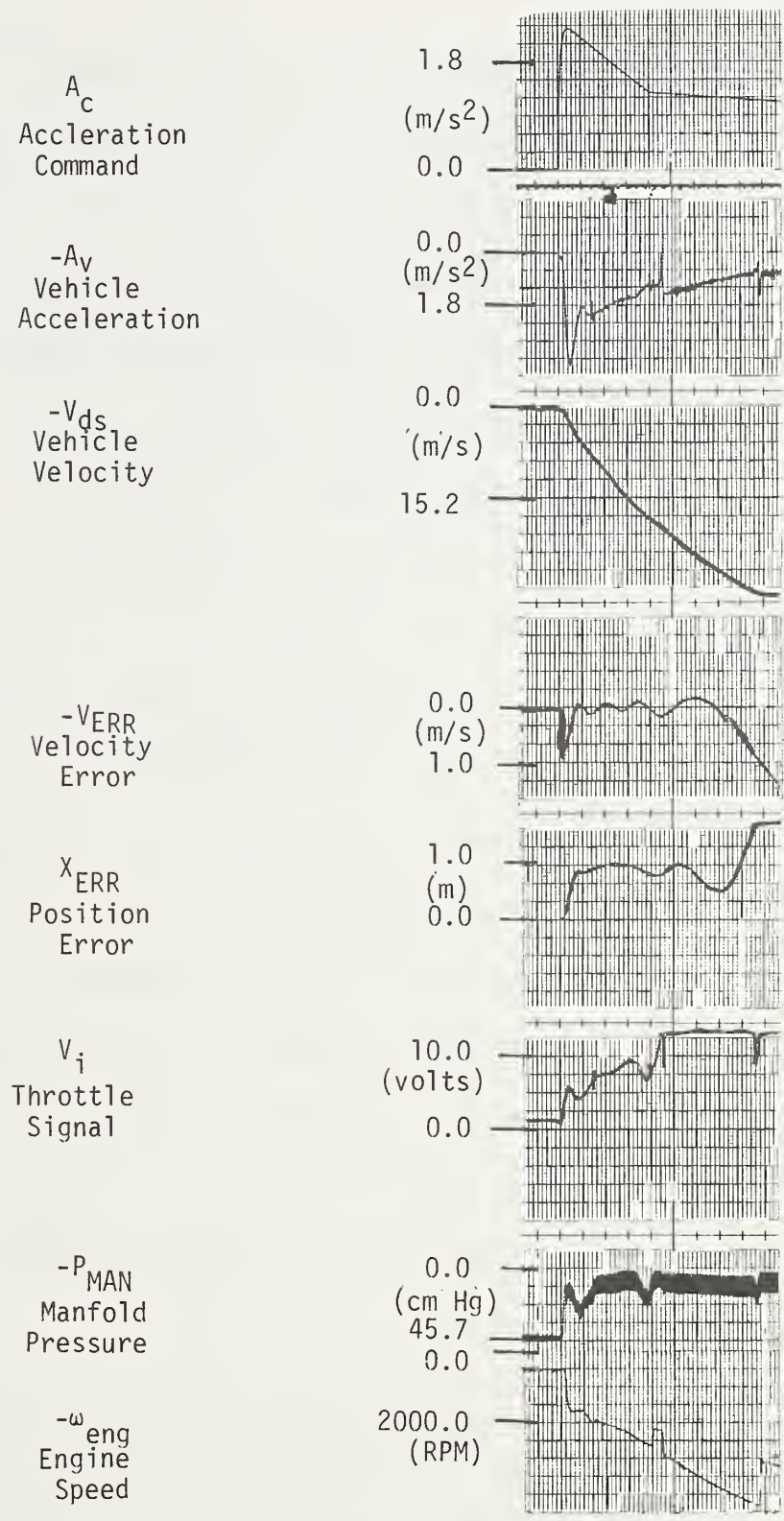


Fig. 6-13: Larger A_C yields less stable system response .

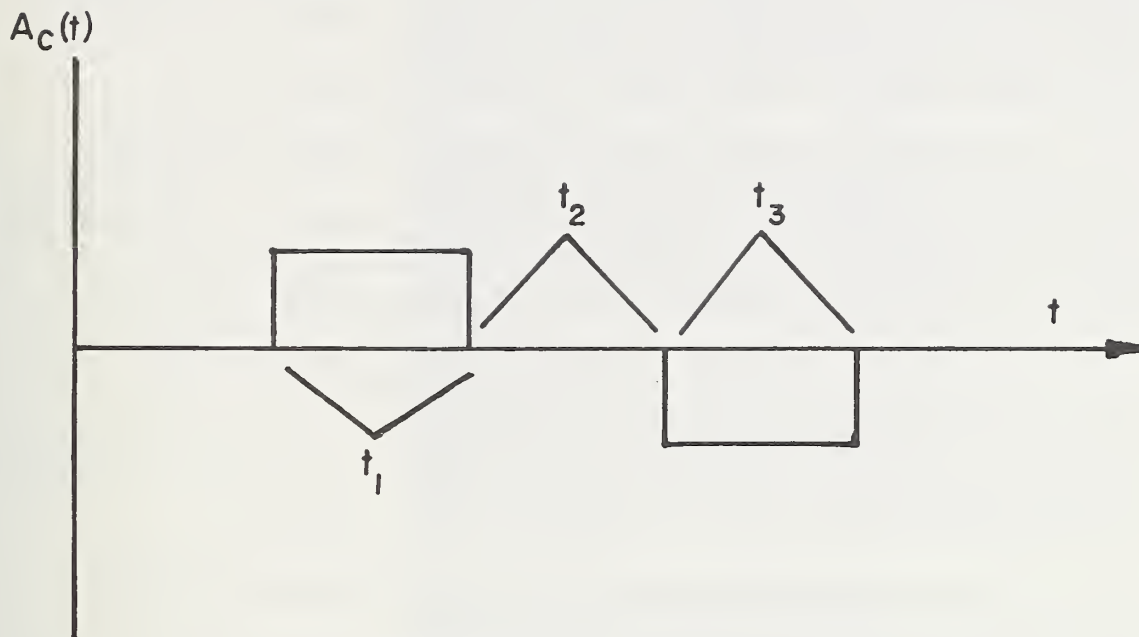
choice of K_X (see Table 6-1 and Fig. 6-8) involves a tradeoff between peak position error and the error of the zero-acceleration point in the command profile. Larger K_X values result in smaller peak position errors to a point; however, such values also result in an increased error at $T = 30$ s (i.e., when the vehicle is inserted into mainline traffic).

b) Small-Signal Tests

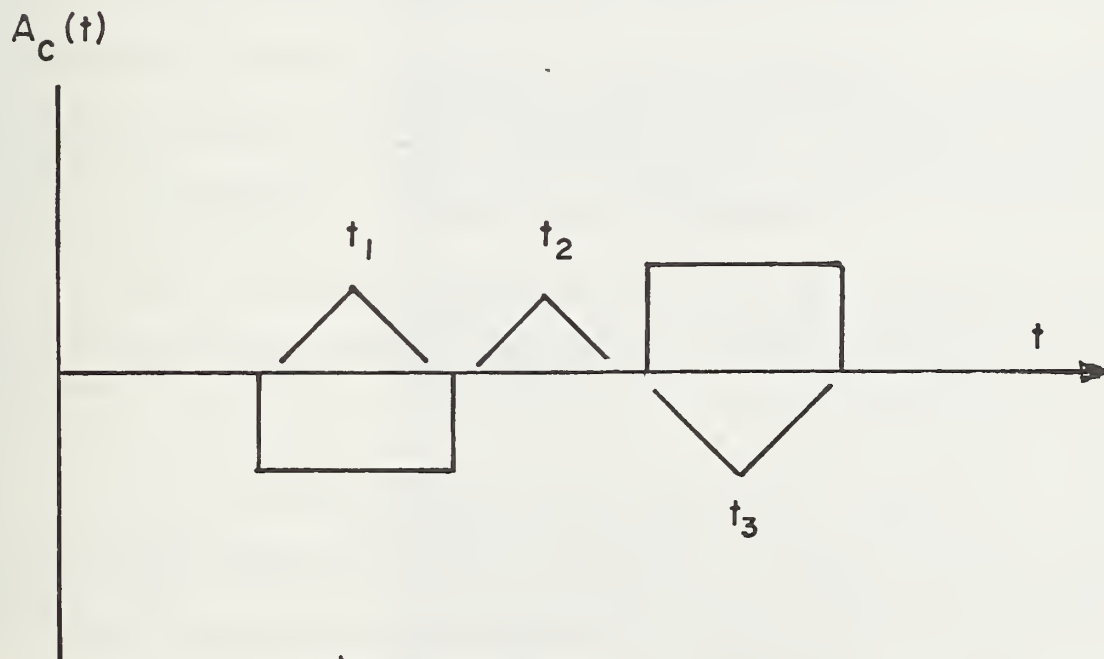
The tracking accuracy achievable for constant velocity operation was observed by fixing V_c at a constant value and recording $X_c - X$. A typical result, which was obtained for $V_c = 26.8$ m/s, was $|X_c - X| < 0.03$ m.

Mainline maneuvering involves both the propulsion and braking controllers. For example, a move-up maneuver would be achieved by employing the acceleration trajectory of Fig. 6-14a. A vehicle would be accelerated from a mainline speed of V_s to a maneuvering speed V_m . The latter would be maintained for a time t_2 , after which its speed would be decreased to V_s . A corresponding moveback maneuver uses the "opposite" commands as is shown in Fig. 6-14b.

In these maneuvers, the propulsion controller would be employed in the acceleration and constant velocity phases, and a braking controller in the deceleration phase. Some typical responses for the former case are shown in Fig. 6-15, where the



a) Move - Up



b) Move - Back

Fig. 6-14: Move-up and move-back command acceleration trajectories.

test vehicle was commanded to accelerate at a rate of 0.1 g from one constant speed to another and remain at that speed until another acceleration command was provided. Typical responses, vehicle acceleration, $V_c - V$, $X_c - X$, V_i , P_{man} , and ω_{eng} , are shown in Fig. 6-15. Note that the maximum position error of 1 m is velocity independent, and that the responses are less oscillatory at the higher speeds.

D. Commentary

The empirical approach to controller design employed here resulted in a reasonable controller from a standpoint of tracking accuracy, ride comfort, and to the extent evaluated, a range of environmental conditions. However, substantial advantages, relative to controller design, could accrue from a propulsion system model which would be sufficiently complex for predicting various higher-order effects and operations over a wide range of environmental conditions and yet simple enough to employ for realistic design.

It will be imperative to integrate the braking and propulsive control systems. In particular, it may be advantageous to make the inner-loop propulsion system dynamics (see Fig. 6-8) "symmetrical" to the braking system dynamics so that one outer-loop configuration could be used for all longitudinal operations.

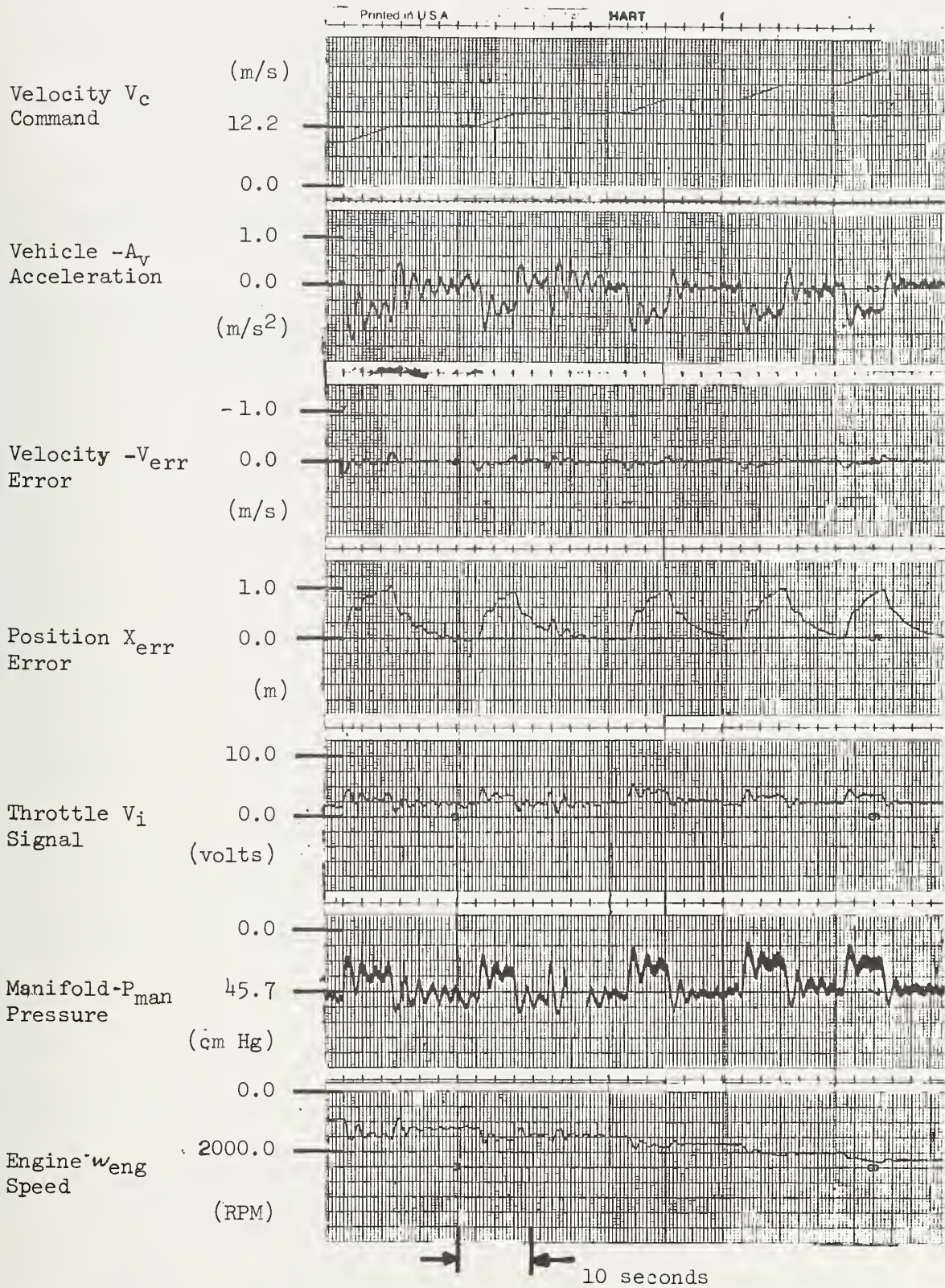


Fig. 6-15: Move-up/move-back acceleration responses.

A digital implementation of the propulsion controller would be desirable as a relative immunity to some analog controller problems such as amplifier noise, circuit drift, and offset biases could be achieved.

These are areas in which future efforts would be desirable.

CHAPTER VII

A MICROCOMPUTER-BASED LONGITUDINAL CONTROLLER

A. Introduction

A longitudinal controller, which was constructed of analog components was discussed in Chapter VI. In this chapter, a start is made toward implementing this controller by a microprocessor-based digital system. The advantages of doing this include the simplicity of command generation, the relative ease of implementing both linear and nonlinear compensation with computer software (as opposed to analog hardware), and its effectiveness in achieving "continuous" dynamic calibrations of various state estimators. In addition, a microcomputer could easily accomplish the monitoring of a vehicle's status (e.g., oil pressure, hydraulic system pressure, water temperature, and position deviation) and be a source of rudimentary intelligence at the vehicle level -- the latter being a necessary capability for a proper reaction to vehicle-level emergencies.

B. Microcomputer Functions

The functions of a microcomputer-based, vehicle longitudinal position controller are shown in Fig. 7-1. These are

command generation, state estimation, and both nonlinear and linear compensation.

a) Command Generation

The command generator would receive an acceleration command (labeled A_c in Fig. 7-1) from the sector computer. This signal would be processed to obtain the corresponding position and velocity commands. These together with A_c , would be compared to an estimate of the vehicle's longitudinal state (i.e., acceleration, velocity, and position) to produce the state error signals for the controller. (in the controller discussed in (d) only velocity deviation (ΔV) and position deviation (ΔX) are required; however, in general, one could use both these and acceleration deviation (ΔA) as shown in Fig. 7-1).

The controller, with its high gain (needed because of stringent performance requirements), must operate on smooth signals;¹ thus, there is a need for finely quantized commands and estimates. To provide the required commands, the command generator must have an output of sufficient word length.²

¹Large steps in error would cause saturation of the electro-hydraulic unit which controls the throttle valve and/or result in uncomfortable changes in acceleration.

²The software for a command generator, based on an INTEL 8085A microprocessor, has been developed by Thayer [55].

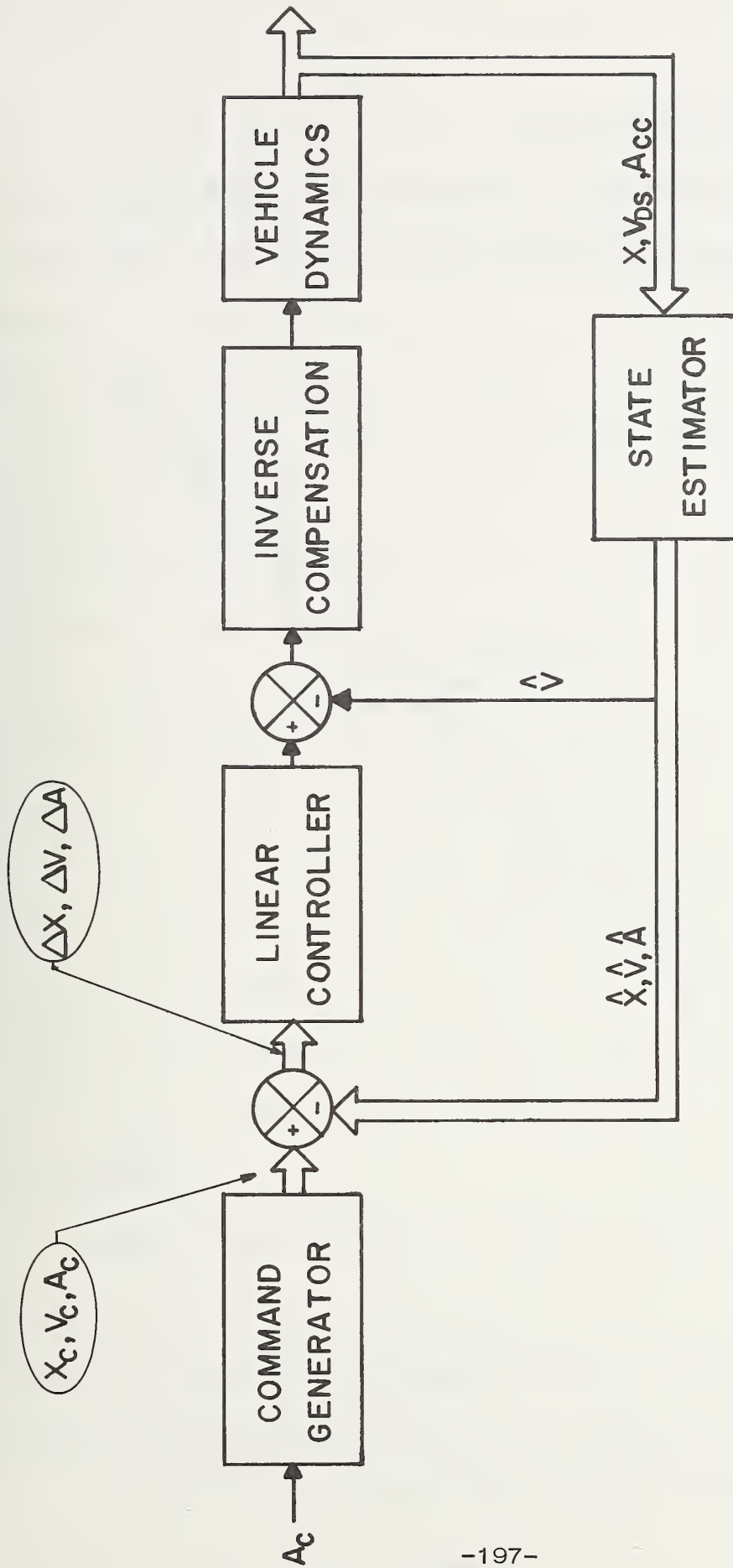


Fig. 7-1. A block diagram of the vehicle longitudinal control system.

b) State Estimation

The required continuous state estimates can be produced by the general technique shown in Fig. 7-2. Here, an

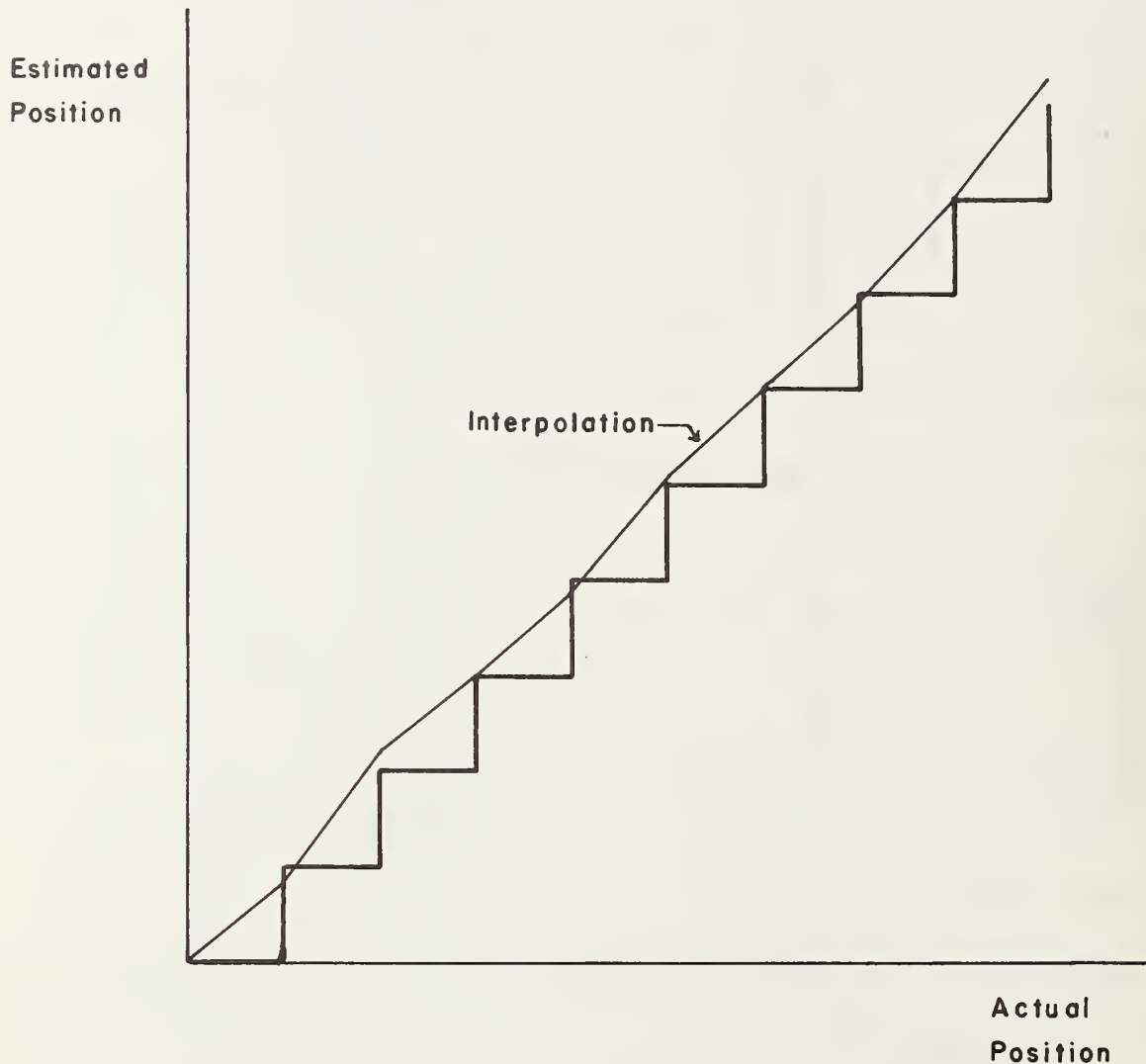


Fig. 7-2 Estimation of position between absolute markers.

absolute signal is available at discrete points along the roadway, and a continuous signal is obtained by interpolating between these points. Takasaki [35] suggested that the discrete points be real-

ized via roadway-implanted markers, spaced at 0.61 m intervals, and the interpolation be achieved by an analog estimator with inputs from an accelerometer and a driveshaft tachometer. This approach was evaluated and satisfactory continuous state estimates were produced under certain conditions.

Two problems resulted: First, absolute position was updated too infrequently at slow speeds to allow for adequate control; and second, much capital investment and subsequent maintenance would be required with such closely spaced markers.

A second approach for state estimation involves the use of a wheel tachometer in place of the closely-spaced roadway markers. The tachometer selected provides position information every 1.8 cm (compared to 61 cm); thus, even at slow speeds, position information is provided frequently. Also, by using online dynamic calibration of the tachometer, absolute position updating would be necessary at intervals of perhaps no less than 150 m. (This value was derived from empirical data provided by Cribbs [53].)

The tachometer output, a train of pulses, would be translated into a position estimate as shown in Fig. 7-3. Note that when each pulse is received, the estimate of position is changed by the discrete amount of 1.8 cm. The latter is too large (i.e.,

too coarsely quantized) and a means of interpolating between pulses must be used.

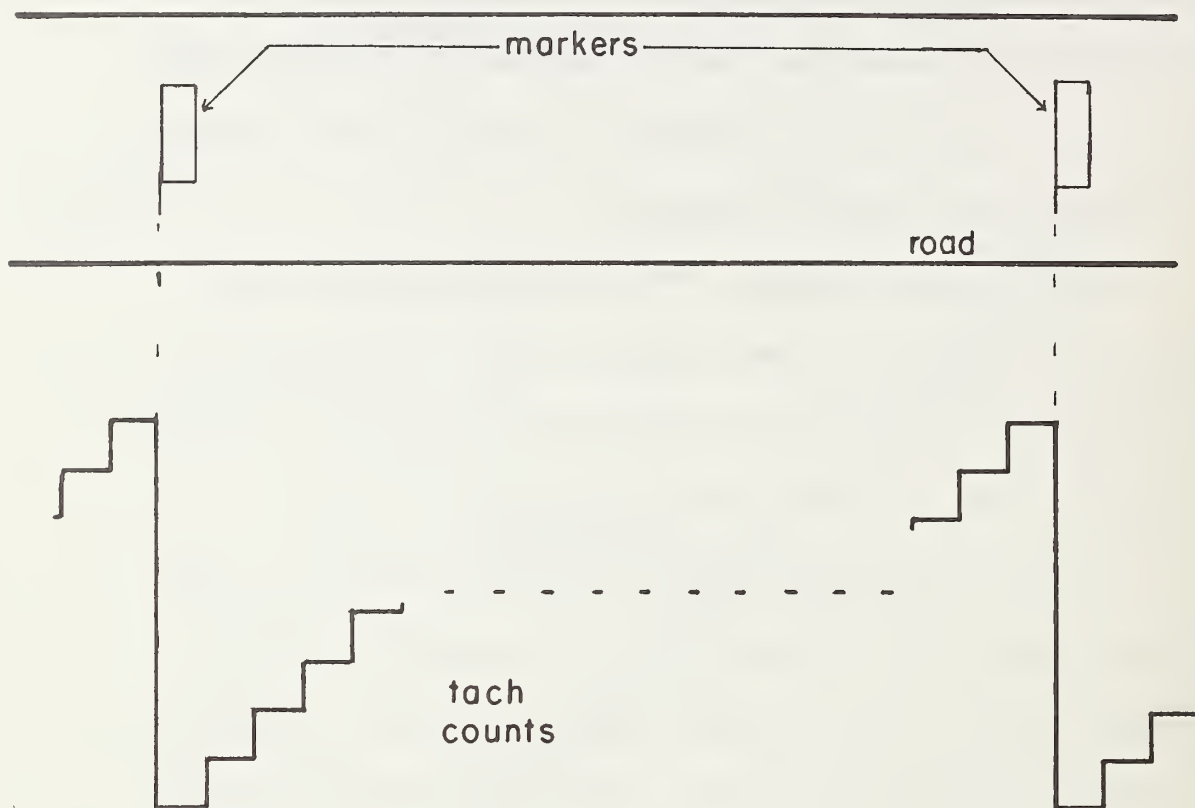


Fig. 7-3. Estimation of position using a wheel tachometer output.

One such technique (see Fig. 7-4) involves the use of velocity information to update the position estimate in the time interval between adjacent pulses. An analog voltage, which is derived from the output of a driveshaft tachometer, controls the output of a voltage-controlled oscillator -- a square wave whose frequency is proportional to vehicle speed. A counter is cleared when a tachometer pulse is registered and incremented each period until the next pulse is received. The result is a position

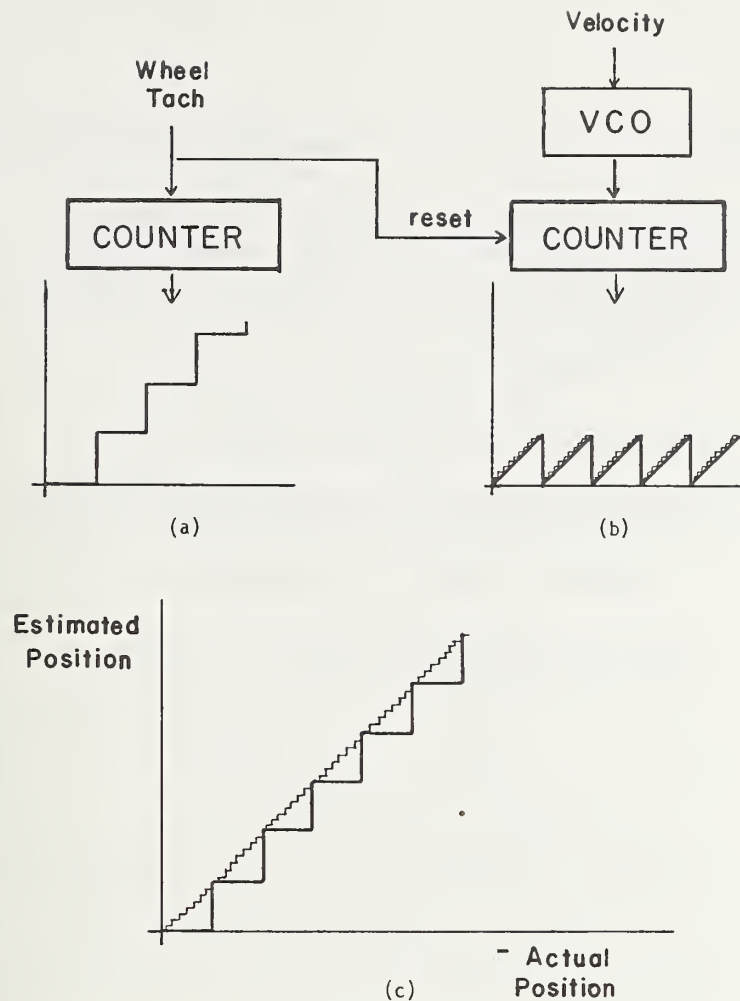


Fig. 7.4 A technique for interpolating between tachometer pulse intervals.

estimate with steps of some 0.2 cm which are acceptable inputs to the longitudinal controller. Similarly, velocity steps are reduced to some 0.03 m/s.

The information derived from the wheel tachometer is dependent on tire pressure and velocity, but is independent of road grade and acceleration for nominal values of both quantities [53]. However, when tire pressure and velocity are fixed, extremely consistent information can be obtained (e.g., a maximum deviation from the mean of 16 cm in a 150-m interval). Clearly, a properly calibrated wheel tachometer can be useful as a primary source for position information.

One algorithm for the online or dynamic calibration of a wheel tachometer can be implemented using a microcomputer and some empirical constants which would be stored in a ROM. These constants are defined as follows:

K_x \equiv distance per tachometer count. (This would be determined from empirical data, in units of meters per tachometer count. This is a velocity-dependent term.)

K_d \equiv distance between wire crossings, measured in meters per wire crossing.

K_d/K_x \equiv number of tachometer counts expected per wire crossing. (This ratio is velocity-dependent.)

In the approach selected, K_d/K_x is subtracted from the tachometer count, (TC), measured during the previous "wire-crossing", (WC), interval to determine how well the tachometer is measuring distance. The difference, " ϵ ", is used to find the error in tachometer counts per meter. Thus,

$$\epsilon^* \equiv \text{error in tachometer counts per meter} = \epsilon/K_d.$$

Similarly, " δ " is defined as the difference between the measured tachometer count from the previous "wire-crossing" interval and the expected count, defined as $(K_d/K_x) (1 + \epsilon^* K_x)$. This difference can be normalized via

$$\delta^* = \delta / K_d .$$

The quantity (\hat{K}_x) for translating tachometer counts into an interpolated distance can then be calculated as ³

$$\hat{K}_x = K_x (1 - \epsilon^* K_x - \delta^* K_x) .$$

Then, position and velocity can be calculated via

$$\hat{X} = \text{position} = (\text{Wire crossings} \times K_d) + [(\text{Tachometer counts} + \delta) \times \hat{K}_x]$$

and

$$\hat{V} = \text{velocity} = [K_x(1 - \epsilon^* K_x) / T_s] \times (TC)_s$$

where $(TC)_s$ is the number of tachometer counts in an interval T_s . The two quantities, \hat{X} and \hat{V} , would then be used in the calculation of propulsion and braking commands for the longitudinal controller.

The following is a numerical example of the workings of the proposed estimator:

Conditions:

1. $K_d = 150 \text{ m};$
2. Velocity at last wire crossing = 30 m/s;
3. The corresponding values of K_x and K_d/K_x (as obtained from ROM) were 0.034884 m/TC

³The quantity \hat{K}_x would be updated at each wire crossing, whereas K_x is constant at each velocity. The quantity ϵ_-^* is the preceding evaluation of ϵ^* .

and 4300 TC/WC, respectively;

4. The tach count over previous 150 m interval was 4295;
5. The tach counts over the next 150 m interval was 4295;
6. Command velocity is constant.

Calculations:

1. At first wire crossing

$$\epsilon = TC - \frac{K_d}{K_x} = 4295 - 4300 = -5$$

$$\epsilon^* = \frac{\epsilon}{K_d} = -.0333 \text{ TC/m}$$

$$\delta = TC - \frac{K_d}{\left(\frac{K_x}{1 + \epsilon^* K_x}\right)} = 4295 - 4300 = -5 \quad 4$$

$$\delta^* = -5/150 = -0.0333 \text{ Tach counts/m.}$$

$$\begin{aligned} \hat{K}_x &= \text{distance estimate/Tach count} \\ &= K_x(1 - \epsilon^* K_x - \delta^* K_x) \\ &= 0.03488 [1 + 2(0.0333)(0.03488)] \\ &= 0.03496 \text{ m/Tach count.} \end{aligned}$$

⁴ Note: Here $\epsilon^* = 0$ as it is assumed that the preceding estimate was exact.

The state estimation of position and velocity results in the following estimates at the instant before the next wire crossing.

$$\hat{X} = [(T.C. + \epsilon) \times \hat{K}_x] = [(4295 - 5)(.03496)] = 150 \text{ m}$$

$$\begin{aligned} \hat{V} &= [K_x(1 - \epsilon^* K_x) / T_s] \times \text{Tach counts in previous} \\ &\quad \text{sample interval.} \\ &= [.03488(1 + (.0333)(.03488)) / 0.1] \times 86 = 30.04 \text{ m/sec.} \end{aligned}$$

2. At second wire crossing

$$\epsilon = -5, \epsilon^* = -0.033 \text{ Tach counts/m.}$$

$$\delta = \delta^* = 0$$

$$\begin{aligned} \hat{K}_x &= 0.03488 [1 + (.0333)(.03488)] \\ &= .03492 \text{ m/Tach count} \end{aligned}$$

$$\hat{X} = (4295)(.03496) = 150 \text{ m}$$

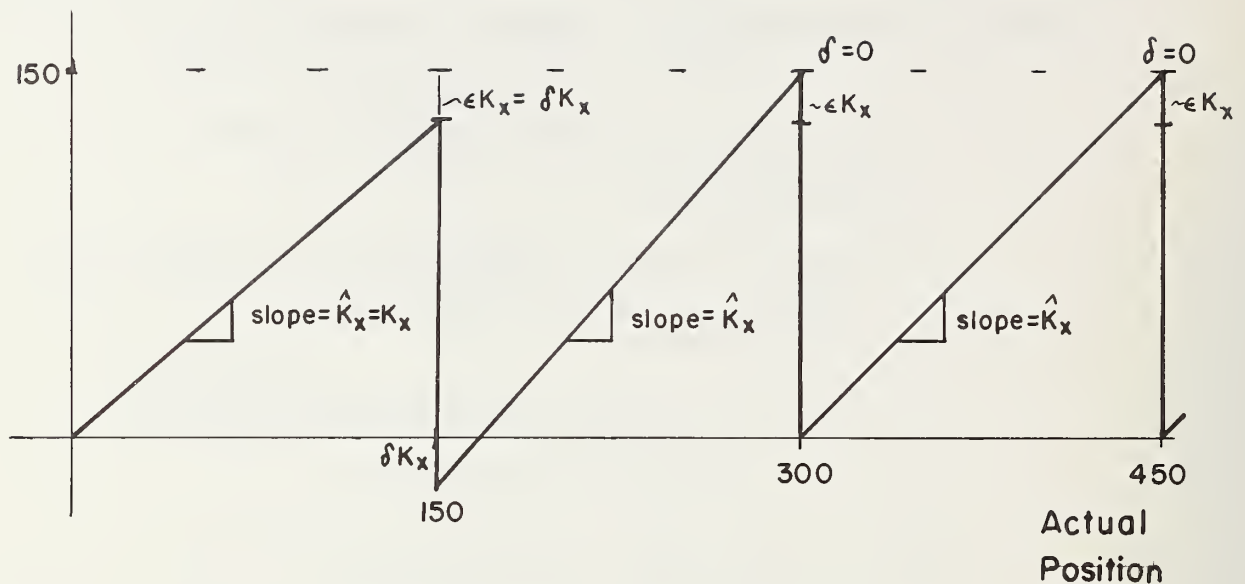
The velocity estimate would be the same as above. Note that the initial error of five tachometer counts has been removed and the position estimate is now exact.

A graphical representation of this example is shown in Fig. 7-5, and a program to perform the necessary calculations has been developed by Thayer [55].

c) Nonlinear Compensation

The state-dependent terms present in a longitudinal dynamics model, such as those presented in Chapter VI, can be linearized by employing inverse compensation. The collective result will be a nominally linear, "fixed" plant.

Estimated
Position



Note: The quality \hat{K}_x is updated every 150 m.

Figure 7-5. Graphical illustration of example of the proposed state estimator.

Inverse compensation can be performed with a digital computer in at least two ways. One is to obtain a piecewise-linear approximation of the non-linear term and calculate its inverse based on the state at which the vehicle is operating. Another is to make a table of the term's inverses at different states (e.g., different velocities and accelerations) and by reading the vehicle's state, use indexed addressing to obtain the proper inverse for cancellation. In both methods, the term would be "multiplied" by its inverse to achieve linearity.⁵ The output

⁵Note that the method of inverse compensation was employed in the design of the steering controller discussed in Chapter V.

of the nonlinear compensator would be the input, through a digital-to-analog converter, to the device which controls the throttle valve.

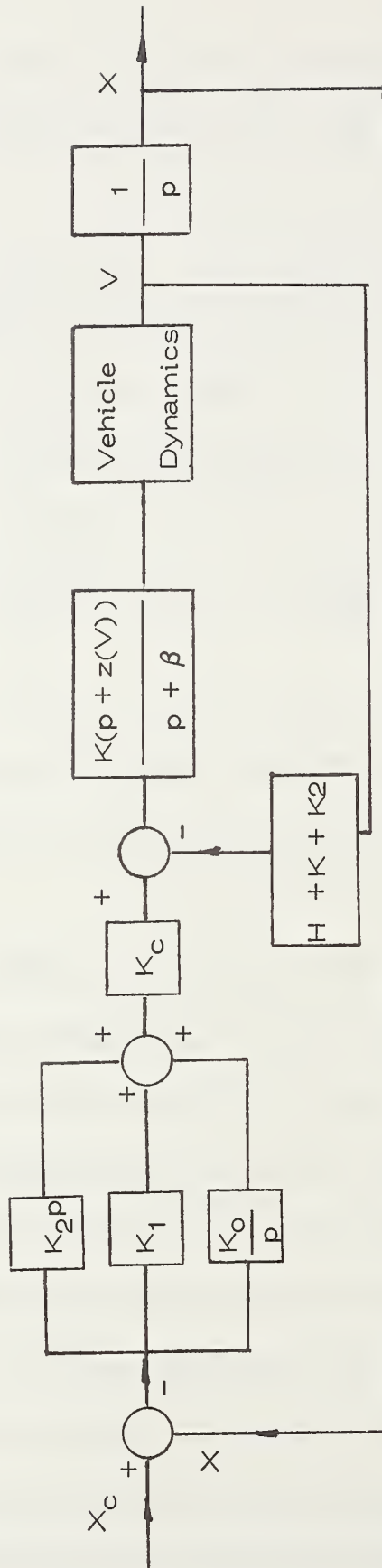
d) Longitudinal Controller

The use of inverse compensation results in a nominally linear plant $G_1(p)$, and the opportunity to employ linear design techniques to specify the necessary compensation $G_2(p)$. For example, in the controller described in Chapter VI,

$$G_2(p) = K_c \frac{K_2 p^2 + K_1 p + K_0}{p}, \quad (7-1)$$

a choice which resulted in the response functions shown in Figs. 6-12 to 6-13. A block diagram of the corresponding closed-loop control system, which is equivalent to that of Fig. 6-8, is shown in Fig. 7-6.

To implement this controller in software (i.e., a discrete equivalent of Eqn. 7-1), the computer must perform three types of operations. The first, multiplication, involves the use of the hardware multiplier. When this function is programmed, it is important to keep track of the assumed decimal point because the multiplications are not "floating point." (Shifting of the product may have to take place for non-integer gains.) The second operation, integration, is implemented by adding the term to be integrated into a given register each sampling period. However, one should be cautioned that with the selected sampling period of 0.1 s,



Note: This structure is equivalent to that of Fig. 6-8

Fig. 7-6. A longitudinal, position controller.

the register's contents would acquire a gain of ten during the integration process. The final operation, addition, takes place near the end of the linear controller program when the three terms (the state errors with their gains) are added before the open-loop gain computation. Addition would be accomplished via the double-precision arithmetic features of the microprocessor.

A flow chart for a linear controller program corresponding to Eqn (7-1) is shown in Fig. 7-7 and a listing of one possible implementation was given by Thayer [55]. His estimate is that the total longitudinal control program would be less than two thousand bytes long and should take less than 10 ms per sampling period to execute. Therefore, there should be time for other vehicle-level functions not directly related to longitudinal control, such as communications and vehicle status monitoring.

e) Microcomputer Hardware

Various microcomputer configurations were examined, and it was concluded that a unit, based on the INTEL 8085A, would be suitable for this application. This unit is described in Appendix D.

C. Velocity Controller Tests

A discrete implementation of the controller discussed in the last section (and in Chapter VI) required more time than was available. Therefore, a decision was made to design and test a

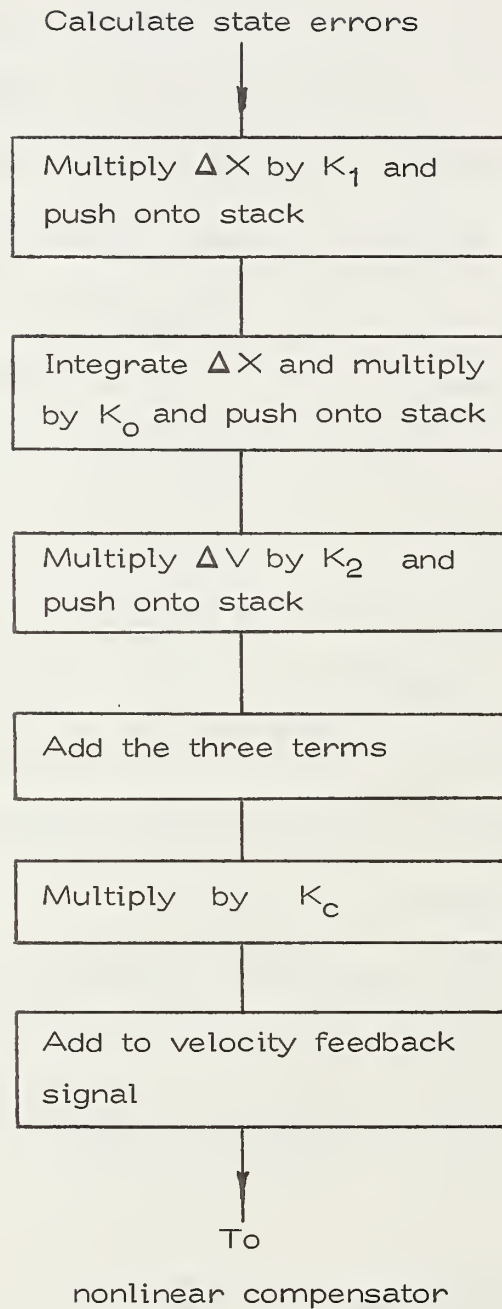


Fig. 7-7. Flow chart for linear controller

simpler controller -- a velocity controller -- as an intermediate step. This would enable an early evaluation of operational problems and, hopefully, a subsequent easy progression to the desired, more-complex controller.

a) Analog Controller Design

The velocity controller used in this implementation is shown in block diagram form in Fig 7-8. The command velocity input, labeled V_C , would, in practice, be transmitted from a sector-level computer, but here consisted of analog signals produced in the vehicle. The signal labeled V_i is the voltage input to an electrohydraulic servo which controls the position of the throttle valve. C_1 and C_2 are parameters of the vehicle model and K_1 is a constant in the compensator. When inner-loop feedback (a gain of 10) is employed as shown, the compensated vehicle model (i.e., $\frac{V_i^*}{V}$) is valid for small-signal inputs over the speed range of 12-24 m/s [52].

The compensator zero was selected to cancel the pole in the "compensated" plant, and the resulting closed-loop function is

$$\frac{V}{V_C} = \frac{1}{0.56 s + 1} .$$

The response of this system to a small step input should be overdamped with a time constant of 0.56 sec.

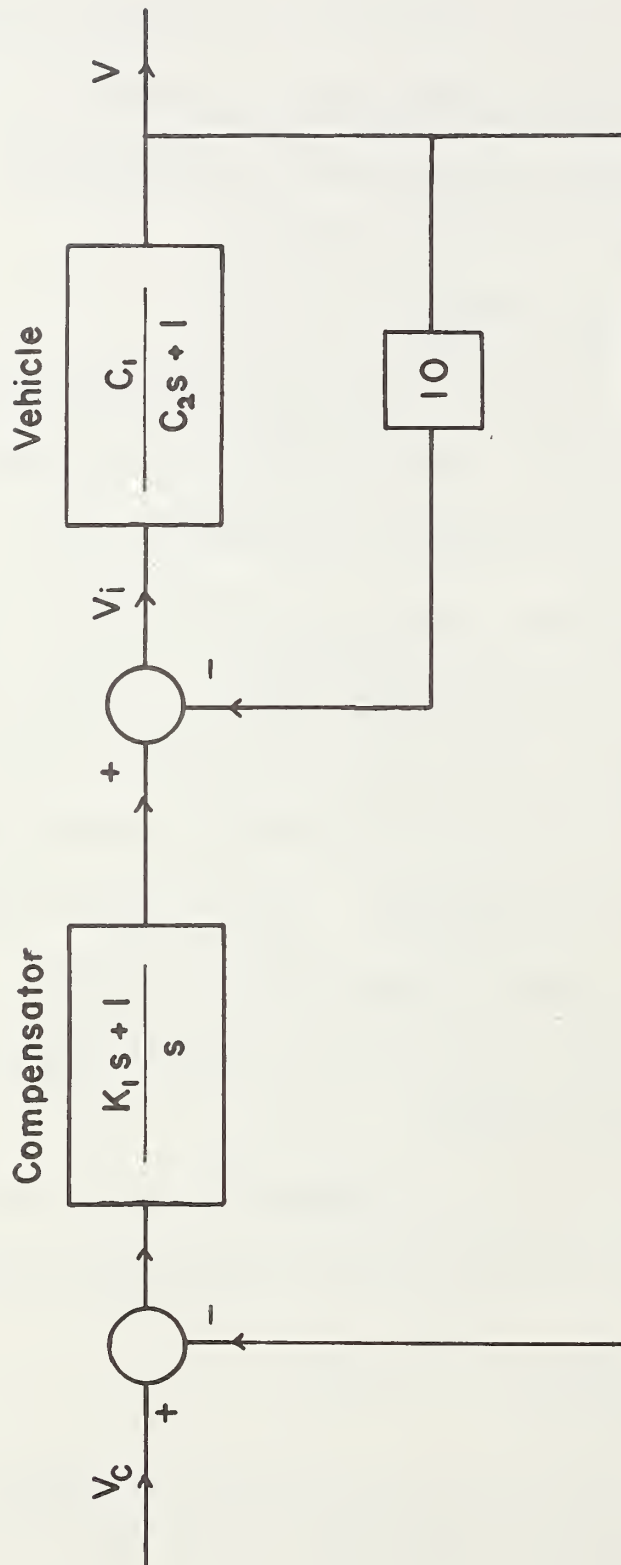


Fig. 7-8. An analog velocity controller.

b) Digital Controller Design

The velocity controller was also implemented by employing a microcomputer as shown in Fig. 7-9. The primary function to be performed by the latter was the realization of the previously selected, proportional-plus-integral compensator. The following conditions must be met by this configuration:

- i) The computer inputs must be in digital form (or easily convertible to that form).
- ii) The quantization levels must be sufficiently small so that all discretized quantities closely approximate their "analog" values.
- iii) All required computations must be fast so that the sampling interval and the transport delay are small.

The first of these was met by using a row of switches to specify the velocity command and appropriately processing the output of a driveshaft-mounted tachometer. This output consisted of a pulse train, and discrete estimates of velocity were obtained by counting the pulses in each sampling interval of 0.1s.⁶ Since, for the wheel tachometer employed, each pulse represented

⁶ This interval was selected to insure that the sampling time did not introduce an excessive time delay into the system.

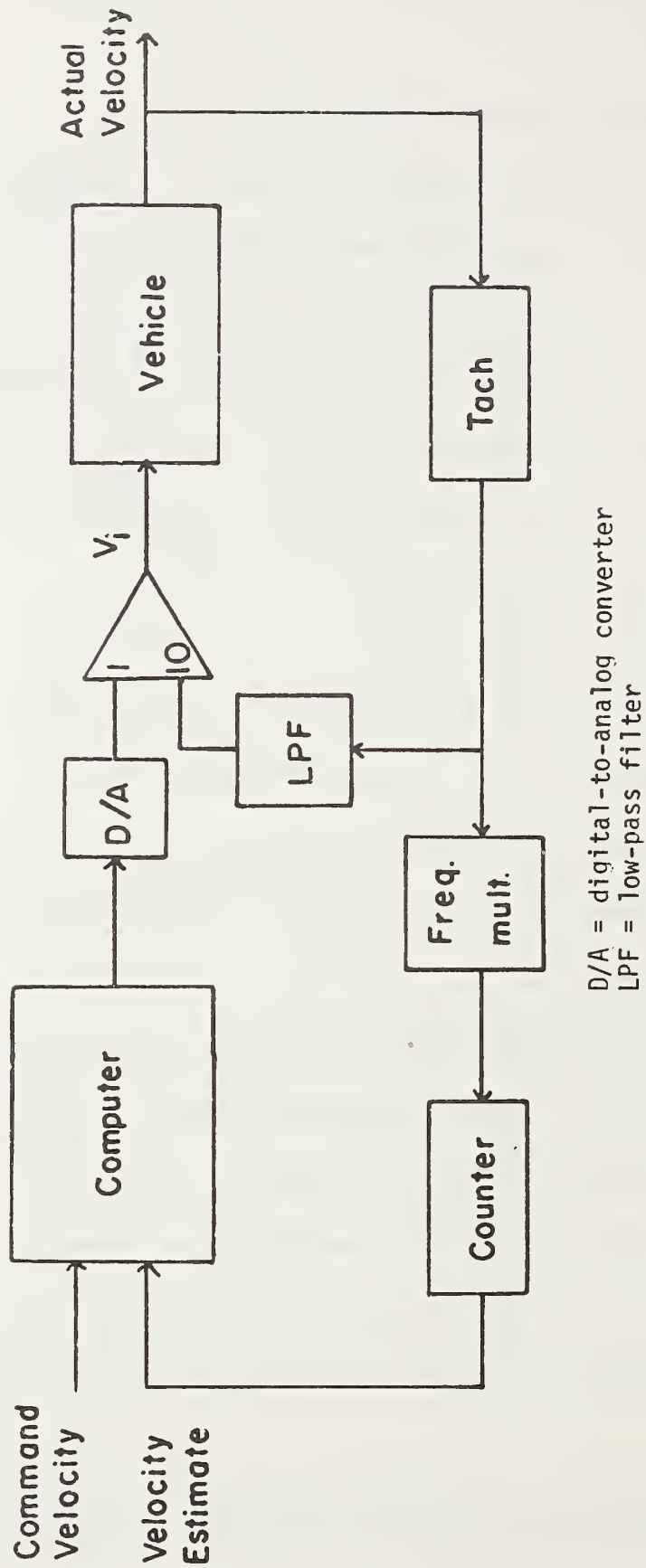


Fig. 7-9. A microcomputer realization of a velocity controller.

a distance traveled of approximately 1 cm, the velocity quantization level was some 0.12 m/s. This value was excessive so a frequency-multiplier circuit was employed to double the pulse rate and reduce the quantization level to 0.06 m/s -- an acceptable value.

The third requirement was met by using the Intel 8085, microprocessor-based system described in Appendix D. This was sufficiently fast (6.144 MHz clock, 1.3 μ s instruction cycle) and the required compensation sufficiently simple so that the transport delay was only 150 μ s -- a value well within the 0.1 s sampling time.

A flow chart of the program used for this controller is shown in Fig. 7-10 and a program listing in Reference [55]. In the first part of the program, the command and actual velocities are read and the error is determined. Then, this error is displayed on the computer readout and is available at an output port for external use. Then the counter, which stores the actual velocity (tach counts per 0.1 s) is cleared by sending a negative voltage pulse into its clear input. The integration and gain operations are performed on ΔV , and the results are added and put through a digital-to-analog converter (DAC) onto an analog summer (see Fig. 7-9).

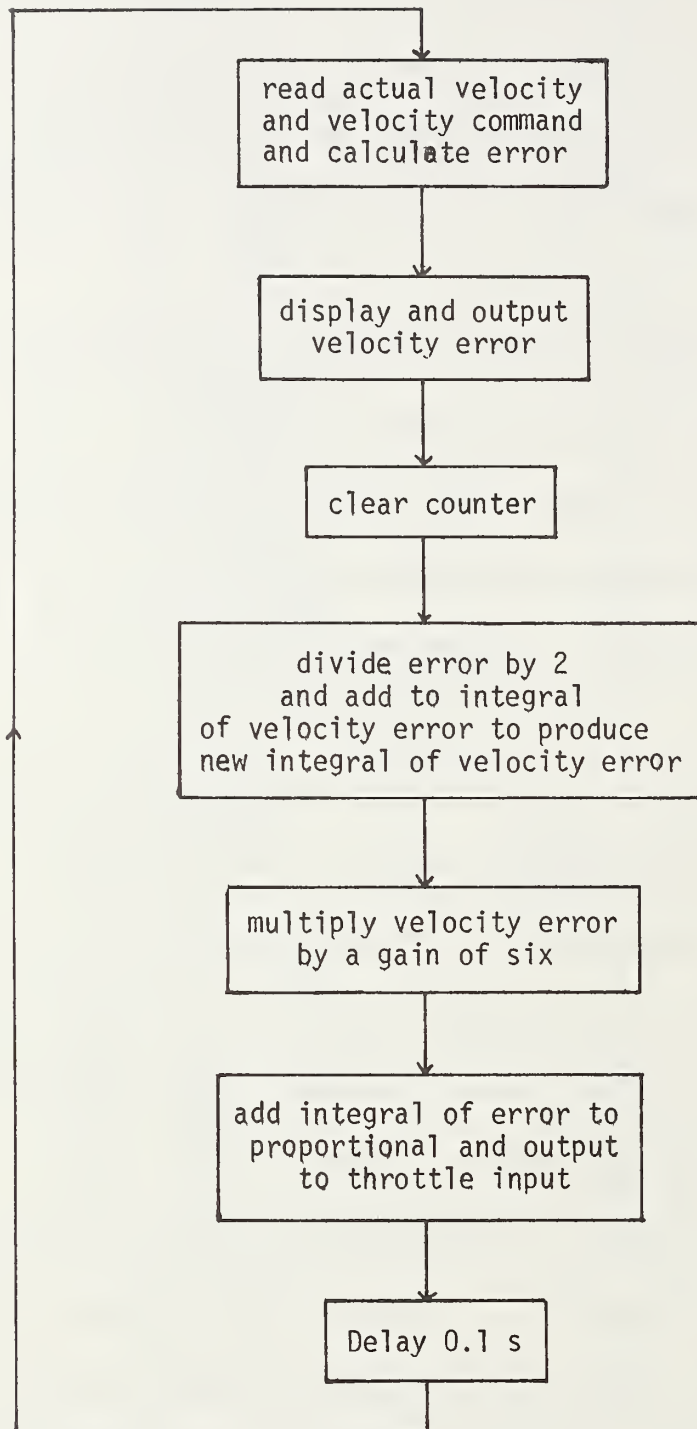


Fig. 7-10. Flow chart for velocity controller.

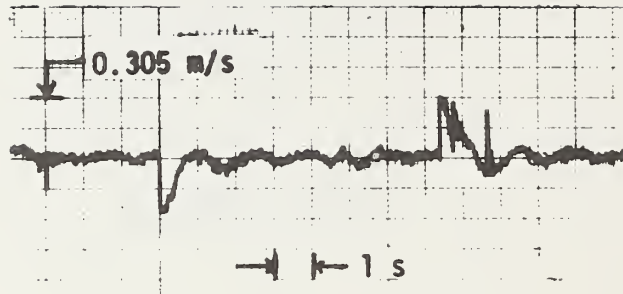
c) Test Results

To compare the operations of the two controllers, both were subjected to nearly identical full-scale tests in which an instrumented, 1965 Plymouth sedan was employed. A step input command speed was applied to this vehicle, which was moving at a constant speed V_{CO} , and as the vehicle responded, $\Delta V = V_C - V$ was recorded. Typical responses, for initial speeds of 9.15, 12.2, 15.3, 18.2, and 21.3 with 0.3 m/s step inputs, are shown in Figs. 7-11 to 7-15.

Note that the responses with both controllers are over-damped as expected. However, while the responses with the analog controller are characterized by a time constant of some 0.56 s, those with the digital controller are somewhat slower. This is at least partly due to the reduced integral gain in the digital controller -- a reduction intended to shorten program length and development time.

The response of the digital controller to disturbance inputs was "synthetically" examined by recording the velocity error as the vehicle entered and traversed a curved portion of track. Note from Fig. 7-16 that this error was always within ± 0.06 m/s of the command velocity.

One operational problem encountered in early digital controller tests was power supply noise which resulted in erratic

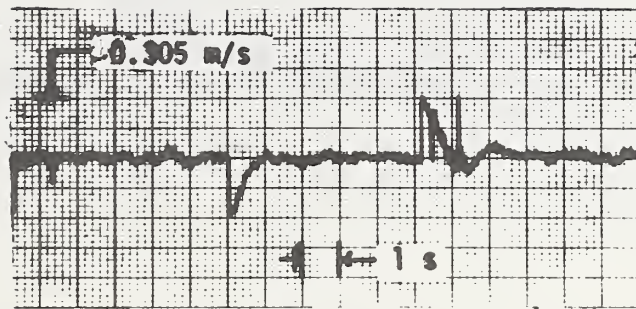


(a) analog controller

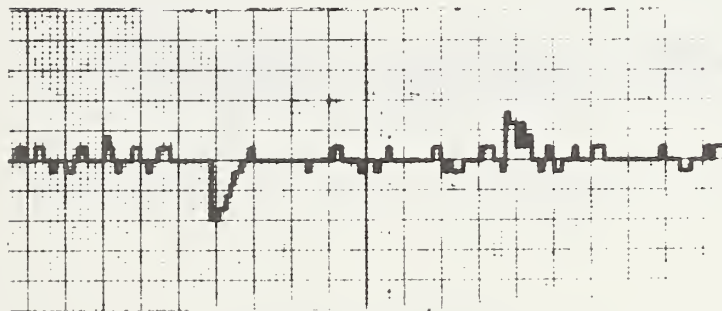


(b) digital controller

Fig. 7-11. Step responses of velocity controllers, $V_{CO} = 9.15$ m/s.

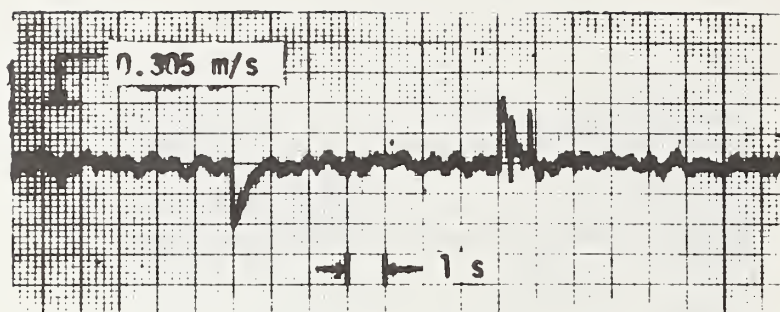


(a) analog controller

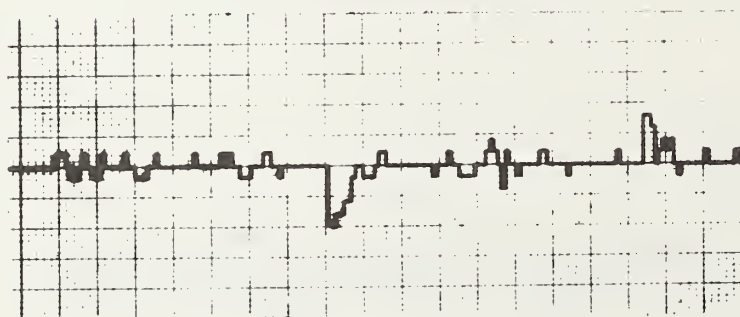


(b) digital controller

Fig. 7-12. Step responses of velocity controllers, $V_{co} = 12.2$ m/s.

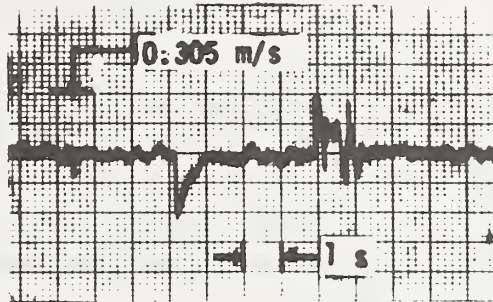


(a) analog controller

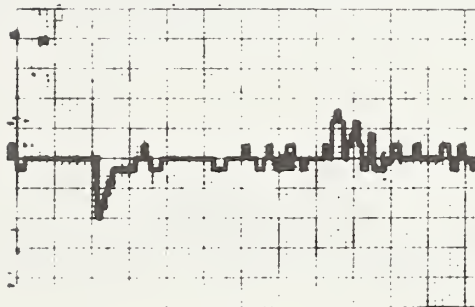


(b) digital controller

Fig. 7-13. Step responses of velocity controllers, $V_{CO} = 15.2$ m/s.

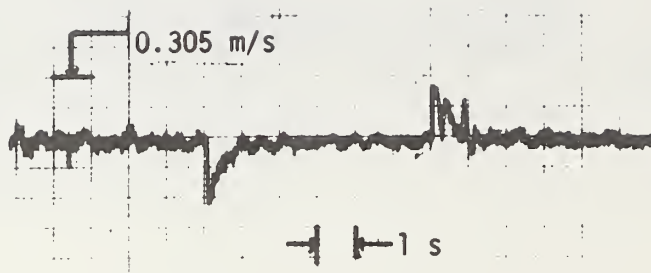


(a) analog controller



(b) digital controller

Fig. 7-14. Step responses of velocity controllers, $V_{CO} = 18.3$ m/s.

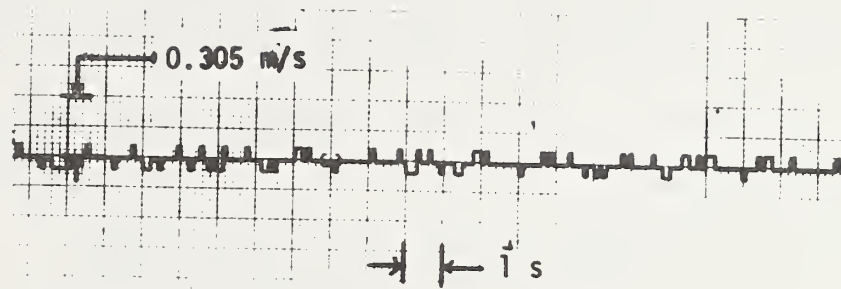


(a) analog controller



(b) digital controller

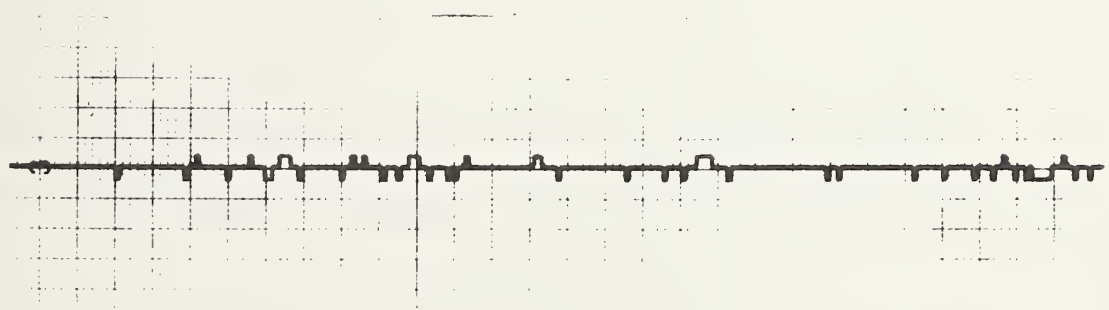
Fig. 7-15. Step responses of velocity controllers, $V_{CO} = 21.3$ m/s.



(a) 9.15 m/s.



(b) 15.2 m/s.



(c) 18.2 m/s.

Fig. 7-16. Steady-state tracking of digital velocity controller around a curved portion of track.

computer operations. This difficulty was overcome by appropriate modification of an AC unit which was employed with other test equipment. Subsequently, there were no operational problems, and the functioning of the digital controller was at least as reliable as the analog one.

D. Longitudinal Position Controller Implementation

The desired longitudinal controller can be implemented using the software concepts discussed here and the hardware configuration discussed in Appendix D. In view of the excellent results obtained from the testing of a simple velocity controller, there appears to be no practical difficulties involved in realizing the more complex position controller of Fig. 7-6.

CHAPTER VIII
SUMMARY AND FUTURE EFFORTS

A. Summary

The control required for an automated highway system can be achieved via a hierarchy wherein a centralized computer would oversee network operations with this including the coordination of activities in the individual geographic regions comprising the network. A second level of control would be at the regional level. Each regional controller would supervise the activity of a number of sectors and control the vehicles in those sectors via appropriate commands to the sector computers which comprise the third level of control. The fourth, and lowest, level of control is that of the individual vehicle. The concern here is with control of the sector level which is comprised of four essential facets:

- a) The specification of the desired state of each vehicle;
- b) The determination of the actual state of each vehicle;
- c) Communications between each vehicle and sector-control; and
- d) The control of each individual vehicle.

Each of the facets can be viewed in the context of either longitudinal or lateral control.

During the past year, which was the final year of a three-year program, the research efforts were focused principally on the continuing development of a physical test facility which will be employed to study control and communication problems at, and below, the sector level. This will be done in the context of high-speed (to 26.8 m/s) operations at time headways as small as 1 s.

The principal accomplishments during this year were:

- 1) The selection of a sector-level control concept, the design and implementation of hardware required for sector-level operations, and the choice of geometrics over which online control would be realized;
- 2) The development and field evaluation of a sector computer-to-controlled vehicle communication link;
- 3) The design, development and field evaluation of a "radar" approach to lateral control; and
- 4) The design and field evaluation of a vehicle longitudinal controller which provided excellent performance -- a small-position error, a comfortable ride, and a relative insensitivity to disturbance forces -- on a consistent basis over a wide range of environmental conditions.

The above were integrated and a demonstration of online control, which involved 2 test vehicles operating at a time headway of 1 s, was given. The highlight of this demonstration involved the merging of an initially stationary vehicle into a position 1 s ahead of a mainline vehicle traveling at a speed of 26.8 m/s.

The secondary activities included the design, construction, and field evaluation of a guidewall structure for use in radar steering, and a start toward converting the analog electronics, employed in the vehicle lateral and longitudinal controllers, to a discrete digital realization. The latter was accomplished using microprocessors and involved the digital realization of both a lateral and a longitudinal controller. The former, which involved a previously designed, velocity-adaptive controller, was extensively tested and yielded excellent performance -- tracking error < 0.063 m, a good insensitivity to disturbance forces, and a comfortable ride. The latter, which involved the realization of a simple velocity controller, originally designed by Bender and Fenton [25], was also field tested with good results; however, it remains to similarly implement the more complex, better-performing longitudinal controller discussed in Chapter VI. The microprocessors employed here can also be employed in a vehicle-based, decision-making role.

B. Future Directions

In view of the results obtained from this study, it is proposed that future AHS technology development efforts should be focused on the following:

- a) The continued development of the automated vehicle test facility at TRCO;
- b) The implementation of an online computing system which could accomplish all sector-level control tasks;
- c) An intensive study of a multi-processor system for in-vehicle use;
- d) Studies of radar-sensing techniques for use in both lateral and longitudinal control; and
- e) Studies in vehicle longitudinal control with an emphasis on both emergency operations and the trade-offs between fuel usage, vehicle tracking accuracy and ride comfort.

REFERENCES

1. Fenton, R.E., "A Headway Safety Policy for Automated Highway Operations", IEEE Transactions on Vehicular Technology, Vol. VT-28, No. 1, February 1977, pp. 22-28.
2. Anon., "Practicality of Automated Highway Systems", Final Report on Contract DOT-FH-11-8903, CALSPAN Corp., Buffalo, N.Y., Nov. 1977.
3. Anon., Proceedings of the First International Conference of Dual-Mode Transportation, Washington, D.C., May 29-31, 1974.
4. Gardels, K., "Automatic Car Controls for Electronic Highways", General Motors Research Laboratories, General Motors Corporation, Warren, Michigan, GMR-276, June 1960.
5. TRW Systems Group, "Study of Synchronous Longitudinal Guidance as Applied to Intercity Automated Highway Networks", Final Report prepared for the Office of High Speed Transportation, Department of Transportation, September 1969.
6. Stefanik, R.G., and Kiselewich, S.J., "Evaluation of the Operating Conditions of a Detroit Dual-Mode Vehicle

- Network", presented at the 1972 SAE Automotive Engr. Congress, Jan. 1972, SAE Paper 720272.
7. Wilson, D.G., Ed., "Automated Guideway Transportation Between and Within Cities", Urban Systems Laboratory Rpt. No. FRA-RT-72-14, Mass. Institute of Technology, Cambridge, Mass., Feb. 1971 (PB 206-269).
 8. Giles, G.C., and Martin, J.A., "Cable Installation for Vehicle Guidance Investigations in the New Research Track at Crowthorne, JAM Road Research Lab., Crowthorne, England, Rpt. RN/40 57/CGG.
 9. Oshima, Y., Kikuchi, E., Kimura, M., and Matsumoto, S., "Control System for Automobile Driving", Proceedings Tokyo IFAC Symposium, 1965, pp. 347-357.
 10. Fenton, R.E., et al., "One Approach to Highway Automation", Proceedings of the IEEE, Vol. 46, No. 4, April 1968, pp. 556-566.
 11. Fenton, R.E., et al., "Advances Toward the Automatic Highway", Highway Research Record, No. 344, Washington, D.C., Jan 1971, pp. 1-20.
 12. Fenton, R.E., and Olson, K.W., "An Investigation of Highway Automation", Rpt. EES 276-6, Dept. of Elec. Engr., The Ohio State University, Columbus, Ohio, March 1969.

13. Anon., "An Investigation of Highway Automation", Rpt. EES 276-A-12, Dept. of Elec. Engr., The Ohio State University, Columbus, Ohio, April 1971.
14. Fenton, R.E., Ed., "An Investigation of Highway Automation", Rpt. No. 276A-15, Dept. of Elec. Engr., The Ohio State University, Columbus, Ohio, September, 1974.
15. Olson, K.W., et al., "Studies in Vehicle Automatic Lateral Control -- Theory and Experiment", Appendix I to "An Investigation of Highway Automation", Rpt. 276A-16, Dept. of Elec. Engr., The Ohio State University, Columbus, Ohio, September 1974.
16. Fenton, R.E., et al., "Studies in Synchronous Longitudinal Control", Transportation Control Laboratory Rpt. EES 276A-17, Dept. of Elec. Engr., The Ohio State University, Cols., Ohio, September 1974.
17. Fenton, R.E., Ed., "Fundamental Studies in the Automatic Longitudinal Control of Vehicles", Final Report on DOT-OS-40100, Transportation Control Laboratory, The Ohio State University, Columbus, Ohio, July 1975 (Available from NTIS).
18. Anon., "Practicality of Automated Highway Systems", Final Report on Contract DOT-FH-11-8903, CALSPAN Corp., Buffalo, N.Y., Nov. 1977 (This report is available from NTIS).

19. Fenton, R.E., et al., "Fundamental Studies in the Longitudinal Control of Automated Ground Vehicles", Transportation Control Lab Report RF 4302A1-1, The Ohio State University, Columbus, Ohio, December 1976.
20. Fenton, R.E., et al., "Fundamental Studies in Automatic Vehicle Control", Interim report on Contract DOT-FH-11-9257, Transportation Control Laboratory, The Ohio State University, Columbus, Ohio, May 1978.
21. Fenton, R.E., et al., "Fundamental Studies in Automatic Vehicle Control," 2nd Interim report on Contract DOT-FH-11-9257, Transportation Control Laboratory, The Ohio State University, Columbus, Ohio, May 15, 1979.
22. Zworykin, V.K. and Flory, L.E., "Electronic Control of Motor Vehicles on the Highway", Highway Research Board (Proceedings of 37th Annual Meeting of Highway Research Board), Vol. 37, 1958, pp 436-451.
23. Bender, J.G., et al., "An Experimental Study of Vehicle Automatic Longitudinal Control", IEEE Trans. on Veh. Tech., VT-20, 1971, pp 114-123.
24. Levis, A.H. and Athans, M., "On the Optimal Sampled-Data Control of a String of Vehicles", Transportation Science, Vol. 1, 1968, pp 362-382.

25. Bender, J.G. and Fenton, R.E., "On the Flow Capacity of Automated Highways", Transportation Science, Vol. 4, 1970, pp 52-63.
26. Gluck, H.D., "Some Design Criteria for an Automated Roadway", M.Sc. Thesis, 1964, M.I.T. Cambridge, Mass.
27. Godfrey, M.B., "Merging in Automated Transportation Systems", Sc.D. Thesis, 1968, M.I.T. Cambridge, Mass.
28. Boyd, R.K. and Lucas, M.P., "How to Run on Automated Transportation System", IEEE Transactions on Systems, Man, and Cybernetics, SMC-2, 1972, pp 331-341.
29. Howson, L.L., "Computer Simulation for an Automated Roadway Network", Gen. Motors Res. Lab., Rep. GMR-1153, 1972.
30. Munson, A.V., "Quasi-Synchronous Control of High-Capacity PRT Networks," in Personal Rapid Transit, Univ. of Minnesota, 1972, pp 325-350.
31. Rule, R.G., "The Dynamic Scheduling Approach to Automated Vehicle Macroscopic Control", Trans.Control Lab. Rpt. EES-276-18, 1974, The Ohio State University.
32. Roseler, W.J. et al, "Comparisons of Synchronous and Quasi-Synchronous PRT Vehicle Management and Some Alternative Routing Algorithms", Personal Rapid Transit II, Univ. of Minnesota, 1974, pp 425-438.

33. Kornhauser, A.L. and McEvaddy, P.J., "A Quantitative Analysis of Synchronous vs. Quasi-Synchronous Network Operations of Automated Transit Systems", Transportation Research, Vol. 9, 1975, pp 241-248.
34. Claffey, P.J. and Associates, "Running Costs of Motor Vehicles as Affected by Road Design and Traffic", National Cooperative Highway Research Program Report 111, Highway Research Board, 1971.
35. G.M. Takasaki, "Some Vehicle and Sector Aspects of Automated Ground Transportation", Ph.D. Dissertation, The Ohio State University, 1977.
36. M. Swartz, Information, Transmission, Modulation and Noise , McGraw Hill Book Co., New York, 1970, pp 416.
37. Smith, Robert T., "Automated Highway Communications Systems" M.Sc. Thesis, Dept. of Elec. Engr., The Ohio State University, Columbus, Ohio 1980.
38. Saxton, L., "Automated Highway Systems -- Consideration for Success," Proceedings of International Conference on Transportation Electronics, Sept. 15-18, 1980, Dearborn, Michigan.
39. Boyer, W.D. and Nilssen, O.K., "Amplitude Modulated CW Radar," IRE Transactions on Aerospace and Navigational Electronics, December, 1962.

40. Marukawa, T., and Namekawa, T., "An Accurate System of FM-CW Radar for Approach Using Phase Detection," Electronics and Communications in Japan, Vol. 58-B, No. 2, 1975.
41. Nicolson, A.M., and Ross, G.F., "A New Radar Concept for Short Range Application," Research Paper, Sensor Systems Department, Sperry Research Center, Sunbury, Massachusetts, February, 1975.
42. Skolnik, Merrill, I., Introduction to Radar Systems, McGraw-Hill Book Company, New York, 1962.
43. Bishel, R.A., "The Design and Development of an Ultra-Short Range Radar for Use in a Lateral Control System for Automated Ground Transportation," M.Sc. Thesis, Department of Electrical Engineering, The Ohio State University, Columbus, Ohio 43210, March 1980.
44. Cormier, W.H., "Experimental Studies in Vehicle Lateral Control," M.Sc. Thesis, Dept. of Elec. Engr., The Ohio State University, Columbus, Ohio, Dec. 1978.
45. Murthy, S.S., "A Microprocessor-Based Vehicle Lateral Controller," M.Sc. Thesis, Dept. of Elec. Engr., The Ohio State University, Columbus, Ohio, 1980.

46. Blumberg, P.N., "Powertrain Simulation: A Tool for the Design and Evaluation of Engine Control Strategies in Vehicles," SAE Paper No. 760158, Society of Automotive Engineers, New York.
47. Waters, W.C., "General Purpose Automotive Vehicle Performance and Economy Simulator," SAE Paper No. 720043, Society of Automotive Engineers, New York, N.Y., 1972.
48. Wollam, J.M., "Generalized Tracked and Wheeled Vehicle Automotive Performance Model," SAE Paper 710628, Society of Automotive Engineers, New York.
49. Blackwell, L.M., "A Study of the Adaptability of the Automobile to Automatic Control," Rept. No. EES 276A-3, Dept. of Elec. Engr., The Ohio State University, Columbus, Ohio, Feb. 1967.
50. Takasaki, G.M., "Vehicle Synchronous Longitudinal Control in Normal Situations," M.Sc. Thesis, Dept. of Elec. Engr., The Ohio State University, Columbus, Ohio 1974.
51. Fenton, R.E., and Chu, P.M., "On Vehicle Automatic Longitudinal Control," Transportation Science, Vol. 11, No. 1, Feb. 1977, pp. 73-91.
52. Bender, J.G., and Fenton, R.E., "On Vehicle Longitudinal Dynamics," Traffic Flow and Transportation, G.N. Newell, Ed., American Elsevier Publ. Co., Inc, New York, 1972.

53. Cribbs, T.B., "Studies in the Longitudinal Control of Automated Vehicle Propulsion," M.Sc. Thesis, Dept. of Elec. Engr., The Ohio State University, Columbus, Ohio, 1979.
54. Kneifel, R.W. II, "On the Development of a Propulsion Controller for an Automated Highway Vehicle," M.Sc. Thesis, Dept. of Elect. Engr., The Ohio State University, Columbus, Ohio, 1980.
55. Thayer, Larry J., "A Microcomputer-Based Longitudinal Controller for Automated Vehicles," M.Sc. Thesis, Dept. of Elect. Engr., The Ohio State University, Columbus, Ohio, 1979.

APPENDIX A
ON THE LATERAL RIDE QUALITY OF
A WIRE-FOLLOWING SYSTEM

In previous test-track evaluations of vehicle lateral controllers, wherein a buried cable was used for reference purposes, ride comfort was generally evaluated subjectively although peak values of lateral acceleration were recorded [1]. This approach was taken since the lateral acceleration (a_{CG}) at the vehicle's center of gravity was generally so small $|a_{CG}| < 0.05 \text{ g}$ that meaningful measurements were difficult to obtain with available accelerometers.

During the past year it was necessary to compare the performance of the wire-following system and the side-mounted radar discussed in Chapter IV, and it was preferable to use quantitative measures of both lateral tracking accuracy and ride comfort in this comparison. The measures selected were the rms values of a_{CG} , a_f , and ΔS_f where a_f is the lateral acceleration as measured at the front center of the vehicle and ΔS_f is the lateral position error at that location.

The three rms measurements were made at each of five speeds -- 10 m/s, 13.4 m/s, 20 m/s, 26.8 m/s, and 35.7 m/s -- and measurement intervals of some 40 s. The test roadway employed was the straight section of the TRCO skid pad (see Fig.

3-12) which is characterized by longitudinal grades ranging from -0.44 to +0.44%.

The test vehicle was a 1965 Plymouth sedan, and its lateral position was obtained by sensing the field from a wire-following configuration. The controller employed was the velocity-adaptive unit designed by Cormier [1] and a crosswind, which varied from 0 - 3.6 m/s, was present during the tests.

Initially, unfiltered measurements of a_{CG} , a_f , and ΔS_f were used as inputs to the rms measuring circuits. As a major portion of both a_{CG} and a_f was due to high-frequency (14 - 25 Hz) engine effects, which do not significantly affect ride comfort, a second series were conducted to reduce these effects on the measurement. This was done by filtering both a_{CG} and a_f with a 7.95-Hz, single-pole filter prior to the computation of the rms values.

The rms accelerations for both cases are shown in Figs. A-1 and A-2. Within each case, the data points are scattered at each speed, an effect which is due to the variable wind force acting, the nonlevel pavement (both in the longitudinal and lateral directions), and the presence of some minor pavement irregularities.

In the unfiltered case, $(a_{CG})_{rms}$ increases from 0.06 m/s² at a forward speed of 10 m/s to 0.26 m/s² at 35.7 m/s, whereas in the filtered case the corresponding range is 0.04 to 0.12 m/s² (see Fig. A-1). The results for $(a_f)_{rms}$, which are

shown in Fig. A-2, are similar in form; however, the measured values are much larger. This is an expected result since

$$a_f = a_{cg} + 3\ddot{\psi},$$

where $\ddot{\psi}$ is the vehicle's yaw acceleration.

In both cases, the differences between the filtered and the unfiltered results can be attributed to engine effects which increase with increasing speed. As the test vehicle is 15 years old and has undergone much severe testing, these effects may be worse than those of a newer vehicle.

The tracking data are shown in Fig. A-3 as a function of speed. In essence, $(\Delta S_f)_{rms}$ increases with increasing speed; e.g., $(\Delta S_f)_{rms} = 0.8$ cm at 9.4 m/s while at 35.7 m/s, it is 1.7 cm.

In summary, the position errors and lateral accelerations were quite low and, on this basis, the tracking capability and the lateral ride quality of this wire-following controller can be described as excellent.

REFERENCE

1. Fenton , R.E., et al, "Fundamental Studies in Automatic Vehicle Control," Interim Report on Contract DOT-FH-11-9257, Transportation Control Laboratory, The Ohio State University, Columbus, Ohio, May 15, 1979.

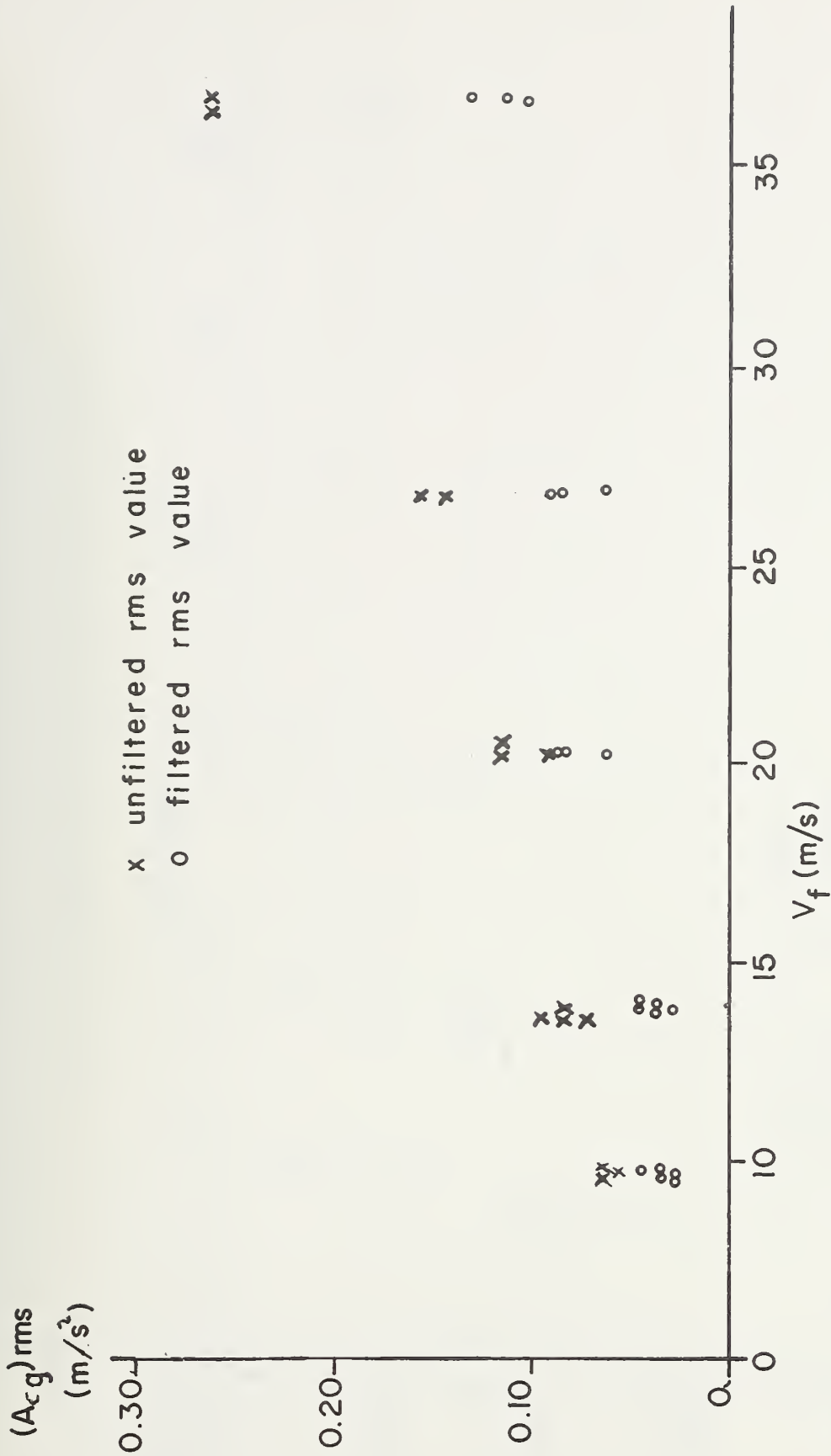


Fig. A-1 Acceleration (rms) at vehicle's cg.

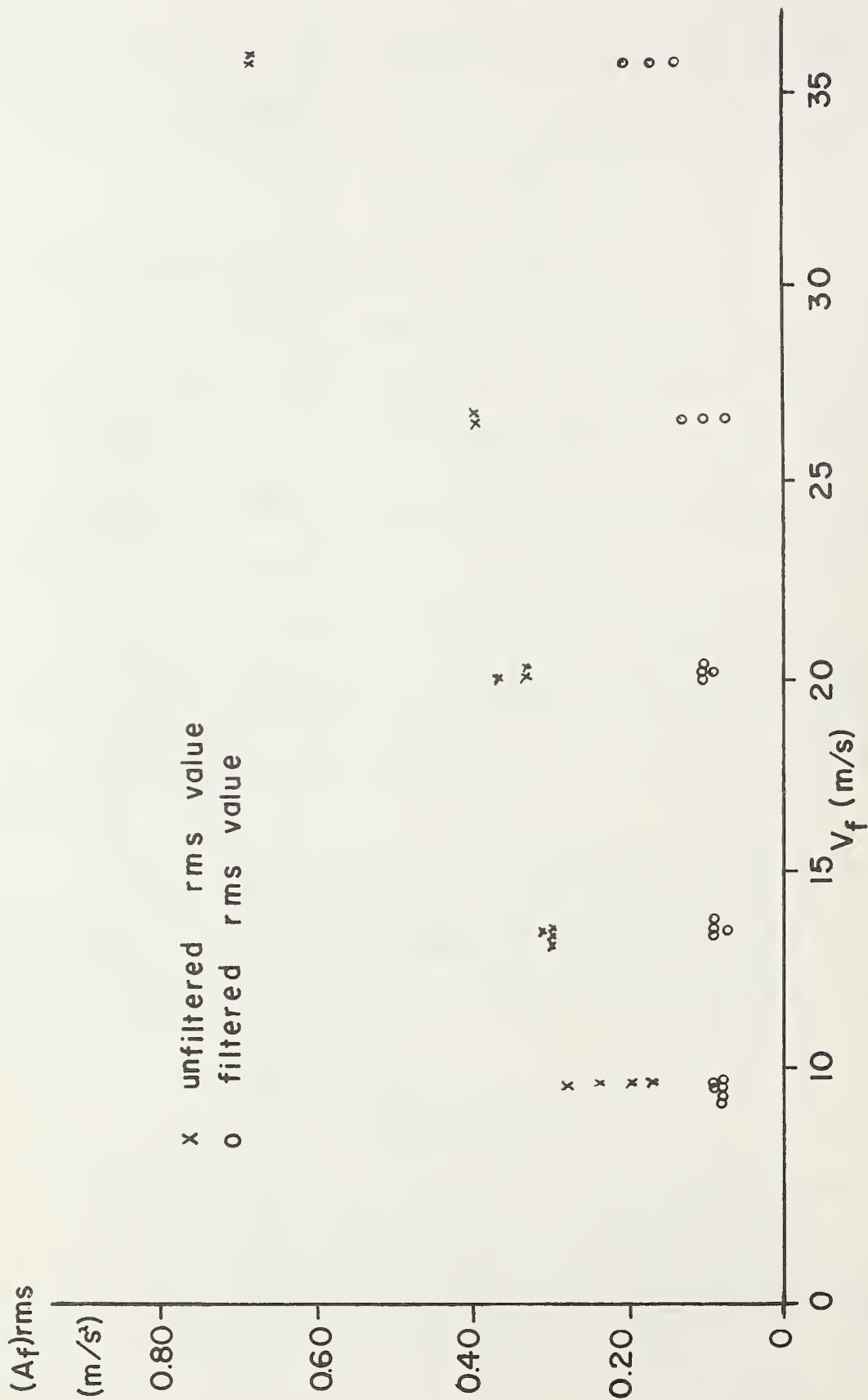


Fig. A-2 Acceleration (rms) at front center of vehicle.

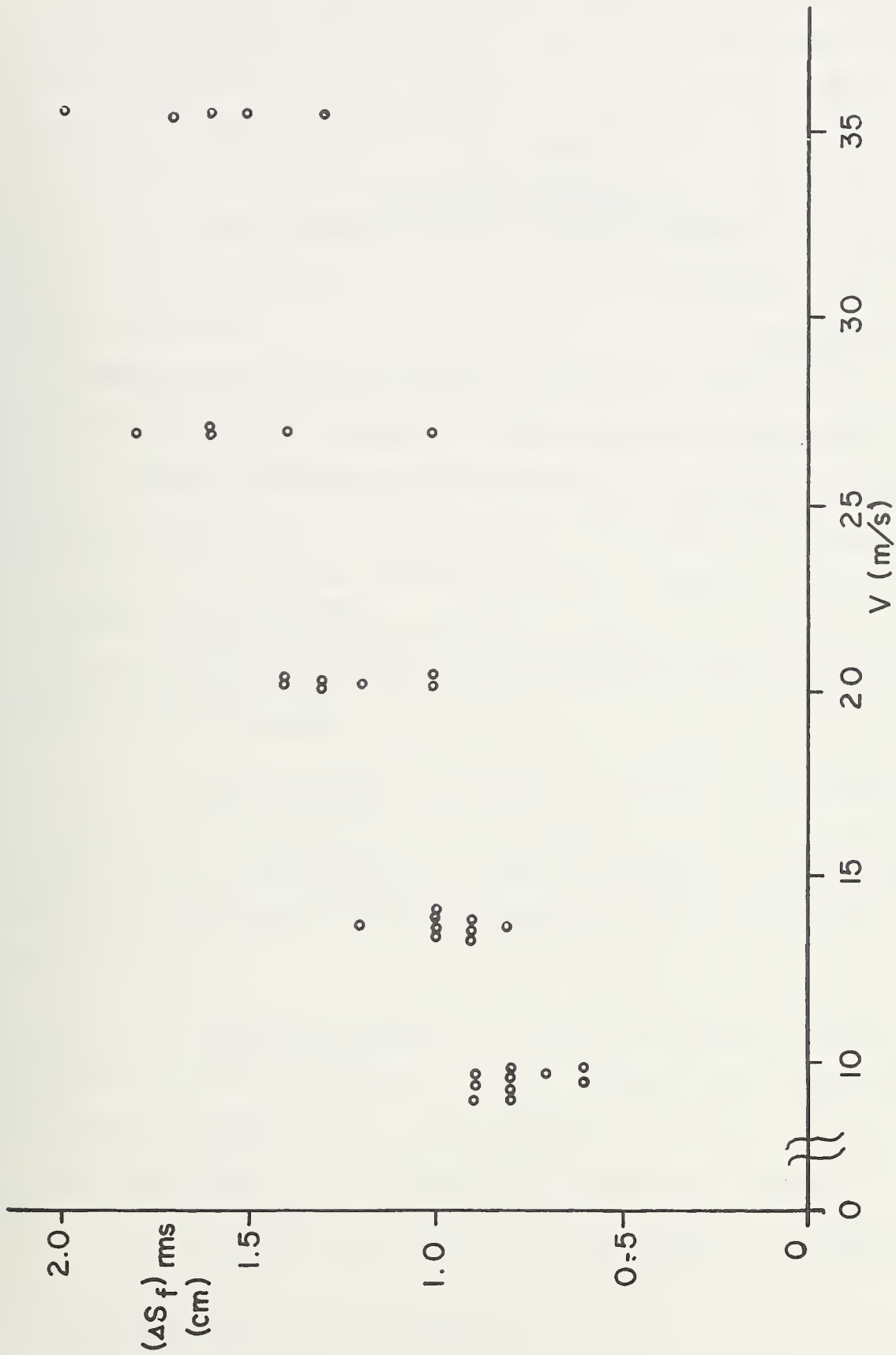


Fig. A-3 Tracking error (rms) at the vehicle's front center.

APPENDIX B
A COORDINATE SYSTEM FOR
AUTOMATIC LATERAL CONTROLLER DESIGN

A. Introduction

Automatic lateral control is an essential function for all classes of automated ground vehicles [1]-[3]. The purpose of such control is to cause a vehicle to follow a desired path even in the presence of disturbance forces (e.g., those due to sidewinds). This path is generally described in a fixed-base, inertial-coordinate system and, as a result, it is very cumbersome to describe a controlled vehicle's motion on anything but a straight path. This is a principal reason why the majority of past designs have considered only this case [4]-[9]. However, as Cormier has demonstrated, good performance (i.e., a small tracking error, a comfortable ride, and a relative insensitivity to disturbances) on a straight-line path doesn't necessarily mean similar performance on a curving one [10]. As a vehicle should be capable of following a variety of paths, the controller must be designed accordingly.

Here, two approaches to describing the desired path and a controlled vehicle's motion are presented. The first involves an inertial coordinate system and the second a path-dependent one. Each of these is examined in detail and reasons for selecting the latter for use in analysis and design are delineated.

In this effort, it is convenient, for illustrative purposes, to represent vehicle lateral dynamics by a linear, 2 degree-of-freedom model. The latter is adequate to describe a vehicle's lateral motions provided the vehicle lateral acceleration is small [11] - [12]. This model is characterized by three inputs F_d , F_e , and δ and two outputs, $\dot{\psi}$ and V_s , as shown in Fig. B-1¹ (A third quantity V_f , which is associated with the longitudinal motion of the vehicle is, for convenience, also shown as available).

There is no loss in generality by setting $F_d = F_e = 0$, since the principal concern here is describing vehicle motion. The effects of $|F_d| > 0$ and/or $|F_e| > 0$ on this motion are easily incorporated as demonstrated in Section III.

B. INERTIAL REFERENCE FRAME

Consider the situation shown in Fig. B-2 where a vehicle is progressing along the desired path

$$\underline{S}_0 = X_0(t)\underline{x} + Y_0(t)\underline{y} \quad (\text{B1})$$

as defined in an inertial coordinate system. The actual vehicle path is obtained by integrating the velocity of the vehicle's center of gravity (cg). Since, from Fig. B-2

$$\dot{X}(t) = V_f \sin \Psi + V_s \cos \Psi \quad (\text{B2})$$

and

$$\dot{Y}(t) = V_f \cos \Psi - V_s \sin \Psi \quad (\text{B3})$$

then

$$X(t) = \frac{1}{\rho} \dot{X}(t) \quad (\rho \equiv \frac{d}{dt}) \quad (\text{B4})$$

¹All symbols are defined in Table B-1

TABLE B-1
DEFINITION OF SYMBOLS

Symbol	Definition
A_1	Distance from cg to front center of vehicle
a_{cg}	Lateral acceleration of the vehicle's cg
a_f	Lateral acceleration of the front center of a vehicle
\underline{F}_d	Disturbance force
F_{dt}	Disturbance force in \underline{T} direction
F_{dN}	Disturbance force in \underline{N} direction
p	Differential operator ($\equiv \frac{d}{dt}$)
$\underline{N}(s)$ (or \underline{N})	Unit vector perpendicular to \underline{S}_D at locations (See Fig. B-5)
$R(s)$	Radius of curvature of path at location s
s	Distance along path from origin
\underline{S}_D	Desired path for vehicle cg (See Fig. B-2 or B-5)
\underline{S}_{DF}	Desired path relative to front center of vehicle
\underline{S}_f	Actual path traveled by front center of vehicle
\underline{S}_{cg}	Location of vehicle cg
ΔS_{cg}	Deviation of vehicle cg from path
$\underline{T}(s)$ (or \underline{T})	Unit vector tangent to \underline{S}_D at location s (See Fig. B-5)
$X_D(t)$	x component of $\underline{S}_D(t)$
$X(t)$	x component fo vehicle cg location (See Fig. B-2)
\underline{x}	Unit vector in x direction (See Fig. B-2)
$Y_D(t)$	y component of $\underline{S}_D(t)$
$Y(t)$	y component of vehicle cg location (See Fig. B-2)

TABLE B-1 (continued)

Symbol	Definition
\underline{y}	Unit vector in y direction (See Fig. B-2)
V_S	Side velocity of vehicle
V_f	Forward velocity of vehicle
\underline{V}	Total velocity of vehicle
ψ	Vehicle yaw angle (See Fig. B-2)
ψ_D	Path yaw angle (See Fig. B-2)
$\Delta\psi$	$= \psi - \psi_D$
δ	Front-wheel angle

Note: A dot over a variable denotes differentiation by time (e.g., $\dot{\psi} = p\psi$).

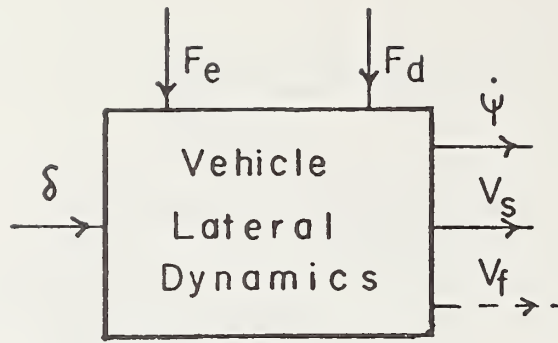


Fig. B-1 A simplified model of a vehicle's lateral dynamics.

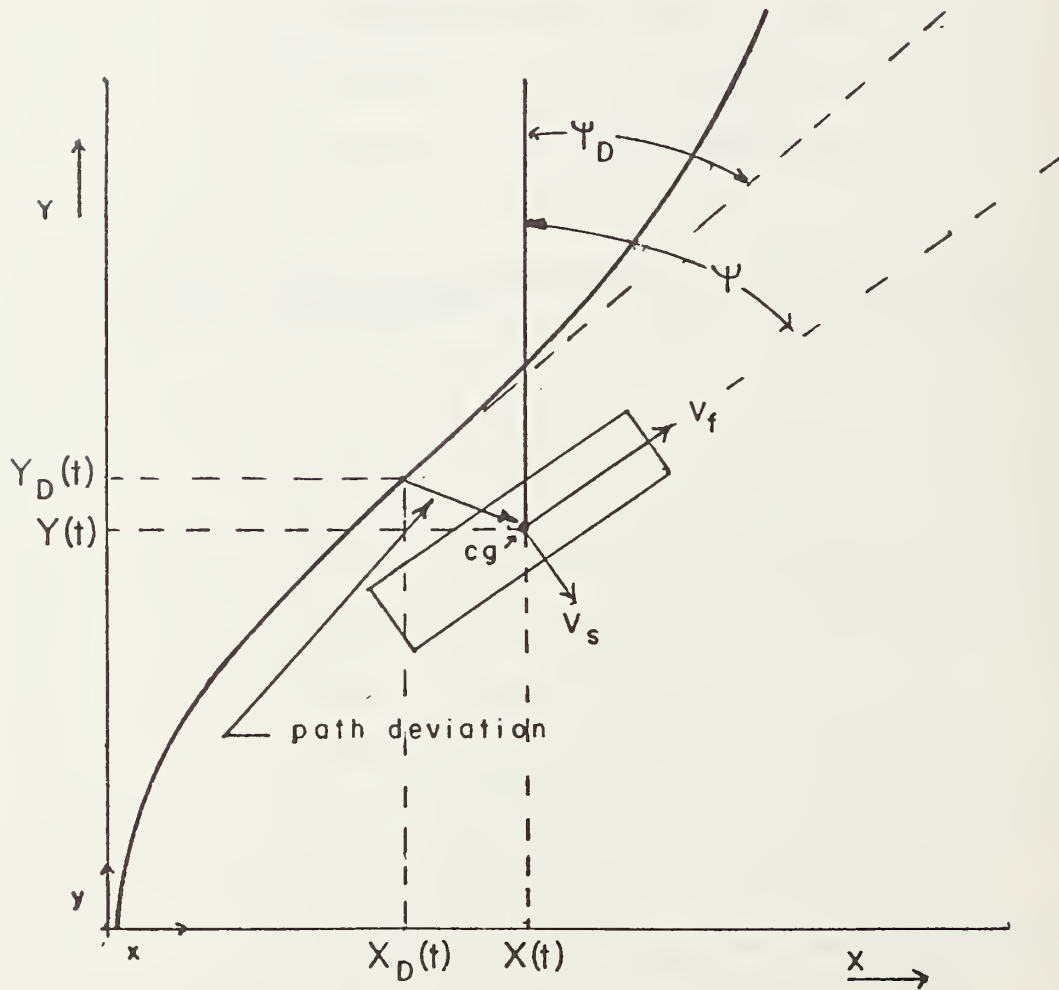


Fig. B-2 Vehicle motion as described in an inertial reference frame.

and

$$Y(t) = \frac{1}{\rho} \dot{Y}(t) \quad (\text{B5})$$

The deviation of the cg from the desired path is

$$[X_D(t) - X(t)] \underline{x} + [Y_D(t) - Y(t)] \underline{y} \quad (\text{B6})$$

This vector is depicted in Fig.B-2 and corresponds to one signal that could be employed by a controller to maintain the vehicle cg on or close to \underline{S}_D . This representation is overly general as the measured quantity would probably be the perpendicular distance from the vehicle longitudinal body axis to \underline{S}_D . Thus, it is convenient to let its intersection with \underline{S}_D be the desired state point.

A measurement, which is employed in wire-following configurations [10] - [11], [13] - [16], is made a distance A_1 ahead of the vehicle's cg (e.g., relative to the vehicle's front center) and relative to the longitudinal body axis. The coordinates of this measurement point are

$$\underline{S}_f = [X(t) + A_1 \sin \psi] \underline{x} + [Y(t) + A_1 \cos \psi] \underline{y} \quad (\text{B7})$$

and those of the corresponding "path point" are

$$\underline{S}_{df} = [X_D(t) + A_1 \sin \psi_D] \underline{x} + [Y_D(t) + A_1 \cos \psi_D] \underline{y} \quad (\text{B8})$$

The resulting deviation is

$$\underline{S}_{df} - \underline{S}_f = [X_D(t) - X(t) + A_1(\sin \psi_D - \sin \psi)] \underline{x} + [Y_D(t) - Y(t) + A_1(\cos \psi_D - \cos \psi)] \underline{y} \quad (\text{B9})$$

If $\psi = \psi_D + \Delta\psi$, where $\Delta\psi$ is small, then

$$\sin \psi_D - \sin(\psi_D + \Delta\psi) \approx -(\cos \psi_D) \Delta\psi$$

and

$$\cos \psi_D - \cos(\psi_D + \Delta\psi) \approx (\sin \psi_D) \Delta\psi$$

Substituting these approximations into Eqn.(B8), results in

$$\begin{aligned} \underline{S}_{df} - \underline{S}_f \approx & \left[X_o(t) - X(t) - A_1 (\cos \psi_o) \Delta \psi \right] \underline{x} \\ & + \left[Y_o(t) - Y(t) + A_1 (\sin \psi_o) \Delta \psi \right] \underline{y} \end{aligned} \quad (B 10)$$

This result is employed in the block diagram of Fig.B-3. The input is \underline{S}_D , the output \underline{S}_f , and the role of the coordinate transformation block is to convert ψ , V_s , V_f and X_D and Y_D into \underline{S}_f by the steps detailed in Eqns. (B2)-(B5) and (B 10). Since

$$\psi_o = \tan^{-1} \frac{dX_o}{dY_o},$$

it would be redundant to include it explicitly as an input to this block.

It is difficult to use this configuration for analysis purposes since the coordinate transformation is nonlinear and the description of the path using vectors is very cumbersome. However, if the restriction is made that the vehicle is traveling at a constant speed on the straight path

$$\underline{S}_o(t) = O \underline{x} + Y_o(t) \underline{y} \quad (B 11)$$

and ψ and V_s are small, then Eqns.(B2) and(B3) reduce to

$$\dot{X}(t) \approx V_f \psi + V_s \quad (B 12)$$

and

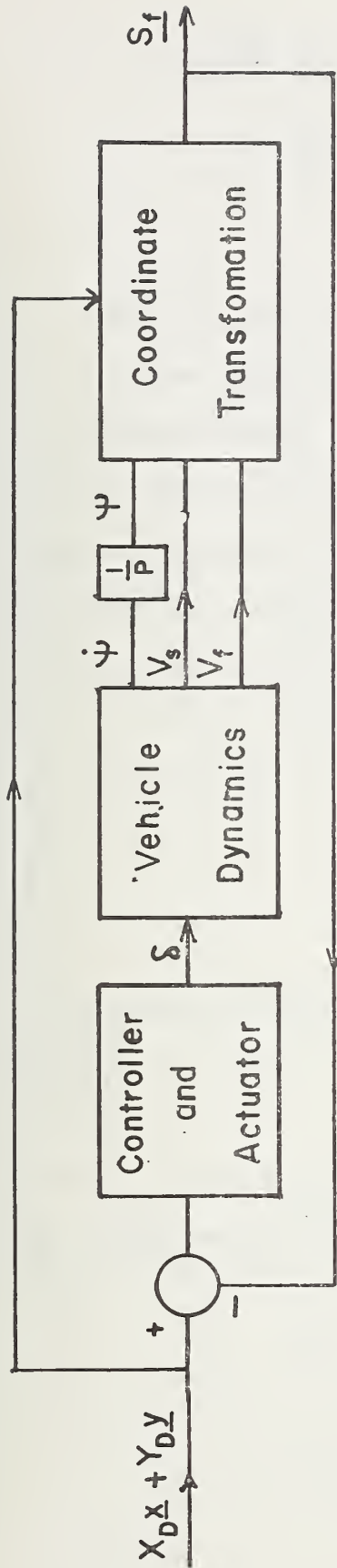
$$\dot{Y}(t) \approx V_f - V_s \psi \approx V_f \quad (B 13)$$

The corresponding distances traveled by the vehicle's cg are

$$X(t) = \frac{1}{\rho} (V_f \psi + V_s)$$

and

$$Y(t) = V_f t.$$



$$[X(t) + A_1(\cos \psi_D) \Delta \psi] \underline{x} + [Y(t) - A_1(\sin \psi_D) \Delta \psi] \underline{y}$$

Fig. B-3 A lateral controller described in inertial coordinates.

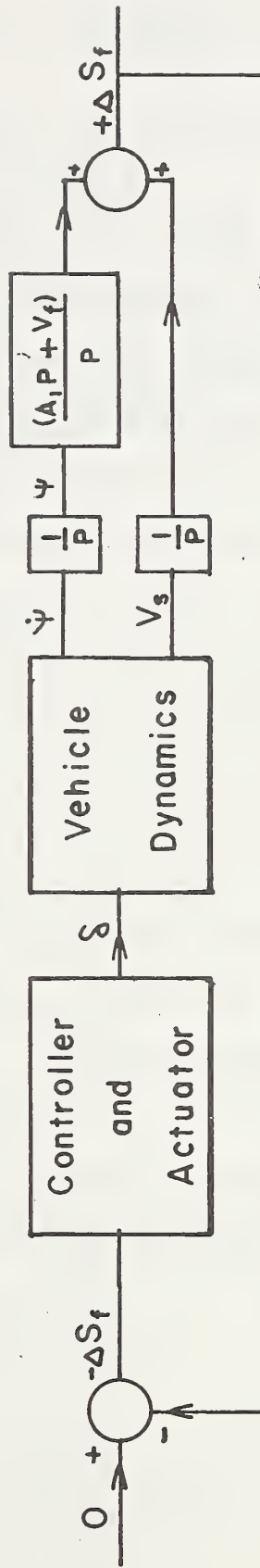


Fig. B-4 Steering controller for operation along a straight-line path (inertial coordinate system).

Thus,

$$\underline{S}_f = \left[\frac{V_f \Psi + V_s}{P} + A, \Psi \right] \underline{x} + \left[Y_D(t) - V_f t - A_1 \right] \underline{y}$$

For perfect tracking in the Y direction, $Y_D(t) = V_f t + A_1$, and

$$\Delta \underline{S}_f = \left[\frac{(A, P + V_f) \Psi + V_s}{P} \right] \underline{x}$$

Under these conditions, the block diagram of Fig. B-3 reduces to that of Fig. B-4. Since $\Delta \underline{S}_f$ only contains an \underline{x} component, the vector notation has been discarded and a relatively simple and easy to analyze configuration results. In particular, if both the vehicle dynamics and controller dynamics are linear (or the combination is linear), the closed-loop system would be linear. However, the use of this configuration is quite restricted as only straight-line tracking and paths involving small value of ψ_D and $\dot{\psi}_D$ can be considered.² For paths characterized by large ψ_D and or $\dot{\psi}_D$ (e.g., when the small-angle approximations of Eqns. (B 12)-(B 13) are not valid), the configuration of Fig. B-3 must be employed.

C. PATH-DEPENDENT COORDINATES

Consider the situation shown in Fig. B-5 where a vehicle is progressing along the path defined by

$$\underline{S}_D = \frac{V_f T(s)}{P}$$

Several representations of this path can be employed for analysis and/or design purposes, and the most convenient of these is considered next.

Note that

$$\frac{dT}{dt} = \frac{dT}{ds} \frac{ds}{dT} = \frac{V_f}{R(s)} \underline{N}$$

and

$$\dot{\psi}_D = \frac{V_f}{R(s)}$$

so that

$$\frac{dT}{dt} = \dot{\psi}_D \underline{N}. \quad (\text{B } 14)$$

²For example, a path defining a lane change.

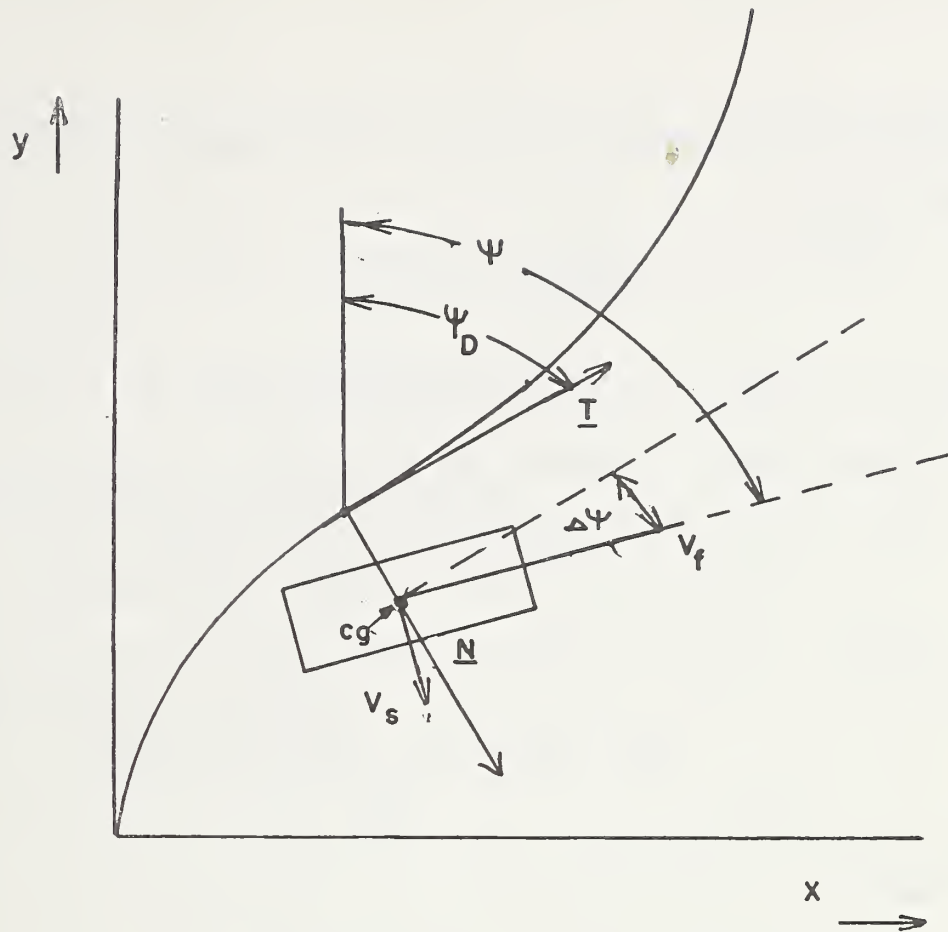


Fig. B-5 A path-dependent coordinate system.

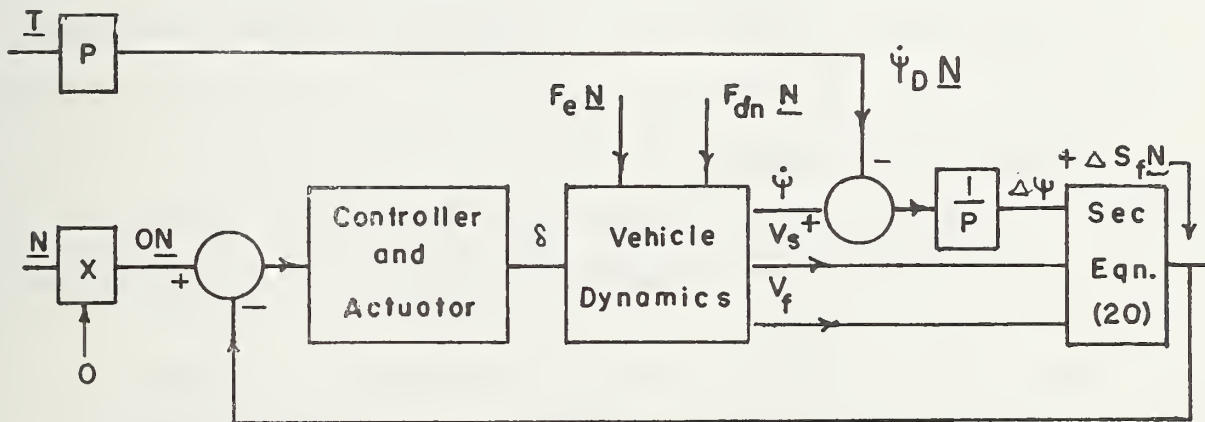


Fig. B-6 Steering controller described in path-dependent coordinates.

Further since a controlled vehicle is to be centered on the path, a second requirement is

$$f(t) \underline{N} = 0 \underline{N}. \quad (\text{B15})$$

Eqns (B14) and (B15), which define the desired path, can be employed as the command inputs to a lateral control system.

Next consider the vehicle deviation from the path. Using Fig. B-5

$$\underline{V}_v = (V_f \cos \Delta \psi - V_s \sin \Delta \psi) \underline{T} + (V_f \sin \Delta \psi + V_s \cos \Delta \psi) \underline{N}$$

Upon integrating, and recognizing that $\Delta \psi$ is small for good tracking,

$$\underline{S}_{cg} = \frac{(V_f - V_s \Delta \psi) \underline{T} + (V_f \Delta \psi + V_s) \underline{N}}{\rho} \quad (\text{B16})$$

Alternatively, from Fig. B-5

$$\underline{S}_{cg} = \frac{V_f \underline{T}}{\rho} + \Delta S_{cg} \underline{N}. \quad (\text{B17})$$

Equating B16 and B17, and cancelling the common $\frac{V_f \underline{T}}{\rho}$ term, there results,

$$\Delta S_{cg} \underline{N} = \frac{-(V_s \Delta \psi) \underline{T}}{\rho} + \frac{(V_f \Delta \psi + V_s) \underline{N}}{\rho} \quad (\text{B18})$$

As demonstrated in the appendix,

$$\Delta S_{cg} \underline{N} \approx \frac{(V_f \Delta \psi + V_s)}{\rho} \underline{N} \quad (\text{B19})$$

for V_s small and moderate values of $\dot{\psi}_D$. The corresponding deviation at the front center of the vehicle (or indeed at any location of the longitudinal axis A_1 units from the cg) is

$$\left[\frac{V_f \Delta \psi + V_s}{\rho} + A_1 \Delta \psi \right] \underline{N} = \Delta S_f \underline{N} \quad (\text{B20})$$

This is the quantity that is usually measured in a wire-following configuration.

If the curving portions of the path were superelevated, then \underline{F}_e would be nonzero and

$$\underline{F}_e = F_e(s) \underline{N}.$$

Another possible input is \underline{F}_d and, in general,

$$\underline{F}_d = F_{dT} \underline{T} + F_{dN} \underline{N}.$$

If this force were not too large, one could employ only the \underline{N} component in the analysis of lateral motion.³

Consider the lateral controller shown in Fig.B-6. Since all inputs (\underline{O}_N , $\dot{\psi}_D \underline{N}$, F_{eN} , and $F_{dN} \underline{N}$) and the output ($\Delta S_f \underline{N}$) are in the \underline{N} direction, the vector notation can be dropped, and the system treated as having scalar inputs and a single scalar output as shown in Fig.B-7. This results in an especially convenient configuration for analysis, as both straight-line paths ($\dot{\psi}_D = 0$) and curved ones ($\dot{\psi}_D \neq 0$) are readily considered. Further, the most important time histories $\Delta S_f(t)$, $V_S(t)$, $\dot{\psi}$, $\Delta\psi$, a_{CG} and a_f are readily obtainable for processing to obtain various desired performance measures (e.g., $(\Delta S_f)_{rms}$ and $(a_f)_{rms}$). The position of the vehicle with respect to an inertial frame is not directly available as with the configurations of Figs.B-3 and B-4 however, for analysis of lateral controller performance this is relatively unimportant.

³For $|F_{dN}|$ large, the vehicle dynamics model employed would probably not be valid.

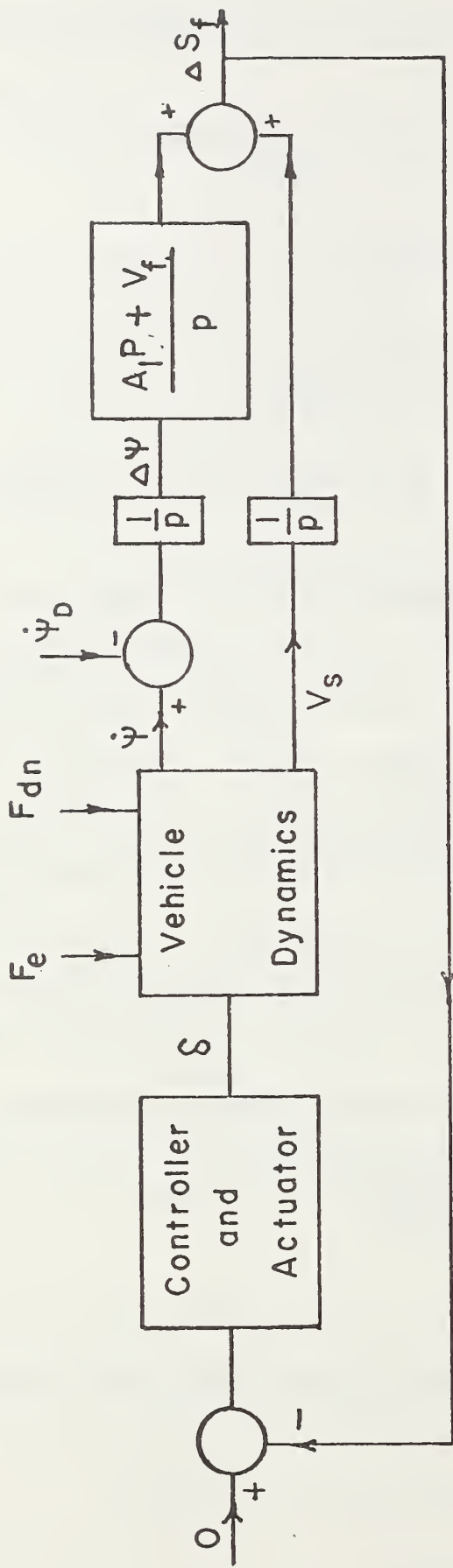


Fig. B-7 Simplified block diagram for a path-dependent coordinate system.

D. CONCLUSIONS

Under the conditions that $\dot{\psi}_D = 0$, the representation of Fig.B-7 reduces to that of Fig.B-4. In this sense, the former is a powerful extension of the latter, as it affords a simple means of accommodating the curving-path inputs which must be considered in lateral control design. This has been done in two studies, and the results obtained for $\dot{\psi}_D \neq 0$ inputs have closely corresponded with those obtained in actual vehicle tests [10] - [11].

A simple two-degree-of-freedom model was employed here for convenience; however, the path-dependent coordinate approach described here is applicable for use with more complex models.

APPENDIX BB

AN APPROXIMATION FOR Δs_{cg} .

It was demonstrated in Section III that

$$\Delta s_{cg} \underline{N} = -\frac{(V_s \Delta \psi) \underline{T}}{\rho} + \frac{(V_f \Delta \psi + V_s) \underline{N}}{\rho} \quad (\text{BB-1})$$

Letting $f(t) = (V_s \Delta \psi + V_s)$ and integrating the second term on the right-hand side by parts results in

$$\frac{f(t) \underline{N}}{\rho} = \frac{f(t)}{\rho} \underline{N} + \frac{1}{\rho} \left[\left(\frac{f(t)}{\rho} \right) \dot{\psi}_b \underline{T} \right]$$

If the resulting second term is integrated by parts, and so on, then

$$\begin{aligned} \frac{f(t) \underline{N}}{\rho} = & \frac{f(t)}{\rho} \underline{N} + \frac{1}{\rho} \left[\left(\frac{f(t)}{\rho} \right) \dot{\psi}_b \right] \underline{T} - \frac{1}{\rho} \left\{ \frac{1}{\rho} \left[\left(\frac{f(t)}{\rho} \right) \dot{\psi}_b \right] \dot{\psi}_b \right\} \underline{N} \\ & - \frac{1}{\rho} \left[\frac{1}{\rho} \left\{ \frac{1}{\rho} \left[\left(\frac{f(t)}{\rho} \right) \dot{\psi}_b \right] \dot{\psi}_b \right\} \dot{\psi}_b \right] \underline{T} - \dots \end{aligned}$$

or

$$\begin{aligned} \frac{f(t) \underline{N}}{\rho} = & \left[\frac{f(t)}{\rho} - \frac{1}{\rho} \left\{ \frac{1}{\rho} \left[\left(\frac{f(t)}{\rho} \right) \dot{\psi}_b \right] \dot{\psi}_b \right\} - \dots \right] \underline{N} \\ & + \left[\frac{1}{\rho} \left[\left(\frac{f(t)}{\rho} \right) \dot{\psi}_b \right] - \frac{1}{\rho} \left(\frac{1}{\rho} \left\{ \frac{1}{\rho} \left[\left(\frac{f(t)}{\rho} \right) \dot{\psi}_b \right] \dot{\psi}_b \right\} \dot{\psi}_b \right) - \dots \right] \underline{T} \quad (\text{BB-2}) \end{aligned}$$

The nature of the higher-order terms in this expression may be examined by considering the special case for which $\dot{\psi}_b(t)$ is constant. Then Eqn. (A-2) becomes

$$\begin{aligned} \frac{f(t) \underline{N}}{\rho} = & \left[\frac{f(t)}{\rho} - (\dot{\psi}_b)^2 \frac{f(t)}{\rho^3} - (\dot{\psi}_b)^4 \frac{f(t)}{\rho^5} - \dots \right] \underline{N} \\ & + \left[\dot{\psi}_b \frac{f(t)}{\rho^2} - (\dot{\psi}_b)^3 \frac{f(t)}{\rho^4} - (\dot{\psi}_b)^5 \frac{f(t)}{\rho^6} - \dots \right] \underline{T} \end{aligned}$$

Under the condition that both $\dot{\psi}_D$ and the successive integrations of $\frac{f(t)}{p}$ are small, then

$$\frac{f(t)N}{p} \approx \frac{f(t)}{p} \underline{N}.$$

Further, since both V_s and $\Delta\psi$ are small for a well-performing lateral controller, the first term in Eqn. (A-1) may be neglected. Then, this equation becomes

$$\Delta s_{eg} \underline{N} \approx \frac{(V_f \Delta\psi + V_s)}{p} \underline{N},$$

which is the result previously employed.

REFERENCES

1. Hacker, R.M., and Osmer, W.D., "AGT Operating Experience at Morgantown and EXPO '75 Okinawa-- A Report from the Field," in Conference Record of 28th IEEE Vehicular Technology Conference, Denver Colorado, March 22 - 24, 1978 (IEEE Cat. No. 78CH1297 - 1VT).
2. Anon., "Dual - Mode Transportation", Special Report 170, Transportation Research Board, Washington, D.C., 1976.
3. Anon., "Systems Studies for Automated Highway Systems", Contract awarded by FHWA/DOT to Transportation Systems Division, General Motors Corp., Detroit, Michigan, April 1980.
4. Pasternak, S., "Modern Control Aspects of Automatically Steered Vehicles", U.S. Dept. of Transportation, Transportation Systems Center, Rep. DOT-TSC-OST-72-3, Dec. 1971.
5. Bonderson, L., "Optimum Lateral Control for Dual-Mode Vehicles", Report GMR-1588, General Motors Research Laboratories, Warren, Michigan, May 1974.
6. Shladover, S.E., et al., "Steering Controller Design for Automated Guideway Transit Vehicles", Journal of Dynamic Systems, Measurement and Control, Vol. 100, March 1978, pp. 1-8.
7. Darenberg, W., et al., "Design of Automatic Lateral Vehicle Controllers," A Link Between Science and Applications of Automatic Control, Proceedings of the 7th IFAC World Congress, Helsinki, Finland, June 1978.
8. Lague, T.L., "Optimization of the Automatic Steering Control of a Vehicle in a Guideway with Positive Mechanical Retension," presented at the TRB Conference on Dual - Mode Transportation, Washington, D.C., May 29-31, 1974.
9. Kasselmann, J.T., and Keranen, T.W., "Adaptive Steering," Bendix Technical Journal, Autumn 1969, pp. 26-35.
10. Cormier, W.H., "Experimental Studies in Vehicle Lateral Control", Master of Science Thesis, Dept. of Elect. Engr., The Ohio State University, Columbus, Ohio, Dec. 1978.
11. Fenton, R.E., Melocik, G., and Olson, K.W., "On the Steering of Automated Vehicles: Theory and Experiment", IEEE Transactions on Automatic Control, Vol. AC-21, No. 3, June 1976, pp. 306-315.
12. Weir, D., et al., "Dynamics of the Automobile Related to Driver Control," Systems Technology Inc., Bureau of Public Roads Tech. Rep. 157-1, July 1966.
13. Gardels, K., "Automatic Car Controls for Electronic Highways," General Motors Research Corp., Warren, MI, Rep. GMR-276, June 1960.

References continued

14. Cardew, K.H.F., "The Automatic Steering of Vehicles-- An Experimental System Fitted to a DS19 Citroen Car", Road Research Laboratory, Great Britian, RRL Rep. LR 340, 1970.
15. Ito. T. et al., "An Automatic Driving System of Automobiles by Guidance Cables, presented at Int. Automotive Engineering Congress, Jan 8-12, 1973, SAE Paper 730127.
16. Smisek, R. and Harder, G., "Automated Control of Guideway Transit Vehicles", Proceedings of 29th IEEE Vehicular Technology Conference, Arlington Heights, Illinois, March 27-30, 1979, pp. 57-64 (IEEE Cat. No. 79CH1378-9VT).

APPENDIX C

A MICROPROCESSOR-BASED LATERAL CONTROLLER -- HARDWARE IMPLEMENTATION

The control algorithm discussed in Chapter V was implemented with an Intel SDK-86 design kit. The resulting microcomputer, which is based on the 8086 microprocessor, is depicted in Fig. C-1. It operates at a 2-MHz (or 4-MHz) clockrate and has 2k bytes of onboard RAM (with provision for an additional 2k), 2k bytes of monitor ROM, and 2k bytes of user PROM. The keypad monitor program, which is resident in the monitor ROM, interprets data and commands from the keypad and displays results on a 10-character, 7-segment display. Input/output is achieved through a programmable peripheral interface, an Intel 8255, which has 3 programmable I/O ports.

A programmable keyboard display, an Intel 8255, divides the processor clock by 1.25×10^4 to provide a 5.1455 ms square wave. This is further divided by 10 using a decade counter, an Intel 7490, to provide a 51.455 ms clock. This clock triggers a monostable multivibrator to produce one $4 \mu\text{s}$ pulse each period. The latter is used to initiate the transformation of both V_f and ΔS_f to a discrete form, and to interrupt the microcomputer which

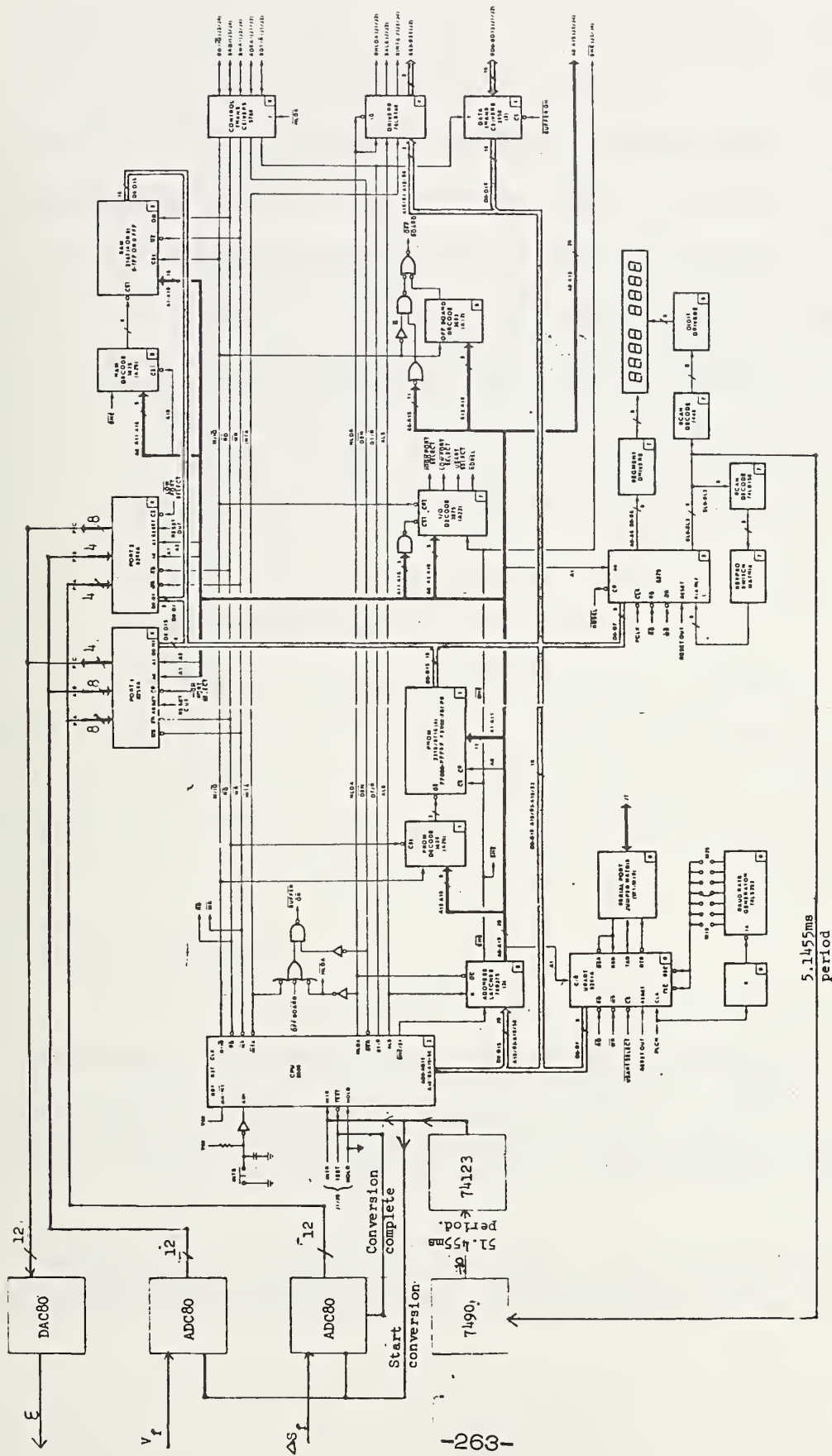


Fig. C-1: Block diagram of SDK-86 microcomputer with hardware modifications.

then starts executing a program to process data. The former is achieved by using two 12-bit A/D converters (two ADC 80's are employed). The conversion-complete signal from the A/D converter (of ΔS_f)¹ is connected to the TEST input of the 8086 processor. On entering the interrupt routine, the processor executes a WAIT instruction¹ so that processing of data begins only after the conversion is complete. Note that Ports A and B of the 8255 are used to input V_f and ΔS_f . The voltage output E_i , which is the input to the electrohydraulic actuator, is the output on Port C.

¹ The conversion of V_f requires approximately the same time as that for ΔS_f . In addition, the V_f signal is used some 4 ms after it is sampled, whereas ΔS_f is used immediately. Hence, the conversion-complete signal of the ΔS_f A/D converter can be used to indicate the completion of conversion for both A/D's.

² The WAIT instruction causes the processor to enter a wait state if the signal on the TEST pin is not asserted. This state is cleared and execution resumes when the TEST signal is asserted.

APPENDIX D

MICROCOMPUTER HARDWARE FOR A LONGITUDINAL CONTROLLER

A. Introduction

The microprocessor selected for use in the longitudinal controller, described in Chapters VI and VII, must meet the following requirements:

- i) The clock frequency and instruction cycle must be fast enough so that the data sampling intervals and transport delays are small, thereby not lessening controller stability;
- ii) There should be one power supply voltage to reduce the necessary auxiliary units; and
- iii) All support hardware must be commercially available.

The device selected, an INTEL 8085 A, is an 8-bit microprocessor with a 1.3 μ s instruction cycle, a single supply voltage (+5V) and commercially available support devices. The 8085A is employed in the computer outlined in Fig. D-1.

B. Address Allocations

A total of 64K memory locations (1K = 1024 bytes) and 256 I/O ports are addressable. The former are divided into blocks for ROM, RAM, memory-mapped multiplying, and user I/O as shown in Fig. D-2.¹ The locations labeled "foldback" are alternative addresses which should be avoided to

¹All addresses presented here are in hexadecimal form.

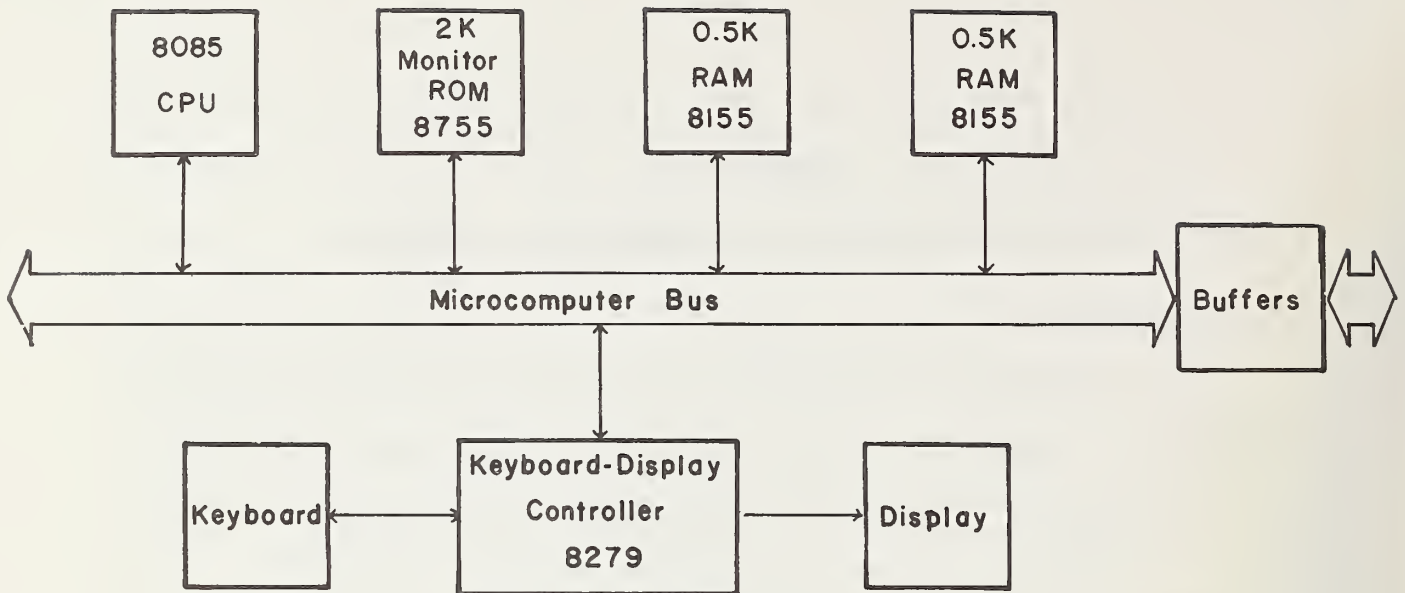


Fig. D-1. Basic microcomputer structure.

reduce the possibility of confusion. Addresses 0000_H through $7FFF_H$ are allocated for the basic system, while addresses 8000_H - $FFFF_H$ are enabled by expansion buffers to implement additions to this system.

C. Program PROM

An INTEL 2758 PROM (programmable read-only memory) was selected for program storage because of its single 5-volt power supply requirement, its low-power dissipation (525-mW active power, 132-mW standby power), its fast access time (450 ns), and the availability of a programming unit.

A diagram of the PROM interface design is shown in Fig. D-3. The chip enable input (\overline{CE}) controls the enabling of the device, and is set "active" when a value between 8000_H and $87FF_H$ is on the address bus. (The PROM is assigned addresses 8000_H - $83FF_H$.)

The 8085 bus-timing was set up to allow for 170 ns between the time the address is valid (i.e., stable) and the read line is activated, and an additional 400 ns before the signals on the data lines are read; thus the total access time is 570 ns. The specified maximum access time of the PROM is 450 ns; therefore, there is a "buffer" of 120 ns in the "READ" cycle.

Memory Locations	
FFFF	Not Used (open for expansion)
C000	
BFFF	Multiplier locations (fold back)
B808	
B807	Multiplier locations
B800	
B7FF	Not Used, Chip selects 1-6 on Device D1
8800	
87FF	Program PROM (fold back)
8400	
83FF	Program PROM (1K)
8000	
7FFF	
	Not Used
3000	
2FFF	Expansion RAM (fold back)
2900	
28FF	Expansion RAM (256 locations)
2800	
27FF	Basic RAM (fold back)
2100	
20FF	Basic RAM (256 locations)
2000	
1FFF	
1800	User I/O
17FF	
	Not Used (2K)
1000	
0FFF	Expansion ROM (2K) (not used)
0800	
07FF	Monitor ROM (2K)
0000	

Fig. D-2. Memory Allocations

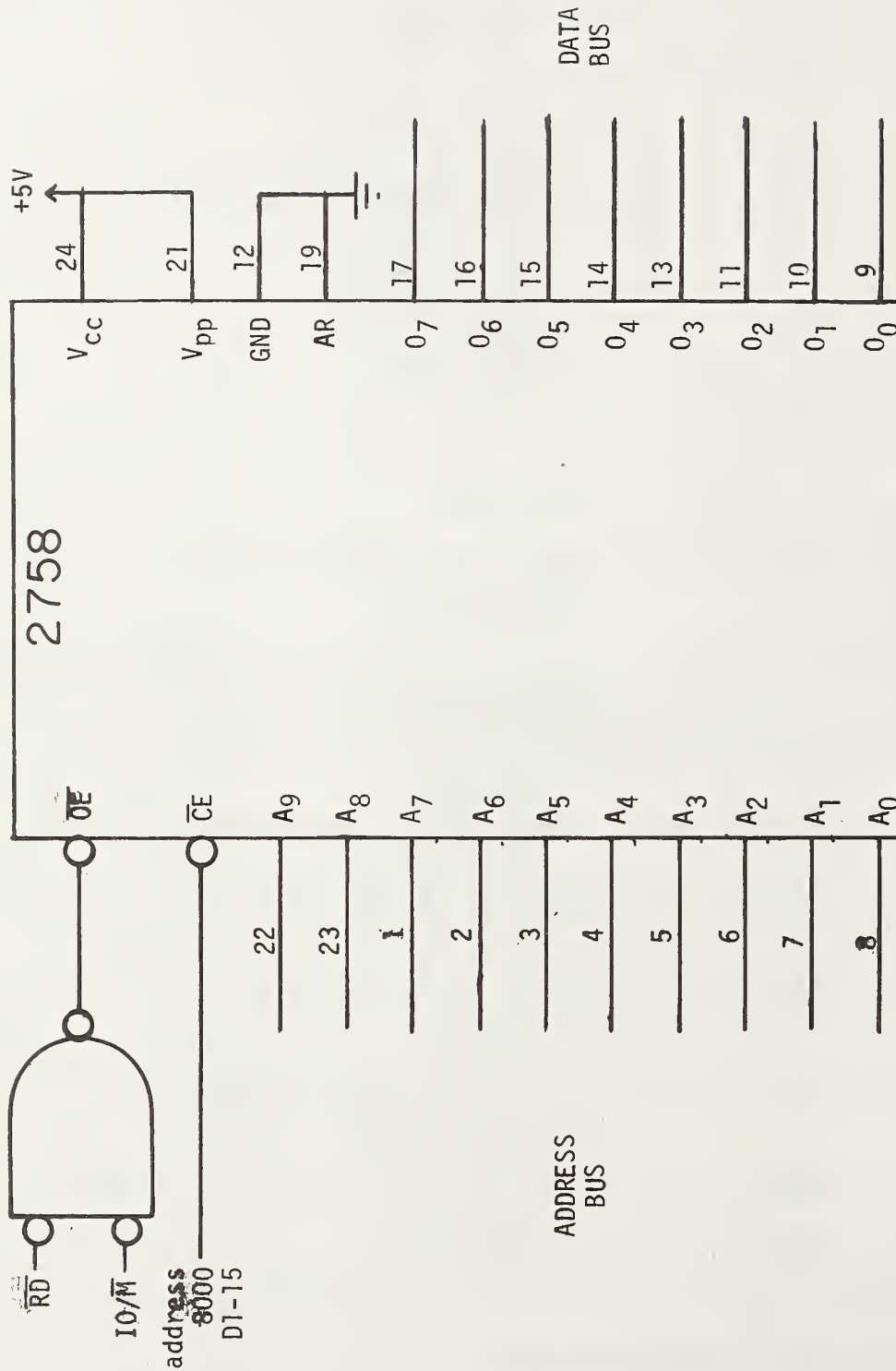


Fig. D-3. PROM Interface.

D. I/O Ports

The information transfers to and from the computer are accomplished via three output and four input ports. These I/O ports operate with the designated hardware and software features of the microprocessor.² The I/O device chosen was the INTEL 8212, which consists of an eight-bit latch,³ a tri-state buffer, and some logic circuitry. The output port (see Fig. D-4) latches data from the microprocessor so that the information is always available on the output pins of the device. The input port (see Fig. D-5) supplies the data bus with the information on the input lines when the proper instruction is executed.

E. Multiplier Interface

A hardware multiplier was added to aid in the numerous and complex computations that must be carried out for longitudinal control. This addition results in a reduction in both software and calculation times by a factor of twenty.

The MPY-16 AJ, manufactured by TRW Corp., was selected because it was the only available multiplier that operated on 16-by-16 bit inputs to produce a 32-bit product. Several problems arose from this choice. First, because the inputs are 16-bits long, external buffers and registers are needed to store and read data. Second, because of the magnitude of power consumption (5W), there is a need for a high-amperage, five-volt supply.

²The I/O ports have eight-bit addresses and are operated with the "IN" and "OUT" instructions.

³A latch is a type of storage register.

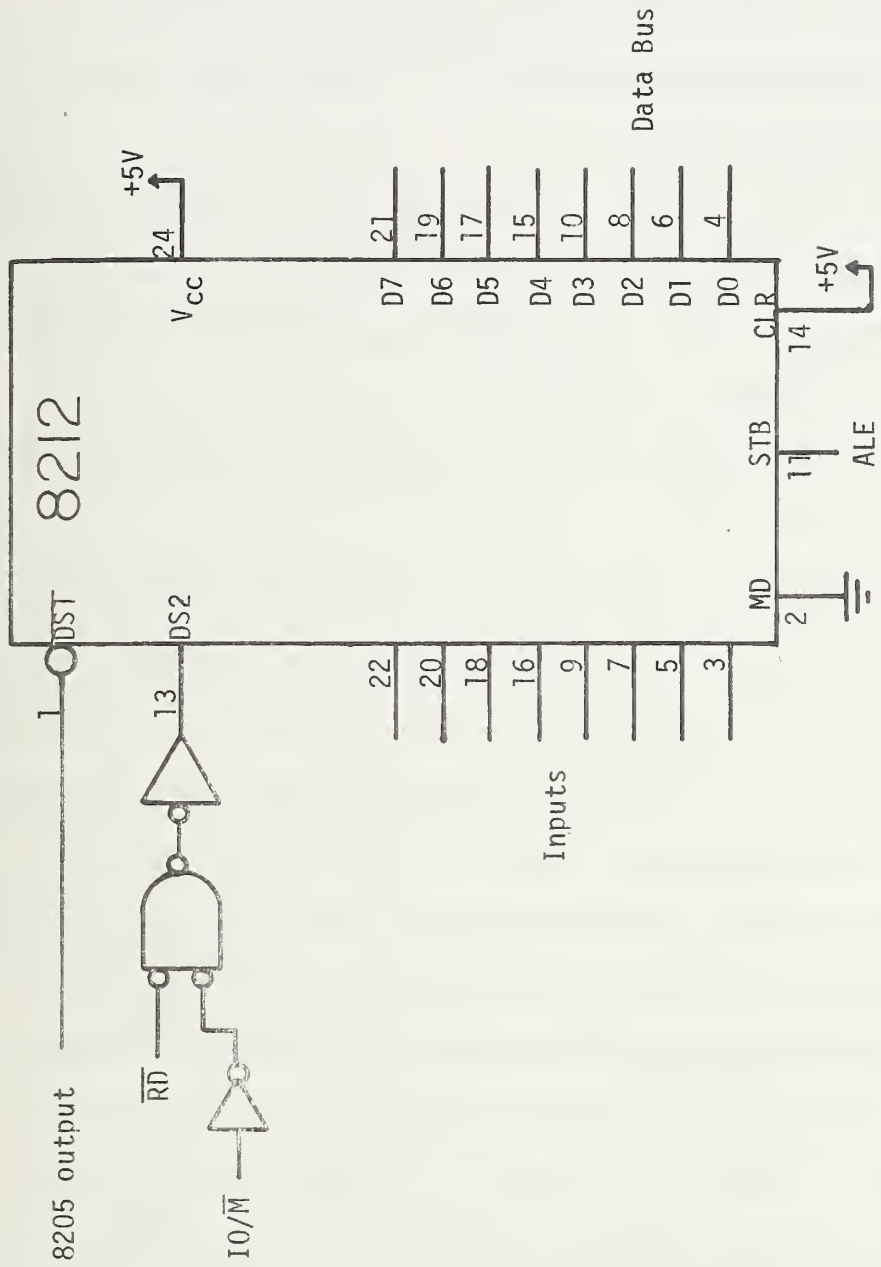


Fig.D-5. Input port interface.

The overall multiplier interface is designed so that the multiplication seems memory-mapped to the programmer. The software procedure for carrying out a 16-by-16 bit, two's-complement multiplication is summarized as follows:

1. The LSB (least significant byte) of the first multiplicand is loaded into address B800 and the MSB (most significant byte) is loaded into address B801.
2. Similarly, the LSB and MSB of the second multiplicand are loaded into addresses B802 and B803, respectively.
3. With these values stored, the product is automatically calculated and stored into output registers.⁴
4. The LSB of the MSP (most significant product) register can be read from B804, and the MSB from location B805.
5. The LSB and the MSB of the LSP (least significant product) can be read from locations B806 and B807, respectively. The sign bit is contained in the highest-order bit in both the MSP and the LSP.

The implemented design involves the use of data latches and tri-state buffers so that the microcomputer's eight-bit data bus can be used to transfer information to and from the multiplier. The package pins which are connected to the first multiplier-input register, the X register, are unique to that register; thus no multiplexing is needed. The only external hardware necessary is a latch (an INTEL 8212) that stores eight bits of data; thus all input digits (eight in the latch and eight on the

⁴The multiplication time is 150 ns, which is very fast compared to the microprocessor instruction cycle.

data bus) are available to the multiplier simultaneously (see Fig. D-6). A decoded timing signal is used to load information into the X register when these bits are available.

The other multiplier input, the Y register (see Fig.D-7) shares external device pins with the LSP output register; thus the required interface to the microprocessor is more complex. Extra buffers and careful timing are needed to ensure that no more than one device activates the data bus at any time.⁵ An INTEL 8212 is used to store the LSB at address B802 and to activate the inputs to the Y register when a byte of data, the MSB, is stored into memory location B803. The latter byte goes through a buffer which is enabled with the same timing signal as the one used to clock the input. In this way, the inputs to the Y register are active only when the decoded address B803, the \overline{WR} signal, and the IO/\overline{M} ⁶ signal are all low voltage.⁷

A combinatorial logic array is used to "multiply" the values in the two input registers. The 32-bit product is transferred to 2, 16-bit registers--the LSP register (see Fig.D-8) and the MSP register. Data is sent from the former register to the device pins by activating the TRI L input when either location B806 or B807 is read. Connected to these pins are two separately-enabled buffers--one is activated when address B806 is read, the other when B807 is read. In this way, the two, eight-bit bytes from the LSP are separately transferred through the same bus.

⁵ Such an occurrence would result in bad data transmission or the destruction of a device.

⁶ \overline{WR} and IO/\overline{M} are microcomputer timing signals.

⁷ This corresponds, in software, to writing into memory location B803.

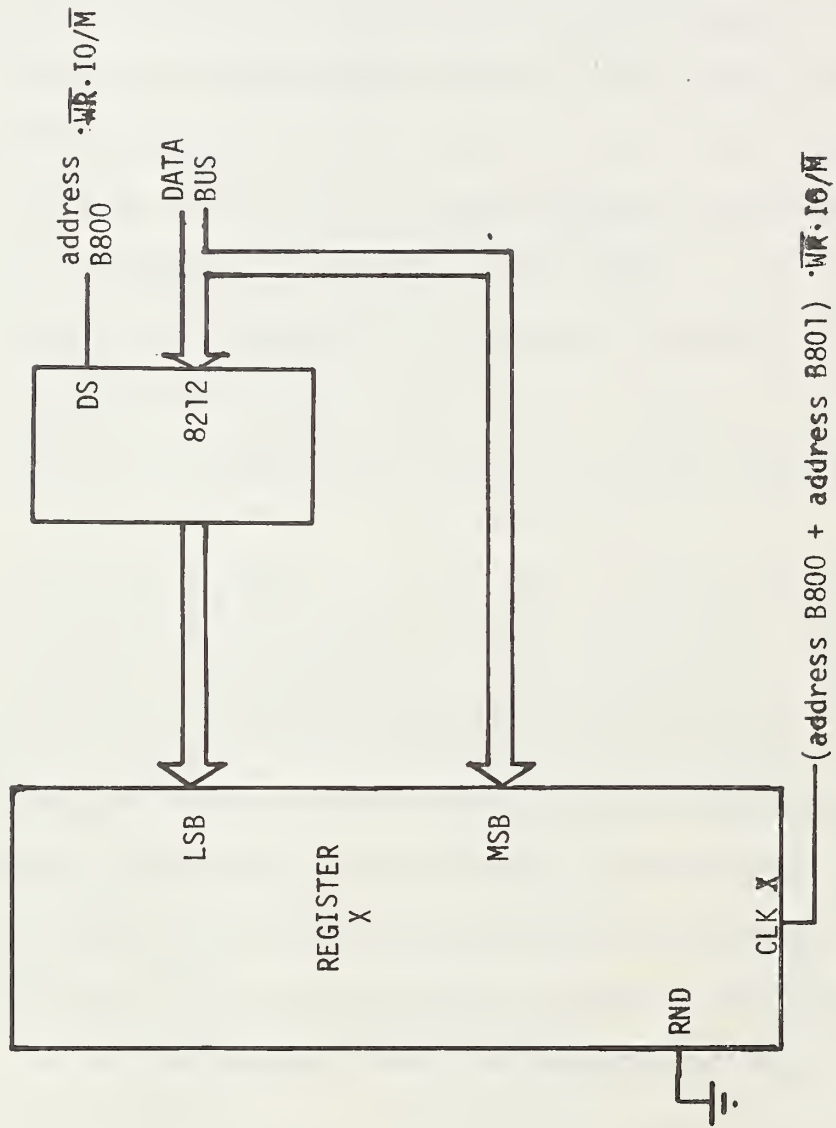


Fig. D-6. Multiplier X-Register Interface.

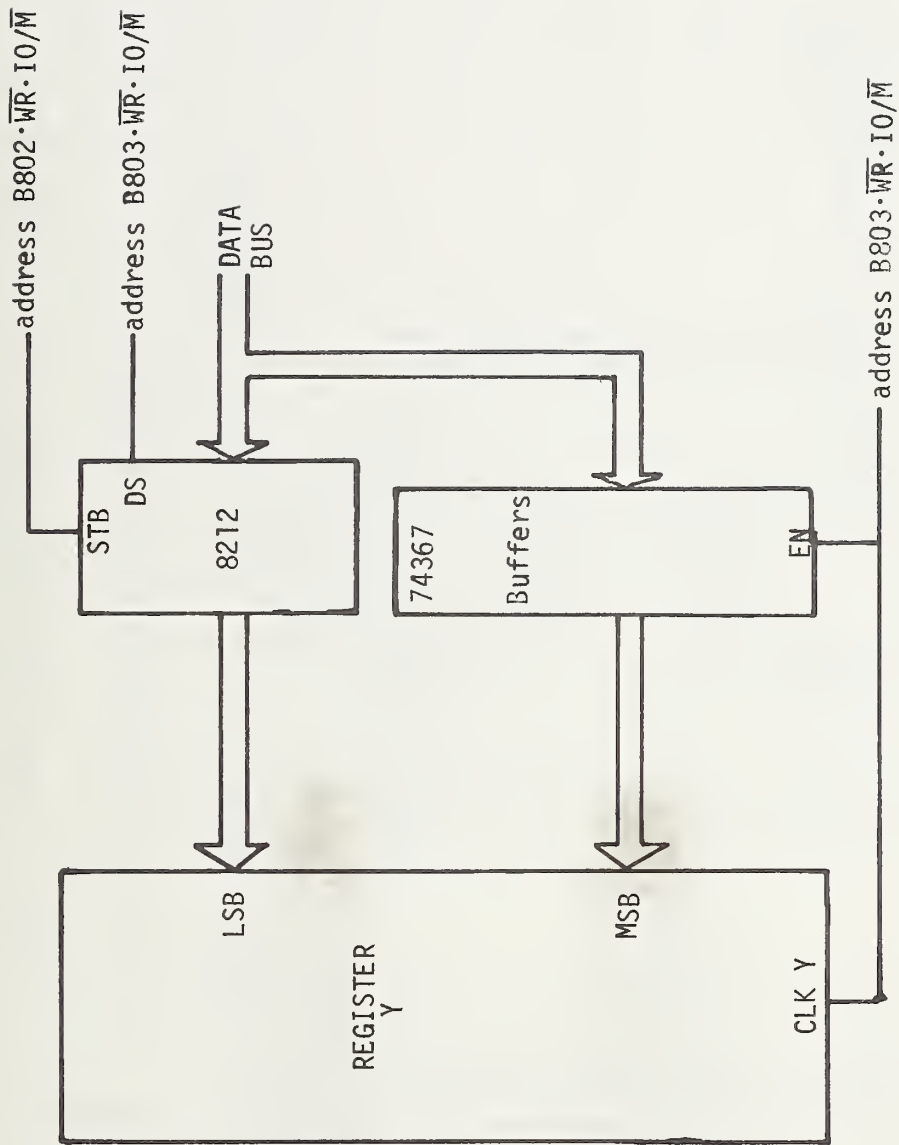


Fig. D-7. Multiplier Y-Register Interface.

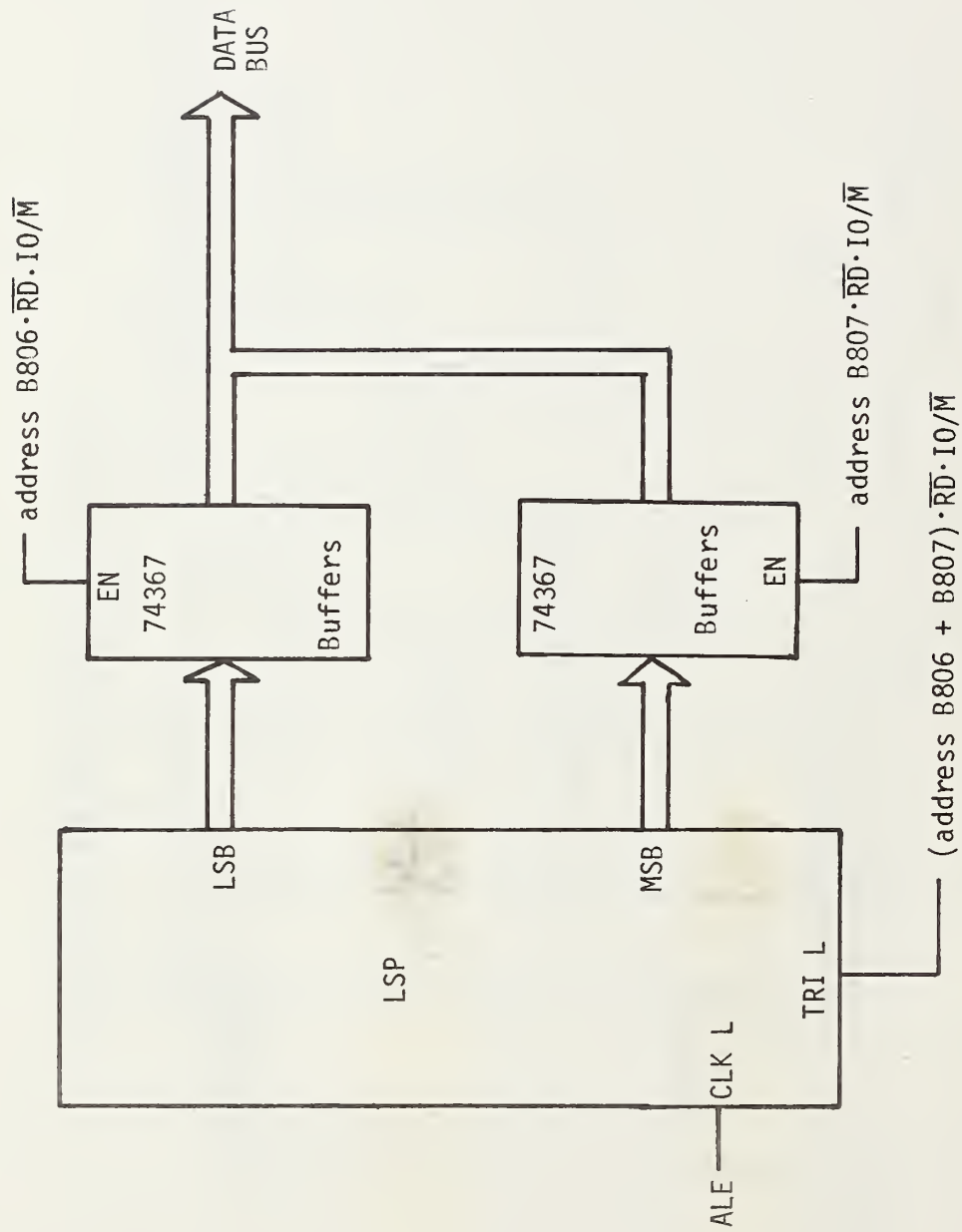


Fig. D-8. Least-Significant, Product-Output Interface.

The other product register is the MSP (see Fig. D-9), whose output operates in the same way as the LSP, except that addresses B804 and B805 are used to enable the external buffers.

F. Interrupt Considerations

During longitudinal control operation, two occurrences warrant the use of a microprocessor interrupt--the reception of a timing signal (every 0.1 s) for the synchronizing sector- and vehicle-level control and communications, and the specification of an emergency either from onboard instruments or from a macro-level computer. Since these two occurrences involve different responses, two separate interrupt lines should be used.

In the basic computer, three interrupts are dedicated to system and user functions and the other two are available for use with the previously described occurrences. The former are the TRAP, which is used for a basic system timing interrupt, the RST 5.5, which is dedicated to the display controller, and the RST 7.5 which is a user-enabled interrupt. The latter should be programmed to allow the operator to halt or alter operations of the computer during testing operations. The two remaining are the RST 6.5 and INTR functions. Since the RST 6.5 is of higher priority than the INTR, the former should be used for emergencies and the latter for the synchronization signal.

G. Summary

The microcomputer described here has been designed for the purpose of longitudinal control--especially the field testing of control algorithms. Expedient testing operations are possible because loading and changing program sections and parameters in memory can be accomplished quickly with either the use of the keyboard input or the insertion of pre-programmed PROM's. Other I/O devices, such as a cassette recorder or a teletype were considered, and it was determined that they could be useful and added later if necessary.

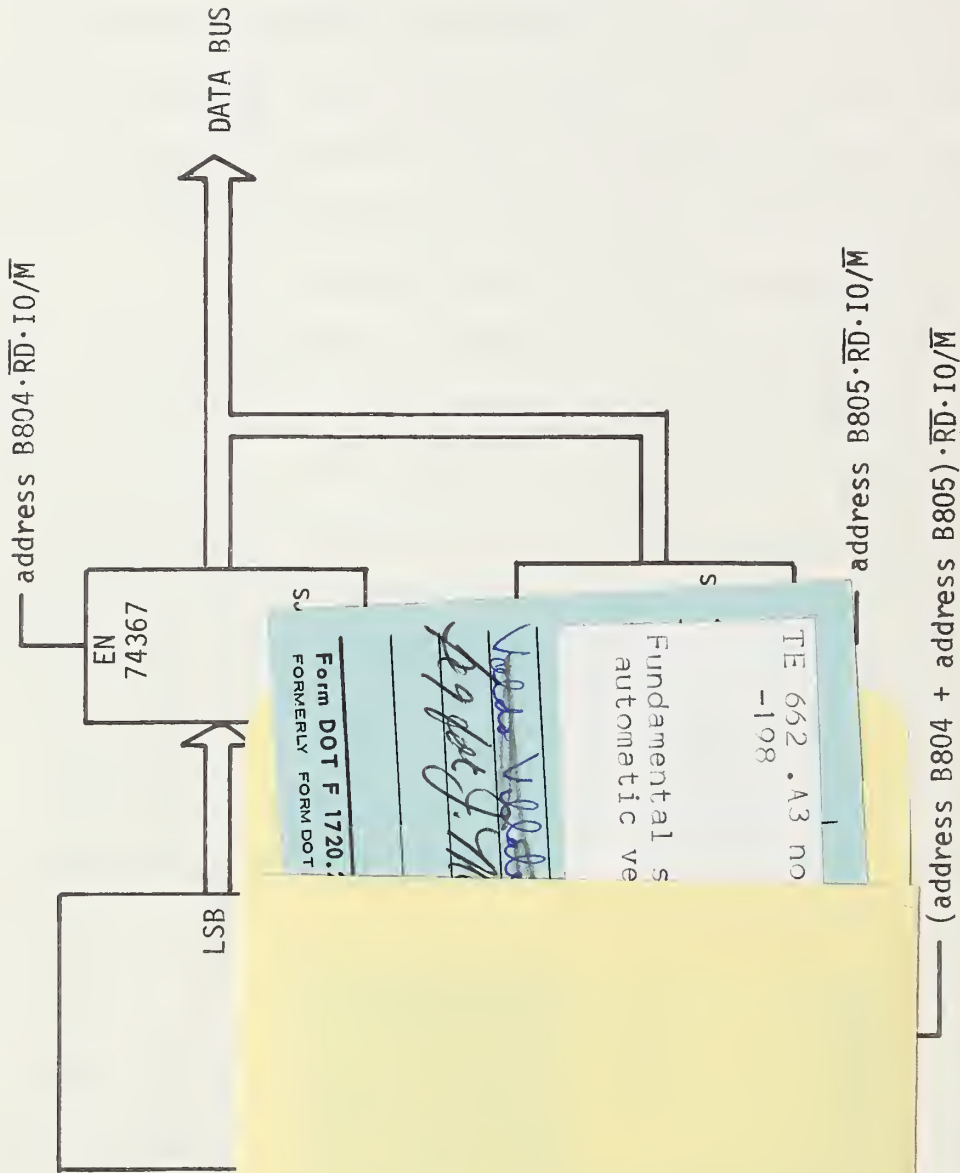


Fig. D-9. Most-Significant, Product-Output Interface

FEDERALLY COORDINATED PROGRAM (FCP) OF HIGHWAY RESEARCH AND DEVELOPMENT

The Offices of Research and Development (R&D) of the Federal Highway Administration (FHWA) are responsible for a broad program of staff and contract research and development and a Federal-aid program, conducted by or through the State highway transportation agencies, that includes the Highway Planning and Research (HP&R) program and the National Cooperative Highway Research Program (NCHRP) managed by the Transportation Research Board. The FCP is a carefully selected group of projects that uses research and development resources to obtain timely solutions to urgent national highway engineering problems.*

The diagonal double stripe on the cover of this report represents a highway and is color-coded to identify the FCP category that the report falls under. A red stripe is used for category 1, dark blue for category 2, light blue for category 3, brown for category 4, gray for category 5, green for categories 6 and 7, and an orange stripe identifies category 0.

FCP Category Descriptions

1. Improved Highway Design and Operation for Safety

Safety R&D addresses problems associated with the responsibilities of the FHWA under the Highway Safety Act and includes investigation of appropriate design standards, roadside hardware, signing, and physical and scientific data for the formulation of improved safety regulations.

2. Reduction of Traffic Congestion, and Improved Operational Efficiency

Traffic R&D is concerned with increasing the operational efficiency of existing highways by advancing technology, by improving designs for existing as well as new facilities, and by balancing the demand-capacity relationship through traffic management techniques such as bus and carpool preferential treatment, motorist information, and rerouting of traffic.

3. Environmental Considerations in Highway Design, Location, Construction, and Operation

Environmental R&D is directed toward identifying and evaluating highway elements that affect

the quality of the human environment. The goals are reduction of adverse highway and traffic impacts, and protection and enhancement of the environment.

4. Improved Materials Utilization and Durability

Materials R&D is concerned with expanding the knowledge and technology of materials properties, using available natural materials, improving structural foundation materials, recycling highway materials, converting industrial wastes into useful highway products, developing extender or substitute materials for those in short supply, and developing more rapid and reliable testing procedures. The goals are lower highway construction costs and extended maintenance-free operation.

5. Improved Design to Reduce Costs, Extend Life Expectancy, and Insure Structural Safety

Structural R&D is concerned with furthering the latest technological advances in structural and hydraulic designs, fabrication processes, and construction techniques to provide safe, efficient highways at reasonable costs.

6. Improved Technology for Highway Construction

This category is concerned with the research, development, and implementation of highway construction technology to increase productivity, reduce energy consumption, conserve dwindling resources, and reduce costs while improving the quality and methods of construction.

7. Improved Technology for Highway Maintenance

This category addresses problems in preserving the Nation's highways and includes activities in physical maintenance, traffic services, management, and equipment. The goal is to maximize operational efficiency and safety to the traveling public while conserving resources.

0. Other New Studies

This category, not included in the seven-volume official statement of the FCP, is concerned with HP&R and NCHRP studies not specifically related to FCP projects. These studies involve R&D support of other FHWA program office research.

* The complete seven-volume official statement of the FCP is available from the National Technical Information Service, Springfield, Va. 22161. Single copies of the introductory volume are available without charge from Program Analysis (HRD-3), Offices of Research and Development, Federal Highway Administration, Washington, D.C. 20590.

DOT LIBRARY



00057010

